Design of a Deployable Structure for a Lunar Greenhouse Module

Vincent Vrakking

Delft University of Technology
Faculty of Aerospace Engineering
Chair of Space Systems Engineering

March 12, 2014

Faculty of Aerospace Engineering
Delft University of Technology
Kluyverweg 1, 2629 HS Delft,
The Netherlands

Preface

This thesis report concludes the final graduation project of the Aerospace Engineering - Master of Science program at the Faculty of Aerospace Engineering at Delft University of Technology. This project was carried out at the chair of Space Systems Engineering and at the department System Analysis – Space Segment of the German Aerospace Center - Institute of Space Systems in Bremen, Germany.

First and foremost, my sincere gratitude to Daniel Schubert for giving me the opportunity to do my thesis work within the System Analysis – Space Segment department at the German Aerospace Center in Bremen and for the invaluable feedback and input. Also, many thanks are due to my supervisor Jian Guo for the useful comments and quick reviews which allowed me to improve my work.

Delft, March 2014,

Vincent Vrakking

Abstract

A design study was carried out at the German Aerospace Center (DLR) in Bremen, investigating the optimal structural design for a lunar greenhouse module. On account of the volume requirements of a lunar greenhouse and the volume constraints of modern launchers, the study has considered only inflatable and hybrid structures.

A literature study was performed on the existing technologies and concepts of fully inflatable and partially inflatable (hybrid) space habitats and structures. Additionally, a review of the lunar environment was carried out and the impact on the lunar greenhouse module structure design was determined.

Using system engineering tools, the structural requirements of the greenhouse module were defined. Concepts, such as a cylinder or semi-cylinder, were developed and assessed using an Analytical Hierarchy Process (AHP).

A preliminary design of the structure was performed for the selected concept, a semi-cylinder with rigid end-caps and a flexible middle section. For the preliminary design, the gas retention properties as well as the micro-meteoroid and radiation shielding capabilities were designed and thermal and load-bearing properties of the structure were analysed. Additionally, a possible configuration of the greenhouse module interior was presented and interfaces between the rigid and flexible sections of the structure, as well as between the structure and other lunar base structures were discussed.

Verification of the preliminary design calculations and the compliance with the requirements was carried out for the thermal and load-bearing structural properties, using the finite element analysis tool MSC Nastran.

The final structure design is a semi-cylindrical hybrid structure with rigid end-caps, 20 m in length and with a 3 m radius and with a total mass of 43786 kg.

Radiation protection is provided by covering the structure with regolith-filled bags. A total thickness of approximately 2,5 m of regolith needs to be applied to the greenhouse to provide sufficient protection for the astronauts and plants within during the envisioned two year mission lifetime.

Table of Contents

List of Figures

List of Tables

Abbreviations

AHP	-	Analytical Hierarchy Process
ALE	-	Arbitrary Lagrangian-Eulerian
ALiSSE	-	Advanced Life Support System Evaluator
AO	-	Atomic Oxygen
ATS-6	-	Applications Technology Satellite 6
BFO	-	Blood Forming Organs
BLE	-	Ballistic Limit Equation
BPC	-	Biomass Production Center
CELSS	-	Controlled Environment and Life Support System
CME	-	Coronal Mass Ejection
CPR	-	Critical Performance Ratio
Csda	-	Continuously slowing down approach
CV	-	Control Volume
DLR	-	German Aerospace Center
DOT	-	Design Option Tree
EDU	-	Engineering Development Unit
ESA	-	European Space Agency
ESM	-	Equivalent System Mass
EVA	-	Extravehicular activity
EVOH	-	Ethylene vinyl alcohol
FARM	-	Food and Revitalization Module
FBD	-	Free Body Diagram
FBS	-	Functional Breakdown Structure
FEM	-	Finite Element Modelling
FFD	-	Functional Flow Diagram
GCR	-	Galactic Cosmic Radiation
GHM	-	Greenhouse Module
GPS	-	General Particle Source
IAE	-	Inflatable Antenna Experiment
IBEX	-	Interstellar Boundary Explorer
IDSS	-	International Docking System Standard
IEO	-	Inflatable Exo-atmospheric objects
ISAS	-	Institute of Space and Astronautical Science
ISS	-	International Space Station
JAXA	-	Japanese Aerospace Exploration Agency
JPL	-	Jet Propulsion Laboratory
LDEF	-	Long Duration Exposure Facility
LED	-	Light Emitting Diode
LET	-	Linear Energy Transfer
LRO	-	Lunar Reconnaissance Orbiter
LSS	-	Life Support System
MLI	-	Multi-Layer Insulation
MMOD	-	Micro-meteoroids and orbital debris
NASA	-	National Aeronautics and Space Agency
NDS	-	Nutrient Delivery System
PHOEBE	-	Permanent Human mOon Exploration BasE

PPF	-	Photosynthetic photon flux
PVC	-	Polyvinyl chloride
RDT	-	Requirements Discovery Tree
RH	-	Relative Humidity
rms	-	root mean square
SEIM	-	Surface Endoskeletal Inflatable Module
SELENE	-	Selenological and Engineering Explorer
SEP	-	Solar Energetic Particles
SHM	-	Structural Health Monitoring
SICSA	-	Sasakawa International Center for Space Architecture
SOHO	-	Solar and Heliospheric Observatory
SoW	-	Statement of Work
TransHab	-	Transit Habitat
VLBI	-	Very Large Basline Interferometry

List of Symbols

A	-	shielding material dependent coefficients
A_c	-	cross-sectional area
A_S	-	exposed surface area of the lunar GHM
AD_b	-	barrier areal density
$AD_{stuffing}$	-	areal density of stuffing
B	-	shielding material dependent coefficients
c	-	speed of light in a vacuum
c_o	-	coefficient
c_b	-	coefficient
$c_{stuffing}$	-	coefficient
c_w	-	coefficient
C	-	coefficient
d_p	-	particle diameter
dE/dx	-	stopping power
D	-	diffusivity
D_S	-	flexural rigidity
e	-	magnitude of electron charge
E	-	Young's modulus
E_e	-	total electron energy
E_k	-	kinetic energy
E_p	-	proton energy (in GeV)
F	-	particle fluence
F_{cr}	-	critical buckling load
F_{ij}	-	view factor of surface i to j
F_{lunar}	-	view factor from GHM surface to lunar surface
F_{solar}	-	view factor from surface to Sun
G_{albedo}	-	incident albedo flux
G_{solar}	-	incident solar flux on the lunar surface
h	-	plate thickness
HB	-	Brinell Hardness
I	-	moment of inertia
I_{eV}	-	mean excitation energy

J	-	steady state permeation flux
k	-	coefficient
k_c	-	thermal conductivity
k_o	-	constant
k_{lat}	-	lateral stiffness
k_{lon}	-	longitudinal stiffness
K	-	material dependent constant
L	-	wall thickness
L_{beam}	-	beam length
m	-	electron rest mass
m_p	-	particle mass
n	-	number of moles [mole]
n_e	-	number of electrons within unit volume material
N	-	number of atoms within unit volume of material
N_o	-	(mono-energetic) photon beam intensity at depth o
N_x, N_y, N_{xy}	-	direct loads
$N(x)$	-	(mono-energetic) photon beam intensity at depth x
P	-	pressure [Pa]
P_{eff}	-	effective permeability
P_h	-	probability of impact
P_i	-	permeability of layer i
P_{lat}	-	lateral load
P_m	-	permeability
P_∞	-	penetration depth
Q	-	Energy loss per collision
Q_{cond}	-	amount of heat conducted
Q_{heat}	-	absorbed UV heat
$Q_{rad,ij}$	-	net radiative heat transfer between surfaces i and j
Q_x, Q_y	-	shear forces
r	-	radius of gyration
R	-	universal gas constant
R_d	-	distance from surface of incidence (in m)
S	-	spacing between bumper and rear wall
S_m	-	solubility
t	-	thickness
t_b	-	bumper thickness
t_i	-	thickness of layer i
t_{total}	-	total thickness
t_w	-	wall thickness
T	-	temperature [K]
T_i, T_j	-	surface temperature
V	-	Volume [m^3]
V_p	-	Particle velocity
w	-	plate deflection function
$W(Q)$	-	Probability density
x	-	depth within the material
x_m	-	x location of material
$\bar{x}$	-	x location of center of gravity
y_m	-	y location of material

$\bar{y}$	-	y location of center of gravity
z	-	atomic number of particle
Z	-	atomic number of material
α	-	ultraviolet absorbtivity
β	-	particle speed as a fraction of light speed
ε	-	infrared emissivity
Δp	-	pressure difference
ΔT	-	temperature difference
θ	-	Angle between velocity vector and shield normal
θ_n	-	angle between neutron velocity vector and proton angle of incidence
μ	-	Probability of electronic collision per unit distance of travel
μ_{lin}	-	linear attenuation coefficient
ν	-	Poisson's ratio
Φ_m	-	particle flux
Φ_n	-	number of neutrons per area per incident proton
ρ_b	-	bumper material density
ρ_p	-	particle density
ρ_s	-	shield material density
ρ_w	-	density of wall material
σ	-	Stefan-Boltzmann constant
σ_w	-	yield stress of rear wall material
σ_y	-	yield stress of rear wall material
τ	-	kinetic energy as a multiple of electron rest energy

1. Introduction

Since the beginning of the early 90's, mankind has had a nearly continuous presence in space with the MIR space station and currently the International Space Station (ISS). With the ISS operating at least until 2020, and taking into account the recent achievements of the Chinese in developing their own space station, it is all but assured that humans will inhabit Low Earth Orbit in the coming decades as well. The various spacefaring nations and mankind in general are not satisfied with remaining on or near Earth forever, though. The vision for future manned space missions is to move beyond Earth's orbit and establish a base on the Moon or on Mars.

As humans move further away from Earth, it will be crucial to supply the basic essentials, such as safe living and working environments, breathable atmosphere, water and other liquids and of course food. To reduce the costs and logistical efforts of supplying a Moon or Mars base with food, oxygen and water, it will be necessary to have an in-situ life support system (LSS), containing, among other systems, a greenhouse for food crop cultivation. A greenhouse module, such as shown in Figure 1 (left), would be capable of (partly) fulfilling many of the functions named in Figure 1 (right), such as waste water recycling, and consequently reduce the amount of supplies which would need to be shipped to a Moon or Mars base.
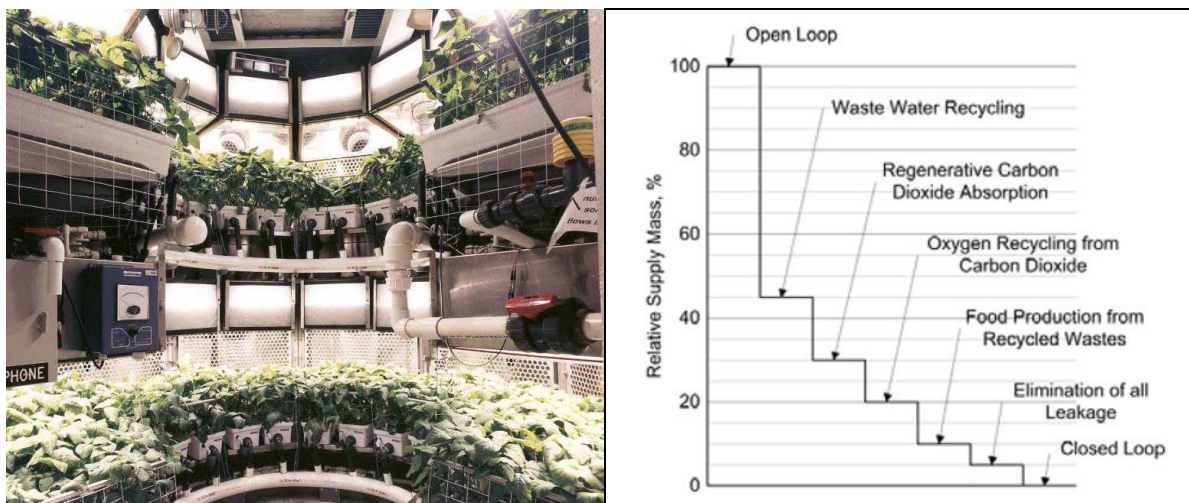
Figure 1: (Left) NASA's Biomass Production Center (BPC) [source: 1]. (Right) Savings in relative supply mass of closed loop versus open loop systems [source: 2].

The harsh environments on the Moon and Mars impose certain requirements on the design of a greenhouse. Particularly, the structure of the greenhouse will need to be capable of withstanding impacts from micro-meteoroids and shield the interior from radiation, among other tasks.

One of the many organizations which are conducting research into the design of greenhouses for the Moon and Mars is the German Aerospace Center (DLR). In line with the efforts of DLR, this work will detail the design of the structure for a Lunar Greenhouse Module. The structure will be deployable, to allow the stowed structure to fit inside an existing launcher, while still providing the required amount of plant cultivation area in the deployed configuration.

The main research question which was formulated for this thesis work was:

What is the optimal design for a (fully-equipped, deployable) Greenhouse module on the Moon?

To facilitate answering this main question, several secondary research questions are formulated. Answering these secondary research questions should make it possible to answer the main question.

- What are the requirements for a Lunar Greenhouse Module? (Specifically with regards to the structure)

Chapters 2, 3 and 4 will be focused on answering this question. First, in Chapter 2, an overview of the research into deployable space structures is presented. Past missions, the current state of the art and other aspects, such as modelling methods and potential materials, are discussed. Then, in Chapter 3, the conditions on the surface of the Moon are analysed, with a focus on their design impact. In Chapter 4, the system analysis of the Lunar Greenhouse Module is covered. Requirements are defined, a subsystem breakdown and corresponding interface definitions are discussed and some necessary assumptions are listed.

- What possible structural designs/configurations would meet the requirements placed on a Lunar Greenhouse Module and which design would be most optimal?

With the assumptions and requirements set up, Chapter 5 presents the different concepts for the Greenhouse Module (GHM) and details the trade-off process and concept selection. Chapter 6 details the (preliminary) design of the structure. Chapter 7 covers the modelling and analysis which is carried out to verify that the structural design meets the requirements. Finally, Chapter 8 presents the conclusions of the work and Chapter 9 discusses (some of) the issues which should be addressed in future design work.

2. Deployable Space Structures Research

In this chapter a non-comprehensive overview of deployable space structures research is presented, detailing (among other things) past missions, current state of the art technologies and modelling methods. First, however, it is necessary to clarify some of the terminology which will be used in this report.

The term deployable will be used for any and all structures which are not launched in their final configuration. Deployable structures can be divided into the three subsets:

- Rigid deployable structures

Rigid deployable structures are defined as deployable structures which require no rigidization to maintain their deployed shape. An example of a rigid deployable structure would be a satellite with (rigid) deployable solar panels.

- Inflatable structures

Inflatable structures are defined to be structures consisting solely of materials which require rigidization or pressurization to maintain the desired shape after deployment, such as the Inflatable Antenna Experiment flown by NASA, which will be discussed later in section 2.1.

- Hybrid structures

Hybrid structures are structures which combine rigid structural elements and inflatable structural elements.

The research discussed in this chapter is limited to inflatable and hybrid structures and the lightweight materials used in the design of such structures. This is done because rigid deployable structures, while technically deployable structures, do not offer the same benefits of low mass and high (deployed) volume which can be achieved using hybrid or inflatable structures. As such, rigid deployable structures are not considered for the current work.

2.1.   Past, present and future missions

Inflatable structures have been considered for use in space missions since the early days of the space era. Werner von Braun already proposed, in 1952, the concept of a wheel-shaped inflatable space station with a diameter of 50 m [3]. Unfortunately, many of the designs never made it past the prototype phase.

One of the inflatable structures which did get launched into space was the ECHO I, seen in Figure 2. The ECHO I was a balloon satellite which was launched in 1960 and inflated from inside a 67,3 cm sphere to a final diameter of 30,48 m. The inflation gas was provided by using sublimating powders [4,5]. The ECHO I acted as a passive satellite, reflecting radio signals as it orbited the Earth at an altitude of about 1600 km. The balloon was coated with a thin layer of aluminium, which work-hardened upon inflation of the balloon, thus rigidizing the structure [6]. The ECHO balloons were invaluable in developing and testing packaging and deployment techniques, which formed the basis for further research.

Figure 2: ECHO I balloon satellite [Source: 6]

Aside from the simple balloon designs of the ECHO balloon satellite series, more complex structures were also being developed using inflatable structures. At that time, Goodyear Aerospace Corporation developed a number of inflatable structures, which are briefly discussed below.

The inflatable search radar antenna, seen in Figure 3 (left), demonstrated the use of a rigidizable truss structure and a metallic mesh was used for the surface of the antenna. The antenna had a length of 10 m, a width of 3m and obtained a parabolic surface profile.

The radar calibration sphere concept used flat hexagonal membrane panels, which were bonded together [4]. Upon inflation, the structure would have a spherical shape, as can be seen from the 6m diameter demonstrator in Figure 3 (center). In principle, it would be possible to obtain any desired size by increasing the number of panels, or the size of the panels.
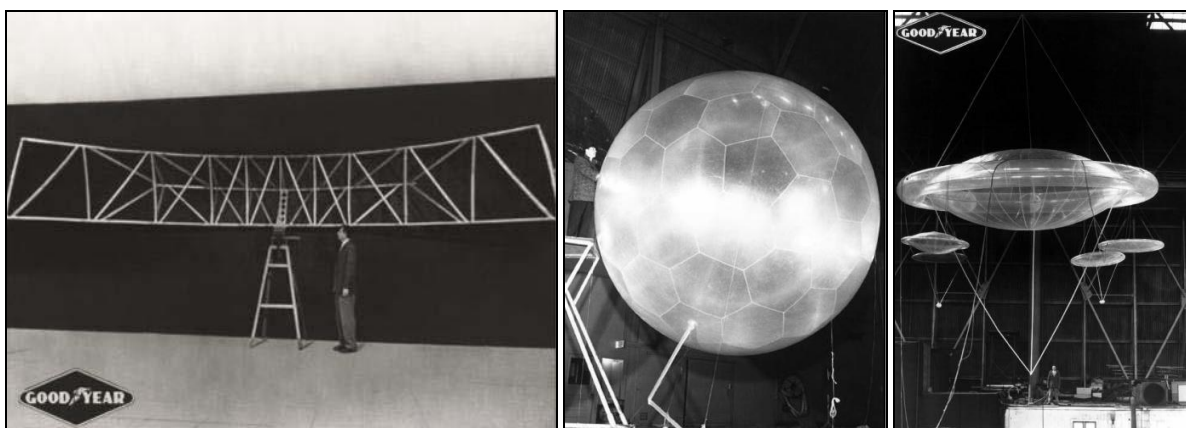
Figure 3: (Left) Inflatable search radar antenna. (Center) Radar calibration sphere. (Right) Lenticular inflatable parabolic reflector [Source: 6]

A different concept developed by Goodyear was the "lenticular inflatable parabolic reflector", consisting of a lenticular reflector, surrounded by a toroidal ring, as can be seen in Figure 3 (right). This concept used the bonding of 'pie-shaped' membrane gores to form a parabolic surface, as well as the bonding of curved segments to produce the toroidal ring. The structure shown in Figure 3 (right) had a total diameter of 12 m, and the reflector diameter was 10 m. A number of rigidization techniques were investigated for this type of inflatable structure, such as foams.

Goodyear also collaborated with NASA to build a prototype inflatable space station in 1961. The station, seen in Figure 4 (left), had a diameter of 7,3 m and was expected to house one or two astronauts. The structure was constructed out of Dacron filaments with a Butyl rubber binder and a Butyl-impregnated nylon internal bladder for gas retention. The structure could be packaged in a hub with a diameter of about 2,4 m and was designed for 5 psi pressure. [7]

Two other habitat designs by Goodyear were a lunar shelter, capable of holding two astronauts for a period of eight to thirty days, and the "Moby Dick" space habitat. The lunar shelter design consisted of a 3-layer laminate with a nylon outer cover over closed-cell vinyl foam and an inner nylon cloth, bonded by polyester adhesive layers. The total length of the structure was around 4,5 m and the diameter was about 2,1 m. The "Moby Dick" was developed as a prototype space habitat. Measuring about 3,9 m in diameter and 11,4 m in length, the structure was designed around a thick gas bladder made from Dacron. This bladder was dipped in a polyester resin bath and sealed by polyvinyl chloride (PVC) foam, after which the structure was covered with flexible polyurethane foam and a nylon film-fabric laminate painted with a thermal coating. [7]

The development of these prototype structures helped develop the knowledge base on inflation, repackaging and gas retention, as well as structural characteristics of inflatable structures.
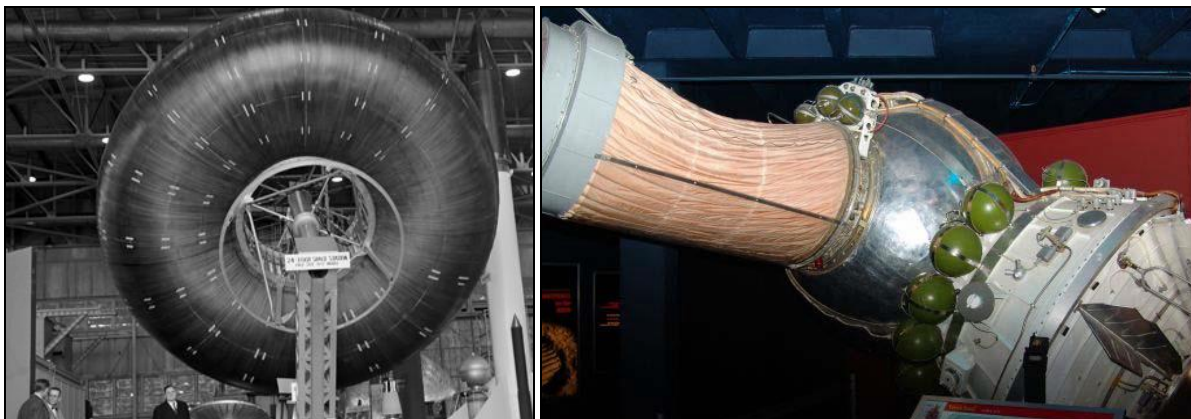
Figure 4: (left) Goodyear 24 foot space station [Source: 8]. (right) Voshkod 2 Inflatable airlock [Source: 9]

Inflatable structures were also being developed by other companies, such as L'Garde Inc. In the late 60's and the 70's this company designed and tested Inflatable Exo-Atmospheric Objects (IEOs) for the US Air Force. These IEOs acted as decoy and target systems and were used to gather flight telemetry data as well as radar and infrared signatures for re-entry vehicles. The structures consisted of a carbon fabric outer skin, with a 'water blanket' directly underneath for temperature control. About one to two meters in length, these structures were capable of inflating within several milliseconds [10].

In 1974, the Applications Technology Satellite 6 (ATS-6) was launched. This satellite carried a deployable antenna reflector designed by Lockheed. Over 9 m in diameter, the antenna was constructed out of aluminium ribs with a metallized Dacron mesh [11].

Outside of the United States, research into inflatable space structures was also being done. One of the more notable achievements is the inflatable airlock, Figure 4 (right), which was flown on the Voshkod 2 and allowed the first ever extravehicular activity (EVA) in 1965 [9,12]. Similar inflatable airlock designs were developed by Lockheed and Goodyear and were later flown by the Americans

[13,14]. The space suits used during an EVA can also be qualified as inflatable structures and these were, of course, also developed during this time period.

In Europe, research into inflatable structures was initiated in the late 1970's. The European Space Agency sponsored the Contraves Space Division and their development of reflector antennas and sun shade structures, seen in Figure 5 [4,6].

One of the results of this effort was the 6 m diameter scale model of a Very Large Baseline Interferometry (VLBI) antenna which was built in the early 80's. This antenna structure was used to test rigidization techniques and materials as well as inflation systems and investigated the achievable surface accuracy of the inflated structure. The pre-rigidization surface precision for the VLBI was found to be on the order of 1 mm rms.

Following this VLBI antenna, a land mobile communications reflector antenna of 10 x 12 m was built. This antenna achieved a surface precision of 2 mm root mean square (rms) and tested rigidization of the structure through solar heating. The third significant result of the Contraves research was a scale model sun shade support structure which was intended for a submillimeter space telescope. The sun shade structure was based on a truss structure and yielded further knowledge on materials and inflation and rigidization techniques [10].

Figure 5: (Top left) VLBI antenna. (Top right) Inflatable sun shade structure. (Bottom) Inflatable communications reflector antenna [Source: 6]

In the late 80's the US Air Force and L'Garde Inc. did similar research into large inflatable reflector structures. Consisting of 18 panels of six-micron thick aluminized Mylar, the Large Offset Reflector Structure had dimensions of 7 x 9 m and achieved a surface precision on the order of a few mm rms [10]. The structure was a technology demonstrator which led the way to the Inflatable Antenna Experiment (IAE) which was flown on the Space Shuttle Endeavour in 1996.

The IAE was a joined project between NASA, the Jet Propulsion Laboratory (JPL) and L'Garde Inc. The structure consisted of a 14 m diameter inflatable reflector and three inflatable struts of 28 m. The deployment of the IAE did not go as intended, due to some residual air inside the stowed volume, but nonetheless the desired deployed shape was successfully obtained [15]. The deployment and final shape of the antenna can be seen in Figure 6.
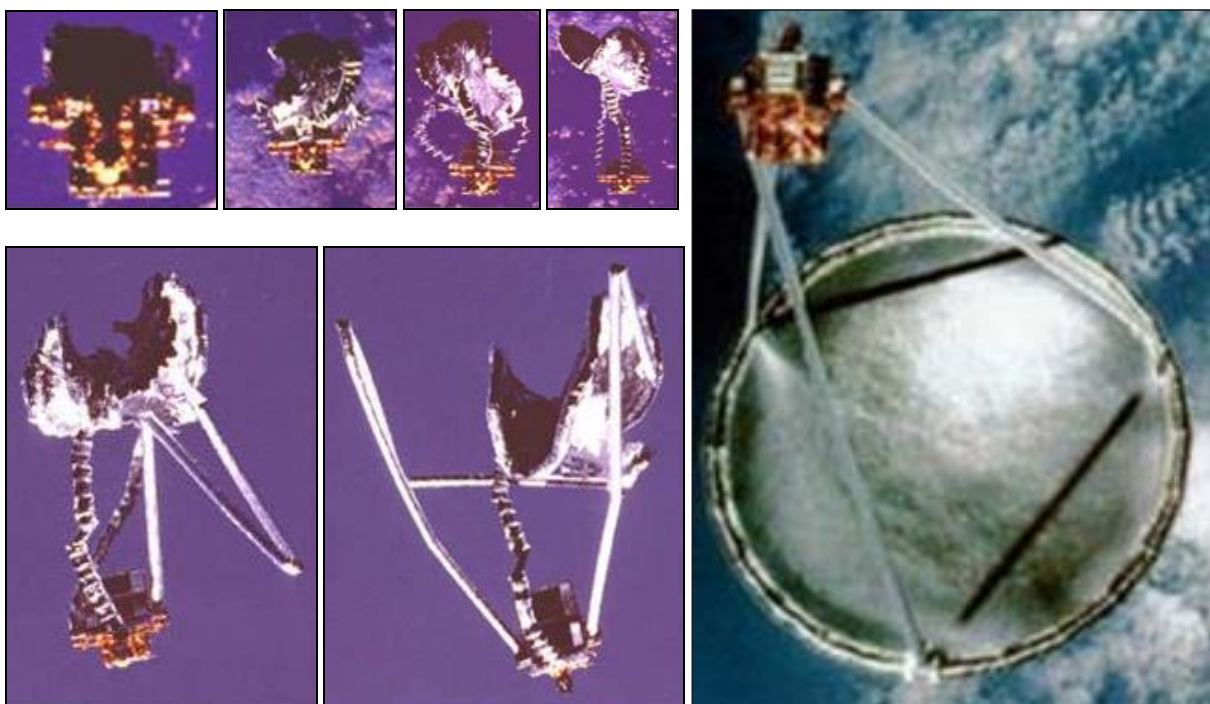
Figure 6: Deployment of the IAE (left) and fully deployed IAE (right) [Source: 6]

Around the same time, ILC Dover, together with the US Air Force and JPL, was developing and, later on, testing a Large Solar Array Structure. Three carbon fibre and thermoplastic, inflatable, beams were used to support the solar cell substrate of the 3 x 10 m solar array. A demonstrator was built and tested and the array structure was intended for flight on the Space Shuttle Columbia and use on the Deep Space 4 Champollion mission, but budget constraints resulted in cancellation of the program in 1999 [16,17].

Another inflatable structures program which was cancelled as a result of budgetary issues was the Transit Habitat (TransHab). The TransHab was considered as habitat module for the International Space Station, where the design and technologies could be proven before being applied in human missions to Mars. The TransHab was a hybrid structure, with a rigid central core and an inflatable outer shell. The inflatable shell consists of five sections, specifically the inner liner, the bladders, the restraint layer, a debris protection system and an outer layer for thermal control and atomic oxygen (AO) protection. In total, the shell is composed of over 60 layers and is about 40,6 cm thick [18,19].
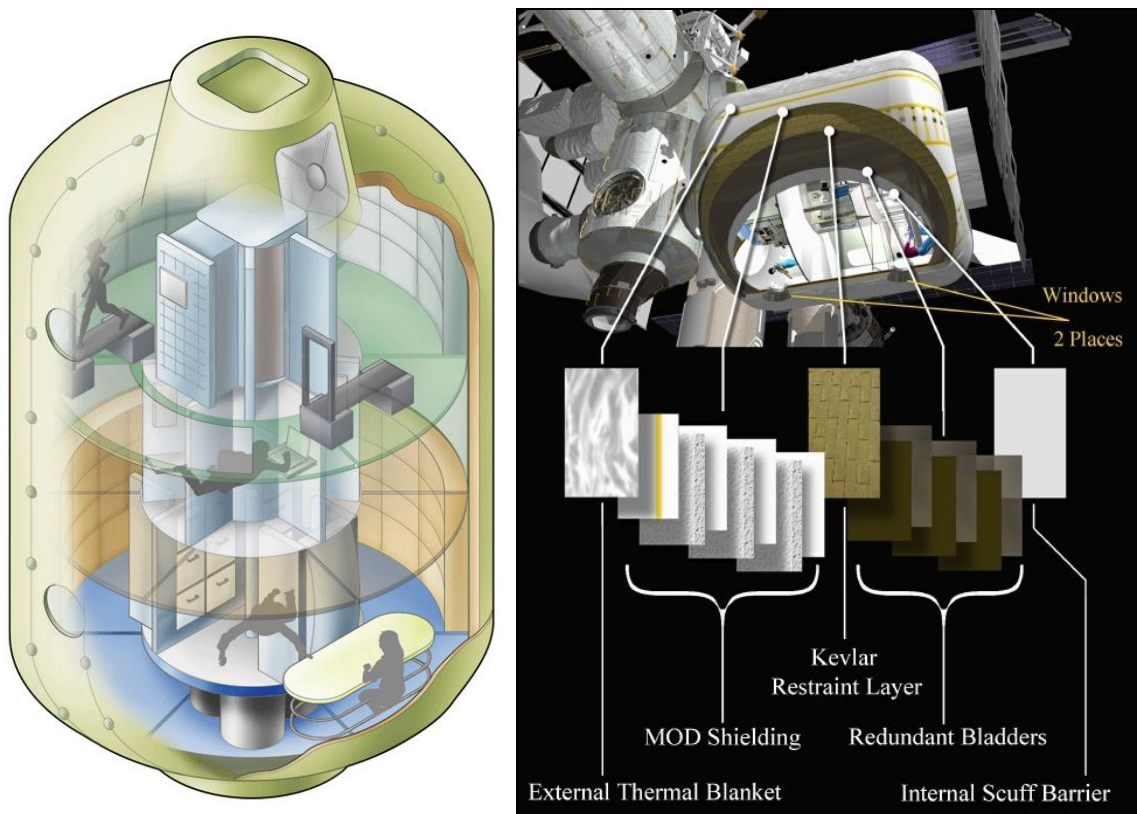
Figure 7: (left) TransHab internal layout schematic [Source: 20]. (right) TransHab shell layers [Source: 21]

The inner liner of the TransHab shell consists of Kevlar and Nomex fabrics, providing a barrier that is durable, easy to clean, flame and puncture resistant and with good acoustic properties. A triple redundant bladder system is used, with the bladders made from Combitherm material, which is a laminate consisting of polyethylene, nylon and vinyl alcohol (EVOH) layers. The bladders are oversized with respect to the restraint layer to maintain a zero stress at the interface between the bladders and the central core. The bladders are surrounded by Kevlar to provide additional puncture resistance. The restraint layer is also constructed out of Kevlar and is designed to hold a pressure of 4 atm. Covering the restraint layer is the debris protection system which is designed to protect against impacts from micro-meteoroids and orbital debris (MMOD). The MMOD shield consists of Nextel ceramic fabric layers, separated by polyurethane foam, with a high strength Kevlar layer at the rear of the shield. Finally, the outer most layers of the TransHab shell are multi-layer insulation (MLI) blankets for thermal control and an aluminized Betaglass fabric for atomic oxygen (AO) protection. The MLI blankets are oversized with respect to the MMOD shield to prevent them from carrying load [18,19].

While the TransHab program was cancelled due to delays and budget constraints, the technology has been used and improved upon by Bigelow Aerospace, leading to the launch of the Genesis I, see Figure 8, and Genesis II in 2006 and 2007, respectively. Several additional inflatable habitats are being developed or have been proposed, and should launch in the coming years [22].

Aside from habitats, the past two decades have seen an increased focus on the development of solar sailing technology and (re-)entry heat shields. In 1993, the Znamya 2 was deployed from the Russian MIR space station, and in 2004, the Japanese Institute of Space and Astronautical Science (ISAS) deployed two prototype solar sails [23]. In 2010, the Japanese IKAROS mission became the first mission to use a solar sail as the main propulsion system [24,25,26,27]. Additional solar sail missions

are being planned by NASA, DLR and ESA, among others [28, 29]. Furthermore, the Deploytech ESA project is aiming to develop three inflatable structure designs [30,31].

Figure 8: (Left) Interior of Genesis I – 'Fly Your Stuff' program (Right). Genesis I in space [Source: 32, 33]

2.1.1. Habitat concepts

A number of habitat designs have been mentioned previously, but many more concepts have been developed. Structures can be created in basically any shape imaginable. The differences in load carrying capabilities, mass and available volume (among other aspects) mean, however, that certain designs are more feasible, from a technical and economic view, than others. The concepts can be subdivided into four categories:

- the (hemi-)sphere
- the cylinder
- the toroid
- atypical shapes (e.g. box-shaped)

Some examples of each of these groups are given below and additional habitat concept illustrations are presented in Appendix A:

(Hemi-)Spheres

Roberts [34] discusses the design issues of inflatable habitats and presents a spherical lunar habitat design. The concept is of a 16 m diameter inflated sphere, with an internal structural cage for support of floors, walls and equipment, see Figure 9. The structural cage would also provide support in case of pressure loss, ensuring that the sphere would not collapse under the weight of the 3 m regolith shielding. Curved radial and concentric beams would run along the inside of the sphere and an open shaft with a 2 m diameter would run from top to bottom in the center of the sphere to allow movement between the different floors.
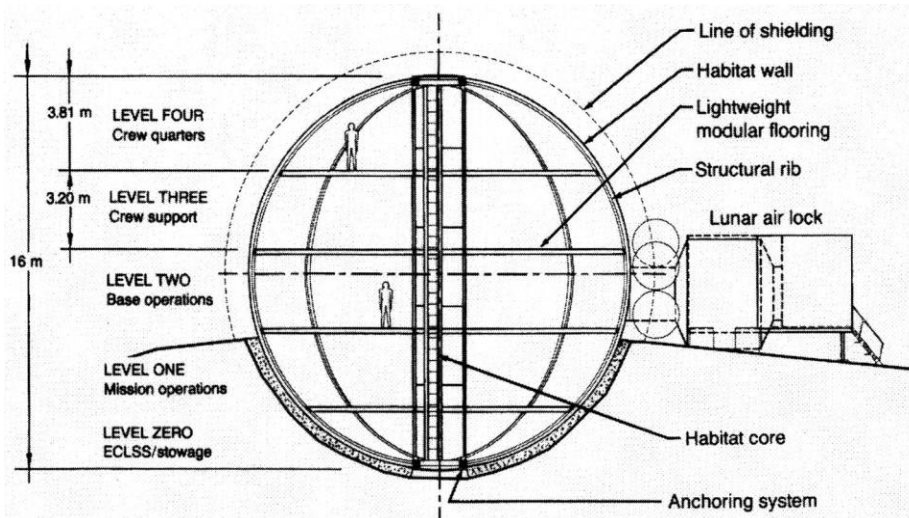
Figure 9: Cross-section of a spherical lunar habitat [Source: 34]

Bucklin et al. have developed a prototype dome structure which serves as a test bed for low pressure (25 kPa) plant cultivation experiments, as seen in Figure 10. A scaled and adapted version of the design could be used as a greenhouse module for the Moon or Mars. The prototype dome has a diameter of 1 m and is made of clear Lexan (polycarbonate thermoplastic) with a stainless steel dome [35].
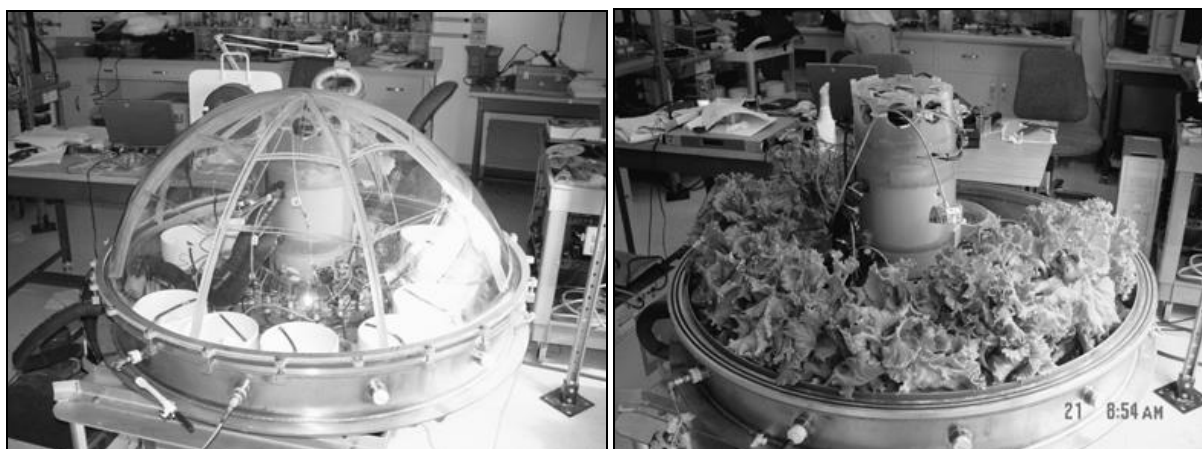
Figure 10: (Left) Mars Greenhouse Dome. (Right) Harvest-ready plants in the Mars Greenhouse Dome [Source: 35]

Fisher [36] compares the advantages and disadvantages of spheres (and domes) compared with toroidal shaped structures to determine the best candidate for a Mars habitat. Several spherical habitats are presented by the author and a number of sphere, dome and torus concepts from other studies are discussed. He concludes that the stability of the torus, the better mass to floor area ratio and reduced construction time and amount of regolith needed for shielding make the toroidal shaped structure a better option than a sphere or dome.

Kozicki and Kozicka [37] have developed several concepts for a Martian Base (see Figure 11) and selected a design with dome-shaped habitats as the best option. Internal layout and initial material selection for the structure are presented, along with a deployment strategy.
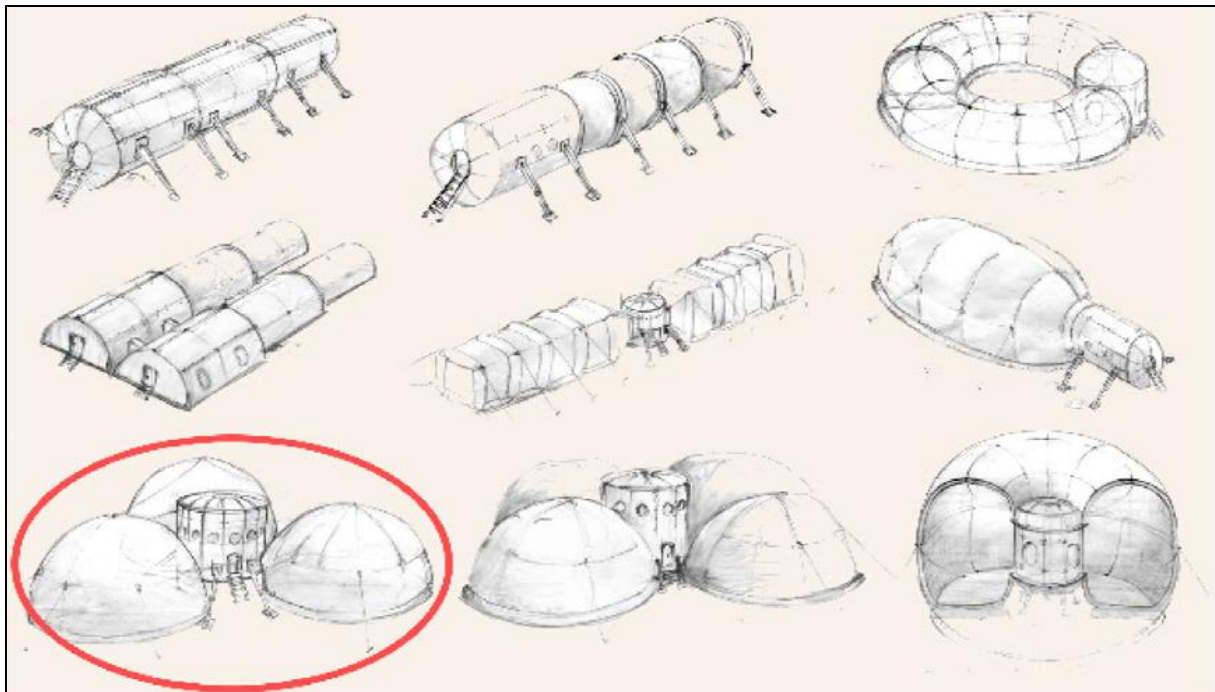
Figure 11: Martian base concepts. In the lower left corner (inside the red ring) is the selected concept [Source: 37]

(Semi-)Cylinders

The University of Arizona is at the forefront of lunar greenhouse development. Building on experience with crop cultivation at a research station on the South Pole, the Controlled Environment Agriculture Center has developed a cylindrical greenhouse demonstrator, see Figure 12 (left). The greenhouse has rigid sections at both ends and extends length-wise during inflation. Plants are placed in flexible, opaque root zone tubes and supported by cables [38].

Figure 12: (Left) Lunar Greenhouse Demonstrator [Source: 38]. (Right) Engineering Development Unit [Source: 39]

The Engineering Development Unit (EDU), see Figure 12 (right), being developed by ILC Dover is another cylindrical structure envisioned to have rigid end caps with a flexible, extendable center section. The habitat has a diameter of 3 m, a deployed length of about 10 m and a stowed length of roughly 5,2 m. The flexible part of the structure consists of a lightweight Vectran fabric with webbing net for additional support and a urethane coating. The EDU is a test bed to demonstrate

the packaging and deployment of the structure, the performance under expected loading conditions and furthermore, it provides a platform for testing of other ideas [39].

Some previous work performed at DLR Bremen by Glasgow [40] analysed different configurations for planetary greenhouses, including a fully rigid cylinder and an inflatable cylinder with rigid ends and a rigid frame, as seen in Figure 13.
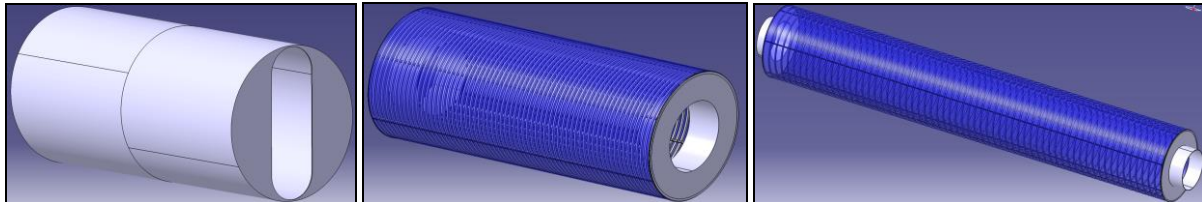
Figure 13: (Left) Fully rigid cylinder. (Middle) Stowed inflatable cylinder with rigid end caps. (Right) Deployed inflatable cylinder with rigid end caps. [Source: 40]

The rigid cylinder had a diameter of 4,48 m and a length of 10 m, which is equal to the size of the stowed inflatable cylinder, which reaches a length of 30 m upon deployment. Only a qualitative trade-off was performed, so no in-depth design was carried out regarding the radiation protection, debris shielding and other structural issues.

Cylindrical habitats were also designed and tested by Goodyear Aerospace Corporation, as mentioned previously in Chapter 2, and ILC Dover. The concept by ILC Dover envisioned a stowed cylindrical habitat on top of a landing craft and upon reaching the surface the structure would deploy, expanding from 2,3 m to 3,7 m in length [41].

Finetto et al. [42] consider rigid and hybrid cylindrical structure concepts for the Lunar Food and Revitalization Module (FARM) which would be part of a Permanent Human mOon Exploration BasE (PHOEBE). The rigid cylinder has a diameter of 8 m, a length of 12 m and at the end caps there are 1 m spherical caps, similar to the (deployed) hybrid design, but suffers from higher mass. The reduced complexity, as well as the fact that it does not require any internal outfitting on the Moon, leads the authors to select the rigid design as the better option.

Hublitz et al. [43] discuss the design of a semi-cylindrical inflatable structure for use as a low- (30 kPa) or high-pressure (59,2 kPa) greenhouse module. Furthermore, the authors examine the impact of using natural, hybrid or artificial lighting on the Equivalent System Mass (ESM) of the design. It was found that the low pressure greenhouse has a lower ESM than the high-pressure design and that hybrid lighting allow for the lowest ESM design, followed by artificial and then natural lighting.

Toroids

Sinn and Doule [44] discuss a torus like structure with a diameter of 26 m and a height of 7.2 m, deploying from a blunt body capsule. The inflatable structure consists of a bladder composite of several layers of polyamide, polyethylene, ethylene vinyl alcohol (EVOH) and adhesive, along with a layer of Kevlar 49. Radiation protection is envisioned to be provided by inflatable water tanks, while trapped air layers near the ground will be used as part of the thermal control system. Figure 14 shows a section view of the proposed capsule and inflatable torus like structure.
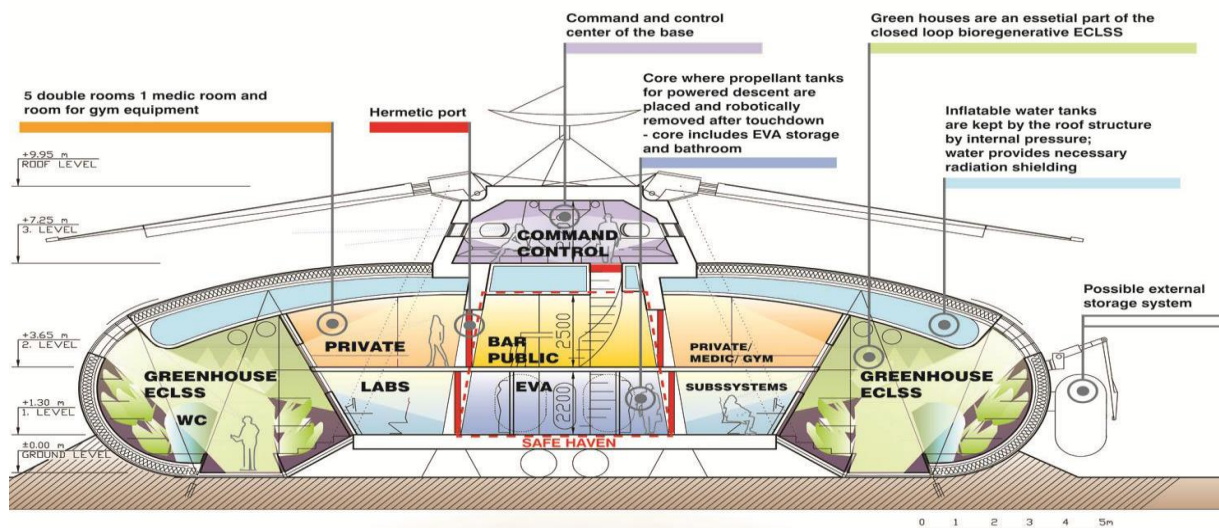
Figure 14: Section view, with functional layout, of the MD10 concept [Source: 44]

A different habitat concept incorporating a torus structure was developed at the Department of Architecture of the University of Wisconsin-Milwaukee. A team of students, with some supervisors, researched different lunar habitat concepts and did further development work on two of the designs, the Domus I and the Dymaxion concept [45]. Figure 15 shows an overall view of the Domus I structure with airlocks (left) , as well as a section view of the interior (right).
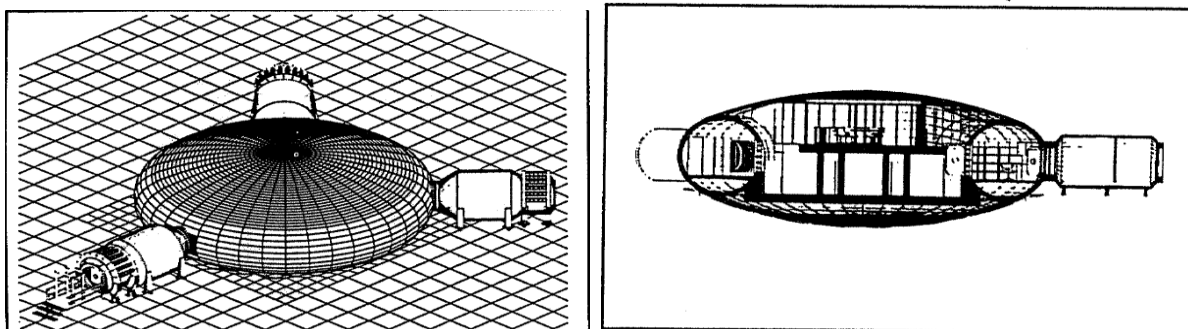
Figure 15: (Left) Overall view of the Domus I concept without regolith shielding. (Right) Section view of the Domus I [Source: 45]

The Domus I concept consists of a rigidizable, inflatable torus within an inflatable ellipsoid. The team uses this design to achieve separation of the work areas (situated in the torus) and the relaxation areas. An option to divide the core area of the structure into two floors would allow separation of private and public crew areas. Structural stiffness is envisioned to come from rigidizing foam injected within two thin layers of the structure membrane walls.

The concept of using toroidal structures within a secondary envelope was also suggested by ILC Dover for the Livermore Habitat Module. The toroidal habitats allowed for compartmentalization of the different work and crew areas, while the secondary structure encompassing the habitats provided redundancy and additional structural support [41].

Several different greenhouse structural concepts are proposed in [46], including a toroidal design similar to the Domus I. The 'TorDome'design has a high pressure torus incorporating the airlock and habitat interface(s), utility interfaces, viewports and workstations, while a dome section encapsulates the torus and allows for a low pressure inner section for plant cultivation.

Miscellaneous

A 'tuft pillow' inflatable structure concept is mentioned in [47]. A single module would be 6,1 x 6,1 x 2,44 m in size and would consist of (slightly) curved walls covering an inflatable frame system of columns and arches. The inflatable frame system needs to be designed to support the structure and any regolith shielding, while the module is unpressurized. A preliminary design of the structure used Kevlar 49 as structural material and used an internal pressure of 69 kPa. It is envisioned that a large number of 'tuft pillow' modules would be combined to form a lunar base, see Figure 16. The use of airlocks between different modules could be used to increase reliability of such a base.
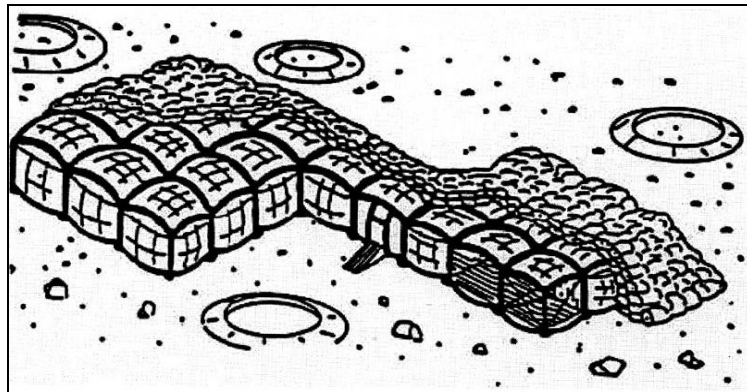
Figure 16: Lunar base layout with 'tuft pillow' inflatable structures [Source: 47]

As mentioned previously, some work has already been carried out at DLR in analysing different greenhouse module configurations. Aside from the cylindrical shapes shown earlier, different concepts were designed based on an octagonal stowed structure with a combination of rigid and flexible parts. Upon deployment, the greenhouse structure could be either a single or a double floored module. The stowed configuration had a length of 10 m and the sides of the octagon were 1,72 m, and in the deployed configuration the floor area was 12,05 by 10 m with a height of 2,55 m or 5,58 m (one or two story building respectively). Figure 17 shows the stowed and deployed configurations of the one sotry design.
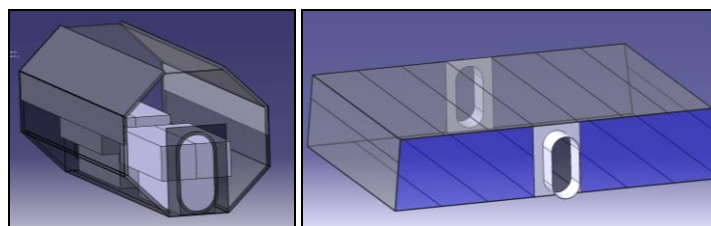
Figure 17: Semi-rigid, octagonal based module with rigid floor, roof and side walls.
(Left) Stowed structures. (Right) Deployed structures [Source: 40]

A team from the Technical University of Vienna developed the Intellihab concept as part of a Lunar Base Design Workshop. The habitat has a maximum width of 12,7 and has a total height between 9,4 and 10,3 m and is shaped more or less like an onion. Accounting for rough terrain at the landing site, the Intellihab uses inflatable supports to level the structure. The habitat is envisioned to deploy itself and to use a robotic 'harvester' to obtain and place regolith shielding on the structure. Some manual labour is needed to attach the outer layers of the structure after deployment and regolith shielding and also for configuration of the interior [48].

The Sasakawa International Center for Space Architecture (SICSA) has developed a number of different concepts for Moon, Mars and space habitats, including the MarsLab concept. This design envisions a lander which, upon reaching the surface, allows deployment of an inflatable habitat from the top of the vehicle. The design incorporates a pop-out tension cable matrix to which astronauts can attach the different systems and components.

The structures discussed here are not a complete representation of all the work done on inflatable structures since the beginning of the space era. It is sufficient to give an indication of the versatility of inflatables however and serves as a good starting point for the review of the state of the art of the various research areas related to inflatable structures.

2.2. State of the Art

As discussed, there have been many technology demonstrators and space missions which have used inflatable structures. As a result, there is a significant knowledge base with regards to packaging and deployment methods as well as different rigidization options. Furthermore, the increase of computing capabilities has led to the development of modelling techniques to analyse the expected behaviour of inflatable structures. Last, but not least, there have been significant advances in material sciences, leading to a wide selection of space-proven materials which can be used for future inflatable structures.

In this section an overview will be presented of current capabilities related to the following research topics:

- Packaging
- Deployment
- Rigidization
- Materials and layers
- Integrated electronics
- Modelling

2.2.1. Packaging

Packaging of inflatable structures is done by a series of (manual or automated) rolling and folding operations. The optimal packaging method for a given structure can be indicated by the packaging efficiency, which is a measure of the efficiency of stowage volume usage. Obviously, packaging methods which require a larger stowage volume are not as attractive.

Aside from the volume of the packaged structure, it is also important to consider the deployment method which will be used. Packaging must be done, such that the structure does not encounter (unwanted) obstructions during deployment. Additionally, stresses and strains resulting from packaging and deployment need to be considered as well as venting to prevent residual air from influencing the deployment process, as was the case for the IAE [10].

Some guidelines were formulated to help develop packaging methods, reflecting the different issues (discussed above) which should be considered for packaging [10]:

- Symmetry of the structure should be maintained in the packaged shape (for packaging efficiency)

-   'Accordion' folds should be used when fast inflation is desired, while rolling should be used for slow deployment.
-   Spherical surfaces should be folded along lines of longitude as much as possible, to prevent wrinkling.
-   Orthogonal folds should be avoided on account of the high stresses which result from such folds.

2.2.2. Deployment

Salama et al. make a rough classification of deployment methods into two classes:

-   'unrestricted free deployment'

In free deployment, the structure, or segments thereof, can move freely in space after being released from the stowage compartment, even if the structure is not yet (fully) inflated.

-   'passively controlled deployment'.

In controlled deployment only the fully inflated segments of the structure are allowed to move in space [10,49].

The Inflatable Antenna Experiment (IAE) is an example of a free deployment. To prevent unstable deployment, the design for the IAE deployment mechanisms incorporated a kick plate. This kick plate was supposed to provide sufficient momentum to the booms to obtain stable deployment in the desired zone. Due to residual air and stress in the packaging folds, the structure moved away from the kick plate slightly, resulting in an actual momentum transfer from the kick plate to the antenna which differed from the expected momentum transfer [10,15,49].

Controlled deployment offers the advantage of increased deployment stability and control with respect to free deployment, but it requires additional components, resulting in added mass, cost and complexity. Different systems have been designed to control deployment of inflatable structures by either controlling the flow of gas during inflation or by using additional forces to counteract the inflation pressure [49].

Gas flow within the deployable structure can be controlled through compartmentalization, where diaphragms separate the different segments of the structure. These diaphragms prevent the gas from flowing to the next segment until a certain pressure is reached, at which point the diaphragm bursts, or check valves are opened, and the next segment will be inflated [49].

Counteracting forces acting against the inflation pressure can be induced through a number of different mechanisms. The so-called roll-out method uses embedded springs or glued on Velcro® strips to provide deployment resistance (Figure 18 (left)). The mandrel method generates friction to counteract inflation pressure by forcing the deployable structure to be pulled over the mandrel during inflation (Figure 18 (right)). Another example of a controlled deployment mechanism is the use of bending strength inherent in the structure to provide deployment resistance as is done in the fan folded method [4].
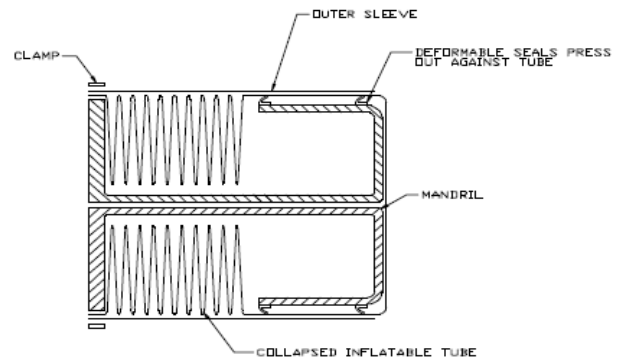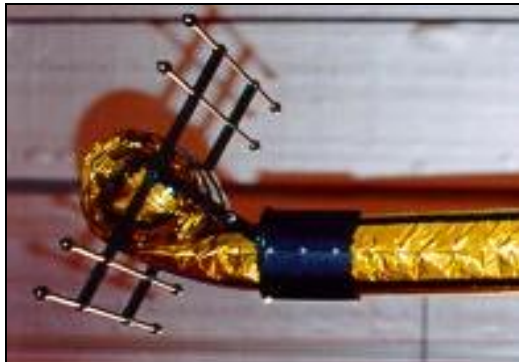
Figure 18: (Left) Velcro® roll up device with membrane tensioning frame. (Right) Columnation device using mandrel method [Source: 50]

2.2.3. Rigidization

The rigidization methods for inflatable structures are directly related to the materials which are used in the design of the structure. Cadogan and Scarborough define rigidizable materials as "*materials that are initially flexible … and become rigid when exposed to an external influence"* [51].

Cadogan and Scarborough classify rigidizable materials into the following three categories, based on the base material properties.

- Thermosetting composite materials
- Thermoplastic (and lightly cross-linked thermoset) composite materials
- Aluminium/polymer laminates

Composite materials consist of a matrix resin and, typically, use fibres and foams to alter specific material properties. The rigidization process involves the hardening ('cross-linking') of the resin. Thermoset composites have a fixed shape, upon rigidization, whereas thermoplastic and lightly cross-linked thermoset composites can be altered through re-heating of the material. A distinction between thermoplastic and lightly cross-linked thermoset materials is that the former can also be set into a new permanent shape, with heating above their forming temperature.

Aluminium/polymer laminates either consist of two layers of aluminium to one polymer film, or vice versa, depending on the specific requirements. Aluminium 1100-0 or 3003-0 is commonly used, in its softest conditions. Polymer films are used as pressure barriers and to provide more resistance to tear. The total aluminium thickness is limited to 0.1 mm to prevent laminate degradation from folding.

Depending on the type of material, different rigidization techniques are possible. For composite materials, these options are [51]:

- Thermal rigidization

Thermal rigidization in composite materials is the process of inducing 'cross-linking' through heating or cooling the material. Rigidization can be initiated passively by heating or UV radiation from the Sun. Aside from using such passive methods, research has been focused on using resistive heating elements and UV lamps to control the curing process. Rigidization through cooling is only possible in so called sub-Tg materials. Sub-Tg materials are materials which have

a glass temperature (Tg) below room temperature and as such, these materials are flexible on Earth. The glass temperature marks the point at which a (amorphous) material transitions from a hard state to a rubber-like state [52]. Upon deployment in space, the material cools and, when the temperature lowers beneath the glass temperature, the material hardens.

- Chemical rigidization

Chemical rigidization selects materials to enable a chemical reaction between the composite resin and a catalyst, such as the inflation gas, to achieve resin curing. The catalyst could be used for initiation of the curing or as support, to accelerate the curing process. The selection of resin/catalyst combination should prevent premature rigidization on Earth, as well as contamination of the spacecraft after outgassing of the unreacted gas.

- 'Solvent boil-off' rigidization

Plasticizer or solvent boil-off rigidization utilizes the outgassing of softening components of composites to achieve a rigid structure upon deployment in space. This method suffers from high mass loss and associated shrinkage of the structure, which can result in reduced shape accuracy, induced laminate stress and changes in final structural performance due to variations in fibre orientation.

- Foam rigidization

A final rigidization method which has been proposed for non-metallic materials is foam rigidization. It is achieved either through foaming of the material upon reaction with an external influence, or through injection of foams into interior cavities of the inflatable structure. The foaming process can also be used for the inflation of the structure, as is done for the pipe in Figure 19.

Figure 19: Inflating cured-pipe by the foaming method [Source: 53]

For aluminium/polymer laminates there is only one rigidization method:

- Work-hardening

The work-hardening rigidization of aluminium is based on the introductions of dislocations in the crystal structure of the metal during deformation. Upon inflation of the structure, the gas pressure results in deformation (deployment) of the aluminium/polymer material, resulting in the aforementioned dislocations in the aluminium crystal structure. With increasing number of

dislocations, the resistance to further dislocation-formation, and thus also to further deformation, also increases, effectively resulting in higher strength and rigidity.

These rigidization techniques were already being researched in the early years of the space era, but, as of 2001, only the work-hardening of aluminium rigidization mechanism has been demonstrated in space. Recent efforts have focused on applying these rigidization methods to new materials and different structural shapes. Some recent examples of the aforementioned rigidization methods being applied in novel structure designs are given below to indicate that, while no new rigidization methods are being developed, research is ongoing to optimize the processes and reduce the drawbacks of the various methods.

Guidanean and Lichodziejewski describe the use of new sub-Tg materials in the design of an inflatable space truss structure [54]. These novel materials are shown to have good radiation resistance and their glass temperature can be custom tailored to fit the needs of the mission. Lichodziejewski, Veal and Derbes discuss the use of aluminium/polymer laminate rigidization technology in solar arrays and deployable booms [55]. Furthermore, by applying spiral-wound filament around the outside of the booms, the limiting hoop stress on the aluminium laminate can be reduced, allowing for higher inflation pressures and better surface accuracy. Allred, Hoyt and Harrah demonstrate the applicability of passive solar radiation in rigidization of inflatable wings [56]. Tinker, Schnell and Leigh Jr. discuss the foam rigidization of inflatable thin-film booms [57]. It was found that the rapid curing times required for rigidization in space requires multiple injection locations to prevent blockage and uneven foam distribution.

2.2.4. Layers and Materials

It is important to realize that there is, in general, no single material which will be able to fulfill all the requirements on an inflatable structure. Some materials may be best suited for load carrying but are susceptible to puncturing by debris, while other materials can be considered for gas retention but are not useful for load carrying and so on. As a result of these specific material 'specializations', the design of inflatable structures is based on layering different materials for the various functions which the structure needs to perform. Figure 20 shows the material layers used for the inflatable TransHab module.

The different layers seen in Figure 20 are an example of an inflatable structure design. For the lunar GHM the number of layers and their specific functions may vary significantly. In case of regolith shielding of the structure for example, atomic oxygen shielding would not be needed and the MMOD shielding could be vastly reduced, if not removed completely. However, a coating would be needed to protect the outer layer from being damaged by the regolith.
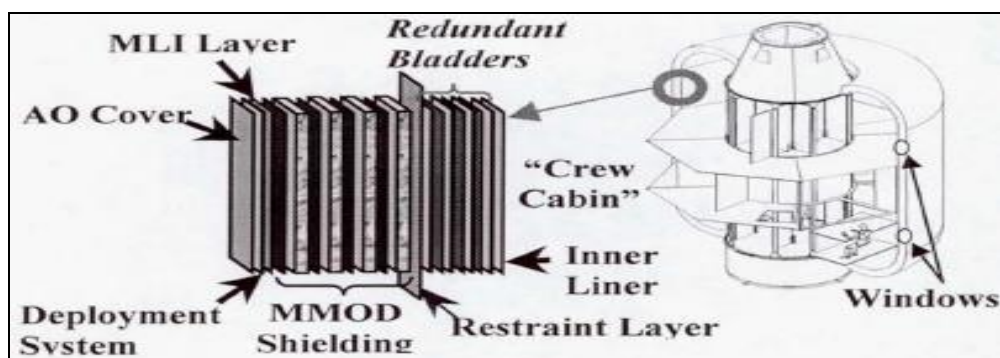
Figure 20: TransHab shell layers [Source: 18]

Materials research for space applications is focused on the characterization of the material characteristics and especially the material degradation as a result of exposure to the harsh space environment. Among others, Aero Sekur (Italy) has performed tests on materials for inflatable structures, subjecting the materials to vacuum conditions, as well as UV and infrared radiation. Specific characteristics which were investigated were the abrasion resistance, tensile strength, mass loss and the capability of the material to recover its shape upon deployment [58].

Flexible materials, such as cloths, have properties which do not solely depend on their constituent materials. Chemical treatment (e.g. coatings) can be used to alter the properties of fibres and cloth. Additionally, the orientation and density of the fibres and the type of weave will also have a significant influence on the overall performance (e.g. permeability, elongation). The relation between physical properties and the geometry of a fabric has been a subject of research for several decades, as can be seen from [59,60]. Figure 21 shows examples of two different weaves of Carbon-Kevlar cloth.
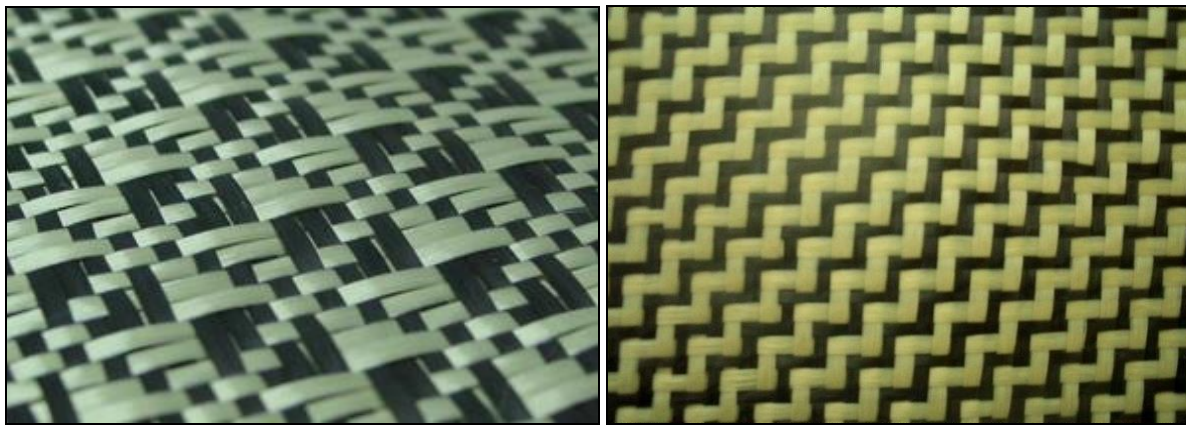
Figure 21: Two different weaves of Carbon-Kevlar cloth [Source: 61,62]

A sample amount of materials which have been investigated for use in inflatable space structures can be seen in Table 1, along with some relevant characteristics. A more detailed, non-comprehensive, overview can be found in Appendix A.

Table 1: Materials for inflatable space structures and relevant characteristics [63]

Material	Tensile strength [MPa]	Tensile modulus [GPa]	Elongation at break [%]	Density [g/cm³]
Kevlar 49	3.600	124	2,9	1,44
Dyneema	3.500	115	3,2	0,975
Vectran HS	2.900	72	3,3	1,41
PBO	5.800	180	3,5	1,56
Technora	3.400	73	4,6	1,39

Additional research is being done to develop new materials to improve specific characteristics, such as areal density or radiation resistance. An example of material development are so-called 'metal foams'. As a result of specific production processes, metal components can be manufactured with a high porosity, hence the term 'metal foam', leading to lower weight, while retaining desired mechanical properties. Potential applications of metal foams in space structures are thermal protection and impact shielding [64,65].

Some other developments are related to 'smart' materials, as well as the integration of electronics into fabrics.

Self-healing Materials

Self-healing materials are of potential interest in the MMOD shields of future inflatable space structures. Wu, Meure and Solomon present an overview of traditional repair methods for composites and thermoplastics and then discuss the different self-healing approaches which have been researched [66]. A brief summary of the various methods is given below:

- Molecular interdiffusion

For thermoplastic materials, so called molecular interdiffusion has been researched since the 1980's as a method of crack healing. When two pieces of the same polymer are brought into contact at high temperatures, above the glass temperature of the polymer, the interface will disappear as the crack heals due to diffusion from one section to the other. Self-healing of materials in response to light, rather than heat, has also been demonstrated. This has a disadvantage that healing is only possible at surfaces exposed to light and as such is not likely to be applicable for internal cracks or thick substrates.

- Chain-end recombination

For certain thermoplastics, recombination of chain ends is another method of self-healing. This method requires that the thermoplastic is capable of a reaction which results in the recombination of chain ends and also requires the presence of a reagent and possibly a catalyst as well.

- Reversible bond formation

Self-healing based on reversible bond formation is likely to be of particular interest to the space sector in the future. The reversible bond formation self-healing method makes use of chain mobility and the inclusion of reversible bonds to provide an approach which does not require external heating, lighting or catalysts.
- Living polymer approach

The living polymer approach, specifically free radical living polymers, could be used for protection against radiation damage, making it another (potentially) attractive method for space structures. Upon exposure to radiation free radicals will be generated and these will recombine with macroradicals at the ends of the living polymer chains, thus mitigating radiation damage.

- Nano-particles and microcapsules

Another potential self-healing method for thermoplastics is the use of nano-particles. Rather than repairing polymer chains as is done in the other approaches, this method would fill cracks with particles. This is similar to the self-healing approaches for thermoset materials, which place healing chemicals within hollow fibres or microcapsules placed withn the material. When cracks occur in the material and hollow fibres and microcapsules are broken, the healing chemicals are released and flow into the crack. Then, through in situ curing, or a reaction with a catalyst

embedded in the material, healing occurs and further crack growth is prevented (see Figure 22). An obvious limitation in these methods is the requirement that healing chemicals are present at the location of the crack.
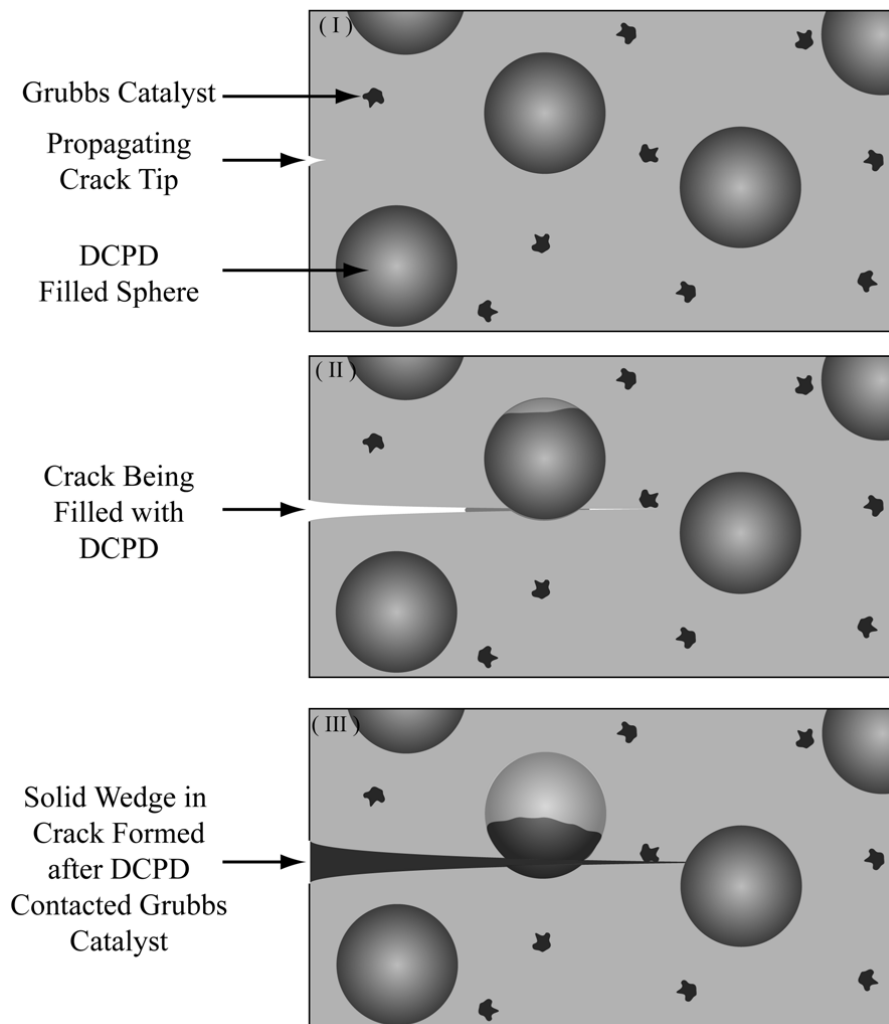
Figure 22: Microencapsulation self-healing concept [Source: 66]

The use of self-healing materials combines well with the possibility of structural health monitoring (SHM), by integrating electronics into the structure. Aside from SHM, integrated electronics can also be used for other purposes, such as shape control of inflatable structures.

Integrated Electronics

The IKAROS solar sail which was developed and launched by the Japanese Aerospace Exploration Agency (JAXA) was made of 7.5 µm thick polyimide. Integrated into this sail were solar cells and liquid crystal devices (LCDs), which were succesfully used to generate power and steer the sail, respectively. The solar cells cover about 5% of the surface area of the sail and will be able to generate about 500 W. The eight LCDs are used for the attitude control of the solar sail. The reflective properties of the LCDs change from diffuse reflection, when the devices are off, to specular reflection when the devices are turned on. By independently controlling the reflective properties of the panels, it is possible to influence the magnitude and direction of the forces

imparted on the solar sail by the impacting photons, which makes it possible to steer the sail [24,25,26,27].

Solar cells and LCDs are only two possible applications of integrated electronics for inflatable space structures. Other options which have been investigated are piezo-electric devices, which have potential applications for shape control of inflatable structures and particularly for antennas and reflectors, as discussed by Salama et al. and Maji and Starnes, among others [67,68]. Figure 23 shows examples of circuits etched or printed onto flexible material.

Figure 23: (Left) Etched copper on Polyurethane Coated Nylon. (Right) Printed Conductive Ink on Aluminized Kapton[TM]. [Source: 69]

2.2.5. Modelling

Modelling of inflatable structures can be subdivided into three parts:

- modelling of the stowed structure
- modelling of the deployment phase
- modelling of the deployed structure

In this section, the information presented will be limited to the modelling of the deployment phase, which differs most from modelling efforts as done for traditional space structures due to the large (non-linear) deformations, fluid-solid interactions and self-contacts. A number of studies are covered to get an overview of the different methods and software tools used for deployment modelling.

The studies discussed in this section do not constitute a comprehensive overview. For a more thorough review, readers are referred to chapter 5 of [10].

Salama et al. [49] distinguish two classes of (simplified) models used to predict deployment:

- 'engineering models'

Engineering models attempt to simulate inflation mechanisms, such as forces at fold lines of a packaged structure, with mechanical analogues, such as forces, torques, springs and dampers.

- 'phenomenological models'.

Phenomenological models attempt to model the effects of inflation gas flowing into the packaged structure, such as the gas flow model described in [70].

Based on this gas flow model, Salama et al. [70] perform deployment simulations of cylindrical tubes with different packaged configurations. To take into account wrinkling, a constitutive model was used relating the effective elastic modulus to the (normalized) inflated volume. Modelling was carried out using commercial non-linear analysis programs LS-DYNA3D and ADAMS. Comparison with a validation experiment showed reasonable agreement between the modelled and observed deployment.

Wang and Johnson use LS-DYNA to simulate the deployment of coiled, Z-folded (see Figure 24) and telescopically folded tube models based on two simulation methods: The Control Volume (CV) method, which models the change in volume as a result of a change in pressure, and the Arbitrary-Lagrangian-Eulerian (ALE) method, which strives to combine the advantages and limit the disadvantages of the Lagrangian modelling approach for solids and the Eulerian modelling approach for fluids. The CV method is less computationally intensive, but is also less accurate as it does not take into account the momentum of the gas as it flows into the structure [71,72].

The ALE method, with underlying equations, transformations and algorithms is discussed in detail by Dunn [73]. The combination of Lagrangian and Eulerian elements is also used by Lienard and Lefevre to model the deployment of a (scaled) coiled beam with Velcro® strips in MSC-Dytran. They estimate that deployment modeling of a 3-m tube to reach the state after 20 seconds would require several hundreds of hours [74].

Further illustrating the high computational cost of the ALE method, Wang and Johnson found that modeling a deployment time of 13 ms required computational times between 1,3 and 1,9 hours depending on the number of processors. In comparison, the less accurate CV method took between 0.2 and 0.3 hours [71].

As mentioned previously, the deployment models can be divided into two classes. The abovementioned work is part of the phenomenological model category. Some engineering models which have been researched include the nonlinear hinge models [10]. This modelling approach simulates folds and wrinkles as non-linear joints or hinges, while the other parts of the structure are modelled as rigid links. Other models use rigid links and non-linear rotational springs, along with linear rotational dampers, to model strut deployment [10].
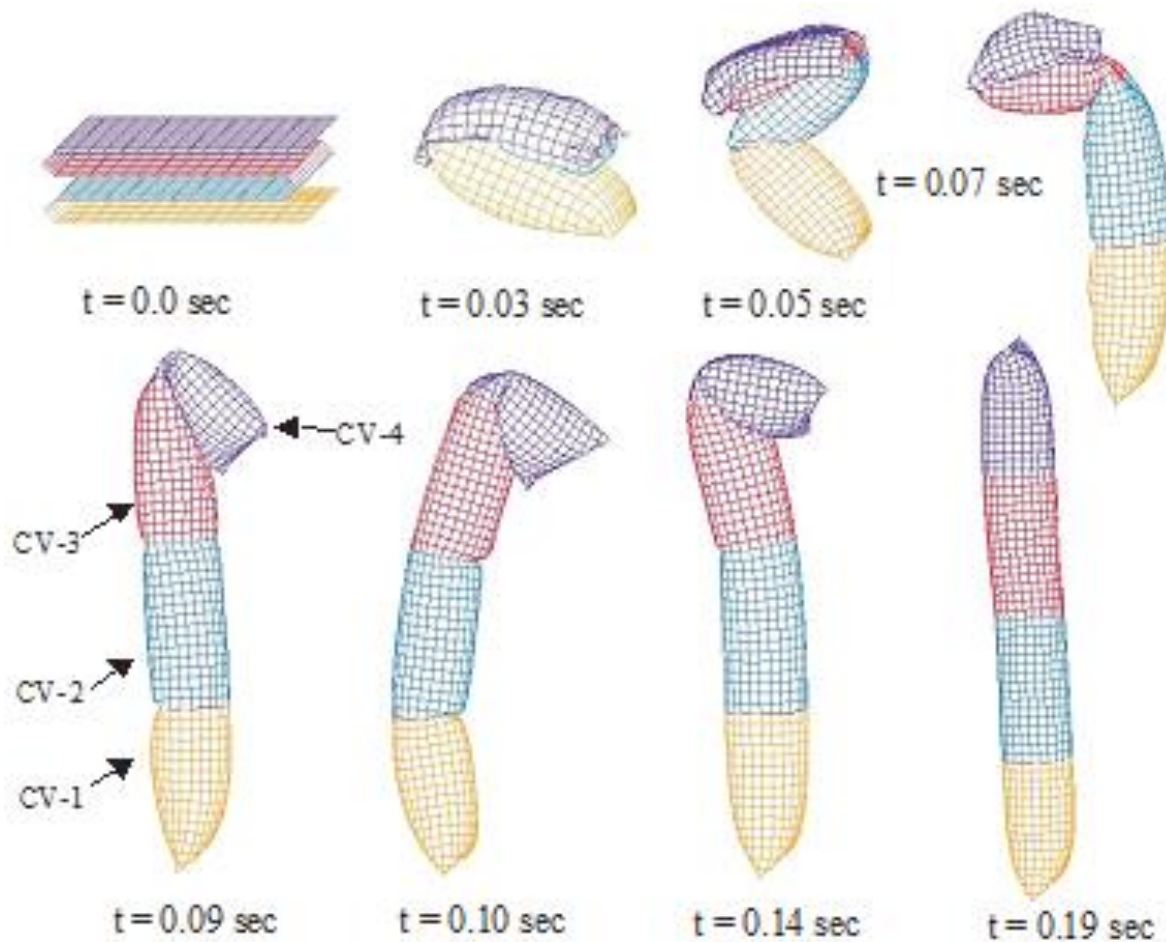
Figure 24: Z-folded tube deployment with no residual air using CV method [Source: 71]

Additional modelling work has been done using other software tools by, among others, Graybeal et al., who use MATLAB/Simulink to simulate the deployment of a Solar Sail spacecraft, based on a number of simplifications to the dynamic equations and the solar sail model [75].

Pollard et al. use ABAQUS to model the deployment of a self-deployable truss structure made of tape-spring elements and shape memory alloy flexures.and then compare the results with data from an experimental deployment [76].

2.3. Summary

This chapter presented a review of inflatable structures which have been designed since the beginning of the space era. It was found that inflatables have been considered for a wide range of applications, such as antennas, reflectors, solar sails, heat shields and pressurized habitats. Through testing and space flight experience has been built with inflation systems, packaging and deployment of structures and the characteristics of inflatable structures.

A classification of different Moon and Mars habitat concepts was made based on the structure shape. Table 2 shows the four categories with an example and a brief summary of some advantages and disadvantages.

Table 2: Advantages and disadvantages of different habitat concept categories

Category	Example	Advantages	Disadvantages
(Hemi-)Sphere		• Spherical shape is optimal for withstanding internal pressure load	• Integration of airlocks and docking ports is relatively complex • Multiple floors will be required, leading to higher complexity
(Semi-)Cylinder		• Integration of airlocks and docking ports is relatively simple • Compartmentali-zation is relatively easy	• Higher wall thickness (and thus mass) needed to withstand pressure loads
Toroid		• High stability (no site exacavation necessary) • Regolith shielding is comparatively easy	• Integration of airlocks and docking ports is relatively complex
Miscellaneous		• Shape can be optimized for greenhouse equipment and systems	• Higher wall thickness (and thus mass) needed to withstand pressure loads
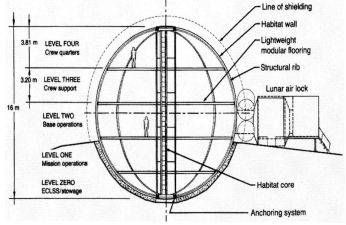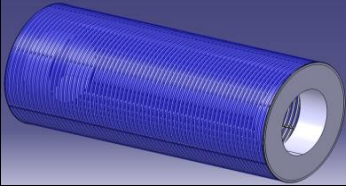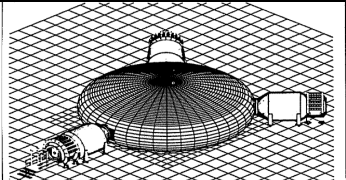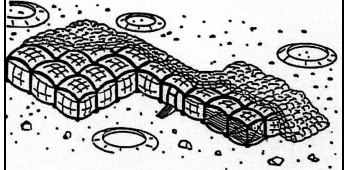
The use of compartmentalization within a habitat or greenhouse structure should be kept in mind to ensure sufficient redundancy within the design. As seen from several of the designs, this compartmentalization might be achieved by encompassing a number of smaller structures within a (secondary) envelope.

The state of the art with respect to inflatable structures technology, modelling and materials was also discussed. It was found that a number of guidelines have been developed for optimal packaging of structures:

- Symmetry of the structure should be maintained in the packaged shape (for packaging efficiency)
- 'Accordion' folds should be used when fast inflation is desired, while rolling should be used for slow deployment.
- Spherical surfaces should be folded along lines of longitude as much as possible, to prevent wrinkling.
- Orthogonal folds should be avoided on account of the high stresses which result from such folds.

With respect to the deployment of inflatable structures, a number of mechanisms were discussed which can be used for controlled deployment, such as compartmentalization, the mandrel method and the roll-out method. By controlling the inflation pressure, or providing a counter-force, the deployment of inflatables can be guided.

Similarly, the different rigidization techniques (e.g. foam rigidization, solvent boil-off rigidization) were reviewed. While the methods remain unchanged, research is ongoing to apply the techniques to new structural shapes and to develop more efficient systems to initiate and control the rigidization.

On the other hand, materials research is focused on developing new materials which can be used in space and which are specialized towards a specific goal. The relationship between fabric structure and fabric properties is also an important aspect which needs to be taken into account. Inflatable structures will typically have multiple layers of various materials to meet the requirements imposed on them and each of the materials will fulfill a different task (e.g. radiation shielding, load bearing). Some promising new developments are metal foams and self-healing materials, which could be used for MMOD shielding for space structures. Equally promising is the potential of integrated electronics, which could find applications in structural health monitoring, shape control and in rigidization systems.

Last, but not least, a review of modelling techniques was performed, with the focus placed on modelling of the deployment process of inflatable structures.

Two classes of models were identified:

- 'engineering models'

Engineering models attempt to simulate inflation mechanisms, such as forces at fold lines of a packaged structure, with mechanical analogues, such as forces, torques, springs and dampers.

- 'phenomenological models'.

Phenomenological models attempt to model the effects of inflation gas flowing into the packaged structure. For these models either the Control Volume method or the Arbitrary-Lagrangian-Eulerian method is used. The Control Volume method model is less computationally intensive, but is also less accurate as it does not take into account the momentum of the gas as it flows into the structure.

3. The Lunar Environment

To design a structure for a lunar Greenhouse Module and formulate requirements for such a structure, it is necessary to review the unique environment which is present on the Moon. In this chapter a brief overview of the lunar environment will be presented, covering the following aspects:

- Topology and Geology
- Gravity
- Magnetic field
- Atmosphere
- Illumination and Temperature
- Radiation
- Micro-meteoroids and Debris

3.1. Topology and Geology

The most widely accepted explanation for the origin of the Moon is that it is the result of the impact of a roughly Mars-sized body on the Earth. The mass expelled during this impact eventually formed the Moon [77].

The most common model for the evolution of the Moon after ejection is the so called magma ocean model. In this model, the newly formed Moon was covered in magma, though the exact depth of this magma layer is unknown. It has been suggested that a seismic discontinuity some 500 km beneath the surface might represent the maximum depth of the magma ocean. Below this discontinuity, frequent 'deep moonquakes' have been detected, while above the discontinuity less frequent, but (in general) more powerful 'shallow moonquakes' occur. Regardless of the precise depth of the magma ocean, modelling and available empirical data indicate that over a period of tens to hundreds of millions of years, the materials in the magma crystallized, forming the different layers that make up the mantle and crust of the Moon [78].

Based on analysis of deep moonquakes (red dots in Figure 25), measured by the Apollo seismograms, Weber et al. [79] conclude that the Moon has a solid inner core, with a fluid outer core and a partially molten layer surrounding it, see Figure 25. There is still uncertainty in the exact size of the core, but it is estimated to have a radius between 250 and 430 km, which amounts to about 15 to 25% of the radius of the Moon, which is roughly 1738 km. According to Weber et al. about 60% of the volume of the core is liquid [79]. Though there is still some uncertainty, it is estimated that the lunar crust is on average between 40 and 50 km and the crust is thicker on the far side than on the near side by about 15 km [78].
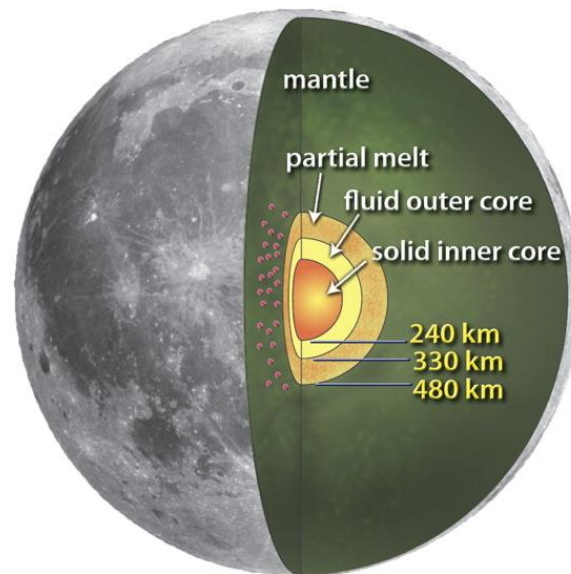
Figure 25: Cross-section of the Moon with probable radii for the core layers. [Source: 79]

3.1.1. Surface Topology

While there is still uncertainty about the precise evolution of the Moon and its interior, the lunar surface has been observed in far more detail. In the absence of plate tectonics and erosion by wind or liquid water, the surface of the Moon has been shaped entirely by volcanism and space weathering.

Space weathering is a term covering the influences of cosmic and solar radiation, as well as impacts from (micro-)meteorites [80]. The impacts of meteorites on the lunar surface are responsible for the macroscopic features, such as impact basins and the basin rings. On a smaller scale, space weathering affects the properties of the material on the surface of the Moon, altering such things as the spectral properties (e.g. albedo) [81].

Lunar features caused by volcanism include the maria, which were basins, most likely caused by impacts, which later filled with lava. Furthermore, past lava flows have been suggested as a possible cause of ridges and rilles in the vicinity of the maria. Finally, and most importantly, volcanism is responsible for lava tubes, natural caverns resulting from underground lava rivers [77].

With expected dimensions of tens or even hundreds of meters and 'roof' thicknesses likely exceeding 10 m, lava tubes have been posited as potential sites for lunar habitats. The thick roofs of such caverns would provide natural shielding against radiation and meteorites and the underground location would have the added benefit of a more stable thermal environment [77, 82].

3.1.2. Regolith composition

Covering the bedrock of the lunar crust is a thick layer of regolith which can range from 4 to 5 m thickness in maria and 10 to 15 m in highland regions [83]. Regolith is a mixture of crystalline rock fragments, mineral fragments, non-crystalline solids (glasses) and agglutinates and breccias. These last two consist of smaller grains of different materials which have been welded together as a result of an impact of a meteorite on the lunar surface [84].

An effect of space weathering is that ionized particles from the solar wind can implant themselves in the topmost layer of the lunar regolith. Concentrations of hydrogen in the order of a hundred µg/g of lunar soil have been found in samples taken during the Apollo missions [84].

The specific minerals and rocks, and thus elements, which are present in regolith depend on the specific location on the Moon. Furthermore, as mentioned previously, space weathering will affect the properties of the exposed regolith material, leading to differences in properties between the top layer of regolith and lower layers of regolith. Thus, the relevant properties of lunar regolith for construction and radiation shielding may vary depending on the location on the Moon.

The Apollo missions brought back roughly 382 kg of rocks, pebbles, sand, dust and core samples from the Moon [80]. Table 3 lists several major elements present in lunar soil and the weight percentages of these elements in selected lunar samples. As of 2005, some 350 kg remains of these samples [85]. NASA maintains an archive of these lunar samples and scientists can request samples for their research. Nonetheless, due to the limited availability and the high value of these lunar samples, simulants are used in research and development related to the Moon. These lunar simulants are materials "manufactured from natural or synthetic terrestrial or meteoritic components for the purpose of simulating one or more physical and/or chemical properties of a lunar rock or soil" [85].

Based on experiments carried out on lunar regolith and simulants, some key engineering values are available. The recommended specific gravity value for lunar regolith is 3,1 g/cm^3, for example [86]. Additionally, radiation testing of lunar regolith suggests that the material has similar shielding properties as aluminium, with a dose reduction of 0,7 to 1,0% per unit areal density (g/cm^2) [87].

Table 3: Chemical composition of several lunar samples [Source: 88,89]

Element *	Sample 10020	Sample 10084	Sample 12001	Sample 15012	Sample 71040
SiO_2 (wt %)	38	41,0	46,0	46,77	39,74
TiO_2 (wt %)	12	7,3	2,8	1,46	9,57
Al_2O_3 (wt %)	11	12,8	12,5	16,75	10,80
Cr_2O_3 (wt %)	0,31	0,305	0,410	0,30	0,47
FeO (wt %)	18	16,2	17,2	12,4	17,73
MnO (wt %)	0,32	0,220	0,220	0,17	0,24
MgO (wt %)	8	9,2	10,4	10,35	9,72

*Only a limited number of elements are listed. Hence the total weight percentages do not equal 100%.

3.1.3. Seismic activity

One part of the payloads of the Apollo missions was seismograms, which, over the period of 8 years during which the instruments were operated, measured seismic activity on the Moon. It was found that the Moon has significantly less seismic activity than the Earth, with some 500 quakes per year measured on the Moon and some 10000 detectable quakes occurring on the Earth each year [84].

Additionally, it was found that moonquakes can be divided into two categories based on the depth at which the quakes originate. As mentioned previously, a seismic discontinuity is located some 500 km below the lunar surface and quakes originating below this discontinuity are called 'deep moonquakes' whereas quakes originating closer to the surface are named 'shallow moonquakes'.

The vast majority of quakes are deep moonquakes, with only about five shallow moonquakes occurring each year [84].

Aside from the reduced number of quakes, the moonquakes, in general, also have a lower magnitude. Deep moonquakes have magnitudes which fall mostly in the range of 1 to 2 on the Richter scale, while shallow moonquakes can reach magnitudes between 5 and 6. In contrast, the largest earthquakes can reach a magnitude between 9 and 10. Taking into account that seismic waves are scattered in the lunar regolith, dispersing the energy of the quakes [84], it can be assumed that moonquakes will have a negligible impact on the lunar GHM.

Aside from moonquakes, the tidal forces acting on the Moon cause deflection of the lunar surface. Since the Moon is tidally locked with respect to the Earth, there is a permanent distortion of the Moon, called a tidal bulge. Transient distortions of the lunar surface also occur as a result of librations (oscillating motions of the Moon relative to the Earth), but this amounts to flexing of some 2 mm over a 10 km distance [84], which is not expected to have an impact on lunar habitats.

3.1.4. Impact on the Lunar Greenhouse Module design

The local (surface) topology at the desired lunar base site will have some impact on the design of the structure and the amount of crew time required for site preparation.

Astronauts or robots will need to prepare the site where the greenhouse will be situated, by removing objects (e.g. protruding rocks) which might otherwise puncture the structure.

If a sufficiently large lava tube is present, the greenhouse structure will be able to take advantage of the provided radiation and meteoroid shielding, as well as the less extreme thermal environment, which such a lava tube would provide and as a result, the structural design will be able to achieve a significant reduction in mass (and wall thickness). However, if the lava tube is not large enough to house the entire lunar base, then the interfaces between structures inside a lava tube and structures on the outside will be significantly heavier and more complex.

If no lava tube is present, then the greenhouse will be placed on the surface and will need to provide its own shielding against radiation and debris, along with thermal control. A possible solution is to place lunar regolith on top of the structure. This will require significant crew effort to dig out regolith and place it on the greenhouse and it will be necessary to incorporate a system in the greenhouse structure which will keep the regolith in place.

As mentioned previously, the seismic activity on the Moon is likely to have a negligible impact on the greenhouse structure, due to the relatively limited strength and frequency of the quakes as well as the energy dispersion behaviour of the lunar regolith. Thus, this will not have an impact on the overall structure design.

3.2. Gravity

The Moon has a (mean) gravitational acceleration at the surface of about 1,622 m/s^2, which is about a sixth of the gravitational acceleration on the surface of the Earth [77]. Consequently, objects of a given mass will weigh roughly six times less on the Moon than on Earth.

Since the Moon, like the Earth, is not a perfect, homogeneous sphere, there is some spatial variation in gravitational acceleration. As can be seen in Figure 26, the minimum and maximum magnitudes of the gravitational acceleration on the surface of the Moon differ by about 0,025 m/s^2, which is just over 1,5% of the mean value [90].
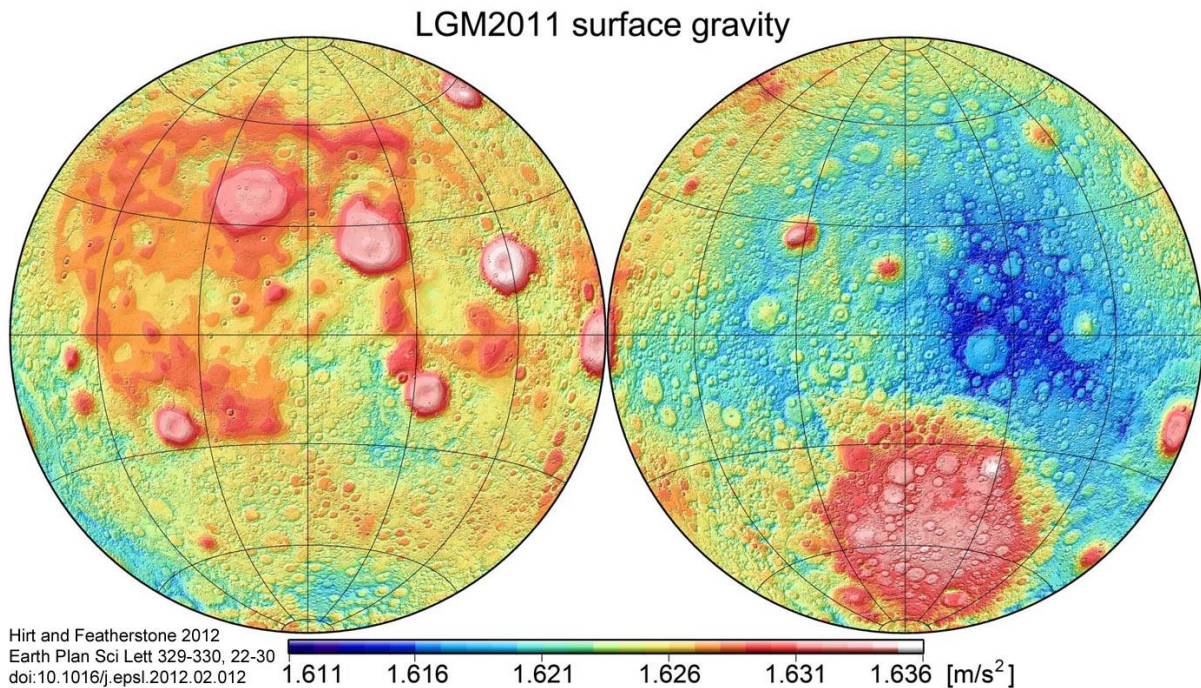
Figure 26: Gravitational acceleration at the lunar surface. (Left) Near side. (Right) Far side. [Source: 90]

During the Apollo program, analysis was carried out to determine the gravity field of the Moon, in order to accurately account for its perturbing effects on the Apollo spacecraft. This effort to characterize the gravity field of the Moon led to the discovery of mass concentrations, or so called mascons, such as the Imbrium and Orientale impact basins [91].

In general, a topographic low, such as an impact basin, results in a local decrease in gravitational acceleration. Based on tracking data from spacecraft orbiting the Moon it was determined however that certain regions of the Moon had local increases in gravitational acceleration which could not be explained on the basis of the geographical features. It was determined that these regions could only have a local increase in gravitational acceleration, due to a local mass concentration.

3.2.1. Impact on the Lunar Greenhouse Module design

Unlike the TransHab, which was designed for use in micro-gravity, the lunar greenhouse will need to be designed to accommodate the gravitational acceleration on the Moon, resulting in a number of additional design issues.

The deployment system of the greenhouse will need to be designed such that the effects of gravity can be overcome. This means that expansion of structures on the lunar surface will be easier in horizontal direction rather than vertical direction. Similarly, for the (re-)positioning of equipment, gravity will need to be overcome, which would be significantly more difficult for a multi-story structure as compared to a single-story structure.

Additionally, gravity will have a large impact on the movement of astronauts. Rather than floating in space, astronauts will be walking upright, which impacts the sizing of doorways and airlocks and results in the need for walkways within the structure.

The comparatively low strength of the gravitational acceleration on the Moon does mean that the loads experienced by the structure as a result of equipment, regolith shielding, and structure mass will be significantly lower. This could potentially lead to a lower mass of the load bearing section of the structure, though this is unlikely since the internal pressure will probably be the main design driver.

3.3. Magnetic Field

On Earth, the presence of a strong magnetic field protects against harmful radiation. Unfortunately, the magnetic field of the Moon is significantly weaker than that of the Earth, with maximum total magnetic field strengths at the lunar surface in the order of 100 nT, see Figure 27 [92]. In comparison, the magnetic field strength at the Earth's surface ranges from 25000 to 65000 nT.
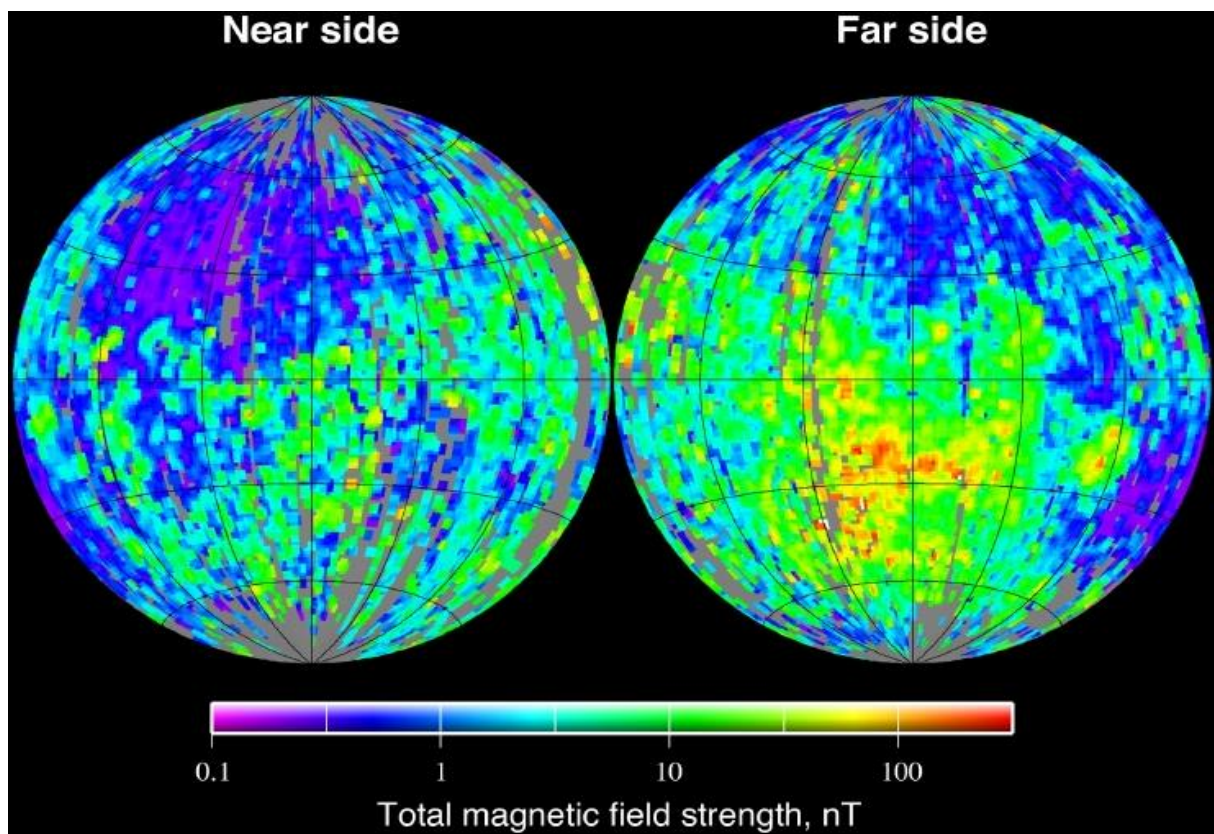
Figure 27: Total magnetic field strength at the lunar surface. (Left) Near side. (Right) Far side. [Source: Lunar Prospector electron reflectometer experiment [92]]

Furthermore, unlike the Earth's magnetic field, the present day magnetic field of the Moon is not a dipolar field generated by a dynamo effect of the core. Instead the magnetic field of the Moon is (almost entirely) due to crustal magnetism [93,94].

This crustal magnetism is a result of remanence, or residual magnetization, of magnetic materials on (or near) the lunar surface. The discovery of magnetized lunar rocks during the Apollo missions,

led to the conclusion that magnetizing fields were present on the Moon in the distant past. It has been hypothesized that a lunar dynamo might have been responsible for these magnetizing fields, but fields generated by impacts or occurring due to solar or terrestrial influence have also been proposed [93,94].

Due to differences in local magnetization, magnetic fields arise. These magnetic anomalies range in size from a few kilometres to hundreds of kilometres and, as seen in Figure 27, the strength of these fields can differ by a factor 1000. The differences in local magnetization can be attributed to, among other things, the type and amount of magnetized material and the strength of the magnetizing field at the time when the material was magnetized [93,94].

It was found that many of the impact basins on the Moon, such as Imbrium and Orientale, are demagnitized. This is due to the fact that large impacts will cause shocks and high temperatures, which result in material around the impact zone being heated above their Curie temperature, resulting in a loss of magnetism. Thus impacts on the lunar surface also influence the variation in local magnetization [93,94].

Despite the limited magnetic field strength at the lunar surface, local magnetospheres have been detected. These so called mini-magnetospheres are regions where the magnetic field deflects the solar wind. By observing the reflectance of energetic neutral hydrogen atoms of the lunar surface, the Chandrayaan-1 satellite was able to detect a region of reduced neutral atom flux with a diameter of 360 km. This reduced flux is caused by a mini-magnetosphere which deflects the incoming solar wind, resulting in a lower number of neutral atoms which are reflected of the surface within this magnetosphere [95].

3.3.1. Impact on the Lunar Greenhouse Module design

The lack of a protective magnetosphere means that the radiation levels on the Moon are significantly higher than on Earth. While mini-magnetospheres have been detected on the Moon, it is unlikely that these will be useful in providing radiation protection for the lunar GHM. Thus, the structural design will need to incorporate radiation shielding to protect the interior.

The presence of crustal magnetism will not impact the design of the greenhouse structure.

The Moon does regularly pass through the magneto-tail of the Earth, but this will not impact the structure design, since the greenhouse will also need to operate when the Moon is not within the magneto-tail of Earth. (The magneto-tail is part of the magnetosphere of the Earth and has been stretched into a 'tail' in the anti-sunward direction by the solar wind pressure.)

3.4. Atmosphere

The exact classification of the lunar atmosphere is a matter of some debate. The density of the atmosphere is so low that the mean free path length exceeds the atmospheric scale height, making the atmosphere a so called surface bounded exosphere. Furthermore, because of the infrequent collisions between atoms and molecules in the lunar atmosphere, it is possible to think of it as a combination of multiple lunar atmospheres, with each one made up of a different gas species [84,96].

The total mass for the lunar atmosphere has been determined to be in the order of 10^4 kg, with nighttime concentrations of $3*10^{-13}$ mol/m³, or, equivalently, between 10^5 and 10^6 molecules/cm³. The major constituents of the atmosphere are argon, neon, helium and hydrogen, with some 10^4-10^5 molecules/cm³. In comparison, the density of the Earth's atmosphere, at sea level, is $3*10^{19}$ molecules/cm³ [84,96].

The exact composition and density of the lunar atmosphere can vary significantly however, due to a number of mechanisms by which atoms and molecules may exit or enter the lunar atmosphere. Loss of atmospheric gas can occur either through particles moving away from the Moon with a velocity exceeding the escape velocity of the Moon (2,38 km/s), or by particles interacting (bonding) with surface material. In [96] a loss rate for the lunar atmosphere of about 10 g/s is stated. Counteracting these losses are various mechanisms resulting in gas entering the lunar atmosphere through 'outgassing' from surface materials, such as the sodium gas detected in 1998 [97], and additionally different gas species are carried towards the Moon on the solar wind.

Of particular interest to engineers designing missions to the Moon is the drastic impact humans can have on the atmosphere. Each of the Apollo lunar landings deposited exhaust and effluent gases amounting to about 20% of the total mass of the lunar atmosphere. Not only did this affect (early) measurements of the lunar atmosphere, but, more importantly, research found that if sufficient mass is injected into the lunar atmosphere it will increase the escape time (of gases from the atmosphere) from days to hundreds of years [83,84,96].

3.4.1. Lunar Dust

The Luna 19 and 22 missions performed measurements to determine the electron content of the lunar atmosphere. These measurements indicated that the peak concentrations were several hundred times higher than could be explained based on photo-ionization of the gases in the atmosphere. The probable explanation for this high electron content is lunar dust which is charged through exposure to ultraviolet radiation [98].

Stubbs et al determine that charging of the lunar surface as a result of solar radiation can lead to negative potentials in the order of 10^2 V on the non-illuminated side of the Moon. Through electrostatic forces acting between the charged surface and charged dust particles, the dust is levitated up to several kilometres above the surface [99]. A follow-up study found that negative potential on the non-illuminated side of the Moon can reach $4*10^3$ V during solar energetic particle (SEP) events [100].

The lunar dust, the component of lunar regolith smaller than 100 μm in size, has been identified as a potential problem by various members of the Apollo missions, such as Cernan (Apollo 17) and Bean (Apollo 12). The adhesion of lunar dust settling on equipment and spacesuits, as well as the effects on visibility and breathing are all issues which need to be addressed when considering manned missions to the Moon [101].

3.4.2. Impact on the Lunar Greenhouse Module design

As mentioned, contamination of the lunar atmosphere by exhaust and effluent gases is a possible concern. This could result in more stringent requirements on the amount of outgassing and the maximum leakage rate which the greenhouse is allowed to have, which would impact the material selection and sizing (and hence mass and cost) for the structure.

The issues of lunar dust and surface charging will definitely need to be addressed. Counteracting the surface charging effects of ionizing radiation will require solutions such as grounding of the structure, applying special coatings or using regolith shielding.

Similarly there are different options to prevent lunar dust from entering the greenhouse. For example, rather than having an airlock the structure could use a suitport. With a suitport, a space suit is attached to the outside of the structure and astronauts are able to enter the suit through a hatch connecting the structure to the suit. Once the astronaut has entered the suit, the hatch is closed and the suit is disconnected from the structure. Upon finishing the lunar surface operations, the astronaut connects the suit to the structure and re-enters through the hatch. This solution, though it has some drawbacks such as increased space suit wear, could significantly reduce the amount of dust entering the greenhouse. Another option would be to use a standard airlock and use overpressure within the greenhouse environment, with respect to the pressurized airlock, to prevent dust from entering.

Regardless of the dust mitigation strategies, it is likely that a system will be needed to clean and remove any dust which does manage to enter the greenhouse. Such a system will result in extra loads on the structure and may require additional volume and interfaces.

3.5. Illumination and Temperature

Crucial aspects of the lunar environment with regards to plant cultivation (and human habitability) are the illumination and temperature. The illumination conditions on the lunar surface need to be known to evaluate the possibility of using natural lighting for plant growth (either completely or as supplement to artificial lighting). Knowledge of the thermal environment is crucial in designing the greenhouse structure and ensuring stable, desired temperatures within.

Analogous to a day on Earth, a Lunar day is the period of time it takes for the Moon to complete one full rotation around its axis. One Lunar day is roughly equal to 28 days on Earth. Locations on the Moon may thus be continuously illuminated over a period of several (Earth) days.

3.5.1. Lighting conditions

The spin axis of the Moon is almost perpendicular to the ecliptic plane, with a tilt angle of about 1,5°. Combined with the rough surface topology, this small tilt angle provides widely varying illumination conditions at different locations on the Moon [102].

For human exploration, the poles are of particular interest. Parts of the impact craters on the Moon's poles are never illuminated by the Sun, while other (nearby) areas of the lunar surface experience continuous sunlight for months at a time and may be illuminated for up to 89% of the year [102,103].

With the topography of the Moon being determined with ever greater accuracy, it is becoming possible to precisely predict the illumination conditions on the Moon. Through orbital mechanics the position of the Moon, the Earth and the Sun can be calculated, which makes it possible to determine the direct and indirect (reflected by Earth) sunlight which illuminate a given area on the Moon. By taking into account the surrounding topography, it is possible to model partial or complete blocking of light by nearby surface features [104]. This method is described by Li et al. and used by Bussey et al. and Noda et al. using lunar topography data from the Japanese Selenological and Engineering Explorere (SELENE), also known as Kaguya [102,103,104].

Of course, such models need to be verified, which requires comparison of the predicted values with observed illumination conditions. Bussey et al. compare the modelled illumination conditions with images from the Clementine satellite. Future work will likely use the more comprehensive and accurate data obtained by the Lunar Reconnaissance Orbiter (LRO) [102].

Using the on-board instruments to make observations of the lunar surface the LRO enables the production of illumination maps for the Moon. Figure 28 shows an illumination map for the lunar South Pole made from images taken by the LRO. This illumination map combines observations taken over a period of 6 lunar days (roughly six months). By taking into account the illumination of each spot during each observation, it was possible to produce a map showing the relative illumination during the entire time period [105].

Figure 28: Illumination map of the lunar South Pole [Source: LRO [105]]

3.5.2. Temperature conditions

Directly related to the illumination conditions, is the temperature which is experienced at a given location. The permanently shadowed craters, for example, are colder than the surrounding areas which do receive sunlight.

Without a protective atmosphere to trap heat, the temperatures on the Moon are far more extreme than on Earth. Surface temperatures near the Apollo 17 landing site varied between 102 and 384 degrees Kelvin (K) over the course of a lunar day. This corresponds to a temperature between roughly -171 and 111 degrees Celsius (°C). As a location moves out of illumination into night time, temperature gradients reach about 5 K/h [84].

As mentioned, the permanently shadowed craters are even colder than the other areas of the Moon, reaching temperatures as low as 40 K, as can be seen in Figure 29 [106]. This figure shows the first global daytime and nighttime thermal maps of the Moon, which were assembled using data from the Lunar Reconnaissance Orbiter. Even lower temperatures of about 25 K have been determined for locations on the other lunar pole [107].

Modelling efforts by Christie et al. show that subsurface temperatures on the Moon are far more stable than surface temperatures, due to the thermal properties of the lunar regolith [108]. Consistent with heat flow measurements obtained during the Apollo program, they find that, at a depth of 30 cm, temperature variations of about 5 K occur and negligible temperature variations occur from a depth of about 60 cm downwards. The average temperature at 30 and 60 cm beneath the lunar surface was modelled to be about 253 K, or -20 °C, which was also consistent with measurement data [83,84,108].

Combining this thermal model for the lunar surface and regolith, with the illumination model and topography data discussed previously, it will be possible to predict the lighting and temperature conditions at any location on the Moon for any desired time.
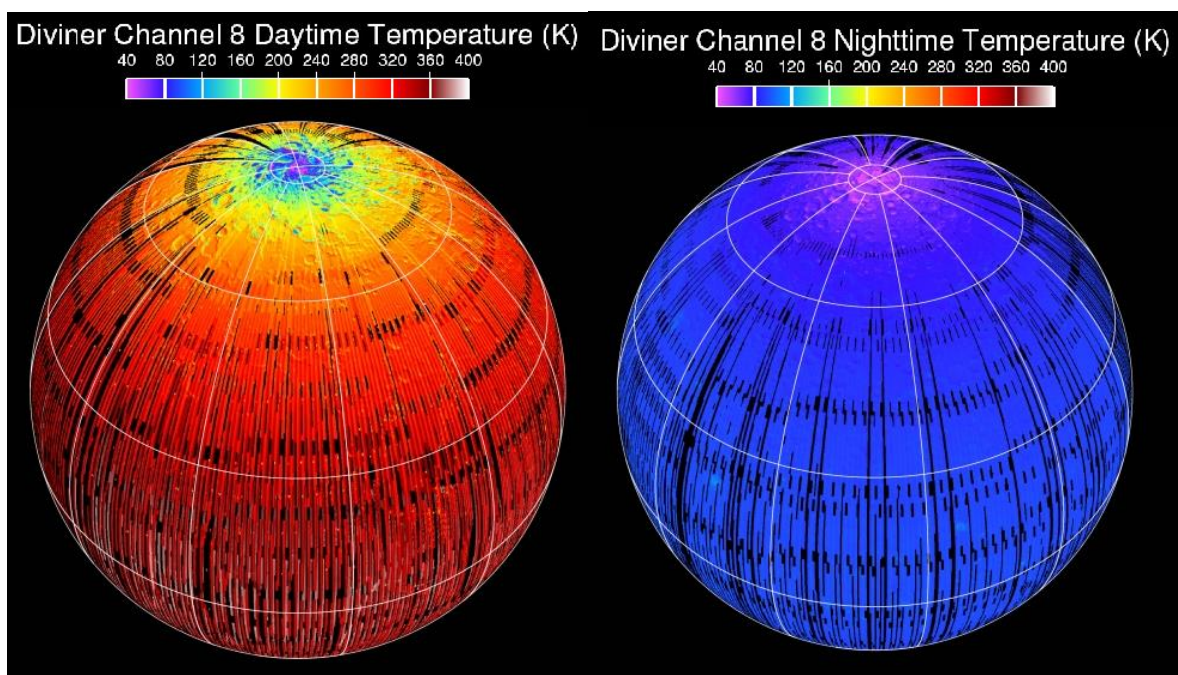
Figure 29: Global thermal maps of the Moon. (Left) Daytime. (Right) Nighttime. [Source: LRO [106]]

3.5.3. Impact on the Lunar Greenhouse Module design

The lighting conditions on the Moon influence the greenhouse design by necessitating the use of hybrid or artificial illumination systems. While certain locations on the Moon are illuminated for more than 80% of the year, the day/night cycle is not suited for optimal plant growth.

The use of artificial lighting adds increased equipment mass and requires additional support harnesses and power interfaces. Furthermore, artificial lighting will add waste heat to the greenhouse system, which requires additional cooling capacity.

To maintain the interior air temperature within the desired range, the greenhouse structure will need to incorporate insulation layers as well as a heating and cooling system. The insulation layers result in a larger wall thickness, which will influence the volume of the stowed structure.
The heating and cooling systems will add equipment mass and, similar to the artificial lighting system, require support harnesses and power interfaces. Depending on the type of thermal control system which is used, it might be necessary to have tanks with cooling fluid and pumps to circulate the fluid through the system, along with radiators for heat dissipation.

3.6. Radiation

The Moon does not have a strong magnetic field and a thick atmosphere to protect the surface from damaging radiation. It should be noted that the Moon does pass through the geomagnetic tail of the Earth and is therefore (partially) shielded by the magnetic field of the Earth for a number of days each month. There is some doubt about the effect this has on the radiation levels on the lunar surface, though. In any case, a lunar Greenhouse Module will need to contain some radiation shielding to ensure proper conditions for the astronauts and plants.

To be able to design this radiation shielding, a brief overview of the radiation environment on the Moon is given. The radiation experienced within a (man-made) structure on the Moon can be divided into four sources:

- Lunar radiation
- Solar radiation
- Galactic radiation
- Secondary radiation, which is radiation emitted by materials as a result of incident (primary) radiation.

Some other minor sources of charged particles have been identified, such as the magnetospheres of Jupiter and Earth, but due to the low flux and low energy of the particles from these sources, as well as limited characterization, these will not be discussed.

Before discussing the different sources of radiation on the Moon in detail, a brief introduction of the different dose units is in order. The radiation dose can be expressed either as the absorbed dose, which only considers the radiation energy absorbed per unit mass, or as the equivalent dose, which takes into account the damage the different charged particles can do to material (most importantly living tissue). Associated to the absorbed dose are the units Gray (Gy) and rad, with 1 Gy equal to 1 J/kg. The relation between Gray and rad is 1 Gy equals 100 rad [77].

For the equivalent dose, the units Sieverts (Sv) and Röntgen Equivalent Man (rem) are common. 1 Sv corresponds to 100 rem. The relation between Sieverts and Grey and rem and rad is based on a radiation weighting factor, also known as quality factor or biological damage factor, for the different particles associated with radiation. This factor represents the ratio between the damage done by a given particle type and the damage done by gamma radiation. For gamma, beta and x-ray radiation the factor is 1, for alpha radiation the factor is 20 and for neutrons and heavy ions it ranges from 5 to 20. The conversion from Gy to Sv is then simply a multiplication of the absorbed doses of the various types of radiation with their respective factors [109,110].

The maximum allowable dose on Earth is 50 mSv/year for radiation workers and 5 mSv/year for a normal person [77]. ESA standards set a career limit of 1 Sv and a maximum radiation dose of 0.5 Sv/year to blood forming organs [111].

3.6.1. Lunar radiation

Every object and substance in the universe produces some radiation, including the Moon. While generally harmless, there are some radioactive elements in the lunar regolith which produce a non-negligible contribution to the radiation environment.

Specifically, radio nuclides ^{40}K (potassium), ^{235}U and ^{238}U (uranium) and ^{232}Th (thorium) are present on the Moon and these produce a combined radiation dose of 0.3 mSv/year [112].

Additionally, though the radiation is technically not lunar in origin, there is a fraction of the incident solar and galactic radiation which is reflected off of the lunar surface. Based on observations by the Interstellar Boundary Explorer (IBEX), Rodriguez M. et al. determine a global flux ratio (reflected energetic neutral atoms to incoming solar wind particles) of 0.09 ± 0.05, which they mention is consistent with other studies. More detailed values, taking into account surface composition and texture variations, will require a greater level of detail in the observations [113].

Adams et al. investigate the albedo of neutrons from the lunar surface for galactic cosmic radiation at solar minimum and maximum conditions, as well as for a solar energetic particle event. Their findings suggest that up to 18% of the effective dose from galactic cosmic radiation can be attributed to albedo neutrons, though they caution that this is likely much lower on account of uncertainties inherent in the used model. For the SEP-event, the albedo was found to account for about 2.4% of the effective dose [114].

3.6.2. Solar radiation

Solar radiation consists of the solar wind and solar energetic particles, related to solar flares. The solar wind is continuously emitted electrically neutral plasma and has a typical velocity in the range of 300 to 800 km/s. The plasma consists of ions and electrons, with mean energies of ~1 keV/nucleon for the ions and energies in the order of 10^0 to 10^2 eV for the electrons [83]. The solar wind density does vary over time, depending strongly on solar activity. Measurements taken by the Advanced Composition Explorer noted a decrease in solar wind density of about 98% in 1999 [115].

The solar wind can be categorized as consisting of different types of streams. 'Slow' solar winds (with velocities around 400 km/s) are associated to the streamer belt, a region around the Sun's equatorial belt. 'Fast' solar winds are thought to originate from coronal holes, which are regions of open field lines in the magnetic field of the Sun [116].

The solar wind consists predominantly (>95%) of roughly equal amounts of electrons and protons, but ions of most chemical elements have been detected as well. Observations made with the Solar and Heliospheric Observatory (SOHO) satellite detected helium, nitrogen and oxygen isotopes for example, among others. Furthermore, alpha particles, consisting of 2 protons and 2 neutrons, have been found to make up about 2% of the solar wind and high-energy photons (e.g. X-rays and gamma rays) are also present [83,117].

The particle flux on the lunar surface, due to the solar wind, is on average of the order of 10^8 to 10^9 protons/cm^2*s. The low energy of the solar wind particles means that the particles do not penetrate materials very deeply (10^{-8} cm in lunar regolith) and pose little risk to astronauts [83,84].

On the other hand, Solar Energetic Particles (SEP) have substantially higher energies, typically in the range of 1 to 100 MeV/nucleon, which is at least a 1000 times higher than the energies of solar wind particles [84]. Particles with energies in the GeV/nucleon range have been detected however, as can be seen in Figure 30, which shows proton fluences versus kinetic energy for six different SEP-events [118].
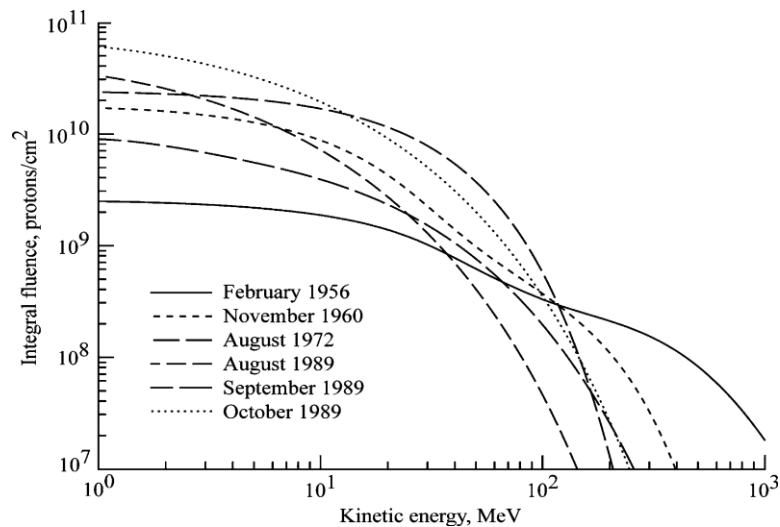
Figure 30: Integral flux (fluences) at 1 AU of SEP-events during solar cycles 19-22 [Source: 118]

SEP output is related to sudden outbursts of solar activity, in the forms of solar flares and coronal mass ejections (CMEs). A distinction can be made between 'impulsive' and 'gradual' SEP-events, based on the underlying method of matter acceleration [117,119].

Impulsive events are associated with flares and the SEP ejected during such an event are accelerated by the flare mechanism itself, through the sudden release of magnetic energy during magnetic reconnection. Gradual events are related to CMEs, which are also believed to be caused by the release of magnetic energy during magnetic reconnection, similar to solar flares. The SEP ejected during a gradual event are accelerated by shock waves produced as a result of the large energy release associated with CMEs [117,119].

Impulsive events have extremely high ^{3}He and heavy element levels which can be 1000 times higher than levels in the corona. For gradual SEP-events, the abundances are typically similar to those of the corona or solar wind [117,119].

3.6.3. Galactic radiation

Another major source of radiation on the lunar surface is the cosmos itself. This Galactic Cosmic Radiation (GCR) has a lower flux than solar radiation, but it consists of more energetic particles, which are more damaging to human tissue.

The GCR consists of 2% electrons, about 85% protons, ~12% alpha particles and the remaining 1% consists of (fully ionized) ions of all chemical elements. The GCR flux on the lunar surface is not constant, but varies as a result of interactions with the solar wind and solar energetic particles. In periods of high solar activity, the amount of galactic radiation on the lunar surface will be lower than in periods of low solar activity.

Figure 31 shows the relationship between particle fluence on the lunar surface and particle energy, for the different components of the GCR [118]. Z is the atomic or proton number, and amu stands for atomic mass unit and has a value of 1,660538921(73) * 10^{-27} kg [120]. The solid lines depict the conditions during the solar minimum in 1977 and the dashed lines indicate fluences for the solar maximum of 1990.

The (relatively) low number of highly energetic particles results in a radiation dose of about 300 mSv/year. [77]
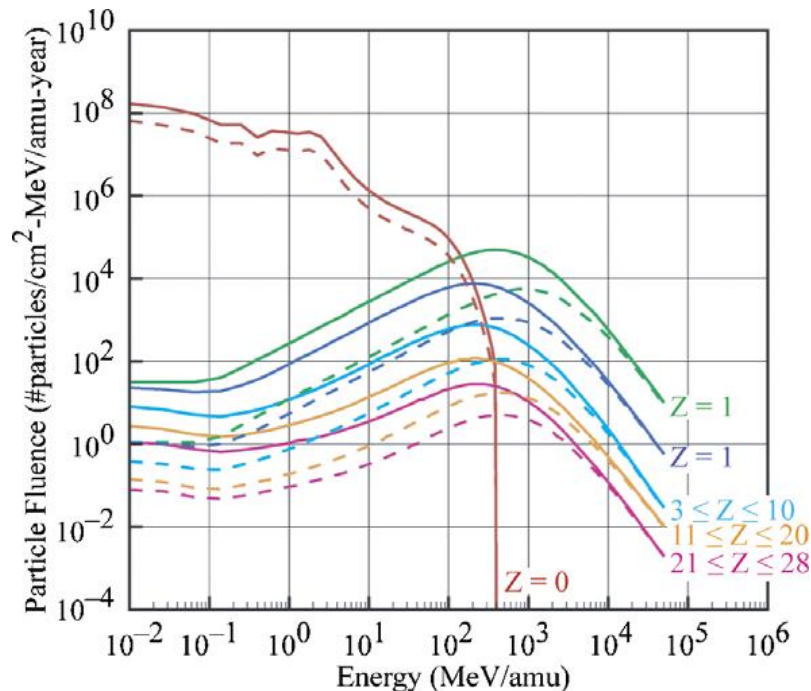
Figure 31: GCR particle fluence on the lunar surface [Source: 118]

3.6.4. Secondary radiation

As charged particles pass through a material, energy is transferred from the particles to the surrounding material via collisions. This can result in a number of different interactions, (e.g. Compton scattering, electron-hole pair generation) which results in secondary radiation [121].

The particles which are thus released from the material can proceed to interact with other atoms and molecules in (potentially) harmful ways. In principle, secondary radiation can transfer enough energy to surrounding material to cause it to eject a particle, resulting in so called tertiary radiation.

Secondary radiation and radiation doses behind a given amount of shielding are determined using radiation transport codes, such as GEANT4 [122]. Using a Linear Energy Transfer (LET) function to describe the energy being transferred to the surrounding material in the immediate vicinity of particle paths, it can be determined whether this is sufficient to eject particles from the atoms and molecules, and thus produce secondary radiation.

Figure 32 shows the flux of (primary) GCR as well as the produced secondary radiation particles as a function of lunar regolith depth [123]. It can be seen that the flux of secondary protons, neutrons and gamma rays is higher than the primary flux and also does not diminish as quickly with increasing regolith depth. Thus, the radiation affecting the astronauts and plants within a structure covered with lunar regolith will consist, for the most part, of secondary radiation.

Adams Jr. et al. indicate that materials with small mean atomic mass are best suited for light-weight radiation shielding, specifically because of the reduced secondary radiation created in such materials [123].
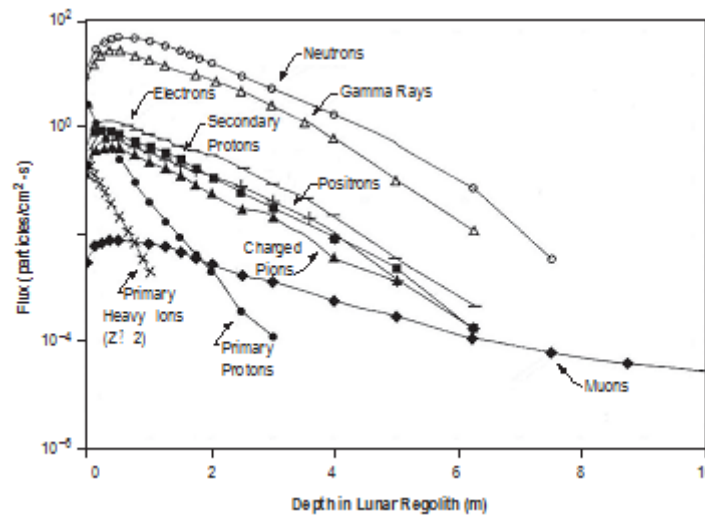
Figure 32: Primary GCR and produced secondary radiation flux in lunar regolith [Source: 123]

3.6.5. Impact on the Lunar Greenhouse Module design

Barring some active radiation shielding methods which are under investigation, the only option for reducing the radiation within the greenhouse to acceptable levels is adding more material to the structure.

The radiation dose from radioactive elements within the lunar regolith is less than 0.1% of the 500 mSv/year limit set by ESA and as such will have a negligible impact on the design. Albedo from the lunar surface will have a minor design impact, since the radiation shielding will be designed to cope with the direct radiation.

Lunar radiation will have a minor impact on the GHM design. The dose from radioactive elements is only a fraction (>0.1%) of the 500 mSv/year limit. The albedo from the lunar surface is small compared to the direct radiation.

Solar wind particles have comparatively low energies and can be stopped with small amounts of radiation shielding material. SEP have energies which can be 1000 times higher than solar wind particle energies. As a result the penetration depth of these particles increases to the order of several centimeters. Extreme SEP-events may occur which require greater shield thicknesses.

The main design drivers are GCR and secondary radiation. GCR particles can have energies of up to several hundred GeV and which will penetrate meters of radiation shielding. High density shielding with heavy elements is preferred, since this increases the number of particle-material interactions and hence the rate of energy loss of the particles. However, as secondary particles are produced as a result of particle-material interactions, materials with small mean atomic mass (e.g. hydrogen) are preferable to limit the amount of secondary radiation.

3.7.   Micro-meteoroids and Debris

As discussed previously, the lunar surface has been shaped predominantly by impacts of large and small bodies. Furthermore, observations of the lunar craters have indicated that in some cases lunar ejecta, mass expelled as a result from the initial impact, was responsible for the formation of additional craters nearby.

3.7.1. (Micro-)Meteoroids

No large scale meteoroids are expected to impact the Moon in the present day, but there are still a great number of smaller micro-meteoroids which strike the lunar surface and which can potentially damage structures placed there.

In [84], Taylor indicates that some 300 craters/m^2*year can be expected, with a crater diameter of 10 µm. Smaller craters will occur even more frequently, while larger impacts happen only on occasion. [124] indicates an average meteoroid velocity of 20 km/s and a mean density of 0,5 g/cm^3. In [86], a non-continuous function for the mass density of meteoroids is mentioned, with values ranging from 2,0 to 0,5 g/cm^3 depending on the mass of the object. Furthermore, based on the model presented in [125] it can be determined that the flux rate for 1 mm micrometeoroids is about 1,35*10^{-3}/m^2*year. In [126], observations of the impact craters on the Long Duration Exposure Facility (LDEF) satellite are used to predict the lunar micrometeoroid flux. Figure 33 compares the results with other models, by plotting the cumulative flux at the lunar surface as a function of micrometeoroid mass.
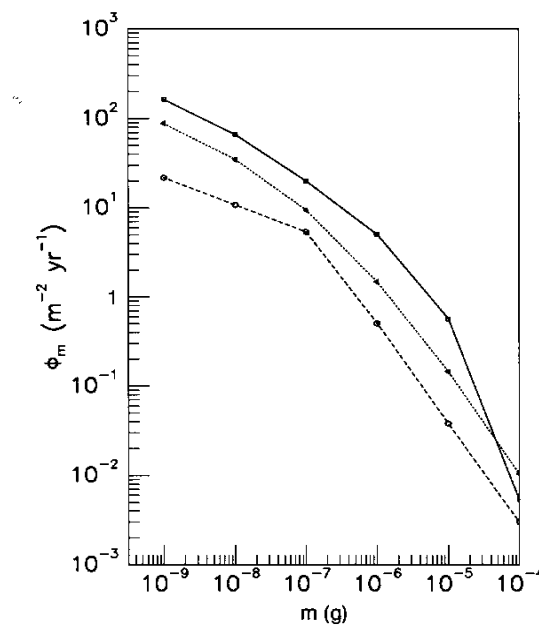
Figure 33: Cumulative lunar micrometeoroid flux versus mass for three different models [Source: 126]

3.7.2. Ejecta

Figure 34 indicates expected ejecta particle flux versus mass for different velocities. Comparing the fluxes in Figure 33 and Figure 34, it can be seen that the ejecta flux for a given particle size will be significantly (up to 10^6 times) higher than the micrometeoroid flux. However, only a fraction of lunar ejecta will be in the vicinity of the lunar greenhouse module, since only a limited amount of micrometeoroids will strike the lunar surface near the structure. Furthermore, the particle velocity is limited to, at most, a few kilometres per second, meaning the energy of each particle will be much lower than the energy of a micrometeoroid. As such, it is expected that the micrometeoroid shielding of lunar structures should provide sufficient protection against lunar ejecta as well.
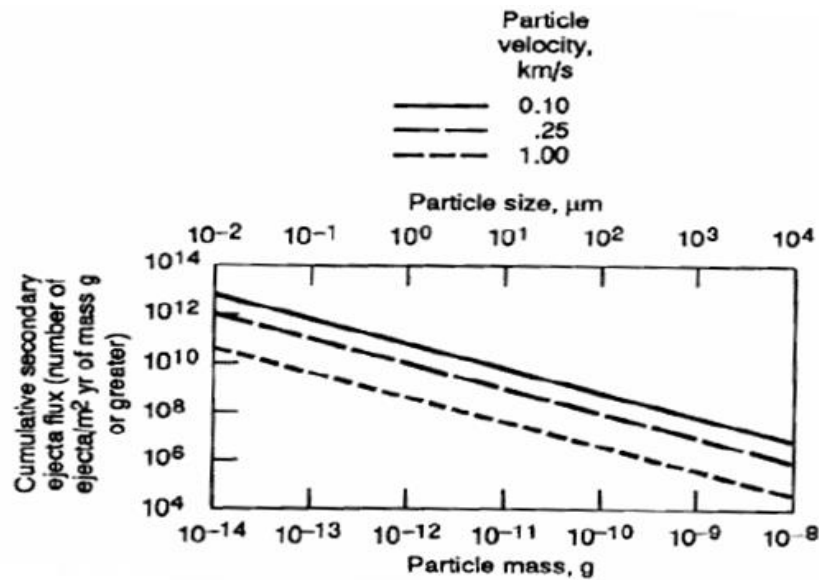
Figure 34: Lunar ejecta flux versus particle mass [Source: 127]

3.7.3. Impact on the Lunar Greenhouse Module design

The (micro-)meteoroid and lunar ejecta flux will impact the design of the MMOD shielding subassembly of the lunar GHM structure. The average number of impacts along with the size and velocity of the particle will determine the number of material layers which will be needed, as well as the distance between the layers, among other things.

3.8. Summary

In this chapter the environmental conditions on the Moon were investigated and the impact on the design of the lunar GHM was determined. Table 4 presents an overview of the different environmental factors with their characteristics as well as their impacts on the system design.

Table 4: Lunar environmental factors and their design impact

Environmental factor	Characteristics	Impact on system design
Topology	• Significant height variation between different points on the lunar surface • Lava tubes have been identified on the Moon	• Local surface topology may require site preparation • Presence of lava tubes may result in reduced design requirements (e.g. radiation shielding)
Regolith composition	• Layer of dust on top of several metres of bedrock. • Exposure to 'space weather' has resulted in changes to regolith properties	• Sufficiently thick regolith layers can be used as radiation and MMOD shield. This might require a design change to the structure to keep the regolith in place.
Seismic activity	• About 500 quakes per year, with highest magnitude between 5 and 6 on the Richter scale	• Negligible impact because of limited quake strength as well as energy dispersion within regolith
Gravity	• Average gravitational acceleration on the Moon is 1,622 m/s^2.	• The presence of a significant gravitational acceleration affects the motion of astronauts and, as a result, the design of airlocks and doors.

Environmental factor	Characteristics	Impact on system design
	• Mascons (Mass concentrations) result in local increases in gravity, despite topological features	• Deployment system should be designed to overcome gravity. • Reduced gravity (w.r.t. Earth) results in reduced loading, which may lead to structural mass savings
Magnetism	• Weak magnetic field is present due to crustal magnetism • Local mini-magnetospheres have been found, which provide limited radiation shielding	• The lack of (significant) magnetic field means that the structure should contain its own radiation shielding system
Lunar atmosphere	• Surface bounded exosphere with night-time concentrations between 10^5 and 10^6 molecules/cm^3	• Atmospheric contamination concerns might result in more stringent requirements on outgassing and leakage rate
Surface charging	• (Negative) potentials of 10^3 V can occur during SEP-events	• Structure will require grounding or the use of (special) coatings and regolith shielding
Lunar dust	• Regolith particles smaller than 100 μm. Adheres to surfaces and causes degradation of spacesuits and equipment.	• Dust mitigation strategies will need to be incorporated into the design (e.g. compartmentalization) • A dust removal system will be needed
Illumination	• Areas on the Moon may be illuminated up to 89% of the time, while others are never illuminated	• Natural lighting is not sufficient to meet the plant growth requirements, hence artificial or hybrid lighting will be required, resulting in additional mass and system size
Temperature	• Surface temperatures may vary from about 25 K in permanently dark area to >400 K in illuminated areas.	• A thermal protection system (e.g. MLI, regolith) will be needed as well as active thermal control
Radiation	• Approximately 0,3 mSv/year from radioactive elements within the lunar regolith • A variable amount of radiation from the Sun (depending on solar activity) due to solar wind and solar flares • About 300 mSv/year from galactic radiation • Variable secondary radiation dose, depending on shielding material	• Radiation shielding and degradation properties will influence material selection for the structure design • The maximum allowable dose on Earth is 50 mSv/year for radiation workers, and 5 mSv/year for a normal person. ESA standards set a career limit of 1 Sv and a maximum radiation dose of 0.5 Sv/year to blood forming organs.

Environmental factor	Characteristics	Impact on system design
Meteoroids and ejecta	• The average flux rate for 1 mm micrometeoroids is about $1,35*10^{-3}/m^2*year$. • The average meteoroid velocity is about 20 km/s and the density is approximately $0,5 – 2,0\ g/cm^3$	• Impact magnitude and frequency will influence structural thickness and material selection

4. System Analysis of the Lunar Greenhouse Module

Before developing designs for a lunar GHM, it is necessary to define the requirements and constraints imposed on the design, specifically related to the GHM structure. Furthermore, the components and interfaces required for the eventual greenhouse design to function properly need to be determined through system analysis. Additionally, a number of assumptions are needed, to be able to start the design process. This chapter describes the design assumptions which have been made, as well as the system analysis and requirement analysis of the GHM.

4.1. Mission Analysis

When designing (the structure of) a lunar greenhouse, it is not sufficient to consider solely the tasks which will need to be performed once the greenhouse is operational on the Moon. A number of activities need to be completed before the lunar GHM is functioning, such as launching and landing, and neglecting to account for these steps can potentially cause requirements to be overlooked.

Thus, in this section, a brief overview of the various mission steps and their influence on the greenhouse structure design will be given:

Cargo vehicle-payload integration

The deployable greenhouse will be stored inside a cargo vehicle which will control the transfer from the initial injection orbit to the Moon and the subsequent landing on the lunar surface.

The greenhouse structure, in its stowed position, will need to be restrained within this spacecraft to prevent any damage from occurring during launch. Depending on the type of restraint mechanism, it may be necessary to incorporate some attachment points within the greenhouse structure. For example, the TransHab design had deployment straps which, in the stowed configuration, would be tied together using cord to restrain the structure [18].

Launcher-cargo vehicle integration

Connecting the cargo vehicle to the selected launcher will not impact the greenhouse structure design directly, though the type of launcher will have some impact.

Launch

Depending on which launcher is selected, the flight profile will be slightly different and the launch loads experienced by the stowed greenhouse will also vary. This could potentially have some impact on the structure, though it is likely to be minimal at worst.

Cruise

There may be some slight exposure to space weather, such as solar radiation, but this will be negligible compared to the lunar environment for which the greenhouse structure is designed. As such, no design impact is expected.

Landing

Landing on the lunar surface will result in some loads on the stowed greenhouse structure, but compared to the launch loads this will be minor. As such, no design impact is expected.

Transport

During the landing phase it is possible for dust and (small) rocks to be blasted aside, as happened during the landing of the Mars rover Curiosity. The dust and rocks could potentially impact any lunar infrastructure which is already present on the Moon at the time of landing, if the landing occurs in close proximity.

To prevent this, as well as to allow for inaccuracies in the landing position, the cargo vehicle should touch down on the lunar surface at a suitable distance from the lunar base. As a result however, it will be necessary to transport the stowed greenhouse structure to the eventual operating site.

By selecting (and designing) a proper transport vehicle and creating proper handling guidelines, the risk of damage due to transport can be made negligibly small. In that case, the transport phase should have no impact on the structure design.

Structure Deployment

Following the transport of the stowed structure to the desired location, it is time for deployment. Depending on the type of restraint mechanism used to keep the structure in the stowed configuration, some type of automated or manual release mechanism will be needed.

For automatic deployment, it will also be necessary for the stowed greenhouse to contain a deployment system, such as tanks filled with inflation gas and gas injection mechanisms. Following the initial inflation, the deployment system should ensure rigidization of the structure, through UV-curing of resin or one of the other rigidization techniques discussed in section 2.2.3.

The structure design and the deployment system will have significant mutual impact. If, for example, foam rigidization is used then the structure will need to be designed with an interior layer which can hold this foam. Conversely, depending on the greenhouse shape, the deployment system design will need to be altered.

Another part of the structure deployment could be the application of layers of regolith to the structure exterior. As mentioned in section 3.1.4, this might require the greenhouse structure to incorporate a system to hold the regolith in place.

Internal System Setup

The deployment of equipment inside the lunar GHM will have some design impact on the greenhouse structure. In multi-story structures for example equipment would need to be moved vertically which requires significantly more effort than horizontal movement.

The internal configuration will also impact the optimal location of interfaces, such as power cables and water feed lines, within the structure.

Lunar base-greenhouse integration

Once the greenhouse structure has been fully deployed and the equipment has been set up, the greenhouse needs to be integrated into the lunar base infrastructure. The greenhouse will be an essential part of the larger closed regenerative life support system as can be seen in Figure 35. It will be necessary to connect power cables and air ducts (among other things) running between other lunar base structures and the greenhouse.

It will be necessary to provide protection from the lunar environment if the interfaces run external to the structure. Alternatively, the structure could be designed such that these cables and other interfaces run along the interior of the structures, but this would result in some restraints on the placement of the different structures forming the lunar base.
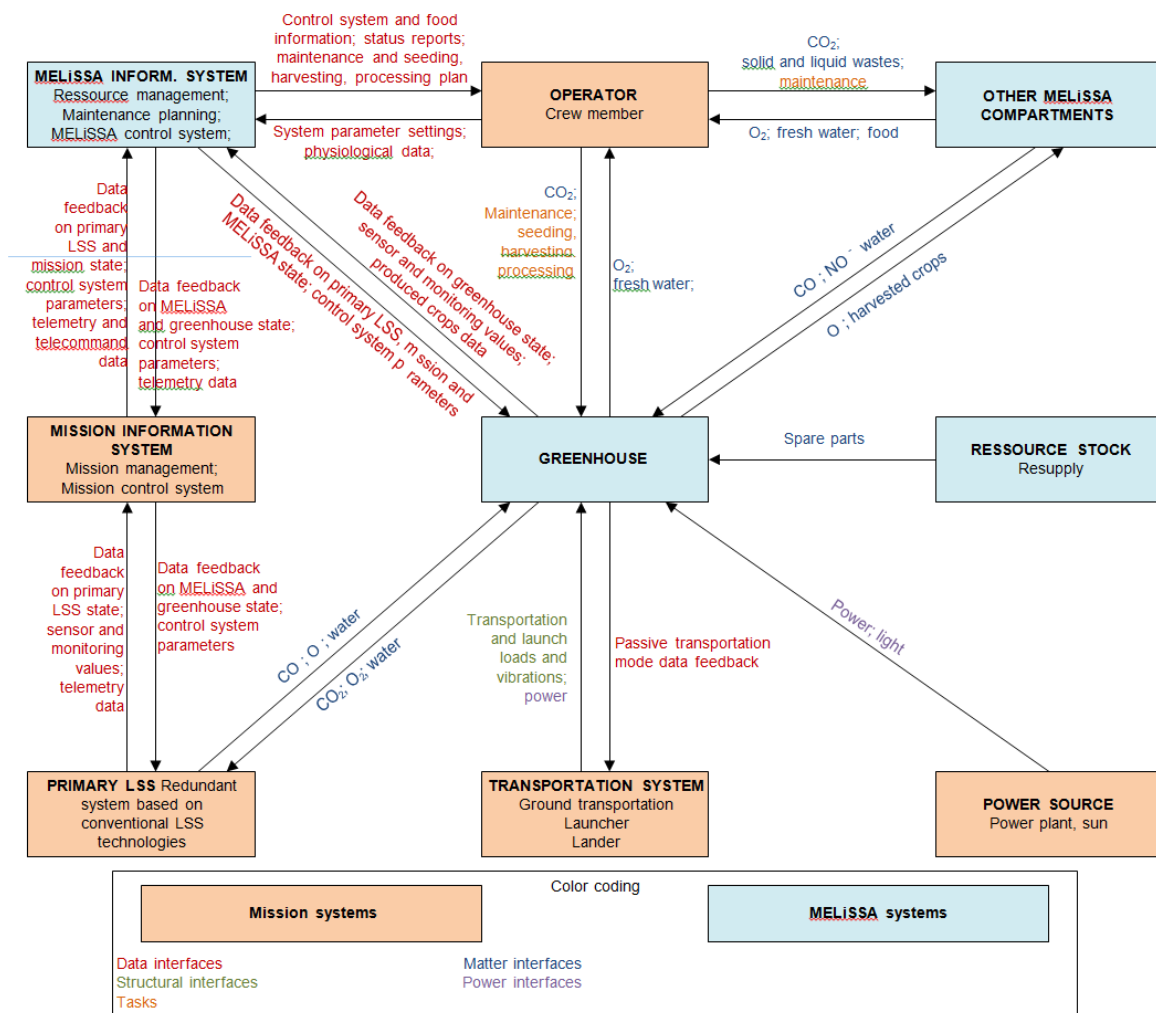
Figure 35: Greenhouse within a closed regenerative life support system [Source: Greenhouse module for space system Statement of Work. [128]]

Greenhouse operation

During the plant cultivation phase, the greenhouse structure will need to withstand the loads (mechanical, thermal) imposed on it, which forms one of the main design drivers. The structure will

also have to withstand the various environmental factors which were already discussed in chapter 3 of this report.

4.2.   Greenhouse System Analysis

As discussed briefly in 'Advanced Greenhouse Modules for use within Planetary Habitats' [129], there are a variety of plant factors which impact the design of a Grow Unit, such as air temperature and humidity, but also the dimensions of the various crop types. An eventual space habitat will require a database of optimal values for all relevant parameters for a wide variety of crops. At present, however, such knowledge is often incomplete and thus assumptions need to be made for design purposes, as can be seen in the next section (4.3).

The lunar GHM will need to fulfil a large number of functions in order to obtain and maintain ideal conditions for plant growth. By defining these functions and interfaces it becomes possible to indicate the (sub-)systems needed to fulfil the desired tasks, which provides information needed for the sizing and design of the GHM structure. The functions, interfaces, internal architecture and systems of the lunar GHM will be discussed in this section.

In the Statement of Work (SoW) document [128] for the "Greenhouse module for space system" project, it is mentioned that the lunar greenhouse should adopt the internal architecture and interfaces with the external habitat as illustrated in Figure 36.
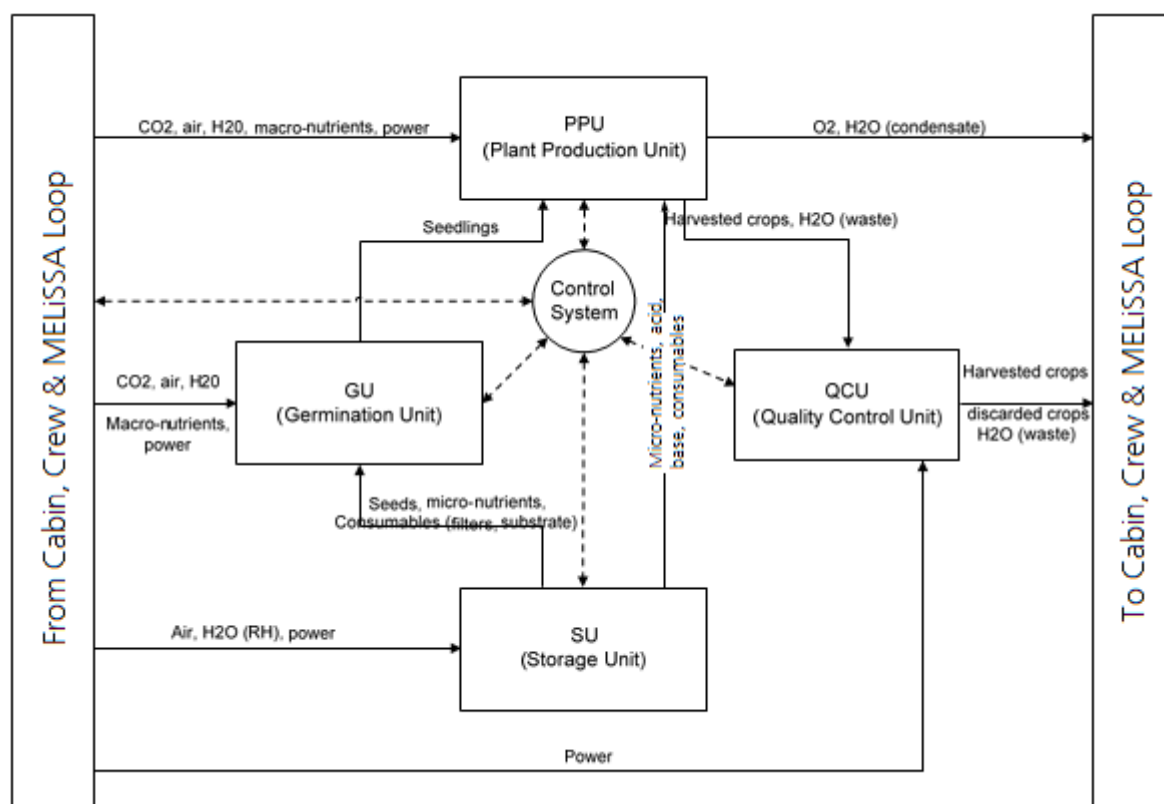
Figure 36: Internal architecture of the lunar greenhouse module [Source: Greenhouse module for space system SoW. [128]]

Based on this architecture and the mission analysis (section 4.1) and functional analysis (section 4.2.1), the configuration of the greenhouse is split into four segments (see Figure 37):

- Structure

The structure is the external shell of the GHM, separating the internal conditions from the harsh environment on the Moon. Included in the structure segment are the MMOD and radiation shielding, gas retention system, thermal protection system, load-bearing structure, interface connections and, possibly, airlocks.

- Deployment Module

The Deployment Module contains the tanks filled with inflation gas, a gas injection system and possibly a rigidization system. The inflation gas should be such that, upon inflation, the internal atmosphere matches the desired composition of the air in the GHM as defined in the SoW. If a rigidization system is required, whether passive or active, then a rigidizable material will need to be incorporated into the structure design.

- Grow Module

The Grow Module is the section of the greenhouse in which the plants are cultivated. This section will contain the Germination Unit and Plant Production Unit indicated in Figure 36, but will also consist of some support equipment, such as sensors and air ducts.

- Service Module

The Service Module encompasses all the support systems needed for plant cultivation, such as the Storage Unit, Quality Control Unit and the Control System from Figure 36, though, as mentioned, some of the components may also be situated within the Grow Module.
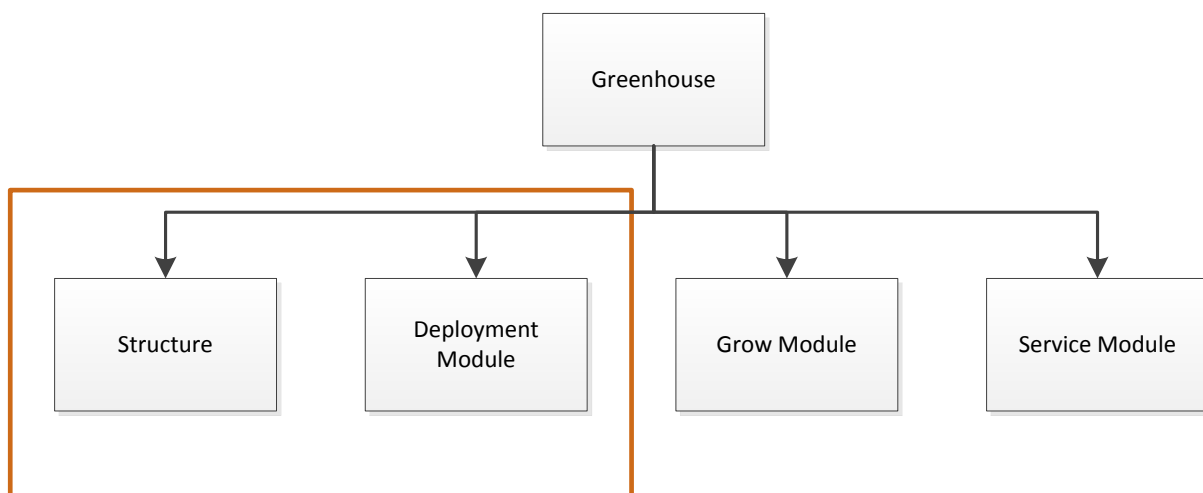
Figure 37: Greenhouse configuration segments and thesis system border

The brown-lined frame in Figure 37 denotes the system borders for this thesis work. As can be seen, only (part of) the structure and the Deployment Module will be considered. Some aspects of these two segments, such as the airlocks, will not be investigated in detail; instead certain assumptions will be made regarding their characteristics (see section 4.3).

4.2.1. Functional Breakdown Analysis

Figure 35 and Figure 36 provide an overview of the resource flows between the different compartments of the greenhouse and the life support system. Neither of the diagrams covers the specific tasks and functionalities of the various compartments however.

To ensure that the final greenhouse design can complete the desired objectives, it is necessary to analyse the required functionality of the system. Based on the functions which need be performed to accomplish successful plant cultivation, it is possible to define subsystems which will handle specific sets of functions and to investigate the components which should be used.

A functional analysis as described above is commonly presented in the form of a Functional Breakdown Structure (FBS) or Functional Flow Diagram (FFD). Starting from the top level function of the greenhouse, which is the successful cultivation of food crops, it is possible to define the lower level functions which are required to achieve this. These lower level functions are then broken down to even smaller tasks, until the desired level of detail is achieved.

The Functional Flow Diagram for a lunar GHM is shown in Figures 38-40. The top row of boxes in the FFD represent the top level functions which need to be fulfilled to achieve mission success. For the greenhouse, these top level functions represent the start-up, the operation and the end-of-life phases.

A number is given to each function, which allows for tracing of the different functions. For example, the function *Deploy Greenhouse* has number *1.2*. This means that it is the second function which is carried out as part of the higher level function *1.0 Perform Pre-operation phase activities*.
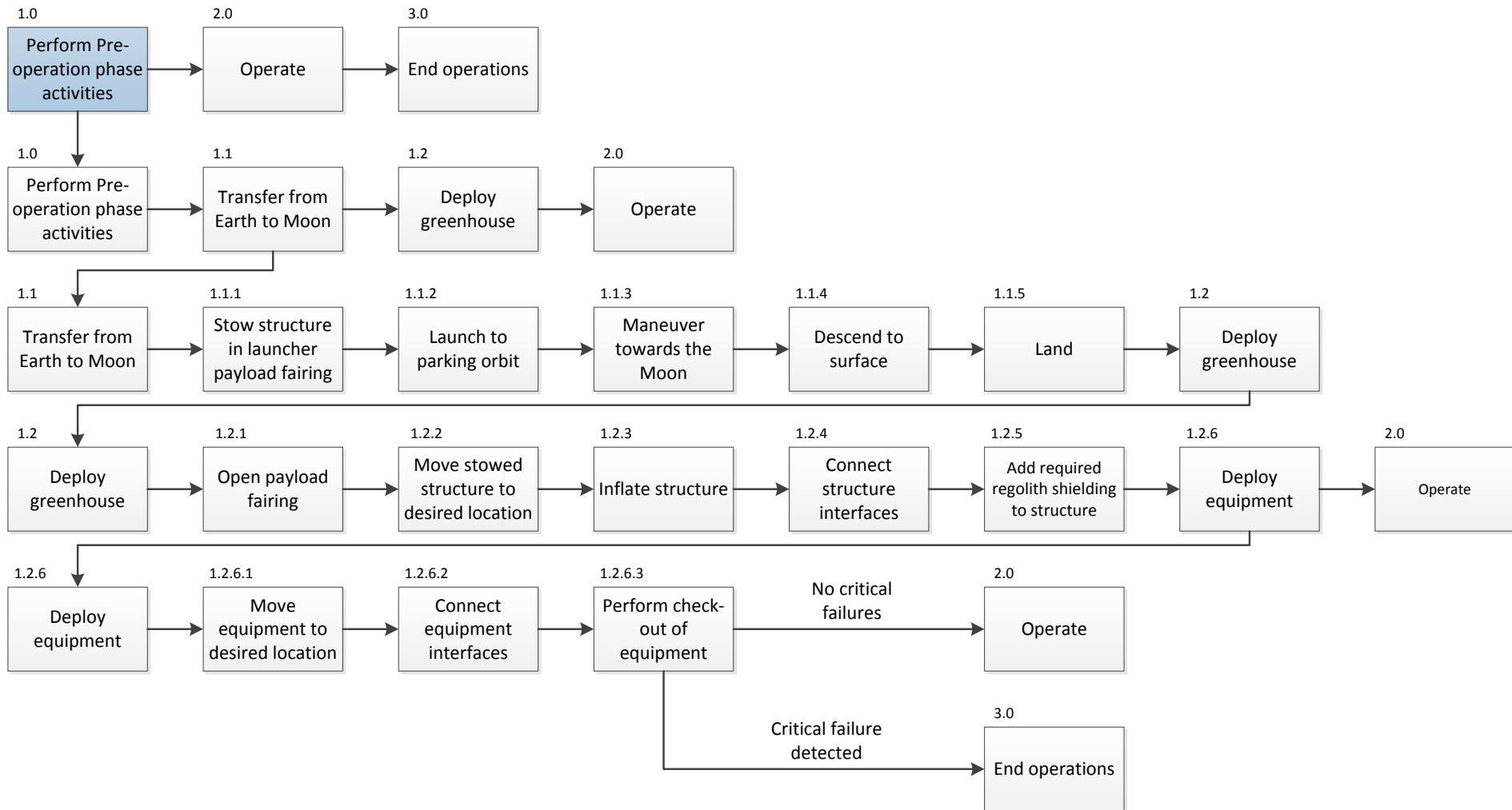
Figure 38: (Part 1 of a) Functional Flow Diagram of a lunar GHM
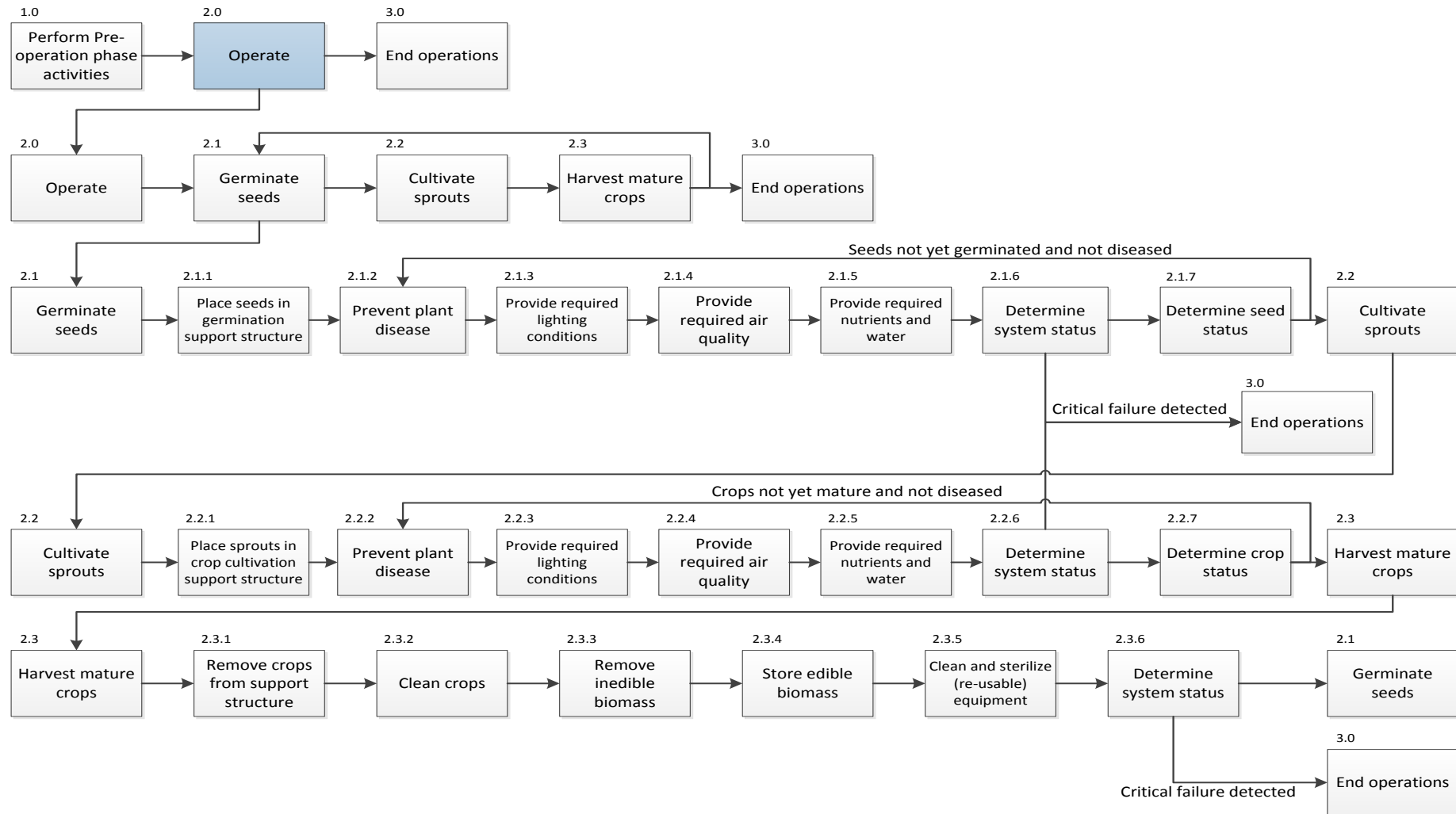
Figure 39: (Part 2 of a) Functional Flow Diagram of a lunar GHM
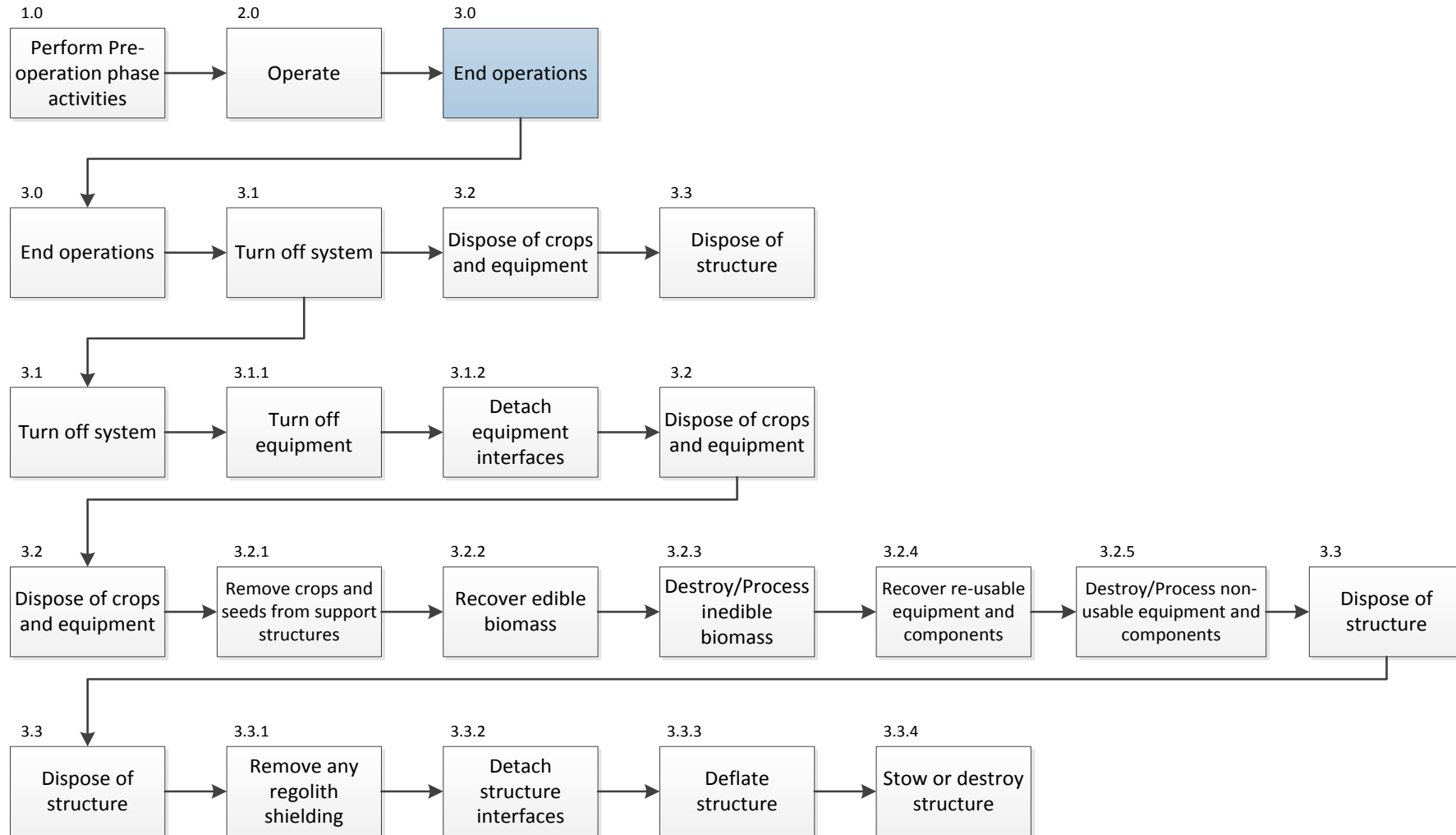
Figure 40: (Part 3 of a) Functional Flow Diagram of a lunar GHM

The FFD provides a straightforward method of determining and depicting the different functions which need to be performed and the sequence of events. When breaking down the functionality to a low level, especially for complex systems, the FFD can become quite large and chaotic, making it more difficult to quickly identify all the different functions.

An alternative graphical representation method is the Functional Breakdown Structure (FBS), which presents the functions in the form of an AND-tree. This means that all the lower level functions need to be fulfilled in order to achieve the higher level functions.

Figure 41 shows (part of) the FBS for the lunar greenhouse module. To limit the required space in the diagram, this part of the FBS only shows the functions related to crop cultivation. It does not address the functionality required for launch, deployment or end-of-life disposal.

The second level of function breakdowns is assigned a colour based on the subsystem which is expected to fulfil that function. A legend is given in the lower left corner of the graph. The functions marked in pink and assigned to "external" may be fulfilled either on Earth or on the Moon. For example, power will be supplied from the lunar base, while harvesting tools and seeds are likely placed within the greenhouse payload before launch.

To illustrate the possibility of breaking functions down even further, a third level function breakdown is shown for the function *Determine delivered lighting conditions*. Again, to limit the size of the diagram this was not done for all second level functions.
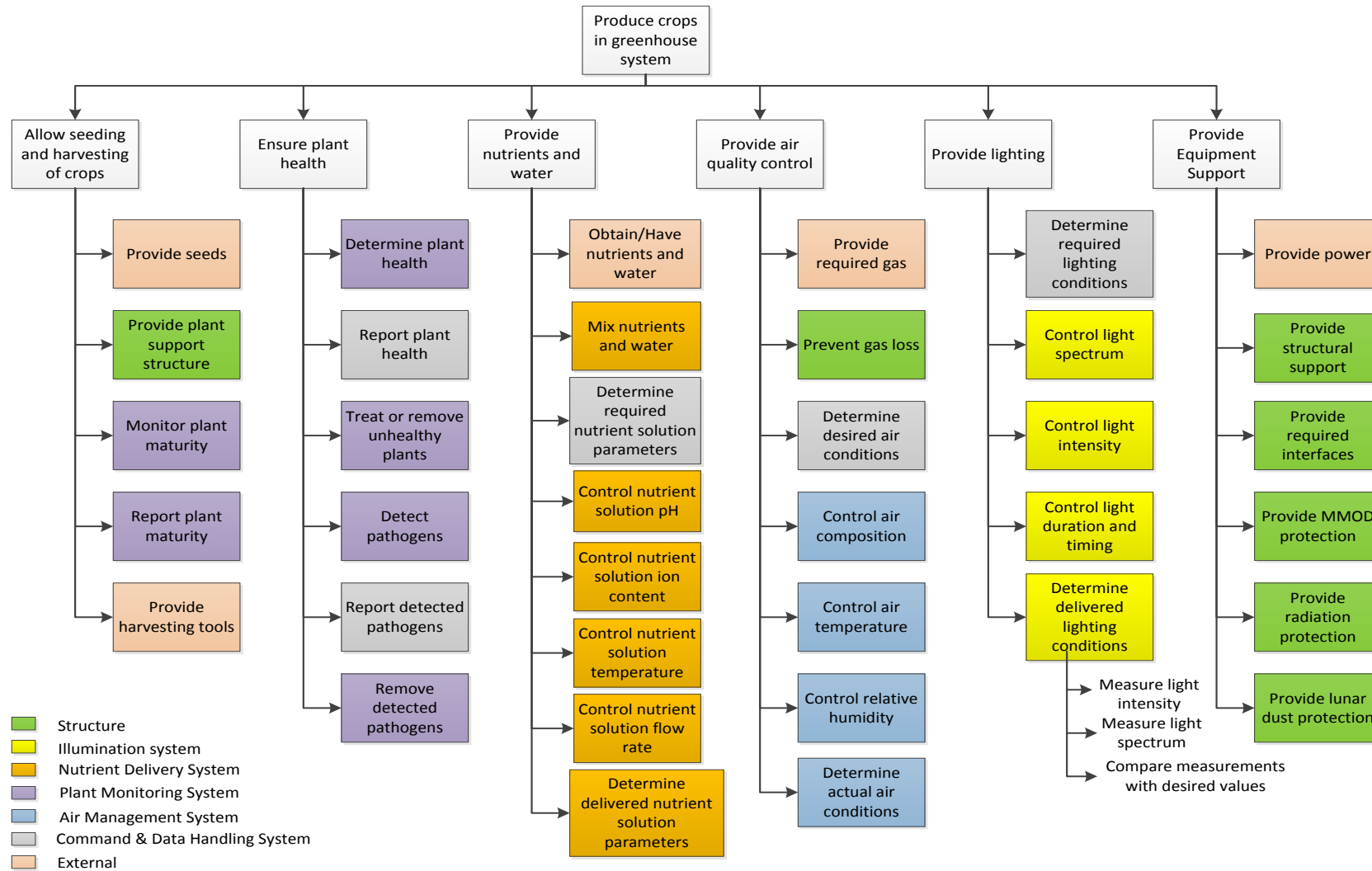
Figure 41: Functional Breakdown Structure of a lunar GHM

4.2.2. Interface Definitions

As mentioned before, it is possible to define subsystems which will perform a specific subset of the functions identified in the FFD or FBS. In Figure 41, different functions have been given colors based on the subsystem they belong to. A legend can be found in Table 5 below.

Table 5: Legend for Figure 41 and Figure 42

Subsystem	Color
Structure	Green
Nutrient Delivery System	Orange
Plant Monitoring System	Purple
Air Management System	Blue
Illumination System	Yellow
Command & Data Handling System	Grey
External system (environment, astronauts, etc…)	Pink
Plants	Brown

The Nutrient Delivery System will be in charge of the delivery of nutrients and water, while the Plant Monitoring System will monitor the plants to detect any diseases and to determine the required amounts of water and nutrients. The Command & Data Handling System will collect data on the plant health and maturity, as well as the system performance and provide data on the required conditions for optimal crop cultivation.

Obviously these systems would need to communicate in some way, since the data gathered by the Plant Monitoring System needs to be available to the Nutrient Delivery System to allow it to function properly. Thus, the Plant Monitoring System will need to send data to the Command & Data Handling System which processes it and sends commands to the Nutrient Delivery System.

Such interdependencies between systems, also known as interfaces, are often shown by means of an N^2 chart [130] and Figure 42 provides such a chart for the lunar GHM and its subsystems.

For clarity, the external environment has been split into the lunar infrastructure with which the lunar GHM has to interface, the astronauts operating and maintaining the system and the space environment (e.g. radiation and meteoroids) acting on the lunar GHM.

	Structure									
Structure	Housing	Housing	Housing	Housing	Housing	Airlock, cable and piping interfaces	Housing, radiation protection		Housing, radiation protection
Corrosion	**NDS**		Waste heat		Nutrient solution data				Nutrients, water
		PM	Waste heat		Plant and disease data				
			AMS		Air composition & quality data	Air composition & quality control	Air composition & quality control		Air composition & quality control
			Waste heat	**IS**	Lighting data			Waste heat	Light
Plant size data	Requests for data, commands	Requests for data, commands	Requests for data, commands	Requests for data, commands	**CDHS**	Warnings, Harvesting prompts, Data	Warnings, Harvesting prompts, Data		
Airlock, cable and piping interfaces	Power, nutrients, water	Power	Power	Power	Power	**Lunar Base**	Housing, radiation protection		
Mainte-nance	Mainte-nance	Mainte-nance	Mainte-nance	Mainte-nance	Mainte-nance	Mainte-nance	**Astronauts**	Lunar surface operations	Seeding, harvesting
Radiation, MMOD, dust					Radiation, MMOD, dust	Radiation, MMOD, dust	**Environ-ment**	Radiation, MMOD, dust
		Plant data	Trace gases, water, oxygen			Inedible biomass	Food		**Plants**

Legend:
- Structure
- Illumination system
- Nutrient Delivery System
- Plant Monitoring System
- Air Management System
- Command & Data Handling System
- External
- Plants

Figure 42: N² chart presentation of interfaces for the lunar GHM

4.2.3. Subsystem Description

Based on the tasks which need to be performed in the greenhouse, an overview can be made of the likely equipment which is needed to fulfil the tasks. As an example, consider the supply of nutrients and water to the various plants. To accomplish this, it is necessary to have tanks to store the water and nutrients, a mixing system which precisely regulates the concentrations of the different nutrients, sensors to detect the various properties of the nutrient solution and many other components.

In this section a description will be given of the different subsystems. Some rough dimensions will be estimated for the systems in chapter 6, to allow sizing of the structure.

Structure

The structure subsystem of the lunar GHM has to provide protection against the lunar environment, but it also has to provide the housing for the equipment as well as interfaces to attach to the lunar base structures.

No windows will be present in the greenhouse module to prevent natural light from entering and changing the actual conditions experienced by the plants from the desired conditions. Some other cut-outs will be required however for such things as fans and ducts, which will allow air flow from and to other areas of the lunar base. Airlocks will be required to allow astronauts to enter and exit the structure from the outside and to ensure that the rest of the base is not affected in case of pressure loss or contamination (e.g. fungi, disease) in the greenhouse. Additionally, mechanisms will be needed to ensure the automated deployment of the equipment into the desired configuration upon deployment of the outer structure.

The structure subsystem does not only comprise structure segment defined earlier though. It also consists of the secondary structure which is needed to hold the seeds and plants as they grow, which is part of the Grow Module.

For these functions, a plant cultivation approach using Grow Lids, Grow Pallets, Germination Units and Grow Units will be used. A Grow Lid is in essence a thin, rigid plate with a number of holes which serve to hold seeds or plant stems (within seed nets or pads). The spacing of the holes as well as the size is dependent on the morphological parameters of the plants, meaning that each crop will have a specialized Grow Lid. Aside from holding the seeds and plant stems, the Grow Lid divides the root zone and the shoot zone of the plants. The possibility of incorporating sensors and parts of the Nutrient Delivery System within the Grow Lid (see Figure 43) has been investigated by the author during earlier work at DLR Bremen.

The Grow Lids, filled with seeds, are placed in a Germination Unit. This is an enclosed structure with LED panels, nutrient solution supply and air management system, which is capable of providing the exact conditions needed for germination of the seeds.
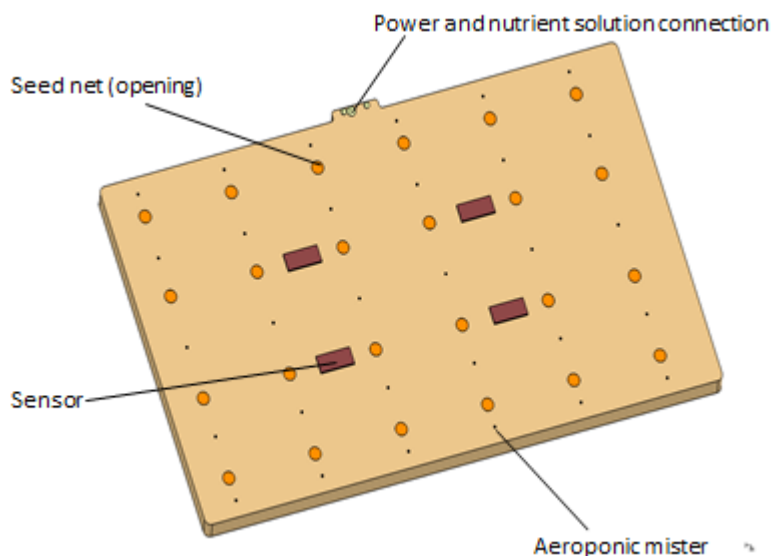
Figure 43: Grow Lid

Upon germination of the seeds, the Grow Lids are retrieved from the Germination Unit and placed on a Grow Pallet. The Grow Pallet provides additional structural support to carry the increasing weight of the growing plants along with an opaque, height-adjustable root zone section. The Grow Pallet is designed to be outfitted with a removable module containing a dedicated Nutrient Delivery System, including a small pump and accumulator tank, as well as some sensors (see Figure 44). The benefit of having such a system for each Grow Pallet is that it allows precise control of the nutrient solution delivered to each set of plants. The modular approach of the Grow Lid, Grow Pallet and NDS module facilitates the cleaning and sterilizing of the equipment after crop harvesting, which is needed to prevent or at least reduce disease and fungi growth.
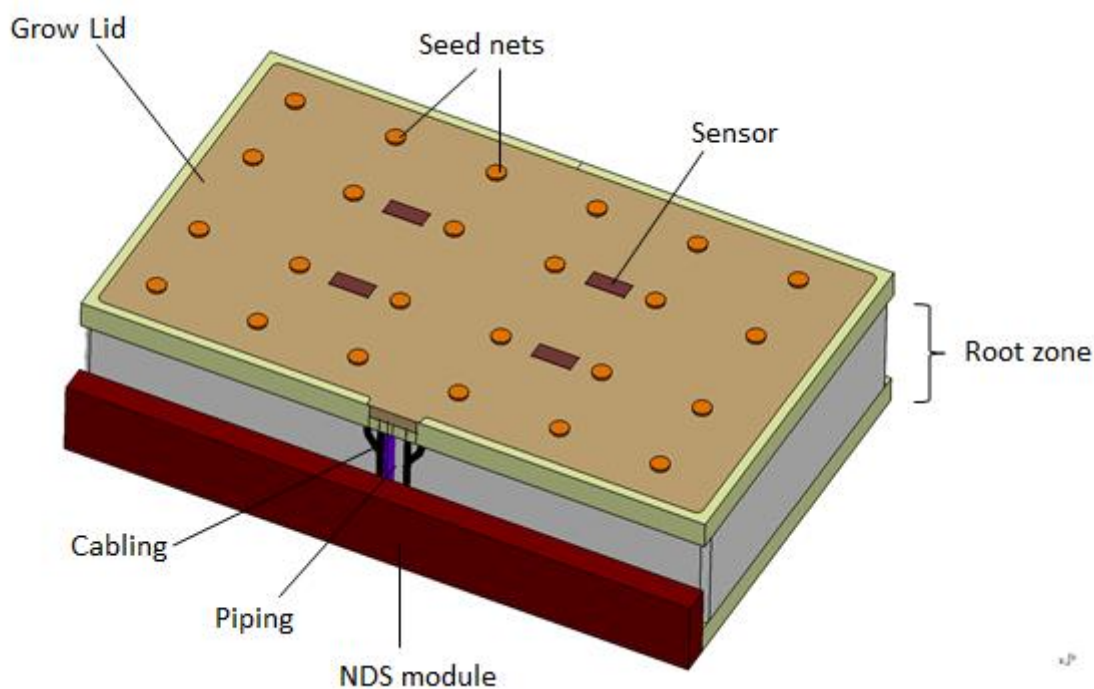
Figure 44: Grow Pallet with Grow Lid and NDS module

Once the Grow Lid has been placed on the Grow Pallet and all the interfaces have been properly connected, the system is placed within a Grow Unit. The Grow Unit, similar to the Germination Unit is an enclosed structure which provides lighting and air management for a number of Grow Pallet/Grow Lid assemblies and houses some additional NDS and power supply infrastructure.

The described approach has been investigated in past studies at DLR Bremen and because of this, it will be applied here. Additional development efforts will be needed to find the best configuration and to develop a prototype. Furthermore, a trade-off between different cultivation approaches, such as the cable culture approach of the University of Arizona, will be beneficial for future studies, but this is outside the scope of this work.

Illumination System

The lighting conditions needed for the optimized germination and cultivation of the different crops will be provided by the Illumination System.

Customized LED panels will be used to provide the exact light spectrum which is needed by the plants at each phase of their life cycle. The panels will have a variable intensity to accommodate the changing photosynthetic photon flux (PPF) demand of the plants over their life. Using digital timers the panels will be kept on predefined day/night cycles to allow for maximum edible biomass yield. The heat from the LED panels will be transported away using a liquid coolant-based heat exchanger system along with some heat dissipating radiators.

The lighting conditions within the Greenhouse will be designed specifically for plant cultivation. When the astronauts are working within the structure, it will be necessary to provide them personal lamps which emit a light spectrum more suitable for humans.

Nutrient Delivery System

The assumption was made that the plant cultivation in the lunar GHM will be done using aeroponics on account of the higher biomass yield and lower resource consumption. To further develop the technologies needed for a fully closed life support system, it is assumed that the aeroponic system which is used will be closed-loop, meaning that waste water is recovered and reused.

A schematic of such a system can be seen in Figure 45, showing the different components which would be needed. The actual system build-up will be slightly altered with respect to the architecture from the figure.

For example, each Grow Pallet/Grow Lid assembly will have its own nutrient solution tank, accumulator tank, digital timer and pump, as well as associated piping and spray jets. Excess solution which is sprayed into the root zone of a Grow Pallet will be collected and flows back into the Grow Pallet nutrient solution tank.

If a nutrient solution tank is nearly empty, or the parameters of the solution (pH, EC, etc…) deviate too much from the baseline value, a warning will be generated and the nutrient solution will be replaced with a new solution mixed by a central mix computer station.

Additionally, piping and assorted infrastructure will be needed to allow the flow of nutrients and water from other compartments of the lunar base to the lunar GHM.
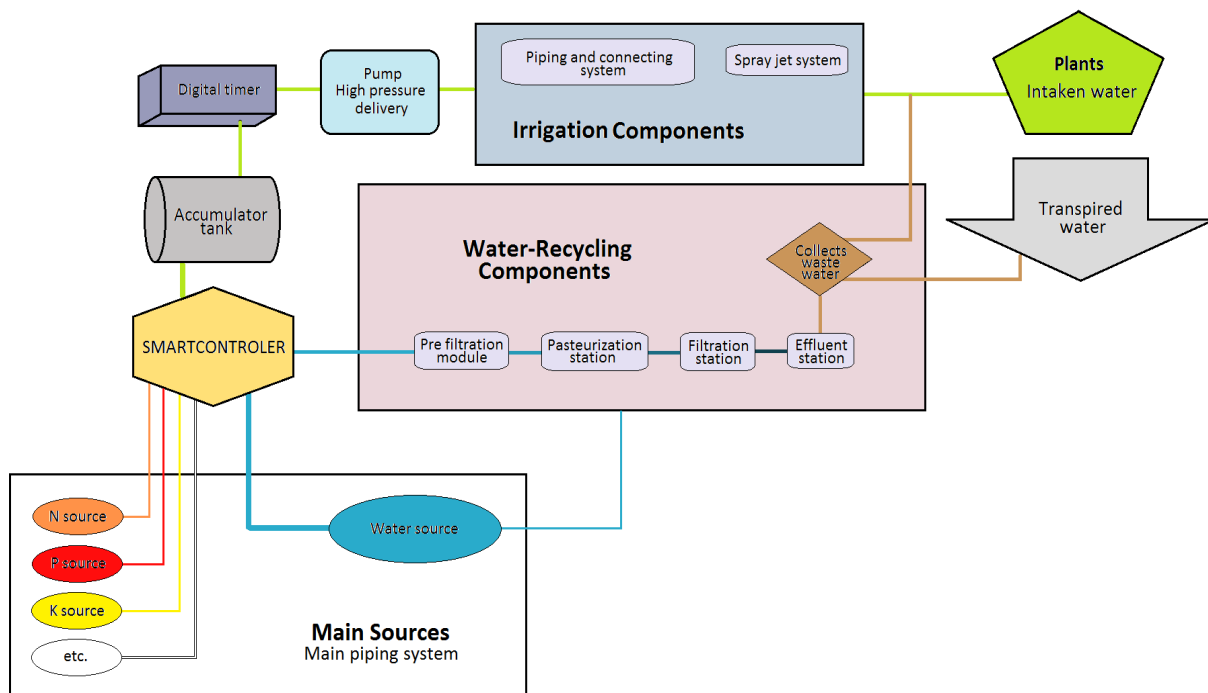
Figure 45: Schematic of the components of a closed-loop aeroponic system [Source: 131]

Plant Monitoring System

The Plant Monitoring System is responsible for health monitoring of the crops, as well as detection of diseases, fungi and other pathogens. Health monitoring is necessary to determine whether the plant has received the proper amounts of nutrient solution and to prevent crop loss due to disease.

Plant health monitoring systems are currently in the early stages of development. Sensors are used to observe crops in a variety of spectra (e.g. VIS, IR) and the data is stored on computers. Based on experiments a database will need to be created which contains the plant response to an off-nominal situation, for example changes in leaf size or coloration as a result of a lack of nitrogen or some other nutrient.

More work is also needed to rapidly and reliably detect pathogens which could adversely affect plants and to identify diseased plants so that these can be removed before the disease can spread.

Air Management System

The composition of the air, the temperature and the relative humidity (RH) are all crucial aspects of an environment in which both humans and plants need to survive and thrive. Since plants absorb CO_2, while releasing oxygen, water and trace gases into the air, these parameters all vary over time.

The Air Management System is needed to counteract these deviations from the desired state, through dehumidifying the air, filtering out trace gases and circulating the air throughout the lunar base. The dehumidification system involves cooling of the air until water condenses. This water should be caught and recycled in the NDS.

Command and Data Handling System

Most, if not all, of the processes within the lunar GHM will be automated. Lighting will be done based on a predefined day/night cycle, which will be controlled using timers. The intensity and spectrum of the light will be adjusted by matching data on the current maturity of the plant with a database indicating the optimal conditions of a plant at each phase of the life cycle.

Similarly, the nutrient delivery will be controlled using timers. Automated signals will indicate insufficient or inadequate nutrient solution, prompting the creation of a fresh mix by the nutrient mix computer station.

A sophisticated command and data handling system will be needed to receive and process all the incoming data from the different processes which are running within the GHM and to generate and distribute commands.

Additionally, a large database will need to be developed containing information on the optimal growth conditions for each plant at each level of maturity as well as the plant response to off-nominal conditions (e.g. nutrient depletion, disease).

Additional

Aside from the above described subsystems and their respective components, there are a number of other items which will be needed, such as storage units and seeds, which do not belong to any of the subsystems.

For the Deployment Module discussed earlier, for example, tanks will be needed to hold the inflation gas. Furthermore, a mechanism will be needed to restrain the structure when it is in its stowed configuration within the cargo vehicle. Additionally, a gas injection system and a rigidization system will be needed.

It was also mentioned earlier that airlocks would be needed in case of pressure loss in the greenhouse, or if fungi and other contaminants were detected. A system will be needed to remove diseased plants and sterilize all areas of the greenhouse which might be exposed to such pathogens. A similar system will be needed to prevent dust build up within the greenhouse and/or to remove dust once it has reached a given threshold concentration. Additionally, equipment will be needed for the harvesting and processing of mature, healthy crops.

4.3.   Design Assumptions

A lunar greenhouse module which is designed to operate as part of a larger lunar base will have a design which differs significantly from a stand-alone lunar greenhouse. A lunar base would be able to provide power and other resources, while a stand-alone greenhouse would need to contain or provide such things independently. Similarly, other factors will impact the design of a greenhouse and its structure.To narrow the design space, a number of assumptions are made. These assumptions are listed below, along with a short rationale.

4.3.1. Lunar base assumptions

Assumption 1: It is assumed that power will be supplied to the greenhouse module from other parts of the lunar base.

Justification: *The 'short' travel time between the Earth and the Moon makes it feasible to set up an initial manned base which can operate without in-situ food production. Such a base will inevitably contain a power generation system.*

Assumption 2: It is assumed that nutrients will be supplied to the greenhouse module from other parts of the lunar base.

Justification: *It is likely that a facility capable of extracting nutrients from human and plant waste will be constructed on the Moon, to further develop closed loop life support systems. Additionally, regular deliveries of supplies from the Earth could contain nutrients, if necessary.*

Assumption 3: It is assumed that astronauts or robots within the base will be involved in the plant cultivation process and carry out such actions as seeding and harvesting and cleaning or sterilizing of equipment.

Justification: *Robots are already being developed for use in greenhouses on Earth. It is likely that such robots could be built and sent to the Moon to operate a lunar greenhouse. Astronauts have already been growing plants on the International Space Station and could do so on the Moon as well.*

4.3.2. Greenhouse assumptions

Assumption 4: The lunar greenhouse module design should meet the requirements and constraints listed in the "Greenhouse module for space system" Statement of Work [128].

Justification: *The thesis work is intended to tie into the larger framework of research and development being carried out at DLR and ESA.*

Assumption 5: It is assumed that the lunar greenhouse module will be located on the lunar surface, rather than placed in a subsurface lava tube.

Justification: *The mapping of the locations and sizes of lava tubes on the Moon is still to be done. As such, it is uncertain whether or not a lava tube of sufficient size will be available in the near vicinity of the desired lunar base location.*

4.3.3. Additional assumptions

Assumption 6: It is assumed that plant cultivation will be done using the aeroponics method.

Justification: *Sources [132,133] indicate that aeroponic plant cultivation allows higher yields than other cultivation methods, with less resource consumption.*

Assumption 7: It is assumed that the plant yield data from the NASA Baseline Values and Assumptions Document [134], is based on hydroponic cultivation.

Justification: *From [135] it was found that the NASA experiments were typically carried out using hydroponic cultivation methods.*

Assumption 8: It is assumed that aeroponic yield of edible and inedible biomass will be a factor of 1,4 higher.

<u>Justification:</u> *According to* [132,133]*, aeroponic yield may be up to 70-80% higher than other plant cultivation methods. A factor of 1,4 is thus a conservative estimate of the yield increase.*

4.4.   Requirements Analysis

This section of the report will focus on the requirements and constraints which are placed on the design of the lunar greenhouse module. For defining the requirements on the structure of the greenhouse a so-called Requirements Discovery Tree (RDT) was developed.

The RDT splits requirements into two branches: constraints and functional requirements. Similar to the FBS, the RDT is an AND-tree, meaning that all of the lower level requirements are needed to fulfil the top level requirements. It provides a convenient graphical tool to trace the origin of a given requirement. This requirement traceability is needed to prevent lower requirements from being applied to a design when there is no actual reason behind it. Furthermore, if a lower level requirement can be rationalized, but there is no associated higher level requirement, then that indicates that there are likely some requirements missing.

As with any of the system engineering tools used in this chapter, it should be used only in so far as it is useful. For the preliminary design presented in this report, for example, it would not make any sense to derive requirements on the precise manufacturing tolerances for various sections of the structure.

The RDT which was created for the structure of the lunar GHM can be seen in Figure 46 (Functional Requirements) and Figure 47 (Constraints). The complete, elaborated requirement lists can be found in Appendix C. These lists contain the top level requirements for the lunar GHM, see Table 6, and the derived requirements for the GHM structure, for a total of 52 requirements.

Table 6: Top level requirements for the lunar GHM

Code	Requirement	Rationale
GHM.1	GHM shall successfully be delivered to the surface of the Moon	*To ensure the mission*
GHM.2	GHM shall successfully be utilized to cultivate fresh food	*Main function of the lunar greenhouse*
GHM.3	GHM shall be designed for a mission lifetime of at least twenty-four lunar days (about two years)	*Requirement from the Statement of Work* [128]
GHM.4	GHM shall be designed to provide a safe environment for humans	*Astronauts may be around the Grow Unit for harvesting or maintenance and should be safe while doing so*
GHM.5	GHM shall be designed such that it has minimal mass	*Cost and launch considerations*
GHM.6	GHM shall be designed such that it has minimal launch volume	*Cost and launch considerations*
GHM.7	GHM shall be designed such that it has minimal power consumption	*Cost reduction*
GHM.8	GHM shall be designed such that it has minimal resource consumption	*Cost reduction, development of closed loop life support systems*
GHM.9	GHM shall be designed such that it has minimal mission cost	*Cost reduction*

Figure 46: Functional Requirements part of the Requirements Discovery Tree for the lunar GHM structure
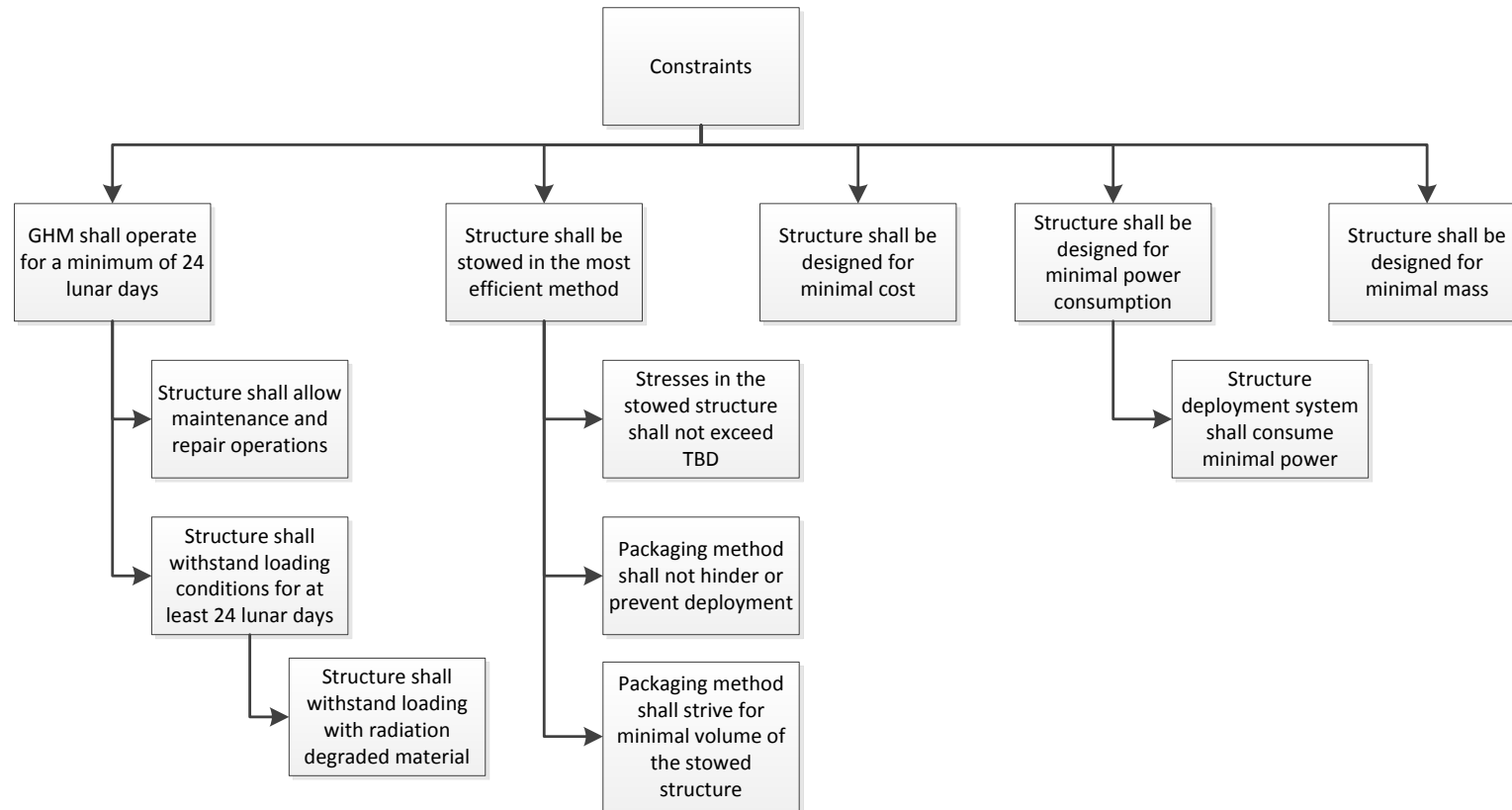
Figure 47: Constraints part of the Requirements Discovery Tree for the lunar GHM structure

4.5.   Summary

An overview of the different mission phases for the lunar GHM was given, starting with integration of the structure within the lunar lander, and the impact on the structure design was discussed.

The main design drivers are the load and environmental conditions which will be encountered during the nominal operating phase. Additionally, the deployment phase, the internal system set-up and the integration into the overall lunar base infrastructure provide key design drivers.
The integration of the stowed structure within the lunar lander and the subsequent launch will also have some (minor) impact on the greenhouse structure design.

The role of the greenhouse in the closed regenerative life support system, as well as the internal architecture of the greenhouse was addressed. The greenhouse was divided into four segments:

- Structure
- Deployment Module
- Grow Module
- Service Module

A functional analysis of the greenhouse was performed and, based on the identified functions, a (sub-)system breakdown was given. An N^2-chart was presented which shows the interfaces between the different greenhouse (sub-)systems, as well as external influences, such as the lunar base and the astronauts.

The system border for this thesis was drawn around the Structure and Deployment Module segments. For the remaining segments, other factors which might impact the structure design, as well as for a few design aspects which (technically) fall within these system borders, assumptions were made.

These assumptions, along with the identified functions and interfaces, were used to develop a list of requirements for the lunar GHM structure.

5. Concept Generation and Selection

Having formulated the requirements on the structural design of the lunar greenhouse module, it is possible to start designing different concepts and subsequently to determine the most suitable option.

In this chapter the concept generation and trade-off phase are covered. First, a number of concepts are developed and presented. Then, as part of the concept trade-off and selection process, different evaluation methods and criteria are discussed. Using one or more of these evaluation methods, along with the evaluation criteria, the different concepts are assessed during a trade-off and the most promising option is selected for the actual preliminary design phase.

5.1. Generation of Lunar Greenhouse Module concepts

Based on the review of existing habitat and greenhouse design concepts which has been discussed in section 2.1.1 of this report, a Design Option Tree (DOT) was created. This DOT can be seen in Figure 48.
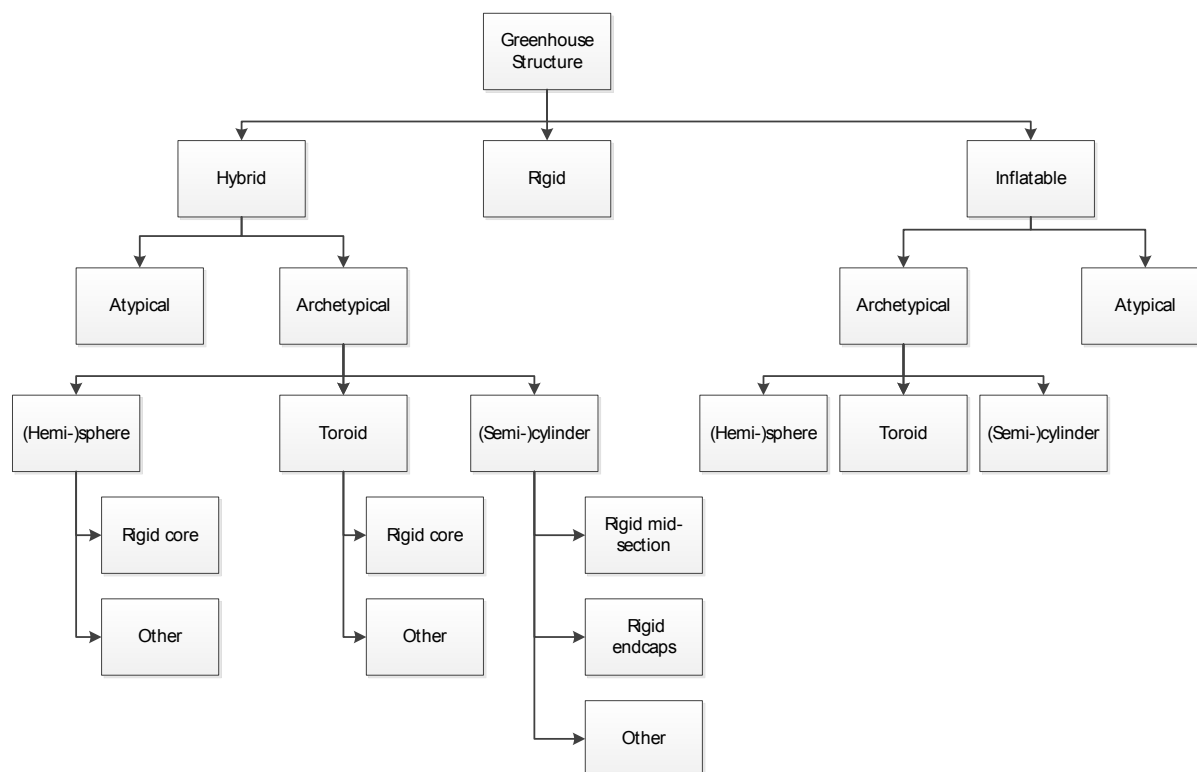
Figure 48: Design Option Tree of greenhouse structure concepts

To limit the size of the diagram, the large number of options for atypical hybrid and inflatable structure concepts is not shown. Similarly, only a limited number of hybrid archetypical structure concepts are shown, with the vast majority combined under the heading 'Other'. In theory, the hybrid design concepts will span the range from almost completely rigid structures to almost fully flexible structures, which would lead to an unfeasibly large DOT diagram.

From the large number of design concepts, a limited number of concepts are chosen, being:

- The cylinder with rigid end-caps
- The cylinder with rigid mid-section
- The inflatable cylinder
- The semi-cylinder with rigid end-caps
- The toroid with rigid core
- The inflatable toroid
- The inflatable sphere
- The inflatable hemi-sphere

By selecting these concepts and performing a trade-off based on the criteria discussed in section 5.2.3, it will be possible to have an initial discussion on a number of aspects of lunar greenhouse and habitat design. Of specific interest are the following three design aspects:

- The optimal amount of rigid material

The cylinder with rigid end-caps, the cylinder with rigid mid-section and the inflatable cylinder will differ only in the amount of rigid material which is used within the concept. The trade-off between the selected concepts will thus provide some insight into whether a lighter, inflatable structure or a more reliable, hybrid structure is preferred.

- The optimal shape

By comparing the final scores of the cylinder with rigid end-caps and the semi-cylinder with rigid end-caps, the structure shape can be optimized. Similarly, the inflatable sphere and hemi-sphere will be compared, as will the three inflatable archetypical structures (cylinder, sphere and toroid).

- Adaptability of space habitats

The toroid with rigid core concept is similar to the TransHab module which was designed for use on the International Space Station. The concept is selected here to see how well such space habitats adapt for use as planetary habitats.

Some preliminary work has been done to determine the best method for integrating the airlocks, 'docking' ports and systems within the structures. Additionally, based on the deployed structure configuration, a possible packing strategy is presented for each of the concepts.

For the concept development it was assumed that at least two airlocks would be needed to allow astronauts to enter or exit the structure in case of emergency (e.g. fire, solar flare). Additionally, at least two 'docking' ports were incorporated in the structures to serve as interface to the rest of the lunar base. The airlocks can function as additional 'docking' ports, in case a direct entrance/exit to and from the lunar surface is not required.

5.1.1. Concept 1: Cylinder with rigid end-caps

The first concept is that of a cylinder with rigid sections at both ends and an inflatable mid-section. The rigid sections house the airlocks and ports, provide structural support and can hold equipment and systems in stowed (and deployed) configuration of the cylinder. The stowed configuration of

the structure is achieved by moving the rigid sections together and folding the inflatable section like an accordion (see Figure 49).

For lateral stability on the lunar surface, the structure will require either support struts or extensive excavation of lunar regolith, resulting in increased mass or crew time demand. Structural mass will already be relatively high due to the large rigid sections of the structure. On the other hand, reliability can be quite good, since compartmentalization of the structure is (relatively) straightforward.

A floor will be required to support the greenhouse equipment, as well as any astronauts and robots which will work within the greenhouse. This floor can be built in within the rigid sections, but part of it needs to be deployed along with the inflatable part of the structure.

The complexity of the concept is fairly low, since the number of rigid-flexible interfaces is very limited (though the interface area is quite large). Additionally, packing and deploying of the structure should be fairly simple. The size of the rigid sections imposes a lower limit on the stowed volume of the structure however, and thus an upper limit on the deployed volume.
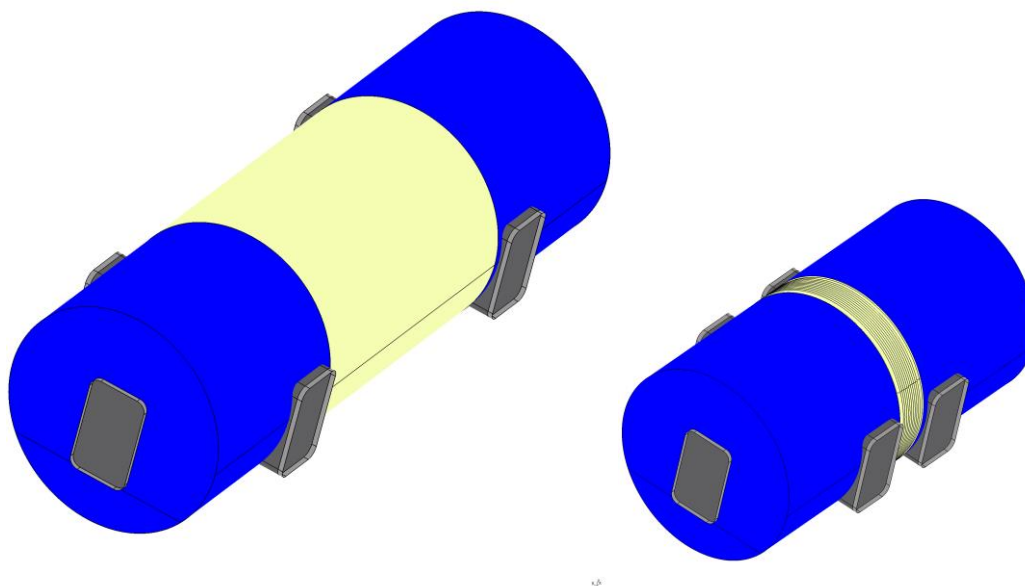
Figure 49: Concept 1 – Cylinder with rigid end-caps. (Left) Deployed structure. (Right) Stowed structure.

The different segments of the lunar greenhouse which were discussed in Chapter 4.2 (Structure, Deployment Module, Service Module and Grow Module) will be integrated into the greenhouse as shown in Figure 50.

Since a floor will be needed within the structure, this provides a natural separation between the equipment used after deployment (on the floor) and the Deployment Module (below the floor). Depending on the size of the rigid end-caps and the space required for the airlocks and ports, the Service Module will be contained either partially or completely within the rigid sections.

If needed part of the Service Module will be placed within the inflatable section, but preferably this is reserved for the Grow Module.
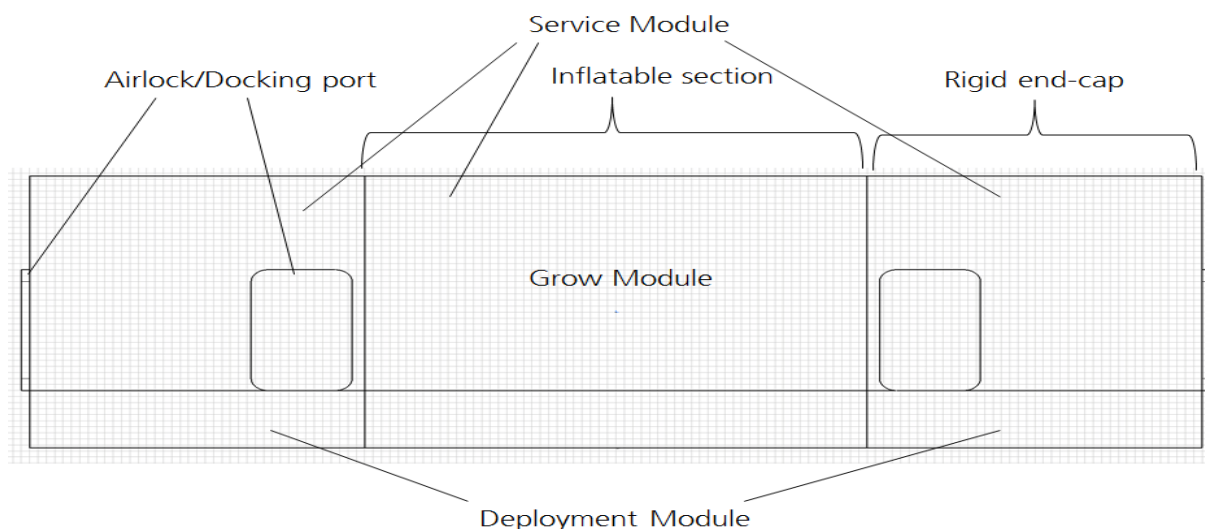
Figure 50: Concept 1 – Side view with greenhouse segment configuration

5.1.2. Concept 2: Cylinder with rigid mid-section

The second concept is also cylindrical, but instead of having two rigid sections at the ends of the cylinder, this design has a single rigid section in the center, as can be seen in Figure 51. This option has a lower rigid to flexible material ratio, which likely results in a lower (relative) mass. Additionally, the packaging efficiency (stowed to deployed volume ratio) will be higher on account of the reduced amount of rigid material.

The two inflatable sections can be packaged using accordion folds, as for the cylinder with rigid end-caps, which is a very low complexity packaging method. This concept has more rigid-flexible material interfaces however, so the manufacturing complexity is slightly higher than for the previous concept.
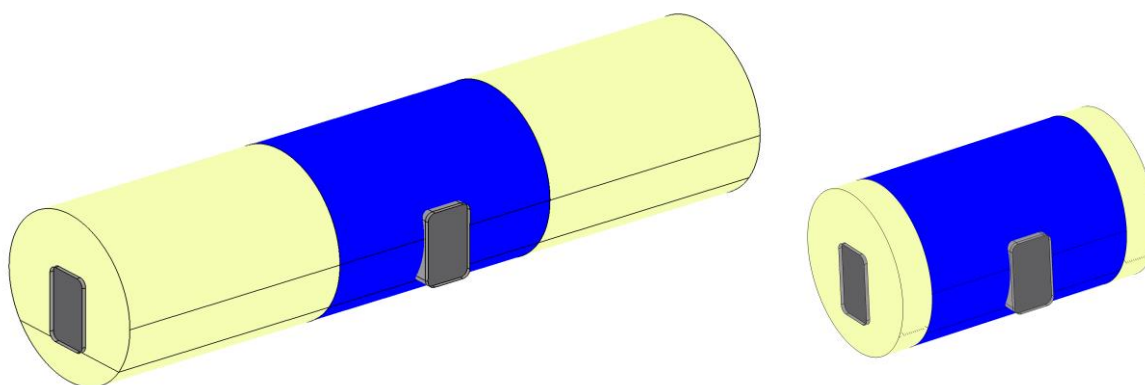
Figure 51: Concept 2 – Cylinder with rigid mid-section. (Left) Deployed configuration. (Right) Stowed structure

The internal layout of the lunar greenhouse segments will likely be as shown in Figure 52. The Deployment Module will probably be installed beneath the floor of the rigid section, with the Service Module taking up the remaining space of this rigid part. The two inflatable sections will house the Grow Module and, if needed, part of the Service Module.
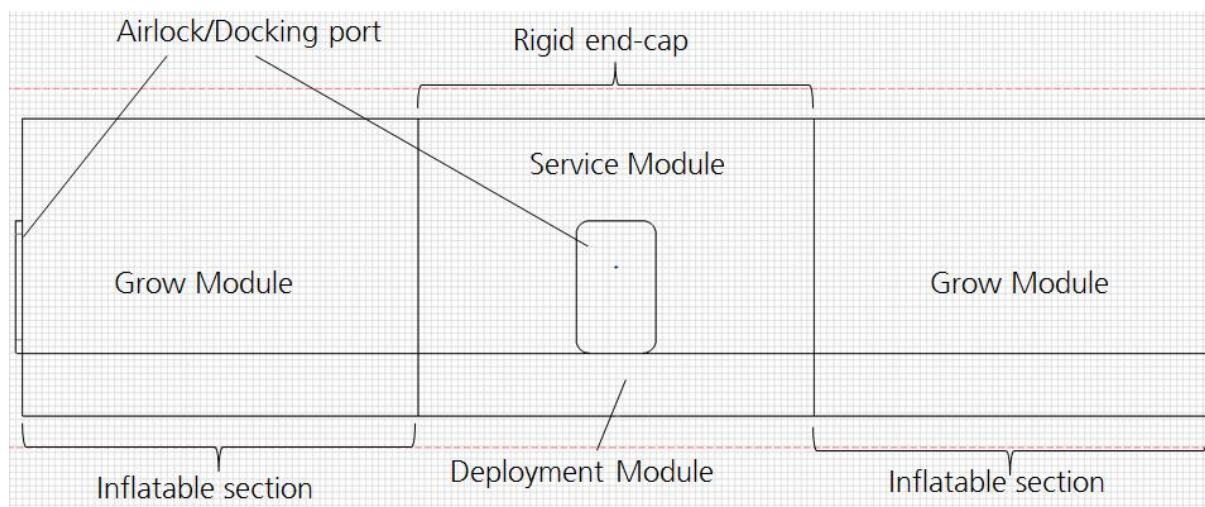
Figure 52: Concept 2 – Side view with greenhouse segment configuration

5.1.3. Concept 3: Inflatable Cylinder

The third concept is the fully inflatable cylinder, shown in Figure 53. The lack of rigid sections, excluding airlocks and docking ports, is expected to lead to a lower relative mass. The presence of the docking ports on the sides of the cylinder mean that a simple accordion folding technique, such as used for the previous cylindrical concepts, is not possible for the entire structure. Thus, either a different packaging method will need to be applied, or only part of the structure will be packaged, resulting in a lower packaging efficiency. In either case, some space will need to be left within the packaged structure to house the Deployment Module. Additionally, the number of rigid-flexible material interfaces has increased with respect to the previous two concepts, resulting in a higher manufacturing complexity.
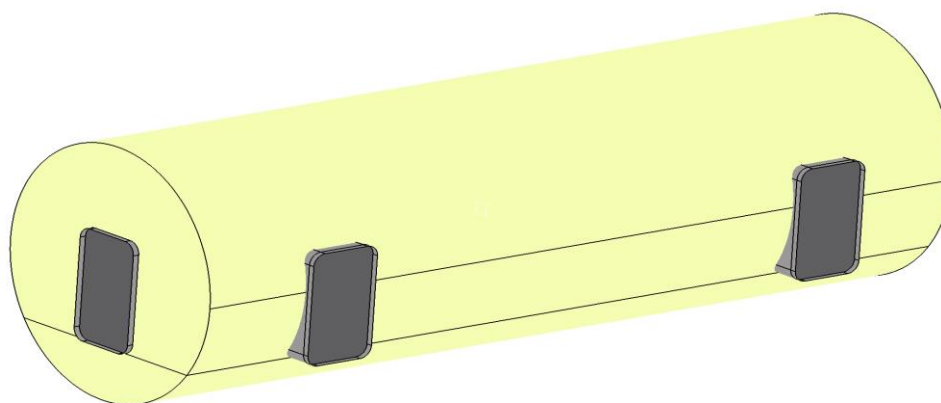
Figure 53: Concept 3 – Inflatable cylinder

The internal configuration of the lunar greenhouse segments will likely be similar to the configuration shown in Figure 50. The only exception is the Deployment Module which may be situated in a different location, depending on the selected packaging method.

5.1.4. Concept 4: Semi-cylinder with rigid end-caps

The semi-cylinder concept is similar to the first cylindrical concept, with rigid sections at both ends and an inflatable middle part. Compared to the cylinder, however, this concept will have reduced mass and requires no regolith excavation.

The reduced size of the rigid sections means that the stowed structure can be either smaller, or that the structure will have more room for inflatable material, allowing for a longer deployed greenhouse. On the other hand, the size reduction will also affect the amount of equipment which can be stored in the structure in the stowed configuration.

It is proposed that the structure will be stowed by folding it in half, bringing the two rigid sections together and leaving the remainder of the available payload volume free for the folded inflatable middle section; see Figure 54 (bottom right).
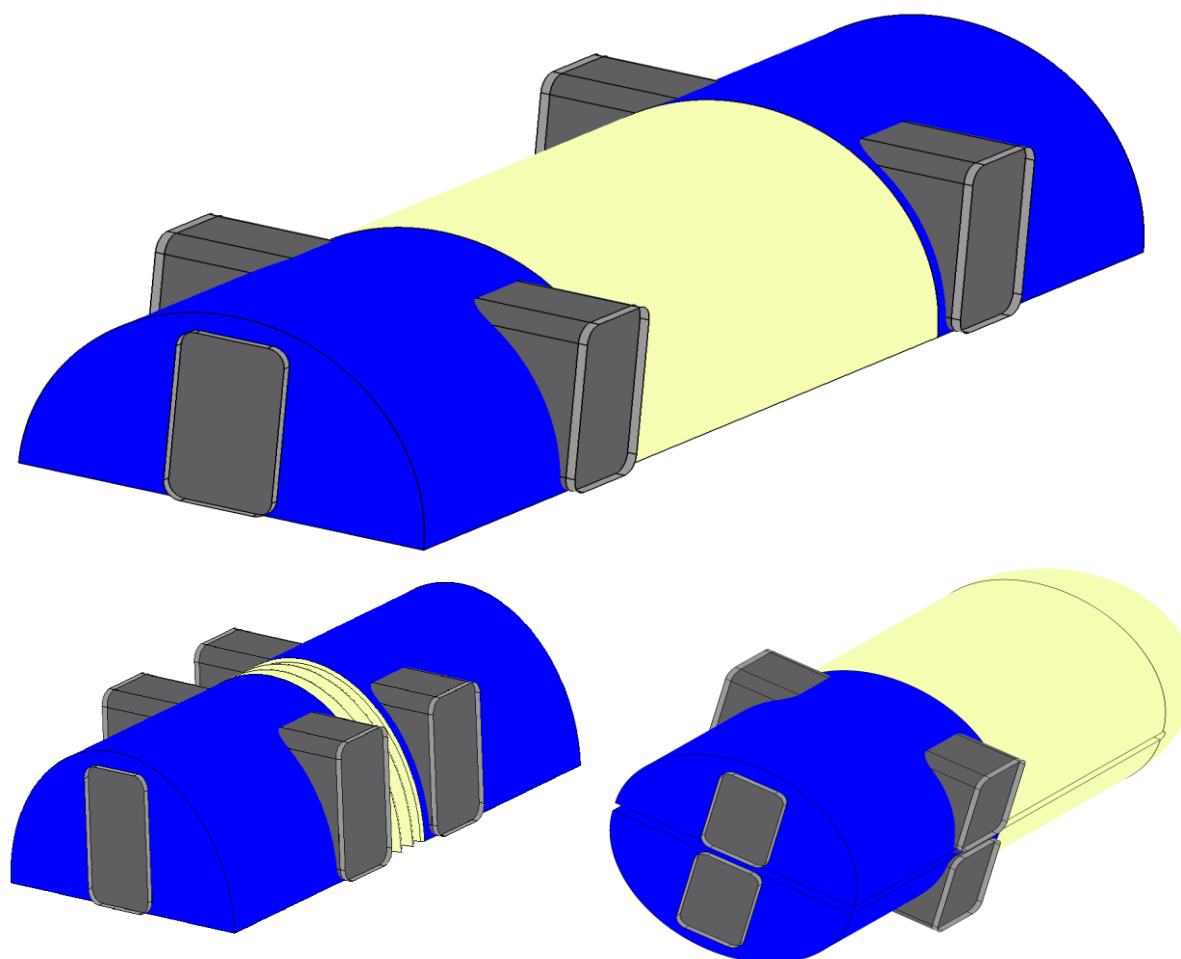
Figure 54: Concept 4 – Semi-cylinder with rigid end caps. (Top) Deployed structure. (Bottom) Two possible configurations for the stowed structure

The semi-cylinder does not have the same natural segmentation as the cylinder concept, since there is no need to add a floor to the semi-cylinder to support equipment. As a result, the Deployment Module, which in the previous concept was housed underneath the floor, now has to be moved to one (or both) of the rigid end-sections (see Figure 55). Consequently, there is less space for the

Service Module in these rigid sections, which increases the likelihood that the inflatable middle section will also be partially used for the Service Module.
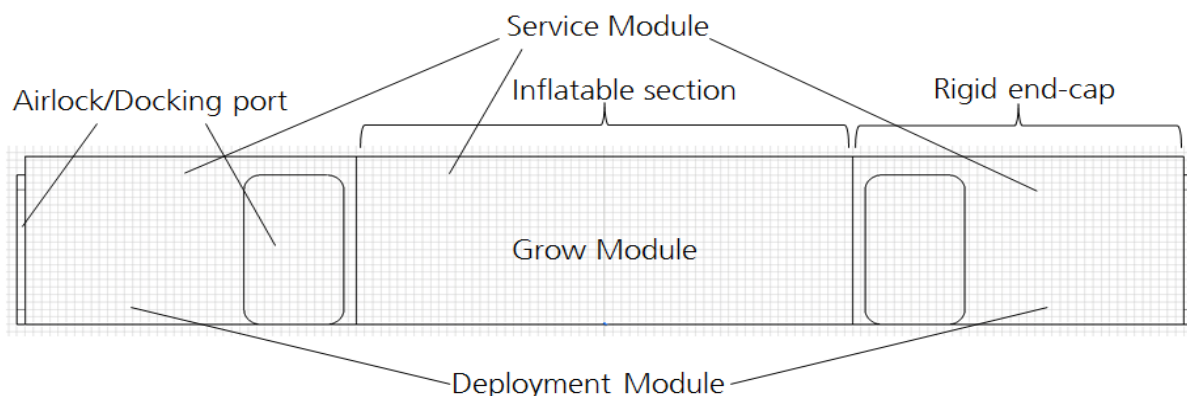
Figure 55: Concept 4 - Side view with greenhouse segment configuration

5.1.5. Concept 5: TransHab

This concept is similar to the TransHab design and is essentially a toroid around a central rigid (hollow) core. The core is hollow, and contains ladders to allow astronauts to move between different floors. The rigid core necessitates a vertical orientation of the structure, which means lateral stability might need to be increased using struts or regolith excavation.

Furthermore, a rigid core, combined with airlocks and ports, results in a high mass and a low deployed to stowed volume ratio. Due to constraints on the available payload fairing it is possible that the rigid core will not have enough space to accommodate all the necessary equipment. As a result, it could be necessary to move equipment into the structure and up several floors, which will require significant amounts of effort and time by the astronauts.

Packaging of the structure will probably be accomplished by pushing in the rigid airlocks and ports towards the inner rigid core and subsequently folding the inflatable sections around the rigid parts, as shown in Figure 56.
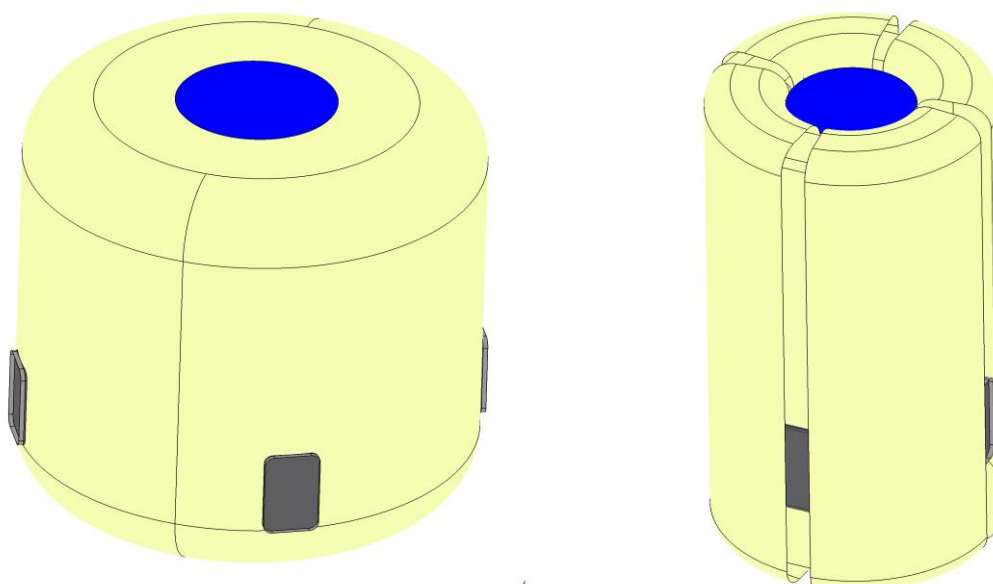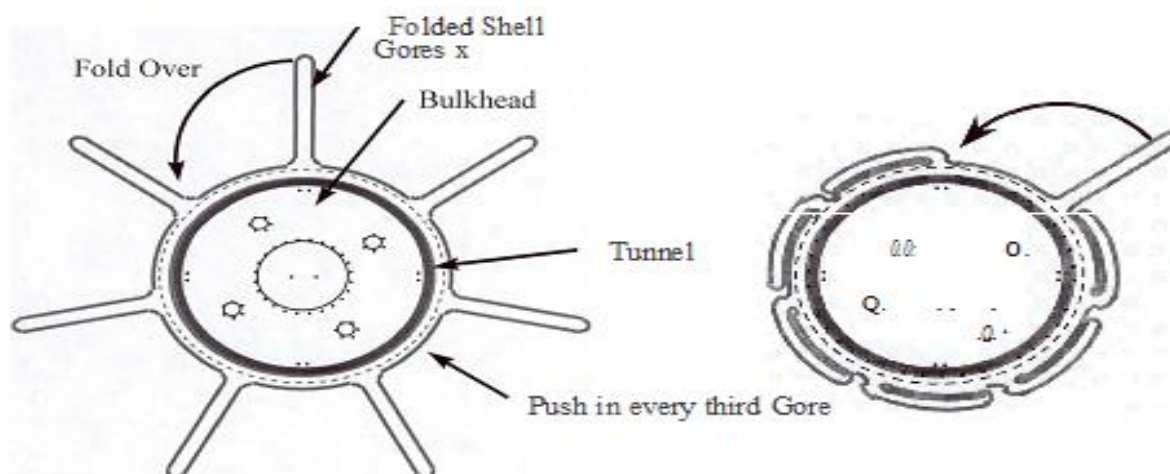
Figure 56: Concept 5 – TransHab (Top left) Deployed structure. (Top right) Stowed structure. (Bottom) Schematic of TransHab folding scheme [Source: 18]

As a result of the rigid core of the structure, as well as the packaging method, it is necessary to have the Deployment Module within the rigid core, as can be seen in Figure 57. After deployment, the first floor will be used for the Service Module, with the remaining floors used for the Grow Module. Depending on the available space, the Deployment Module may need to be removed or relocated to allow free movement between the different floors.
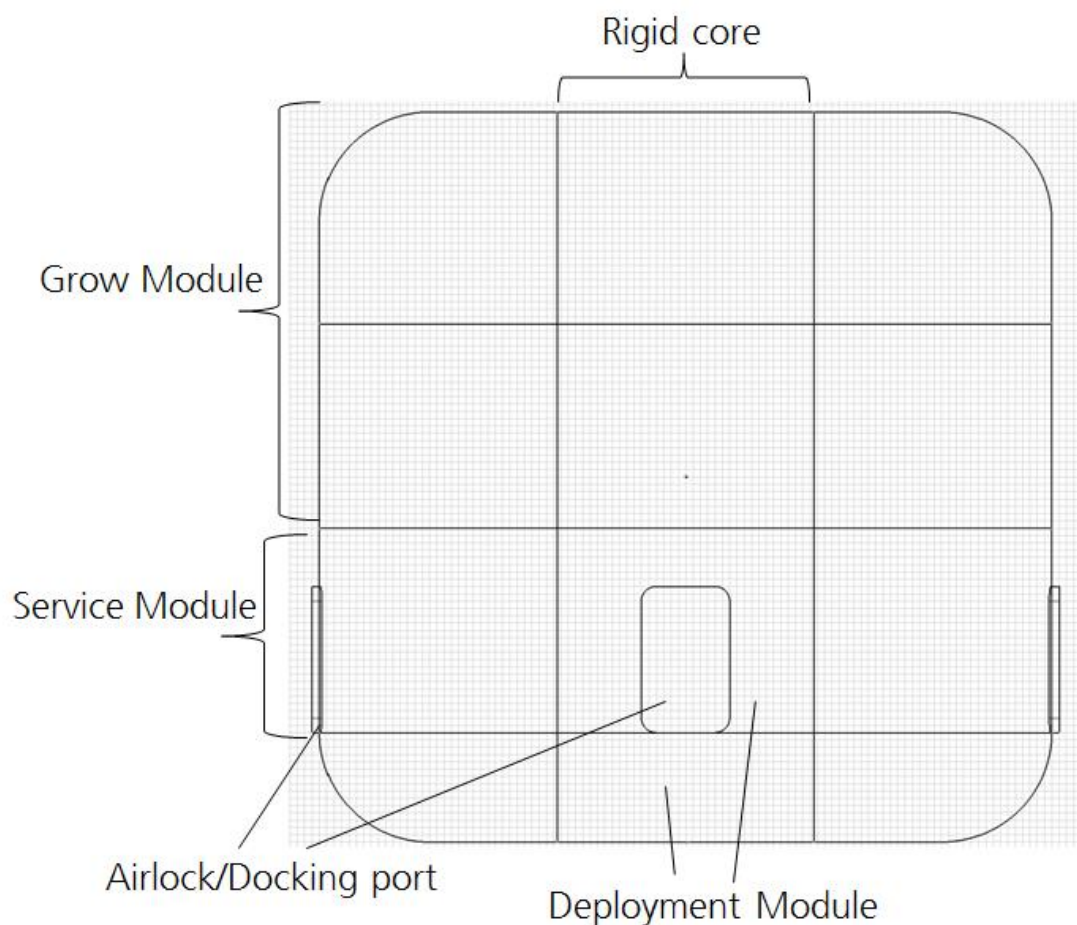
Figure 57: Concept 5 – Side view with greenhouse segment configuration

5.1.6. Concept 6: Inflatable Toroid

The next concept (see Figure 58) is similar to the Domus I concept discussed in chapter 2, in that the outer structure is an ellipsoid and the internal structure is split into a toroidal outer ring and a central area.

The curvature of the ellipsoid is small enough to allow the structure to be stable on the lunar surface, meaning that no support structure or site excavation is needed. Nonetheless, a deployable floor will be used to support the greenhouse equipment and astronauts.

Aside from the airlocks and docking ports, the entire structure will be made from flexible (rigidizable) materials, resulting in a much lower (relative) mass compared to the hybrid concepts. Additionally, the minimum stowed volume of the structure (excluding any equipment or systems, can (probably) be much smaller for a structure with a similar deployed volume, or, alternatively, the structure can achieve a much larger deployed volume for a similar stowed volume.

The complexity of the structure is higher than for the first several concepts though, since the structure will require a more extensive rigidization system. Additionally, the packaging strategy for this concept is expected to be more complex. One proposed method involves folding the airlocks and docking ports inwards by 180 degrees. The flexible material making up the top of the structure will need to be folded in some manner, while leaving sufficient room in the center for the Deployment Module.
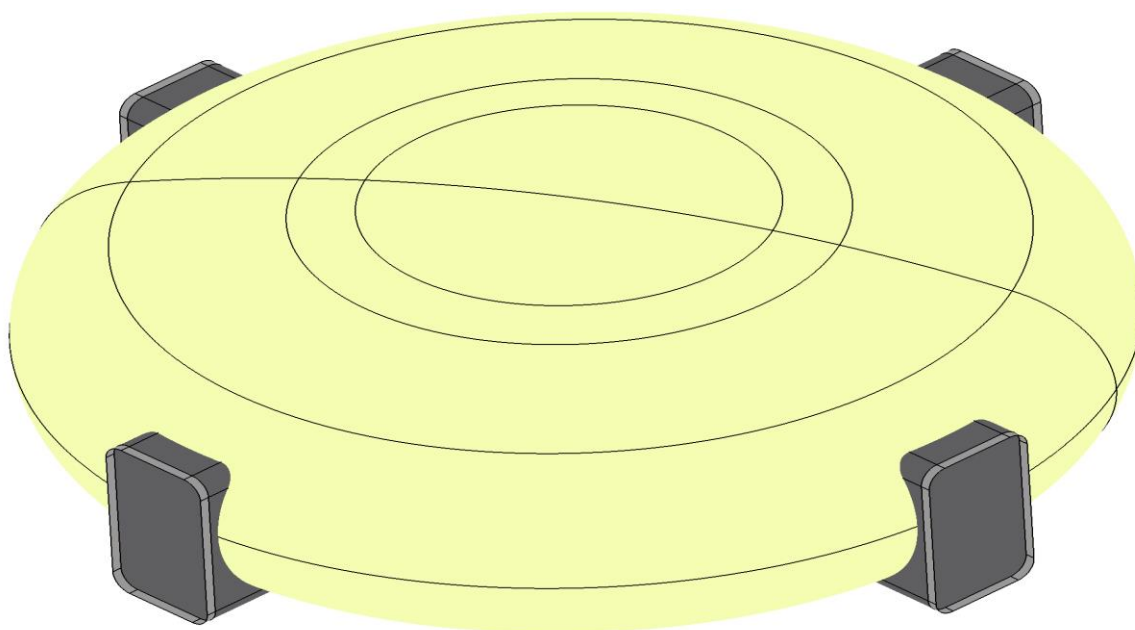
Figure 58: Concept 6 – Domus. Deployed structure

As briefly mentioned, during the description of the possible packaging method, the Deployment Module will be within the central area of the Domus. Upon deployment of the structure, the remainder of this area will be used for the Service Module, while the outer ring will be used for the Grow Module (see Figure 59)
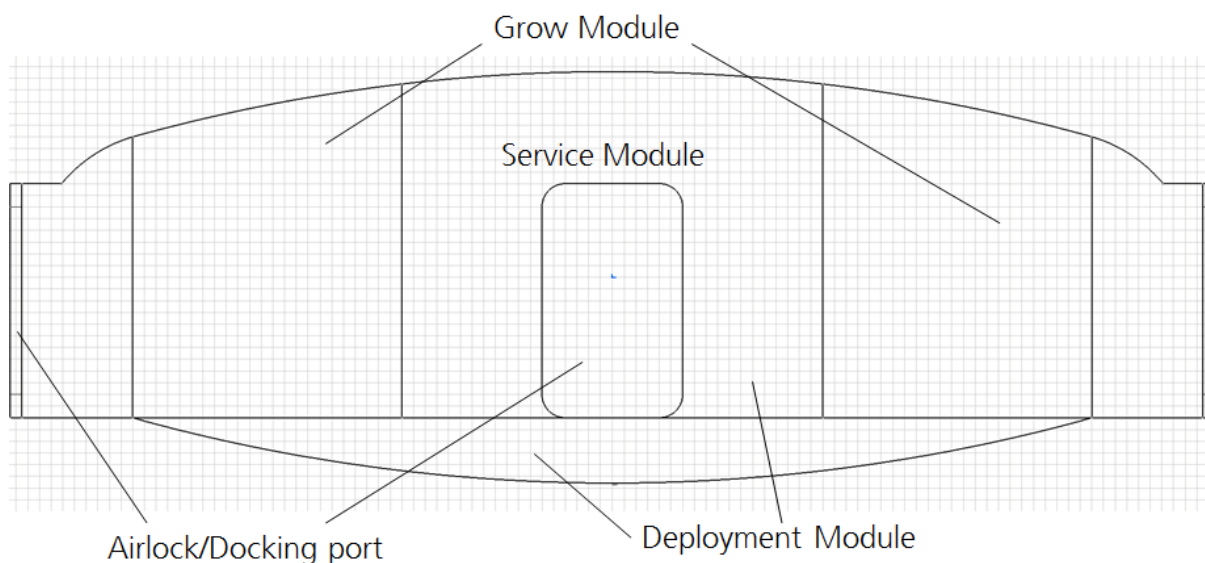
Figure 59: Concept 6 – Side view with greenhouse segment configuration

5.1.7. Concept 7: Inflatable Hemi-sphere

The seventh concept is the hemi-sphere, shown in Figure 60. This concept provides additional volume with respect to the Domus concept discussed previously, by adding extra height. To use the extra height will require an additional floor however, which adds mass and complexity. Furthermore, as with the other multi-story concepts, it will require significant time and effort to move the required equipment up to the extra floor(s).

A central section of the hemi-sphere will be used for movement between the floors, as well as for storage of the Deployment Module. To support the upper floor, this central section will almost certainly require a rigid (or rigidized) load-bearing structure, which would also be able to serve as compartmentalization method, separating the different segments of the greenhouse. The packaging method which was proposed for the previous concept could also be applied to the hemi-sphere.

The extra floor which this concept offers will house (part of) the Grow Module, with the ground floor housing the remainder of the Grow Module (see Figure 61). As mentioned, the Deployment Module will be housed in the central section of the structure. The same is the case for the Service Module, though, depending on the available size, some additional space may be required on the ground floor to house the Service Module.
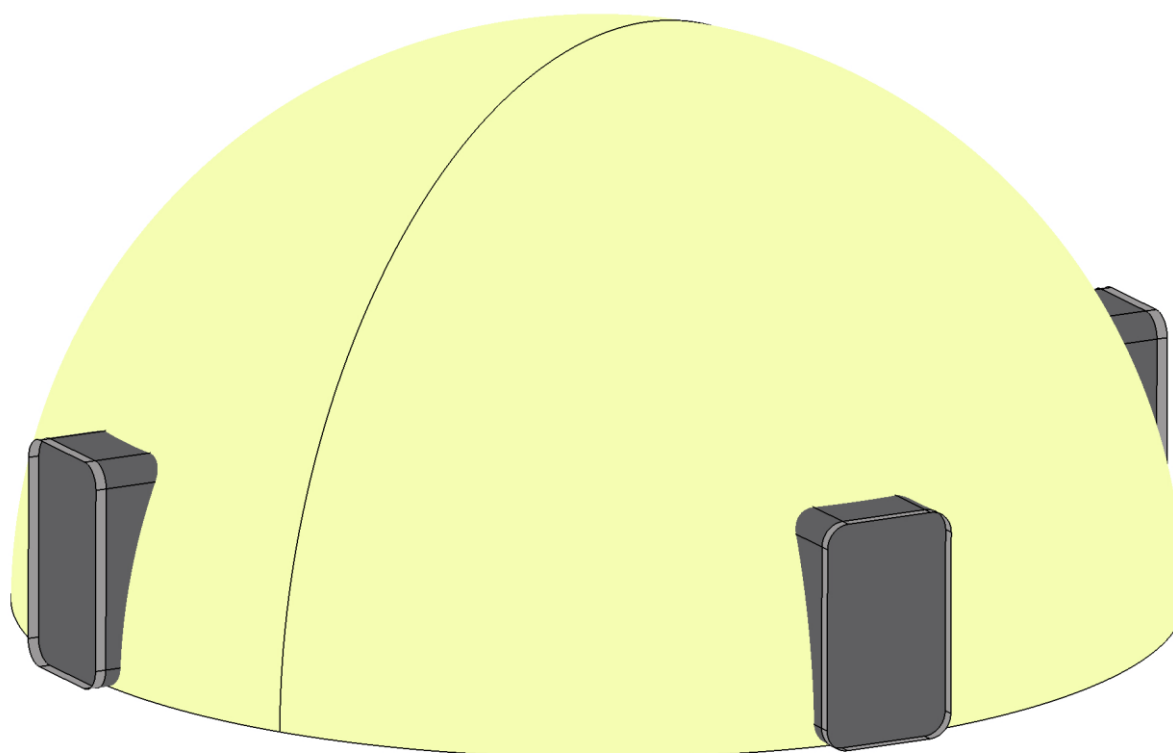
Figure 60: Concept 7 – Hemi-sphere, deployed structure.
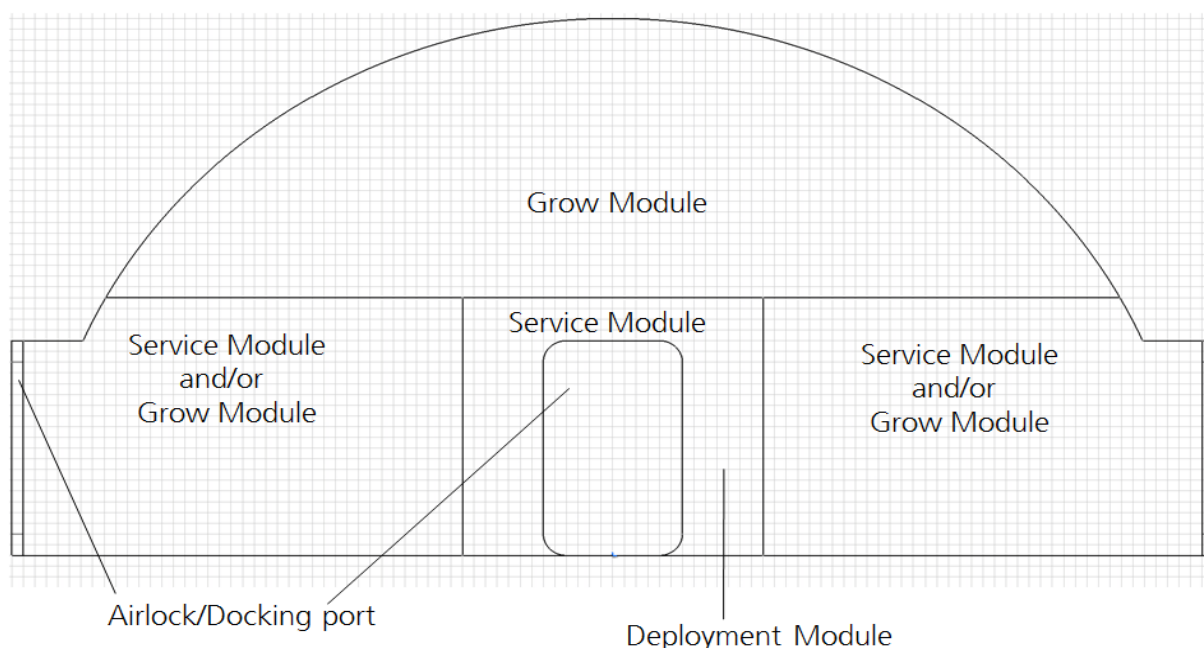
Figure 61: Concept 7 – Side view with greenhouse segment configuration

5.1.8. Concept 8: Inflatable Sphere

The final concept is the inflatable sphere, shown in Figure 62 (left). Compared with the hemi-sphere, the sphere offers a significant increase in available volume. The complexity is significantly higher though, due to the floor(s) and the associated support structure. The packaging method can likely be (almost) the same as for the hemi-sphere and the inflatable toroid concept.
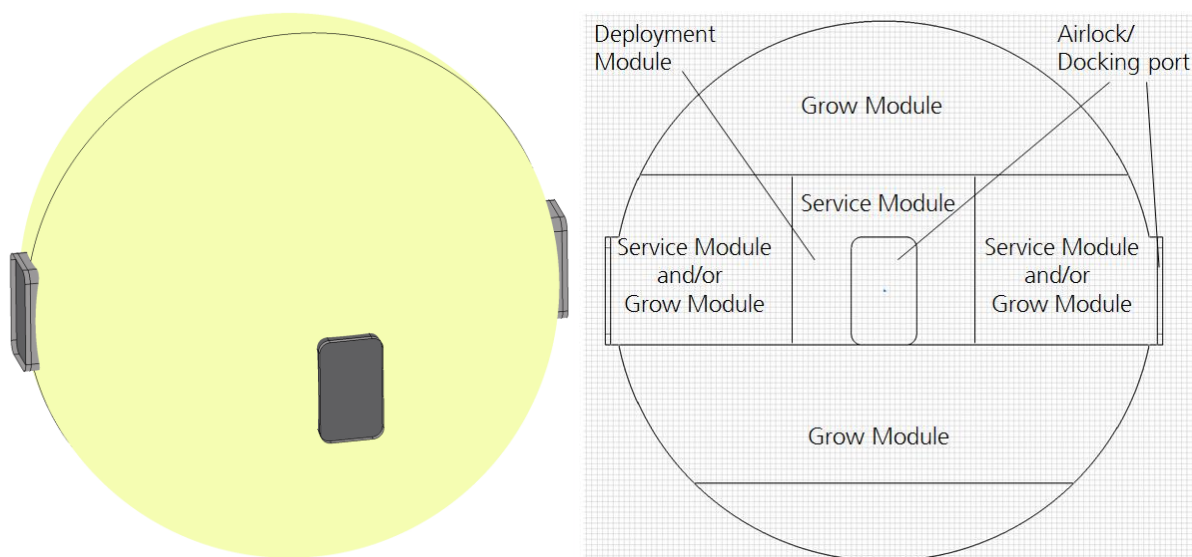
Figure 62: Concept 8 – Sphere. (Left) Deployed Structure. (Right) Side view with greenhouse segment configuration

The crew time required for the sphere will be significantly higher, on account of the extra site preparation required, as well as the extra time needed for outfitting.

The proposed configuration of the lunar greenhouse segments is shown in Figure 62 (right). The 'ground floor' where the astronauts enter will be used for the Service Module, with extra space used for the Grow Module. The other floors will be dedicated entirely to the Grow Module. Depending on the size of the sphere, and the required height per floor, it may be that there is some left-over space which cannot be used as a separate floor, such as the bottom section of the sphere in Figure 62 (right). Such space can be used for storage of resources and spare equipment for example.

5.2.   Evaluation method selection

Selecting the most suitable greenhouse design concept depends on a trade-off with respect to a number of factors, both tangible and intangible, which affect the overall performance. The trade-off process is further complicated by the fact that, early in a design process, the characteristics of the different concepts cannot easily be quantified. A number of evaluation methods have been developed and applied as tools in the trade-off process and a variety of factors are taken into account in each specific method.

In this section a brief overview of the most important evaluation methods and criteria will be given. The most suitable method and criteria will be selected for use in the subsequent concept selection process, which is discussed afterwards. For a more detailed discussion of the different evaluation methods and criteria, the reader is referred to [136,137].

5.2.1. Evaluation methods

Equivalent System Mass

The first evaluation method which will be discussed is the Equivalent System Mass (ESM) approach developed by NASA. As the name suggests, the equivalent system mass evaluation method involves

the transformation of the various units of different evaluation criteria (e.g. volume, power) into a mass unit.

Five different components are considered for the ESM method, specifically, the actual mass of the system and the equivalent masses of the volume, power requirement, cooling requirement and crew time demand. The ESM is calculated for each subsystem and summed to get an overall score for the entire system. The concept with the lowest ESM value would be the most suitable for further development.

A drawback of the ESM evaluation method is that determination of the different components mentioned above is not always straightforward and may require significant experience with greenhouse design. Furthermore, in case the different concepts have different specifications, for example due to the use of different technologies (e.g. bio-regenerative or physio-chemical), the ESM scores need to be adjusted accordingly, which also demands a large amount of experience.

Advanced Life Support System Evaluator

The Advanced Life Support System Evaluator (ALiSSE) has been developed by ESA to serve as a tool for evaluation of different Life Support System (LSS) or subsystems thereof.

ALiSSE considers seven criteria to determine the (relative) performance of LSS designs. Aside from the system mass, the evaluation method considers the crew time demand, energy and/or power consumption, efficiency, reliability, volume and the risk to humans [138].

To determine the performance of each concept with respect to the different criteria, various factors have been suggested along with corresponding indicators. System mass, for example, can be broken down into the following factors: dry mass, mass of fluids, mass of secondary resources and mass of spare parts and tools. To compare between different concepts with widely varying production (in terms of food, recycled water, etc...), the proposed indicators (units) for these mass factors are expressed in kilograms per produced amount of end-product per time period (e.g. kg/kcal end-product/h).

The ALiSSE method is still being developed further and the factors and indicators for several criteria will need to be decided upon. Furthermore, it will depend on the assigned importance of specific criteria to make the final trade-off. Additionally, the ALiSSE method will require the maturation of simulation software to adequately model the LSS loops and architectures [139].

Analytical Hierarchy Process

In contrast to the previous two evaluation methods, the analytical hierarchy process (AHP) has not been developed specifically for LSS evaluation. Rather, the AHP is a tool for any problem in which a decision needs to be made based on multiple criteria.

The AHP uses pairwise comparison of different criteria, which are assigned a ranking based on their (perceived) relative importance. A number of hierarchy levels and corresponding criteria are defined for the complete problem (e.g. LSS) and for each of these levels pairwise comparisons between criteria are carried out. The pairwise rankings are entered into comparison matrices, which are normalized to obtain weighting matrices.

The AHP relies on the subjective ratings of the evaluator(s) and experts, which can influence the final results. To mitigate the subjectiveness of the method, a consistency check and sensitivity analysis should be performed.

The consistency check ensures that the ratings assigned to the various pairs do not conflict, while the sensitivity analysis investigates the effects which varying said ratings would have on the overall result.

The AHP method was used for the evaluation of space greenhouse concepts and the process and results are detailed in [136]. Additionally, in [40] the AHP approach was used to perform the trade-off between different greenhouse structure concepts.

Critical Performance Ratios

Each of the evaluation methods discussed previously have drawbacks, requiring either significant expertise with regards to greenhouses and life support systems (ESM and AHP methods) or requiring further development of the evaluation method (ALiSSE).

Aiming to allow inexperienced analysts to perform trade-offs between greenhouse concepts, while building on the previously mentioned evaluation methods, a novel method was developed and detailed in [137].

A total of 51 Critical Performance Ratios (CPRs) are defined, similar to the ALiSSE criteria, expressing for example amount of end-product output in terms of area. The calculations are converted to a per day basis to allow for easy comparison.

The values for each CPR for a given greenhouse concept based on available technical data and then normalized. Depending on whether the CPR has a positive or negative influence on the overall performance a rating factor is applied and the relevant value is either added to the final score or the reciprocal is taken and added. The final sums of the CPR values for each concept, the so called Critical Performance Scores, are compared, with the highest scoring concept being the optimal choice.

To cope with the problem of incomplete data, established equivalent ratios are used as well as some assumptions. Applying data from the NASA Advanced Life Support Baseline Values and Assumptions Document [134], for example, it is possible to determine an estimate for the power consumption based on the greenhouse crop area.

An analysis of several greenhouse designs is done using the newly developed method and the results are compared with an AHP evaluation. The results show that the CPR approach results in a similar ranking of the concepts as the AHP.

5.2.2. Selected method

For the generation of the concepts presented previously, the assumption was made that all of them should contain the same subsystems and components. As a result, the trade-off between concepts is not between different approaches to CELSS or greenhouse design, but rather it is a trade-off between different configurations of a greenhouse with fixed performance.

Due to this assumption, the power consumption, mass and volume of the subsystems is taken to be the same for all concepts, as is the crew time for maintenance and operation of the subsystems. In reality, variations in mass may occur due to the internal layout (e.g. more cabling required) and the thermal control system may require more power depending on the shape and size of the overall structure. These variations are assumed to be minor and hence are neglected.

The differences between the concepts are thus only in the (outer) structure, such as for example the total deployed volume, stowed volume, mass and the crew time for deployment and maintenance.

Given the limited number of variables which differ from one concept to the next, the most suitable evaluation methods for the trade-off process are the ESM and AHP approaches. The CPR method would require calculating 51 ratios, most of which would be (roughly) the same for the various concepts. The ALiSSE method is still being developed and includes some intangible criteria which cannot be applied in a straightforward manner.

The AHP method will be used to account for the fact that it is not possible to accurately quantify the mass or crew time for the different concepts. Rather, the relative performance of the concepts with respect to the evaluation criteria will be determined in a qualitative (subjective) manner and rated with a value from 1 to 5. Multiplying these ratings with the weights determined by the AHP approach, will allow the selection of the most promising concept. A more detailed description of the AHP process can be found in Appendix D.

5.2.3. Evaluation criteria

As mentioned above, the only differences in the performance of the greenhouse concepts are assumed to result from the structure. A number of criteria (and sub-criteria) have been determined for use in the AHP approach. These evaluation criteria will briefly be discussed below.

Mass

For any space mission the mass is of very high importance and such is also the case for the lunar GHM. A larger size structure will have more material and hence more mass, while the shape will impact the load carrying capability and may result in a higher or lower wall thickness requirement. For example, for a pressurized vessel the sphere or torus is a more optimal (load carrying) shape than a cylinder. Rigid sections will use heavier materials and as such concepts with more rigid material will probably be heavier than other concepts, although the greater wall thickness for inflatable structures may counteract the effect of the lighter materials used.

The average mass per unit volume of structure can be related to the overall ratio of rigid to flexible material used in the structure, assuming similar wall thicknesses and materials for each concept. As such, the concept rating will be done according to the rigid-flexible material ratio ranges listed in Table 7. A lower (estimated) rigid to flexible material ratio is assumed to result in a lower structural mass (per unit volume of structure) and as such is rated higher.

Table 7: Rating scheme for mass

Mass					
Rigid-flexible material ratio (Area-wise)	0-20%	20-40%	40-60%	60-80%	80-100%
Rating	5	4	3	2	1

Volume

The higher the (internal) volume of the deployed structure, the more capacity the greenhouse will have to contain crop cultivation systems and equipment. Of course, due to the shape the actual usable volume may be slightly lower depending on the shapes of the different components. The deployed volume is limited by the stowed volume, which needs to fit within the lunar lander.

The stowed volume of the structure impacts the launcher selection and as a result the launcher and mission cost. If the structure contains more rigid components, the stowed volume is expected to be higher. For more complex flexible structures the packaging efficiency will probably be lower and hence the stowed volume will also be higher.

To take into account these different factors, the achievable packaging efficiency and the effective work area per unit of deployed volume are estimated and rated according to the schemes shown in Table 8. Summing the ratings and dividing by two leads to an overall score for the Volume criteria.

Table 8: Rating scheme for volume

Volume					
Available Volume					
Packaging efficiency (Stowed/Deployed Volume)	0-20%	20-40%	40-60%	60-80%	80-100%
Rating	5	4	3	2	1
Usable area					
Work area / Volume	<0,2	0,2-0,3	0,3-0,4	0,4-0,5	>0,5
Rating	1	2	3	4	5

Reliability

Some of the concepts discussed in the review of existing habitat and greenhouse designs considered the impact of loss of pressurization. A concept with internal compartmentalization will have a higher reliability than a concept which does not. Additionally, due to the very extensive experience with rigid structures, structures with rigid sections will be more reliable than fully inflatable structures. The reliability criteria takes into account the likelihood of failures of (part of) the structure, such as punctures by meteorites, as well as the influence of such failures on the operations of the greenhouse and is therefore rated according to the level of risk (see Table 9).

Table 9: Rating scheme for reliability

Reliability					
Risk	Very Low	Low	Medium	Medium-High	High
Rating	5	4	3	2	1

Complexity

An increase in complexity of a structure results in a higher chance of manufacturing errors and/or failures during operation. Complexity is increased by rigid-flexible interfaces and also depends on structure shape (e.g. sharp corners) and use of compartmentalization. Additionally, the packaging and deployment methods for the structure need to be considered to judge the overall complexity.

Both the manufacturing complexity and the packaging deployment method are rated separately, according to the schemes shown in Table 10. Summing the scores obtained from these ratings and dividing by three gives an overall indication of the complexity of the concepts.

Table 10: Rating scheme for complexity

Complexity					
Manufacturing complexity					
Number of rigid-flexible interfaces	<2	2	3	4	>4
Rating	5	4	3	2	1
Number of deployable floors	0	1	2	3	4
Rating	5	4	3	2	1
Penalty of -2 for concepts with (sharp) corners. (semi-cylinder and hemi-sphere)					
Packaging & Deployment complexity					
Packaging method	Inflatable folding, one direction	Inflatable + airlock folding, one direction	Inflatable folding, multiple directions	Inflatable + airlock folding, multiple directions	Inflatable + airlock folding, multiple directions, additional constraints
Rating	5	4	3	2	1

Crew time

The assumption has been made that astronauts and robots are present on the Moon when the lunar GHM lands. Upon landing it may be necessary to move the stowed structure to the desired location and possibly the crew will need to aid in the deployment process. If this is the case, more time and effort will be required for multi-story structures. Additionally, the crew may be required to spend time preparing the site (e.g. digging a hole/crater) and for the purposes of this trade-off it is also assumed that the crew will be responsible for applying regolith shielding to the structure. The amount of time needed for regolith shielding is mainly dependent on the surface area of the structure.

Preliminary estimates of the crew time needed for each concept are made for three aspects (pre-deployment, outfitting and post-deployment) and then rated according to the scheme shown in Table 11. The total score for the crew time criterion is obtained by summing the three ratings and dividing by three. It is assumed that post-deployment work (e.g. regolith shielding) will require more effort for multi-story structures compared with single story structures with the same outer surface, which is reflected in a penalty to the post-deployment work rating.

Table 11: Rating scheme for crew time

Crew Time					
Pre-deployment work					
Excavation required	None	Minimal (excavation for 0-1 floors)	Significant (excavation for 1 floor)	Extensive (excavation for 1-2 floors)	Extreme (excavation for >2 floors)
Rating	5	4	3	2	1
Outfitting work					
Number of floors	1 floor	2 floors	3 floors	4 floors	>4 floors
Rating	5	4	3	2	1
Post-deployment work					
Surface area to volume ratio	<0,3	0,3-0,4	0,4-0,5	0,5-0,6	>0,6
Rating	5	4	3	2	1
Penalty of -1/extra floor for multi-story structures					

5.3.   Concept selection

With the concepts developed and the trade-off method and criteria selected, it is possible to decide which concept will be selected for further development.

5.3.1. Trade-off

As discussed, the trade-off method consists of pair-wise comparison of the trade-off criteria, using the AHP method, and a qualitative rating of the concepts with respect to each criterion. The pair-wise comparison of the trade-off criteria, as well as the intermediate results from the AHP process can be found in Appendix D. The final weights obtained by applying the process are shown in Table 12.

Table 12: Trade-off criteria weights

Criteria	Weight
Mass	0,1454
Volume	0,3755
Reliability	0,3593
Complexity	0,0851
Crew Time	0,0347

In the previous section it was mentioned that the concepts would be assigned a qualitative rating. Ratings will range from 1 to 5, with 5 being the optimal (e.g. lowest mass, highest reliability). The ratings for each concept per criterion are discussed below.

Mass

The rigid-flexible material ratio of the cylinder with rigid end-caps is estimated to be between 40 and 60%, resulting in a rating of 3 for the mass criterion. Assuming the rigid section in the cylinder with rigid mid-section has a similar size as one of the end-caps from the first concept, the amount of rigid material for this option is half of the first. As a result, the rigid-flexible material ratio is estimated to be between 20 and 40%, which leads to a rating of 4.

The fully inflatable cylinder and the other inflatable concepts are given a rating of 5, because it is estimated that the airlocks and docking ports do not result in a rigid to flexible material ratio higher than 20%.

The semi-cylinder with rigid end-caps will have the same rigid-flexible material ratio as the cylinder and therefore is also given a score of 3. This score is also given to the TransHab, since it is estimated that the amount of rigid material used for the core will result in a 40-60% ratio of rigid to flexible material. An overview of the scores of all the concepts with respect to the Mass criteria is given in Table 13.

Table 13: Mass criteria scores

Concept	Score
Semi-cylinder with rigid end-caps	3
Inflatable sphere	5
Inflatable hemi-sphere	5
Cylinder with rigid end-caps	3
Inflatable toroid	5
Cylinder with rigid mid-section	4
Inflatable cylinder	5
TransHab	3

Volume

The Volume criterion rating is based on the packaging efficiency and the effective work area per unit of volume. The packaging efficiency is estimated based on the amount of rigid material, as well as on the type and complexity of the packaging method.

The cylinder with rigid end-caps is assigned a score of 3 for the packaging efficiency, because, while the packaging method is very simple and efficient, this concept has a significant amount of rigid material which limits the minimum achievable stowed volume. Based on geometry, the ratio of effective work area (amount of floor area) to internal volume of the deployed structure is expected to be between 0,2 and 0,3, and therefore a score of 2 is assigned. Summing and dividing by two gives an overall value of 2,5 for the cylinder with rigid end-caps with respect to the volume criterion.

Due to the reduced amount of rigid material, the cylinder with rigid mid-section receives a rating of 4 for the packaging efficiency. The inflatable cylinder has even less rigid material and can still be packaged in a fairly simple manner, so a rating of 5 is assigned to this concept. Both of these concepts receive a value of 2 for the work area to volume ratio, resulting in overall values of 3 and 3,5 respectively.

The packaging efficiency of the semi-cylinder with rigid end-caps is estimated to be between 40 and 60%, similar to the cylinder with rigid end-caps, and thus a score of 3 is given to this concept. The semi-cylinder provides roughly the same amount of work area as the cylinder, but has only half the volume, leading to a much higher work area to volume ratio and a rating of 5. Combining the two ratings leads to an overall rating of 4 for this concept.

The TransHab, on account of the large rigid core, gets a rating of 3 for its packaging efficiency. The inflatable toroid, hemi-sphere and sphere have no rigid material, except for the airlocks and docking ports, but the packaging method is significantly more complex so a rating of 4 is assigned to these concepts.

Based on geometry and the expected number of floors in the various concepts, the work area to volume ratio of the concepts is estimated. It is estimated that the TransHab will have a work area to volume ratio between 0,3 and 0,4 which would correspond to a rating of 3. The inflatable toroid is estimated to have a ratio between 0,2 and 0,4, giving it a score of 4, and the inflatable sphere and hemi-sphere are expected to have the best work area to volume ratio and are assigned a score of 5.

The work area and volume were estimated using some assumed dimensions for the radius and length. For the cylinder and semi-cylinder concepts, a radius of 2,5 m and a length of 20 m was assumed. The inflatable toroid was approximated as a cylinder with radius 5 m and length 2,5 m. The inflatable sphere and hemi-sphere were estimated to have a radius of 5 m, while the TransHab concept was approximated as a cylinder of outer radius radius 5 m, inner radius 1 m and length 10 m. Four floors are assumed for the TransHab and sphere, 2 for the hemi-sphere and 1 for all other concepts.

Table 14: Volume criteria scores

Concept	Work area	Volume	Packaging efficiency score	Work area/Volume score	Total Score
Semi-cylinder with rigid end-caps	100	159	3	5	4
Inflatable sphere	314	524	4	5	4,5
Inflatable hemi-sphere	157	262	4	5	4,5
Cylinder with rigid end-caps	100	318	3	2	2,5
Inflatable toroid	79	196	4	4	4
Cylinder with rigid mid-section	100	318	4	2	3
Inflatable cylinder	100	318	5	2	3,5
TransHab	302	785	3	3	3

Reliability

To assess the reliability of the concept, the chance of structural failure and the impact of structural failure on greenhouse operations is estimated and combined into a rating of the overall risk. For the inflatable concepts the chance of structural failure is estimated to be higher than for hybrid concepts. As such, the inflatable concepts are assigned a score of 2.

The cylinder with a rigid mid-section is expected to have a lower chance of failure, on account of the rigid section which is estimated to be more reliable than the inflatable sections. This concept is therefore assigned a score of 3. The cylinder and semi-cylinder with rigid end-caps contain even more rigid sections, which leads to a higher estimated reliability. These concepts are given a score of 4.

The TransHab concept also contains a large amount of rigid material, but the placement of the rigid material in the core of the structure reduces the benefits this provides to the reliability of the concept. As such the rating assigned to this concept is lower than the cylinder and semi-cylinder with rigid end-caps, with a score of 3.

Table 15: Reliabiliy criteria scores

Concept	Score
Semi-cylinder with rigid end-caps	4
Inflatable sphere	2
Inflatable hemi-sphere	2
Cylinder with rigid end-caps	4
Inflatable toroid	2
Cylinder with rigid mid-section	3
Inflatable cylinder	2
TransHab	3

Complexity

The cylinder with rigid end-caps has two rigid-flexible interfaces, one deployable floor and no (sharp) corners, which results in a score of 8 for the manufacturing complexity. Packaging of the structure is done by folding the inflatable material in one direction, which corresponds to a complexity rating of 5. Summing these values and dividing by three gives an overall complexity rating of 4,33.

The cylinder with rigid mid-section has four rigid-flexible interfaces, which reduces the manufacturing complexity rating to 6. The packaging complexity for this concept is similar to the complexity for the cylinder with rigid end-caps and thus a score of 5 is assigned to the concept, for an overall score of 3,67.

The inflatable cylinder has more than four rigid-flexible interfaces and one deployable floor, resulting in a manufacturing complexity score of 5. The packaging method is expected to involve folding of inflatable material with integrated airlocks in one direction, which leads to a packaging complexity score of 4.

The semi-cylinder concept has two rigid-flexible interfaces and does not need a (separate) deployable floor since the structure floor can serve as system support. The corners present in the semi-cylinder lead to a penalty of -2 however, for a total manufacturing complexity score of 7. The packaging method involves folding of inflatable material in a single direction, which gives a score of 5, for an overall complexity rating of 4.

The TransHab is expected to have three deployable floors and more than four rigid-flexible material interfaces and as a result scores a 3 for manufacturing complexity. The packaging method involves folding of inflatable material with integrated airlocks in multiple directions (inwards and radial), and this corresponds to a value of 2. Combining the scores and dividing by three results in a complexity rating of 1,67.

The inflatable toroid has four interfaces and one deployable floor, leading to a manufacturing complexity score of 6. The packaging method requires folding inflatable material with integrated airlocks in multiple directions, with the added constraint that space needs to be left in the center of the stowed structure to house the Deployment Module. This further complicates the packaging strategy, leading to a rating of 1.

The inflatable hemi-sphere has four interfaces and one deployable floor, but also receives a penalty of -2 on account of the (sharp) corners of the outer structure. Thus, the manufacturing complexity

rating is 4. The packaging strategy is expected to be as complex as for the inflatable toroid and hence a packaging complexity score of 1 is assigned to this concept.

The inflatable sphere is assigned the same packaging complexity score of 1. This concept has four rigid-flexible material interfaces and at least three deployable floors, which gives a manufacturing complexity rating of 4 and the overall complexity rating is 1,67.

Table 16: Complexity criteria scores

Concept	Manufacturing score	Packaging score	Total Score
Semi-cylinder with rigid end-caps	7	5	4
Inflatable sphere	4	1	1,67
Inflatable hemi-sphere	4	1	1,67
Cylinder with rigid end-caps	8	5	4,33
Inflatable toroid	6	1	2,33
Cylinder with rigid mid-section	6	5	3,67
Inflatable cylinder	5	4	3
TransHab	3	2	1,67

Crew Time

According to the scheme shown in Table 11, the cylindrical concepts all score a 4 for the pre-deployment work required, since these concepts require minimal site excavation. The same goes for the TransHab and inflatable Toroid, though, depending on the exact design, these concepts might not need any site excavation at all. The semi-cylinder and the hemi-sphere, having a flat bottom surface, do not require any excavation and therefore receive a score of 5. The inflatable sphere requires extensive or, depending on the final size, extreme pre-deployment work, resulting in a rating of 2.

For the outfitting work, the cylindrical concepts as well as the semi-cylinder and the inflatable toroid all receive a score of 5, since these are single-story designs. The inflatable hemi-sphere is expected to be a two-story structure, resulting in a score of 4, while the TransHab and inflatable sphere receive a score of 3.

The outer surface area to volume ratio can be estimated from the geometry of the concepts. The cylindrical concepts, as well as the semi-cylinder concept, are assigned scores of 3, because it is estimated that the outer surface area to volume ratio is between 0,4 and 0,5 and no penalty needs to be applied since these are single-story buildings.

The TransHab, the inflatable sphere and the inflatable hemi-sphere concepts are all multi-story concepts and therefore receive penalties to their scores. Combining these penalties, with the estimated surface to volume ratios leads to a rating of 1 for all these concepts for the post-deployment work. The inflatable toroid does not receive such a penalty, but, on account of its poor surface to volume ratio it is assigned a score of 2.

The final concept scores for the crew time criteria are found by summing the ratings for pre-deployment work, outfitting work and post-deployment work and dividing by three. These scores, are listed in Table 17.

Table 17: Crew Time criteria scores

Concept	Pre-deployment score	Outfitting score	Post-deployment score	Total Score
Semi-cylinder with rigid end-caps	5	5	3	4,33
Inflatable sphere	2	3	1	2
Inflatable hemi-sphere	5	4	1	3,33
Cylinder with rigid end-caps	4	5	3	4
Inflatable toroid	4	5	2	3,67
Cylinder with rigid mid-section	4	5	3	4
Inflatable cylinder	4	5	3	4
TransHab	4	3	1	2,67

By multiplying the criteria scores with the criteria weights from Table 12, scores are obtained for each concept, as seen in Table 18. The selected concept is the one with the highest overall score, which, as can be seen, is the semi-cylinder with rigid end-caps.

Table 18: Trade-off results

	Mass		Volume		Reliability		Complexity		Crew Time		
Criteria Weight	0,1454		0,3755		0,3593		0,0851		0,0347		
Greenhouse Concept	Score	Weighted score	Score	Weighted score	Score	Weighted score	Score	Weighted score	Score	Weighted score	Overall score
Semi-cylinder with rigid end-caps	3	0,44	4	1,5	4	1,44	4	0,34	4,33	0,15	**3,87**
Inflatable hemi-sphere	5	0,73	4,5	1,69	2	0,72	1,67	0,14	3,33	0,12	3,4
Inflatable sphere	5	0,73	4,5	1,69	2	0,72	1,67	0,14	2	0,07	3,35
Cylinder with rigid end-caps	3	0,44	2,5	0,94	4	1,44	4,33	0,37	4	0,14	3,33
Inflatable toroid	5	0,73	4	1,5	2	0,72	2,33	0,2	3,67	0,13	3,28
Cylinder with rigid mid-section	4	0,58	3	1,13	3	1,08	3,67	0,31	4	0,14	3,24
Inflatable cylinder	5	0,73	3,5	1,31	2	0,72	3	0,26	4	0,14	3,16
TransHab	3	0,44	3	1,13	3	1,08	1,67	0,14	2,67	0,09	2,88

From the trade-off results it can furthermore be concluded that the space habitat (TransHab) does not adapt well to use on a planetary body. Additionally, it seems that the sphere has a slight advantage over the toroid and cylinder, the semi-cylinder and hemi-sphere are preferred over the cylinder and semi-cylinder, and hybrid concepts with higher amounts of rigid material are rated better than the inflatable concept. However, due to the subjective nature of the trade-off process, these results could be slightly different when the trade-off is performed by a different person.

5.3.2. Sensitivity Analysis

To account for the subjective nature of the AHP, it is customary to perform a sensitivity analysis, which aims to determine how sensitive the results of the AHP are to changes in the criteria weighting.

Here, the sensitivity analysis will be done in two parts. First, the weight of the most important criterion (Volume) will be changed to determine the upper and lower bounds within which the semi-

cylinder with rigid end-caps remains the highest scoring concept. The sum of the weights of all the criteria has to remain 1, so the other weights will be allowed to vary, though the relative importance between these other four criteria (mass, reliability, complexity and crew time) will be fixed.

The second part involves the same process, but it focuses on the second most important criterion (Reliability). Again, the upper and lower bounds for the weight are determined, with the weights of the other criteria allowed to vary (though with a fixed relative importance).

The results of the sensitivity analysis are shown in Figure 63. Five scenarios are presented, representing the nominal case, the lower bound case for the Volume criterion, the upper bound case for the Volume criterion and the lower and upper bound case for the Reliability criterion.

The colored bars indicate the overall scores of the concepts for each scenario and the weights for the different criteria are listed below the graphs.

It can be seen that changes in weight of more than 40% in either the Volume or the Reliability criteria are possible, without it leading to a different trade-off winner. Thus, it can be said that the trade-off result is quite robust.

Concept ranking - Nominal case

Mass: 0,1454   Reliability: 0,3593
Volume: 0,3755   Complexity: 0,0851
Crew Time: 0,0347

Concept ranking - Volume lower-bound case

Mass: 0,2287   Reliability: 0,5652
Volume: 0,0177   Complexity: 0,1339
Crew Time: 0,0545

Concept ranking - Volume upper-bound case

Mass: 0,0747   Reliability: 0,1846
Volume: 0,6792   Complexity: 0,0437
Crew Time: 0,0178
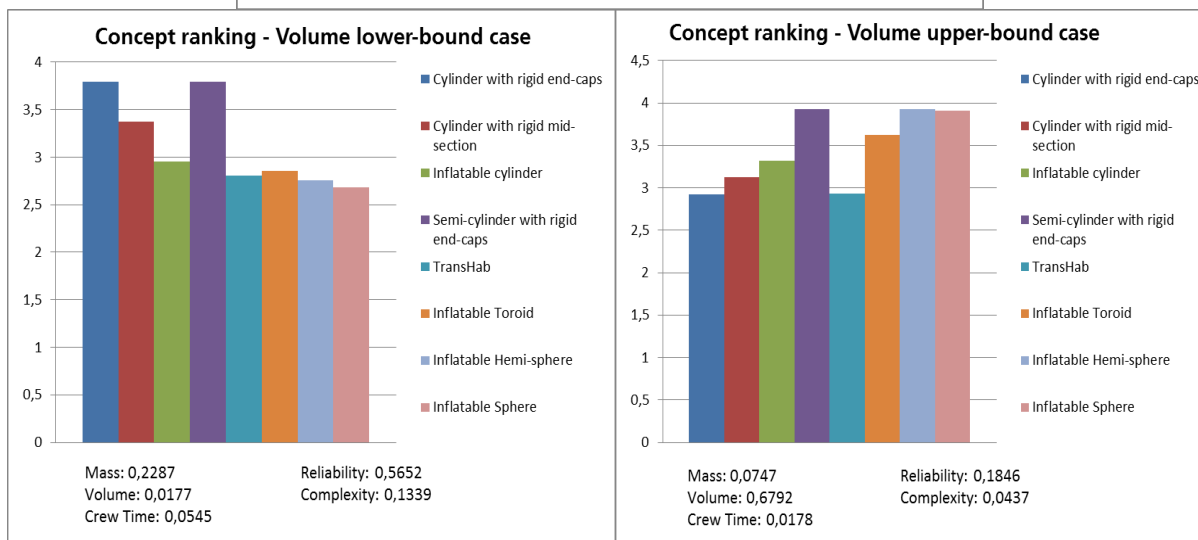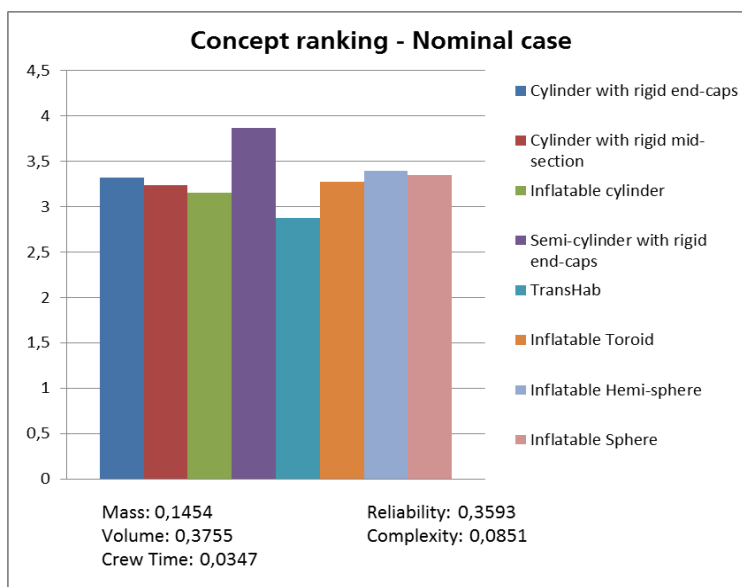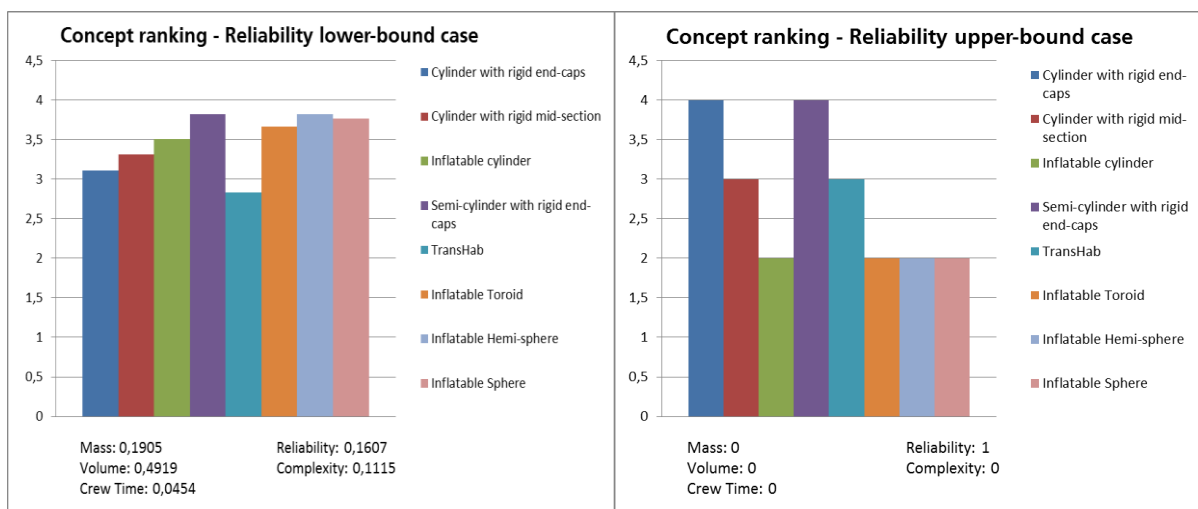
Figure 63: Concept rankings for the nominal case and the lower- and upper-bound cases for Volume and Reliability

5.4.   Summary

A Design Option Tree was presented to give an overview of the different greenhouse structure concepts. From this DOT eight concepts were selected, specifically to obtain some insight into:

- The optimal amount of rigid material for lunar greenhouses
- The optimal shape for lunar greenhouses
- The adaptability of space habitats as lunar greenhouses

Preliminary work was done on the concepts to allow a trade-off between the different designs. For this trade-off, the Analytical Hierarchy Process was selected from a number of possible evaluation methods and subsequently used to determine the weights of the five trade-off criteria:

- Mass
- Volume
- Reliability
- Complexity
- Crew Time

Qualitative ratings were assigned to each concept for all five criteria and then multiplied by the corresponding weights obtained using the AHP. Summing the weighted scores led to an overall score for each design, with the semi-cylinder with rigid end-caps scoring best, as seen in Table 19.

Table 19: Overall trade-off scores ranked in descending order

Concept	Overall score
Semi-cylinder with rigid end-caps	**3,8662**
Inflatable sphere	3,3928
Inflatable hemi-sphere	3,3466
Cylinder with rigid end-caps	3,3197
Inflatable toroid	3,2734
Cylinder with rigid mid-section	3,2368
Inflatable cylinder	3,1539
TransHab	2,8750

To account for the subjective nature of the trade-off, a sensitivity analysis was performed on the AHP weights. This was done by varying the weights of the two most important criteria (Volume and Reliability) and determining the upper and lower bounds at which the semi-cylinder concept remains the highest-ranked design. It was found that changes of more than 40% in either the Volume or Reliability criteria weight would be needed for the top-ranking concept to change.

6. Preliminary Design of the Structure

Having selected the semi-cylinder concept in the previous chapter, it is now possible to start the preliminary design of the structure. First and foremost the required size of the structure will be determined, by calculating the space needed for the Grow Module, Service Module and Deployment Module. A probable configuration will be presented, including rigid to flexible material interfaces and attachments from the greenhouse to the lunar base.

After determining the required dimensions of the lunar GHM, the functional layers (e.g. gas retention, radiation shielding) will be designed. Each layer (of the inflatable section) will be designed separately, using the assumption that the other layers will not influence the overall performance of the structure. For example, the radiation shielding is assumed to have negligible gas retention characteristics, which in reality is unlikely to be true, but this assumption does lead to a conservative design.

6.1. Structure sizing

The main task of the lunar GHM is to provide sufficient food for the astronauts. Based on the total edible biomass requirements, it is possible to determine the required crop grow area. Then, based on the total grow area, it is possible to determine the size of the support equipment. Combining the total required areas, it is possible to size the structure of the lunar GHM.

6.1.1. Grow Module sizing

As mentioned, the first step in sizing the structure of the lunar greenhouse module is to size the required grow area. The required edible mass production is found from [128] and baseline values on the biomass production per unit area are taken from [134]. The assumption was made that the achievable yield with an aeroponic cultivation system is 1,4 times as large as the baseline value.

The required production, the productivity (with aeroponic yield increase factor) and the calculated required grow area are listed in Table 20.

Table 20: Monthly crop production requirements and corresponding grow area

Higher plant	Soybean	Durum wheat	Bread wheat	Potato	Lettuce	Beet	Rice
Edible Dry Mass (g/month)*	25000	31000	33000	41200	1000	2200	4320
Corresponding edible fresh mass (g/month)	27800	33700	35100	51600	20000	22000	43200
Dry basis edible biomass productivity (g/m^2*day)**	6,356	28,00	28,00	29,484	9,198	9,10	12,698
Dry basis edible biomass productivity (g/m^2*month)**	190,68	840,00	840,00	884,52	275,94	273,00	380,94
Required grow area (m^2)	131,11	36,91	39,29	46,58	3,63	8,06	11,35

*: ±10% deviation from the dry mass requested is acceptable
**: NASA baseline values multiplied by the assumed aeroponic yield increase factor of 1,4.
***: Month is assumed to be 30 days

The set-up of the plant cultivation system with Grow Units, Grow Pallets and Grow Lids was discussed in section 4.2.3. In essence, it means that crops will be grown on multiple, vertically stacked, levels, which allows for an increase in total grow area for a given footprint area.

To determine the total footprint area, the minimum number of levels of a crop within a Grow Unit is determined based on the height of the Grow Unit, the mature plant height, which is obtained from [134], and an assumed spacing between levels. The data and results are shown in Table 21.

Table 21: Grow Pallets per Grow Unit and total required number of Grow Units

Higher plant	Soybean	Durum wheat	Bread wheat	Potato	Lettuce	Beet	Rice
Mature Plant Height (m)	0,55	0,50	0,50	0,65	0,25	0,45	0,80
Minimum number of levels per Grow Unit *	2	2	2	2	4	3	2
Minimum grow area per Grow Unit	1,0	1,0	1,0	1,0	2,0	1,5	1,0
Required number of Grow Units	132	37	40	47	2	6	12

*: Grow Unit height of 2,0 m. Spacing between levels at least 0,2 m. 0,5 m^2 grow area per level/ Grow Pallet.

The Grow Units have a height of either 2,0 or 2,4 m and a footprint area of about 0,7 x 1 m^2. From Table 21 it can be seen that a maximum total of 276 Grow Units is needed to ensure that the required edible biomass is produced, which corresponds to a total footprint area of 193,2 m^2. By using the larger Grow Units (of 2,4 m) this number can be reduced to 207. Either way, this would lead to an unfeasibly large greenhouse structure, since, even with four parallel rows of Grow Units, the Grow Module would be roughly 50 m. Add to that the Service and Deployment Modules and the structure size will increase even further.

Instead of designing a structure of this size, it was decided to limit the size of the structure to 20 m and to determine the achievable production for a structure of that size.

6.1.2. Service Module sizing

Following some iteration of the internal configuration, the total number of Grow Units within the 20 m greenhouse was found to be 40. Assuming a grow area of 2,0 m^2 per Grow Unit the total grow area in the greenhouse is 80 m^2

Based on the grow area, it is possible to determine the mass and size of the necessary support equipment (and spare equipment, etc...). While not all system masses will scale linearly with increasing grow area, for convenience such relationships are assumed here. In [140] three different plant growth system concepts are mentioned, along with estimated system masses and this data is used to estimate the mass (per unit grow area) of the different systems (see Table 22). To determine the volumes of the different systems, scaling, based on the number of Grow Units, was applied to a previous design by the author for a 40 foot (High-Cube) container greenhouse.

Table 22: Service Module systems mass estimation

System	Specific mass [kg/m² Grow Area]	Mass [kg]
Illumination System	5,0	400
Nutrient Delivery System	20,4	1632

System	Specific mass [kg/m² Grow Area]	Mass [kg]
Air Management System	8,1	648
Plant Monitoring System	1,5	120
Command & Data Handling System	1,5	120
Other (e.g. sterilization equipment)	32,5	2600
Total	69	5520

6.1.3. Deployment Module sizing

The Deployment Module will consist of the tanks containing the required gases for inflation of the structure as well as a system to control the gas flow out of the tanks into the structure.

As mentioned previously, it was decided to limit the length of the greenhouse to 20 m. The radius of the semi-cylinder was set at 3 m to allow for four rows of Grow Units as will be shown in the next section. From these structure dimensions it can be determined that the internal volume of the structure is approximately 283 m^3. Using this known volume, along with the requirements on the internal atmosphere, it is possible to determine the amount of gas needed in the Deployment Module.

The required internal atmospheric pressure is 1010 mbar [128] and the atmospheric composition should be as shown in Table 23.

Table 23: Required atmospheric composition [128]

Gas	Concentration
Oxygen	20 +/- 1%
Carbon dioxide	300 – 2000 ppm
Nitrogen	~80%
Other (Trace gases)	tbd

The required amount of gas can be determined using the ideal gas law (equation (1)) and the atmospheric composition given in Table 23.

$$P*V = n*R*T .$$
(1)

Here, R is the universal gas constant (8,314462175 J/mol*K), T is the air temperature which should be at least 20 °C [128], and n is the number of moles of gas. Since the pressure and temperature are known and the volume of each gas can be calculated from the total volume and the concentrations listed in Table 23, it is possible to determine the number of moles present for each gas. These values are then multiplied by the molecular weight, to obtain the gas mass in kg, see Table 24.

Filling in all the numbers, yields the total amount of each gas which is required to obtain the initial atmospheric pressure. During the lifetime of the lunar greenhouse, there will be some gas loss through leakages, which means that it is necessary to have additional gas available to replace these losses.

Any variations in gas pressure or composition due to the absorption of CO_2 and the production of O_2 and water vapour in the greenhouse are neglected here. It is assumed that these variations are cancelled out through effects in the other structures of the lunar base.

The requirement on the maximum allowable leakage rate was determined from [128]. It was found that the maximum pressure variation (de- or increase) is 20 mbar/hour. A pressure loss rate of 20 mbar/hour would, however, result in a pressure loss of 480 mbar/day, which is nearly half of the internal atmospheric pressure in the greenhouse. With such a large pressure loss rate, it would not be feasible to operate the lunar greenhouse for any extended period of time due to the large quantities of replacement gas which would need to be produced and/or transported to the structure. Thus, the requirement on the maximum gas loss rate was made more stringent and was set to 0,025 mbar/day, which corresponds to roughly 1% pressure loss per year.

Assuming a constant volume and a temperature of 20 °C, it is possible to determine the amount of gas lost when the pressure decreases by 0,025 mbar. Taking this value as the daily leakage rate and integrating over the minimum mission lifetime (approximately 2 years) yields the total gas loss during the mission.

For the sizing of the Deployment Module the total amount of gas within the tanks is taken to be the sum of the initial gas required and the replacement gas required, with a margin of 10%. Assuming the gases can be stored at a pressure of 200 bar, which was the pressure used for the Skylab airlock system [141], the total tank volume which is required can be calculated using equation (1). The results of the calculations described above are listed in Table 24.

Table 24: Gas requirements for the lunar GHM Deployment Module

	Initial gas required [kg]	Gas leakage rate [g/day]	Replacement gas required [kg]	Total gas required [kg] *	Tank Volume required [m³]
Oxygen	78,9	1,96	1,43	88,37	0,34
Carbon dioxide	1,1	0,03	0,02	1,24	0,004
Nitrogen	262,9	6,51	4,75	294,42	1,28
Total	342,9	8,5	6,2	384,03	1,624

*: (Initial gas + Replacement gas) + 10% margin

6.1.4. Configuration and Interface design

As mentioned previously, the length of the greenhouse structure was limited to 20 m. Furthermore, the required equipment for the Service Module, as well as the dimensions of said equipment, was based on a design created for a container greenhouse. After a number of iterations, the design shown in Figure 64 was developed.

The structure has a radius of 3 m and its total length of 20 m is divided into a flexible mid-section of approximately 10 m and the two rigid end-sections with a length of about 5 m each. The flexible mid-section holds 40 Grow Units, for a (conservatively) estimated 80 m² grow area.
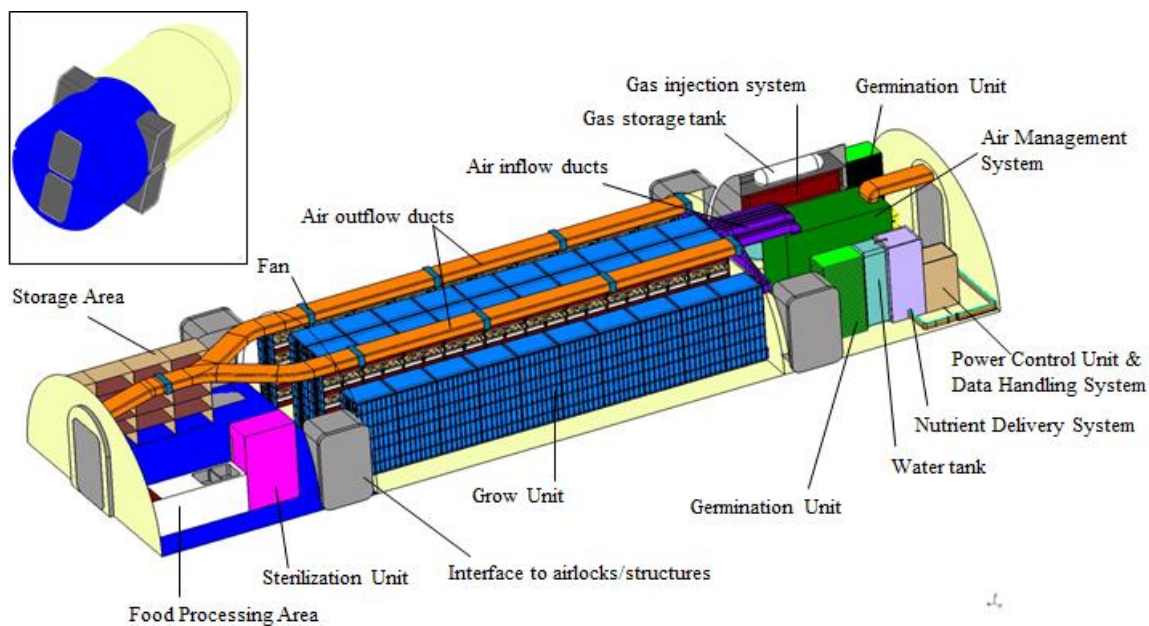
Figure 64: Internal configuration of the lunar GHM. (Inset) Stowed configuration

A number of different rigid-flexible interface designs were found during a review of existing and proposed systems [142,143,144]. Comparing the various interfaces, the design from [143] was selected as it should allow for a reduced mass and size with respect to the design options using clamps and bolts.

The selected solution, see   Figure 65, consists of a cavity within the rigid material. The flexible material layers are wrapped around a wire or cable and then the incoming and outgoing flexible material layers are stitched together. Subsequently, the wire and fabric are inserted into the cavity after which the cavity is filled by casting a low melting point material into it. Upon solidifying, the rigid material, wire, fabric and cast-able material form a strong attachment with a relatively light weight and size. Further investigation is needed to determine if there is a need for an adhesive layer between the rigid material and the cast-able material, as well as for a sealant material which will allow for a reduced stress concentration at the interface, as proposed in [143].
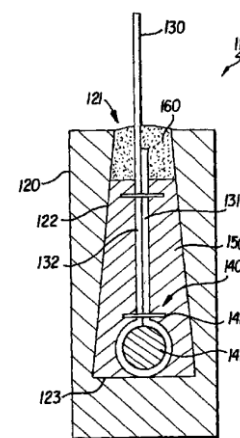
Figure 65: Proposed Rigid-Flexible Interface design

For the interface from the structure to the airlock system and/or the other lunar base structures an androgynous system as opposed to a male/female system is deemed most suitable. The androgynous system requires a design which can connect with its mirror image. Figure 66 shows an axial view of the International Docking System Standard (IDSS) Androgynous Docking Interface [145], which could be used as the basis for the lunar GHM to airlock interface.
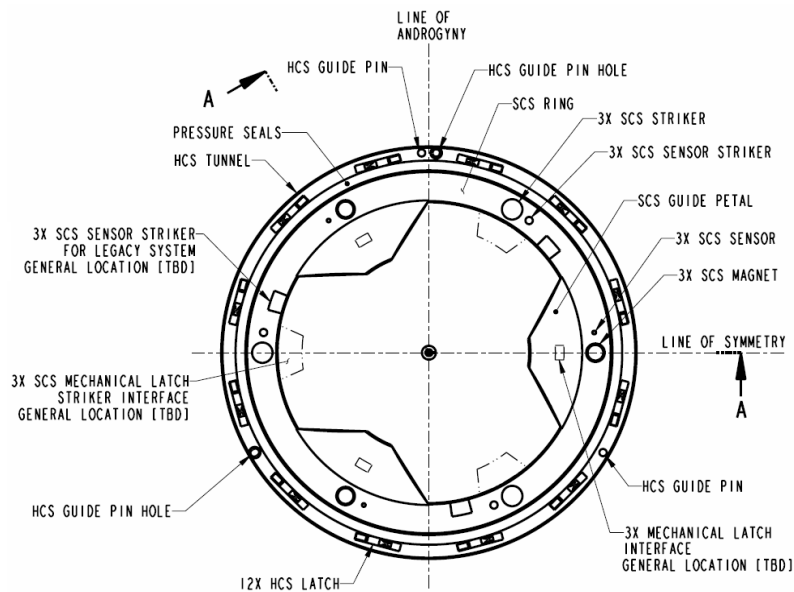
Figure 66: IDSS Androgynous Docking Interface.

6.2. Gas retention layer design

As mentioned previously, each of the different functional layers of the lunar GHM structure will be designed separately. One of these functional layers is the gas retention layer, which is responsible for preventing the gas inside the greenhouse from escaping at too high a rate. To fulfil this function, the gas retention layer will need to be designed to reduce the gas flux to below the maximum allowable permeation. Additionally, the mass should be minimized.

A brief overview of the relevant theory and formulae will be given and subsequently applied to the design of the gas retention layer.

6.2.1. Theory and Formulae

The theory for gas permeation through polymeric materials was developed by Thomas Graham around 1866. Based on observations, Graham proposed that permeation of gas occurred through a solution-diffusion process. This model involved the dissolution of penetrant (gas), followed by diffusion of the dissolved gas through the polymeric material [146]. The solution-diffusion process assumes a uniform pressure throughout the membrane which is equal to the upstream pressure. The pore-flow model is an adaptation of this model where the pressure is assumed to drop uniformly over the membrane. The solution-diffusion model is used for the calculations done in this section.

The relationships which describe these models are based on Fick's first law and Henry's law, governing, respectively, diffusion and solubility. The overall permeation is given by:

$$P_m = D * S_m,$$ (2)

where P_m is the permeability, D is the diffusivity and S_m is the solubility.

Typically, the diffusivity and solubility are determined experimentally using a so-called time-lag experiment. The permeability is then calculated using equation (2).

In the case of a multi-layer membrane, consisting of n layers, the effective permeability of the total membrane can be determined using the following relationship:

$$\frac{t_{total}}{P_{eff}} = \sum_{i=1}^{n} \frac{t_i}{P_i}.$$ (3)

Assuming that the diffusivity and the solubility are independent of (gas) concentration, the steady state permeation flux, J, can be determined by multiplying the permeability, P_m, with the pressure gradient, Δp, and dividing by the membrane thickness, t:

$$J = P_m * \left(\frac{\Delta p}{t} \right).$$ (4)

In reality, the permeability, diffusivity and solubility will depend on pressure and temperature, but for the preliminary design discussed in this report these effects will not be taken into account.

6.2.2. Design

As discussed in section 6.1.3, the requirement on the maximum allowable gas (and water vapour) leakage rate was set to be 0,025 mbar/day.

Using the ideal gas law and assuming a constant temperature and volume, it can be found that a change in pressure of 0,025 mbar is equivalent to a loss of 0,29 moles of gas. The composition of the gases inside the greenhouse is similar to that of air so a molar mass of 28,97 g/mol [147] is taken for the gas mixture. Thus a pressure drop of 2,5 Pa/day in the GHM would correspond to a gas loss of 8,5 g/day.

The pressure difference between the inside of the greenhouse and the lunar environment is approximately 1 atm, since the atmospheric pressure on the Moon is negligible.

Using these known variables, in combination with equation (4) it is possible to determine the required effective permeability for a given thickness. From this effective permeability, and the total thickness, it will be possible to determine the number of layers and the thickness of each material layer.

The permeability of several materials with respect to a number of gases is listed in Table 25. As can be seen, certain materials have better gas retention properties for oxygen and other gases, while other materials provide better characteristics for retention of water vapour.

Table 25: Permeability properties of candidate materials with respect to different permeants [146,148]

Material	N_2	O_2	CO_2	Water (vapour)
	[ml*mm/m²*day*atm]			[g*mm/m²*day]
LDPE	36,61	142,14	631,0	4553,28
HDPE	1,26	9,28	17,41	2,71
PVDC	0,02	0,1	1,42	456,69
PA-6 nylon	0,55	1,73	7,50	987,52

The highest effective permeability with respect to one of the gases or with respect to water vapour should still be lower than the maximum allowable permeability for the given thickness.

Calculating the required thicknesses, and corresponding weights, for the different materials listed in Table 25 it was found that HDPE was the most appropriate material. A thickness of 0,15 mm is required to limit the gas loss to an acceptable value, which leads to a weight of 144 g/m^2.

Lacking data on the probability and risk of failure, the redundancy used for the gas retention layer is based on literature on inflatable space structure designs. A doubly-redundant design is selected, meaning three gas retention layers will be incorporated in the structure. To prevent a single puncture from piercing all three layers, the gas retention layers will be separated by a bleeder layer of 0,1 mm Kevlar felt cloth.

6.3.   MMOD shielding design

To prevent (micro-)meteoroids from puncturing the lunar GHM structure, causing leaks and damaging equipment, it is necessary to add layers of material to protect against such impacts.

This section will determine the optimal MMOD shielding configuration, materials and the required layer thickness to withstand the expected meteoroid impacts on the lunar surface. First the relevant formulae will be discussed and then the trade-off will be presented. The effects of the other material layers and any regolith shielding which may be applied are not taken into account for the calculations in this section.

6.3.1. Theory and Formulae

From [149] it is found that NASA's preferred reliability practice is to design (spacecraft) external surfaces to ensure a 95% probability of no mission critical failures. If it is assumed that each penetration of the MMOD shielding has a unity probability of causing a critical failure, then it is necessary to have a 95% probability of no penetration during the mission lifetime in order to meet the NASA preferred practice guideline. Given that astronauts will work within the lunar GHM, it was decided that there should be a 99% probability of no penetration.

An alternate way of stating this requirement is that the MMOD shielding should be designed in such a way that there is a 99% probability that there will be no impacts of particles with sufficient momentum to penetrate the shielding or, assuming a constant velocity, a 99% probability that there will be no impacts of particles with a mass higher than the MMOD shielding can withstand.

Since the relation between particle flux and particle size is a random distribution, a statistical model needs to be fitted to the data. Then, using that model, the probability that a particle larger than a mass m will hit the lunar GHM can be calculated using the equation below:

$$P_h = 1 - e^{(-A_S * F)},$$ (5)

where P$_h$ is the probability, A$_S$ is the exposed surface of the lunar GHM and F is the fluence.

Figure 33 in section 3.7 of this report shows the (micro-)meteoroid flux versus size as experienced on the lunar surface. The cumulative flux values for each particle size were read from this graph and then plotted along with a power trendline. This graph can be seen in Figure 67.
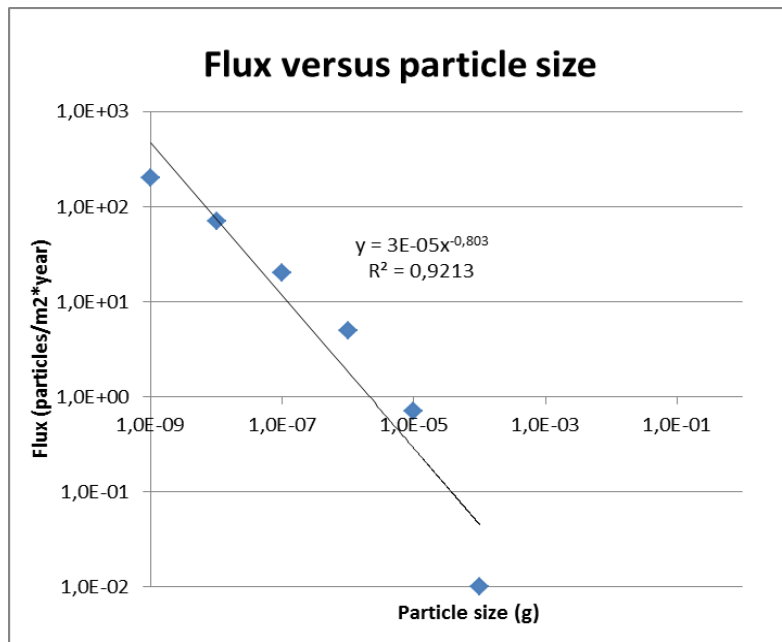
Figure 67: Cumulative particle flux versus size with power series trendline

From this graph, it can be seen that the relationship between flux, Φ_m, and particle mass, m_p, is approximately described by:

$$\Phi_m = 3 * 10^{-5} * m_p^{-0,803} . \qquad\qquad (6)$$

The fluence, F, is the total flux over the duration of the mission. Assuming a constant flux, the fluence is simply the mission duration (approximately 2 years) multiplied by the flux.

Using equations (5) and (6) it can be found that the MMOD shielding should be designed to withstand an impact of a particle of about 1,16 g. Using the fact that the average velocity of the micro-meteoroids is about 20 km/s as discussed in chapter 3, it is possible to design the MMOD shielding. Assuming a spherical particle with a mean density of 0,5 kg/m³, the diameter of a particle of 1,16 g will be about 1,65 cm.

Depending on the type of shield configuration which is selected and the materials used in the shield, the performance of the MMOD shielding is described by different equations. Here four configurations (seen in Figure 68) will be briefly addressed and their corresponding formulae presented. Additional shield configurations exist, but will not be discussed in detail to limit the size of this section of the report.
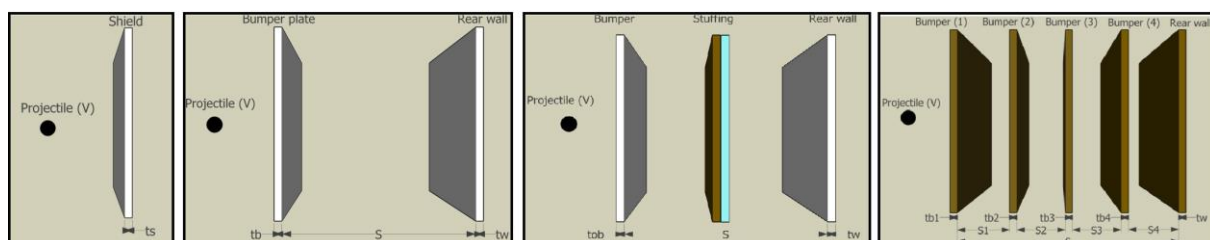
Figure 68: MMOD shield configurations [Source: 150]
(Left to right) Single wall, Whipple, stuffed Whipple and flexible multi-shock configurations

The single wall shield is the least effective configuration for MMOD protection, since the MMOD shield consists only of the satellite wall. This was primarily used in the early days of spaceflight. The penetration depth of a particle into the shield can be calculated using the equations in (7).

$$
\left.
\begin{aligned}
P_\infty &= 5,24 * d_p^{19/18} * HB^{-0,25} * \left(\rho_p \middle/ \rho_s \right)^{0,5} \left(V_p \cos\theta \middle/ C \right)^{2/3} \quad if \left(\rho_p \middle/ \rho_s \right) < 1,5 \\
P_\infty &= 5,24 * d_p^{19/18} * HB^{-0,25} * \left(\rho_p \middle/ \rho_s \right)^{2/3} \left(V_p \cos\theta \middle/ C \right)^{2/3} \quad if \left(\rho_p \middle/ \rho_s \right) \ge 1,5
\end{aligned}
\right\}
\tag{7}
$$

where P is the penetration depth, d_p is the particle diameter, HB is the Brinell hardness, ρ_p and ρ_s are the particle and shield density respectively, V is the particle velocity, θ is the angle between the velocity vector and the shield normal and C is a coefficient.

From the penetration depth calculated using these equations, the wall thickness can be found by applying a safety factor. The recommended safety factor depends on the shield configuration, the shield material and the allowable damage to the shield. Typically though a factor of 3,0 is used to prevent perforation and spallation (ejection of material from the shield due to impact or stress) and this factor will be used here for the MMOD shield design.

The Whipple shield was developed to provide additional protection from meteoroids and debris. It offers improved protection over the single wall shield by adding a bumper wall at some offset, S, from the satellite wall. Equations (8) and (9) are used to determine the thickness of the bumper and satellite wall for a metallic Whipple shield.

$$
t_b = c_b * d_p * \frac{\rho_p}{\rho_b}
\tag{8}
$$

$$
t_w = c_w * d_p^{0,5} * \left(\rho_p \rho_b \right)^{1/6} m_p^{1/3} \left(V_p \cos\theta \middle/ S^{0,5} \right) \left(70 \middle/ \sigma_y \right)^{0,5},
\tag{9}
$$

where t_b and t_w are the bumper and wall thicknesses respectively, c_b and c_w are coefficients, ρ_b is the bumper density, m_p is the particle mass, S is the spacing between the bumper and the rear wall and σ_y is the yield stress of the rear wall material. All other variables are as explained earlier.

The stuffed Whipple shield and the flexible multi-shock shields further improve shielding performance by adding additional layers. The stuffed Whipple shield adds a layer of (flexible) material (e.g. Nextel, Kevlar) between the front bumper and the satellite wall, while the flexible multi-shock shield uses several ceramic bumpers to shield a flexible satellite wall. The barrier, stuffing and wall thicknesses for the stuffed Whipple shield can be calculated using equations (8) and (10) through (12).

$$
AD_{stuffing} = c_{stuffing} * d_p * \rho_p
\tag{10}
$$

$$
AD_b = t_b * \rho_b + AD_{stuffing}
\tag{11}
$$

$$t_w = c_w * \left(\frac{AD_b}{c_0 * d_p * \rho_p} \right)^{-1,1} * \frac{m_p * \left(V_p \cos^{3/2} \theta \right)}{\rho_w S^2 \left(\frac{\sigma_w}{40} \right)^{1/2}},$$ (12)

where $AD_{stuffing}$ and AD_b are the stuffing and barrier areal densities respectively, c_o and $c_{stuffing}$ are coefficients and σ_w is the yield stress of the rear wall

For a multi-shock shield with four equally spaced ceramic fabric bumpers and a flexible rear wall, the areal densities of the bumper(s) and the wall are given by equations (13) and (14)

$$AD_b = 0,19 * d_p * \rho_p$$ (13)

$$AD_w = K * m_p * \frac{\left(V_p \cos \theta \right)}{S^2},$$ (14)

where AD_w is the areal density of the rear wall and K is a material dependent constant (K =43,6 for Nextel and K = 29,0 for Kevlar).

The above listed equations, along with additional formulae for different types of shields and other velocity ranges, can be found in [150].

6.3.2. Design

By varying the configuration and the materials used in the design, it is again possible to minimize the mass while still meeting the requirements. Table 26 lists different materials which have been considered for use in the debris shield, along with the relevant properties needed to perform the design calculations.

Table 26: MMOD shield material candidates with relevant properties [63,150,151,152,153,154]

Material	Density [g/cm³]	Brinell hardness [BN]	Yield stress [MPa]
Kevlar 49	1,44	-	-
Nextel 312 AF10	2,7	-	-
Ti-5Al-2.5Sn ELI	4,48	311	720
Ti-15V-3Cr-3Al-3Sn	4,73	257	772
Al 7075-O	2,81	60	103
Al 2024-T4	2,78	120	324

For the inflatable section of the habitat the flexible multi-shock shield was selected, using Kevlar as the material. The shield has a total spacing between the first and last layer of 25 cm and an areal density of 2,65 kg/m².

For the rigid section of the habitat, a Whipple shield made from Aluminium 2024-T4 was chosen. With a spacing of 25 cm between the two layers, the shield has a total thickness of roughly 26,5 cm and a weight per unit area of 42,43 kg/m².

6.4. Radiation shielding design

The expected radiation dose on the lunar surface, without shielding, due to the different radiation sources was discussed in section 3.6 of this report. As mentioned, the ESA standard for the allowable radiation dose is 0,5 Sv/year and a 1 Sv career limit. With an unshielded radiation dose of ~300 mSv/year due to galactic cosmic radiation and (potentially) several solar flares per year, each resulting in a radiation dose of up to 1 Sv, it will be necessary to have radiation shielding to reduce the expected dose to below the allowable dose. This radiation shielding will be discussed in this section, starting with a brief overview of the theory and formula, followed by the trade-off of shielding options.

6.4.1. Theory and Formulae

Barring exotic solutions such as generating electromagnetic fields to protect against radiation, shielding is done by placing mass between the radiation source and the object which is to be shielded. Through interaction between the radiation and the mass, the (potentially) harmful energy of the radiation is reduced, resulting in a lower amount of energy impacting on the object.

Radiation consists of photons, charged particles and neutrons with a large range of energies and each of the radiation components has different interaction mechanisms with matter. As a result, materials which provide excellent protection against a certain type of radiation may not be the optimal choice for other types of radiation.

For protons and heavy ions, energy transfer from the charged particle to matter is done through ionization and excitation of atoms. Energy transfer through nuclear collisions is neglected, based on the assumptions that the particles will have high velocities.

Based on the expected energy loss per interaction, an average rate of energy loss can be determined. This so called stopping power is calculated using equation (15) [155]:

$$-\frac{dE}{dx} = \mu Q_{avg} = \mu \int_{Q_{min}}^{Q_{max}} Q W(Q) dQ. \tag{15}$$

Based on relativistic quantum mechanics, Bethe developed a relationship for the stopping power (see equation (16)) which can be used to determine the general formula (given in equation (17)) for the stopping power of any material with respect to a proton (or heavy ion) of arbitrary energy.

$$-\frac{dE}{dx} = \frac{4\pi k_0^2 z^2 e^4 n}{m_0 c^2 \beta^2} * \left[\ln \frac{2 m_0 c^2 \beta^2}{I_{eV}\left(1 - \beta^2\right)} - \beta^2 \right] \tag{16}$$

$$-\frac{dE}{dx} = \frac{5{,}08 * 10^{-31} * z^2 * n}{\beta^2} \left[\ln \frac{1{,}02 * 10^6 * \beta^2}{I_{eV} * \left(1 - \beta^2\right)} - \beta^2 \right], \tag{17}$$

where

k_0 is a constant ($8{,}99 * 10^9$ N*m^2/C^2),
z is the atomic number of the particle,
e is the magnitude of the electron charge,

n is the number of electrons within a unit volume of the material,

m_o is the electron rest mass,

c is the speed of light in a vacuum,

β is $\frac{V}{c}$ (the particle speed as a fraction of light speed),

I_{eV} is the mean excitation energy of the medium and is approximated using equation (18) for elements and equations (18) and (19) for compounds.

$$I_{eV} \cong \begin{cases} 19,0\,eV & Z=1\,(hydrogen) \\ 11,2+11,7*Z\,eV & 2 \le Z \le 13 \\ 52,8+8,71*Z\,eV & Z > 13 \end{cases} , \qquad (18)$$

$$n*\ln I_{eV} = \sum_i N_i * Z_i * \ln I_i . \qquad (19)$$

For electrons (and positrons), energy transfer from the charged particle to matter is done through the following mechanisms [155]:

- Collisions
- Bremsstrahlung

The stopping power is subdivided into collisional and radiative stopping power. The collisional stopping power is calculated using equation (20).

$$\left(-\frac{dE}{dx}\right)_{col}^- = \frac{5,08*10^{-31}*n}{\beta^2} * \left[\ln \frac{3,61*10^5 * \tau * \sqrt{\tau+2}}{I_{eV}} + F^-(\beta) \right], \qquad (20)$$

where τ is $\frac{T}{mc^2}$ (kinetic energy of the particle as a multiple of electron rest energy), and $F^-(\beta)$ is calculated using the formula given in (21):

$$F^-(\beta) = \frac{1-\beta^2}{2} \left[1 + \frac{\tau^2}{8} - (2\tau+1)\ln 2 \right]. \qquad (21)$$

No analytic formula exists for calculating the radiative stopping power but an approximate relationship between the radiative and collision stopping power is given by equation (22):

$$\frac{\left(-dE/dx\right)_{rad}^-}{\left(-dE/dx\right)_{col}^-} \cong \frac{ZE_e}{800}, \qquad (22)$$

with E the total energy of the electron and Z the (effective) atomic number of the material.

After calculating the collision stopping power, the radiative stopping power can thus be determined using the previous formula and the two values are summed to obtain the total stopping power.

$$\left(-\frac{dE}{dx}\right)_{tot}^{-} = \left(-\frac{dE}{dx}\right)_{col}^{-} + \left(-\frac{dE}{dx}\right)_{rad}^{-}. \tag{23}$$

Photons are electrically neutral and as such only lose energy through direct interaction (read: collision) with particles in matter. The number of photons which penetrate a certain thickness of matter can be described with equation (24) [155]:

$$N(x) = N_0 e^{-\mu_{lin} x}, \tag{24}$$

where N_0 is the number of (mono-energetic) photons entering the material, x is the thickness (or depth) of the material and μ_{lin} is the (material- and photon energy-dependent) linear attenuation coefficient.

The final type of energetic particle is the neutron. Neutrons will be produced within the shielding material due to interaction between the previously mentioned particles (e.g. protons, heavy ions) and the atoms in the material. A relationship between the incident flux of protons and the secondary flux of neutrons was found from [156] and is shown in equation (25):

$$\Phi_n = \frac{A*\left(1-\exp\left(-3,6*E_p^{1,6}\right)\right)}{R_d^{\ 2}*\left(B*\theta_n + 40*E_p^{-0,5}\right)^2}. \tag{25}$$

Here Φ_n is the number of neutrons per area per incident proton. A and B are coefficients depending on the shielding material, E_p is the proton energy in GeV, R_d is the distance in meters from the surface of incidence and θ_n is the angle in degrees to the direction of incidence of the protons. The relationship in (25) is only given for protons, but will be applied for alpha particles and heavy ions as well. The initial average energy of the neutrons is estimated at 10% of the incident particle energy.

From [157] the stopping power of a material with regards to neutrons is found to be:

$$-\frac{dE}{dx} = 1,53*10^{-32}*N*Z*\left(\gamma^2 - 1\right)*\left(\gamma^2 + 3\right), \tag{26}$$

where N is the number of atoms per unit volume, Z is the atomic number of the material and γ is described by equation (26).

$$\gamma = \left(1-\beta^2\right)^{-\frac{1}{2}} = \left(1-\left(\frac{V_p}{c}\right)^2\right)^{-\frac{1}{2}}, \tag{27}$$

with v the velocity of the neutron and c the speed of light in a vacuum.

The velocity of the different particles can be determined using formula (27) below [158]:

$$E_t = mc^2 = \frac{m_0 c^2}{\sqrt{1 - \dfrac{V_p^{\,2}}{c^2}}}, \qquad\qquad (28)$$

with m_o is the rest mass of the considered particle, E_t the particle energy and V_p and c as defined for equation (26). The rest masses of protons, electrons and neutrons are given in Table 27.

Table 27: Particles and their rest mass [159,160]

Particle	Rest mass [eV]	Particle	Rest mass [eV]
Electron	$5{,}11*10^5$	Neutron	$9{,}39*10^8$
Proton	$9{,}38*10^8$	Alpha	$3{,}73*10^9$

It is mentioned in [161] that when the kinetic energy of the particle is small compared to the rest mass the classic relationship between energy and velocity (29) is sufficiently accurate.

$$E_k = \frac{m_p}{2V_p^{\,2}} \qquad\qquad (29)$$

Figure 69 shows the velocity versus kinetic energy of different particle types as calculated using the classic and relativistic equations. It can be seen that the classic relationship does not limit the particle velocity to the speed of light, furthermore, it can be seen that (as expected) due to the high rest mass of alpha particles, the classic and relativistic velocities agree reasonably well up to a very high kinetic energy (approx. 500 MeV). For heavier particles, the two relationships will produce similar results for kinetic energies even higher than 1 GeV. Thus, the classic relationship will be used for particles with a rest mass higher than an alpha particle (e.g. heavy ions with Z>2).
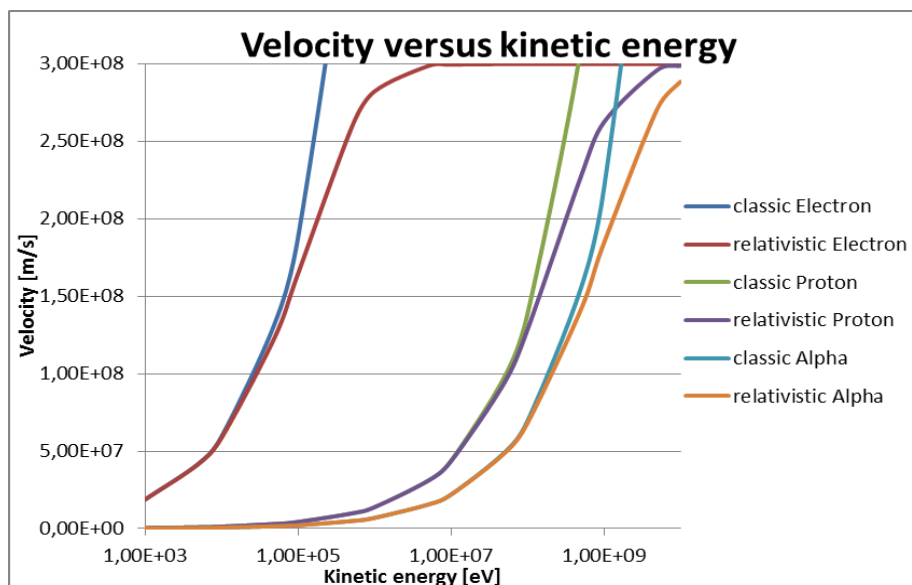
Figure 69: Comparison of classic and relativistic velocity-energy relationships for various particles

6.4.2. Design

The different sources of radiation, such as solar wind and SPEs, are modelled in terms of the types of particles and the energy of those particles. See Table 28 for discretized standard flux and Table 29 for the (additional) particle fluence of an SPE.

Table 28: Particle flux and particle energy for average lunar conditions

Particle	Flux [particles/m²*s] (Energy [eV])				
Electron	$1*10^{14}$ ($1*10^3$)	$1*10^{14}$ ($1*10^4$)	$1*10^{12}$ ($1*10^5$)	$1*10^{10}$ ($1*10^6$)	$1*10^8$ ($1*10^7$)
Proton	$5*10^{13}$ ($1*10^3$)	$5*10^{13}$ ($1*10^5$)	$5*10^{12}$ ($1*10^7$)	$1*10^9$ ($1*10^8$)	$5*10^5$ ($1*10^{11}$)
Alpha	$1*10^6$ ($1*10^4$)	$1*10^7$ ($1*10^6$)	$5*10^7$ ($1*10^7$)	$1*10^8$ ($1*10^8$)	$6*10^5$ ($1*10^{11}$)
Ion	$1*10^6$ ($1*10^4$)	$1*10^6$ ($1*10^5$)	$2.5*10^8$($1*10^6$)	$2.5*10^8$ ($1*10^8$)	$2.5*10^5$ ($1*10^{11}$)
Photon	$1*10^8$ ($1*10^3$)	$5*10^8$ ($1*10^4$)	$5*10^7$ ($1*10^5$)	$1*10^7$ ($1*10^6$)	$2.5*10^6$ ($1*10^8$)

Table 29: Particle fluence and particle energy for a (large) SPE

Particle	Flux [particles/m²*s] (Energy [eV])				
Electron	$5*10^{13}$ ($1*10^3$)	$5*10^{13}$ ($1*10^4$)	$1*10^{12}$ ($1*10^5$)	$2.5*10^{11}$ ($1*10^6$)	$1*10^9$ ($1*10^7$)
Proton	$1*10^{13}$ ($1*10^3$)	$1*10^{13}$ ($1*10^5$)	$1*10^{12}$ ($1*10^7$)	$1*10^9$ ($1*10^8$)	$1*10^6$ ($1*10^{11}$)
Alpha	$2.5*10^{12}$ ($1*10^4$)	$2.5*10^{12}$($1*10^6$)	$5*10^{10}$ ($1*10^7$)	$1*10^9$ ($1*10^8$)	$5*10^5$ ($1*10^{11}$)
Ion	$1*10^{12}$ ($1*10^4$)	$1*10^{10}$ ($1*10^5$)	$2.5*10^8$ ($1*10^6$)	$5*10^7$ ($1*10^8$)	$1*10^5$ ($1*10^{11}$)
Photon	$1*10^{12}$ ($1*10^3$)	$1*10^{12}$ ($1*10^4$)	$5*10^{10}$ ($1*10^5$)	$1*10^9$ ($1*10^6$)	$4*10^8$ ($1*10^7$)

Using the 'continuously slowing down approach' (csda) [155], in which the assumption is made that the particles lose a constant amount of energy per unit distance travelled through a material, it is possible to determine the amount of energy which is lost and how much energy is left in the particles which make it through the shielding material.

CSDA is applied for all particle types except photons. For photons, the assumption is made that a photon loses all of its energy upon interaction with matter and that no energy is lost otherwise.

By determining the number of particles which pass through the shield and the remaining energy the particles have at that point, it is possible to determine the amount of radiation. As mentioned in section 3.6, not all types of radiation are equally damaging though and as such the quality factors listed in Table 30 are applied to obtain the final estimate of the shielded radiation dose.

Table 30: Biological Damage Factor, or Quality Factor, for different particle types

Particle	Quality Factor
Photons	1
Protons and electrons	10
Neutrons	10
Heavy ions	20
Alpha particles	20

The required shielding thickness was calculated for different materials to ensure that the shielded dose over the mission lifetime was less than the allowable limit. Some of the material-specific properties required for the calculations can be seen in Table 31.

Table 31: Relevant properties for different radiation shielding material options

Material	Number of atoms per unit volume	Effective atomic number (Z)	Mean excitation energy [eV]	Density [g/cm³]
Aluminium	$6,03*10^{28}$	13	163,3	2,78
Water	$3,35*10^{28}$	7,42	74,59	1,0
Regolith	$8,23*10^{28}$	11,16	150,16	3,1

The photon attenuation coefficients for the different materials and photon energies were determined using the web-based version of XCOM [162], which can calculate the total and partial attenuation coefficients for the first hundred elements and compounds and mixtures made of those elements for photon energies from 1 keV to 100 GeV. For the materials listed in Table 31, the total photon attenuation coefficient (with coherent scattering) was plotted against photon energy and the result can be seen in Figure 70. The regolith composition shown in Table 32 was used to determine the photon attenuation coefficients.

Table 32: Regolith composition [163]

Element	Wt. %	Element	Wt. %	Element	Wt. %
Oxygen	42,64	Calcium	7,71	Natrium	0,35
Titanium	3,2	Magnesium	6,09	Chromium	0,25
Aluminium	7,55	Manganese	0,15	Silicium	20,22
Iron	11,69	Kalium	0,16		
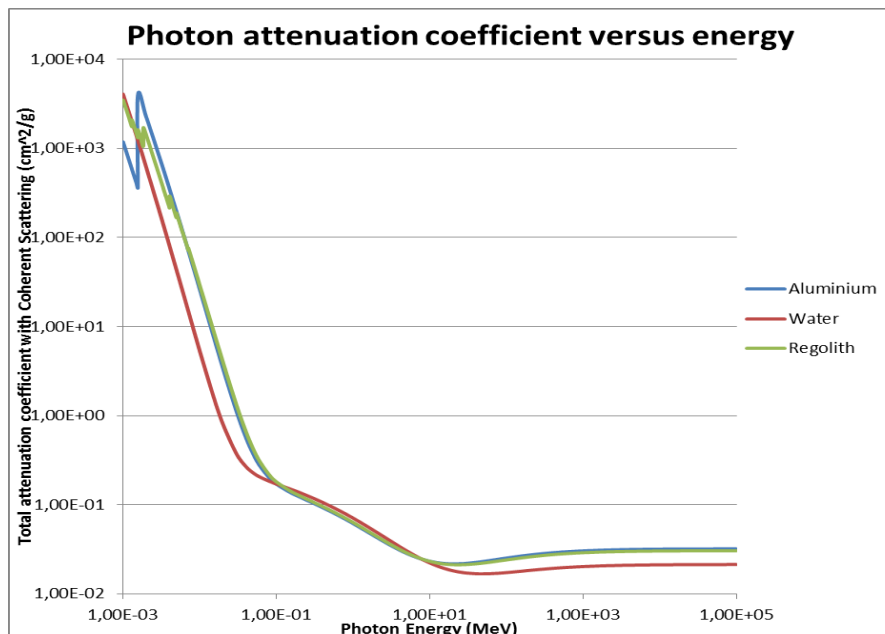
Figure 70: Photon attenuation coefficient versus photon energy for radiation shielding materials

A MatLab script was written to determine the shielding thickness which is required to reduce the absorbed radiation dose to below acceptable levels. The results are listed in Table 33. Radiation dose calculations were based on an average astronaut having a mass of 80 kg.

As mentioned in section 3.6, ESA has a radiation limit of 0.5 Sv/year. To obtain a conservative design, the allowed radiation dose within the shielded structure is taken to be 0.25 Sv/year.

Table 33: Minimum radiation shielding thickness and mass for various materials

Material	Shield thickness [m]	Shield mass [kg]	Radiation dose [mSv]
Aluminium	2,69	$4,37*10^6$	249,93
Water	5,91	$4,67*10^6$	249,99
Regolith	2,29	$3,97*10^6$	249,89

The regolith shielding option will be selected, since this option has the lowest shield mass and thickness and requires no transport of shielding mass from Earth to the Moon. Additionally, the regolith shielding option can be applied to both the rigid as well as the flexible sections of the structure, whereas aluminium for example cannot.

6.5.   Thermal protection design

The design of the lunar structure needs to consider the thermal environment in which it will operate to allow for proper design of the cooling and/or heating components which are needed. Additionally, temperature differences between different parts of a structure can lead to displacements and stresses which may need to be prevented or mitigated.

Thus, in this section, the performance of the lunar GHM in the expected thermal environment will be assessed. First, the relevant equations will be discussed, followed by application of these formulae to the design case.

6.5.1. Theory and Formulae

Being situated on the surface of the Moon, the lunar greenhouse module will be subjected to varying amounts of solar radiation, depending on the exact location and the time of the lunar day. The incident solar UV radiation results in heat being absorbed by the structure. The amount of absorbed heat, Q_{heat}, can be calculated with the following formula [164]:

$$Q_{heat} = \alpha A_S \left(F_{solar} G_{solar} + F_{lunar} G_{albedo} \right),$$ (30)

with α the ultraviolet absorption coefficient (absorbtivity), A_S the surface area, G_{solar} the incident solar flux on the lunar surface (~1353 W/m²), G_{albedo} is the incident albedo flux, F_{solar} is the view factor from the surface to the Sun and F_{lunar} is the view factor from the GHM surface to the lunar surface. The view factor indicates the percentage of view a surface has to another surface.

Aside from the absorption of solar radiation, the external surface(s) of the lunar GHM will have heat transfer to/from space and the lunar surface through IR radiation. The net heat transfer between two surfaces due to IR radiation, $Q_{rad,ij}$, can be calculated using equation (31) [164]:

$$Q_{rad,ij} = F_{ij} A_i \varepsilon \sigma \left(T_i^4 - T_j^4 \right),$$ (31)

where A_i is the area of the surface on which the radiation is incident, ε is the (infrared) emissivity, σ is the Stefan-Boltzmann constant ($5,67051*10^{-8}$ W/m*K⁴), T_i and T_j are the temperatures of the two surfaces and F_{ij} is the view factor of surface i to surface j.
Neglecting (momentarily) the heat flow from the external surface to the interior of the GHM (and vice versa), a steady state temperature can be determined for the external surface of the structure by equating the incoming heat to the outgoing heat. Since the atmosphere on the Moon is

negligible, heat convection between the external surface and a fluid flowing past it (e.g. air) can also be neglected. Also neglecting the influence of the (nearby) buildings of the lunar base, the heat balance for a surface of the lunar GHM can be written as equation (32)

$$\alpha A_S \left(F_{solar} G_{solar} + F_{lunar} G_{albedo} \right) = F_{space} A_S \varepsilon \sigma \left(T_{surface}^4 - T_{space}^4 \right) + F_{ground} A_S \varepsilon \sigma \left(T_{surface}^4 - T_{ground}^4 \right), \quad (32)$$

with F_{space} the view factor from the surface to space, F_{ground} the view factor from the GHM surface to the lunar surface and $T_{surface}$, T_{space} and T_{ground} the temperatures of the GHM surface, space and the lunar surface respectively.

In reality, some heat will flow between the exterior and interior surface of the lunar GHM through heat conduction. For a (one-dimensional) situation with a given exterior and interior surface temperature, the amount of heat conducted is calculated using (33)

$$Q_{cond} = \frac{k_c A_S}{L} \Delta T, \quad (33)$$

where k_c is the thermal conductivity of the structure wall, A_S is the wall surface area, L is the wall thickness and ΔT is the temperature difference.

The structure shape is modelled as a rectangle to simplify the calculation of the view factors. The view factors from the Sun to the surfaces of the structure, as well as the lunar surface to the structure are calculated using relations from [165]. For simplicity it is assumed that the Sun is precisely in the zenith direction with respect to the greenhouse.

6.5.2. Design

The first step in the thermal design is to define the hot and cold worst cases, which have, respectively, the maximum and minimum heat flux to and minimum and maximum heat flux from the structure.

From [128] it is found that the temperature at the lunar surface at the selected operating site is 89 K and 292 K for dark and illuminated conditions respectively. The minimum and maximum solar thermal radiation levels correspond to the scenarios where the greenhouse is, respectively, not illuminated at all, or completely illuminated. The solar flux on the lunar surface is approximately 1353 W/m², and additionally 7% of incident solar flux is reflected as albedo which will also impact the thermal loading of the greenhouse [165].

From [134] a linear relationship between the power consumption and the growing area in a plant growth chamber is found, where 2,6 kW of power is used per square meter of crop area. Taking this value and assuming that at least 50% and as much as 70% of the consumed power is lost as heat, the internal heat load within the lunar greenhouse ranges from 104 kW to 145,6 kW.

Potential heat entering into the greenhouse due to radioactive decay of elements within the lunar soil or through resource flows between lunar base buildings is assumed to be minor and is thus neglected for the preliminary analysis done here. An overview of the relevant data for the hot and cold cases is presented in Table 34 and the thermal optical material properties are listed in Table 35. For the temperature of outer space a value of 8 K is used and for the thermal optical properties it is assumed that the emissivity for a given wavelength (range) is equal to the absorptivity.

Table 34: Thermal parameters for hot and cold case lunar GHM thermal environment [128,165]

Parameter	Hot case	Cold case
Solar flux [W/m²]	1353	0
Albedo [W/m²]	94,7	0
Outer space temperature [K]	8	8
Lunar surface temperature [K]	292	89
Internal GHM temperature [K]	303	293
Internal heat load [kW]	145,6	104

Table 35: Thermal-Optical material properties [153,166,167,168,169]

Parameter	Regolith	Aluminium	Kevlar
UV absorptivity/emissivity	0.93	0.1	0.95
IR absorptivity/emissivity	0.83	0.1	0.95
Conductivity [W/m*K]	0.011	121	0.04
Specific heat capacity [J/g*K]	0.76	0.875	1.42

The structure wall is modelled as a 2-layer wall, with the first layer being the regolith radiation shield, while the second layer is the load-bearing structure layer. Only one-dimensional heat transfer is considered.

A MatLab script was used to determine the external surface temperature and the interior wall temperature. Because of the very small thickness of the interior wall (compared to the regolith thickness), it is assumed that the temperature throughout the load bearing structure material is constant. Table 36 contains the calculated temperatures for the hot and cold cases. For the cold case an eclipse period of 94 hours [128] was considered. The temperature of the regolith underneath the structure is assumed to be equal to the hot case temperature of the lunar surface (292 K).

Table 36: Structure wall temperatures for hot and cold cases

	Hot Case Temperatures [K]		Cold Case Temperatures [K]	
Structure Section	1*	2**	1*	2**
Top, rigid	387	303	341	293
Top, flexible	387	303	341	293
Front / Back	251	303	241	293
Left / Right, rigid	251	303	241	293
Left / Right, flexible	251	303	241	293
Bottom, rigid	292	303	292	293
Bottom, flexible	292	303	292	293

*: External surface temperature regolith
**: Internal surface temperature

It was determined that the amount of heat being transferred from the air inside the GHM (assuming a constant air temperature) to the structure and regolith shield is significantly less than the available internal heat load for both the hot and cold cases. Thus, this 'waste' heat will need to be processed using a thermal control system.

It is assumed that the materials are in a zero (thermal) stress state at a temperature of 293 K. Assuming that all elongation due to temperature variation is blocked, the thermal stresses can be determined in a straightforward manner. These are then added to the nominal load case discussed in the next section.

6.6. Load bearing structure design

The load-bearing capabilities of the lunar GHM need to be assessed for a variety of different loading conditions, both for the stowed and deployed configuration. These loading conditions, along with the (simplified) models and equations used will be briefly addressed in section 6.6.1 after which the design calculations are performed and discussed in section 6.6.2.

6.6.1. Theory and Formulae

The structural analysis can be divided into two parts: static and dynamic analysis. Static analysis focuses on the response of the (stowed or deployed) structure to a steady loading case, while dynamic analysis determines the behaviour of the structure when exposed to a transient load (e.g. an impact).

For the preliminary design simplified models of the structure will be used to allow determination of the relevant characteristics of the structural behaviour while limiting the complexity of the calculations.

Free Body Diagrams (FBDs) are drawn for the complete models and for sections of the models and the corresponding equations are derived. Solving the equations allows for determination of for example reaction forces and internal stresses, among other parameters.

The stowed greenhouse is expected to have a configuration as discussed previously in section 5.1.4, with the floors of the two rigid end-caps touching each other. Two caps will be attached to the stowed structure. The bottom cap will be fixed in some fashion to the payload adapter, while the top cap will ensure that the rigid sections remain fixed with respect to each other and that the flexible section cannot move. The flexible section, in the stowed configuration, is not expected to carry any load.

The stowed configuration of the structure is modelled as a thin-walled beam of approximately 5 meters length, which is clamped at one end. The cross-section of the beam is circular, with a stiffener (simulating the two floors of the rigid sections) bisecting it.

The main characteristics of relevance for the stowed configuration are the eigenfrequencies, which determine the structural response to launch shocks, and the critical buckling load, which should be such that the structure will not buckle when subjected to launch accelerations.

The eigenfrequencies of the column model are determined using the general relationship between stiffness, mass and the eigenfrequency, along with the standard relationships for the stiffness, longitudinal (eq. 34) and lateral (eq. 35), of a beam.

$$k_{lon} = \frac{EA}{L_{beam}},$$
(34)

$$k_{lat} = \frac{3EI}{L_{beam}^3},$$
(35)

where E is the Young's modulus of the material, I is the moment of inertia, A is the cross-sectional area, and L_{beam} is the beam length.

The moments of inertia of the column model are calculated using equations (36) and (37):

$$I_x = \int_A (y - \bar{y})^2 \, dA,$$ (36)

$$I_y = \int_A (x - \bar{x})^2 \, dA.$$ (37)

The critical buckling load is determined by applying either the Euler relationship (eq. 38) or the Johnson formula (eq. 39), depending on whether the beam is strength-limited or not.

$$F_{cr} = \frac{\pi^2 E A}{4 \left(L_{beam} \middle/ r \right)^2},$$ (38)

$$F_{cr} = A \left[\sigma_y - \left(\frac{\sigma_y L_{beam}}{2 \pi r} \right)^2 \frac{1}{kE} \right],$$ (39)

where r is the radius of gyration and is calculated using equation (40):

$$r = \sqrt{\frac{I}{A}}.$$ (40)

The beam is strength-limited, meaning that the yield stress is reached before Euler buckling occurs, if the inequality in (eq. 41) is true [170]:

$$\frac{L_{beam}}{r} < \sqrt{\frac{2 \pi^2 E k}{\sigma_y}}.$$ (41)

For the deployed structure, three design cases were considered; a burst pressure case, in which an internal pressure of 4 times the nominal was applied, a nominal case and a case involving a loss of pressure inside the structure.

It is expected that the thicknesses will be significantly smaller than the other dimensions of the greenhouse structural elements and therefore the structure will be modelled as a collection of plate and shell elements. Since finding an analytical solution for the behaviour of plates and shells with specific loads and boundary conditions is not always an option, it was decided to use formulas from [171] for similar situations and apply additional safety factors to account for the differences in Poisson's ratio or boundary conditions, among others.

The stress in the semi-circular end caps was determined using the formula, see equation 42, for case #30 from Table 11.2 [171], which describes a solid semicircular plate with a uniformly distributed load and with all edges fixed, and substituting the design values.

$$\sigma_{max} = -0.42 * \frac{q R^2}{t^2}$$ (42)

Here q is the distributed (pressure) load, R is the radius of the semicircular plate and t is the plate thickness.

As a comparison for the results of equation 42, the thickness of the end caps was calculated using equation 43, which gives the minimum thickness for flat heads on cylindrical pressure vessels according to ASME standards [172].

$$t = d * \sqrt{\frac{C * P_{design}}{S * E_{joint}}}$$ (43)

Here d is the outer diameter of the flat head, C is a factor dependent on the geometry, P_{design} is the design pressure, S is the maximum allowable stress in tension and E_{joint} is a factor representing the joint efficiency.

The stress in the floor plates as a result of the internal pressure was determined using cases #9a and #6, for the rigid and flexible sections respectively, from Table 11.4. The first case corresponds to a rectangular plate with three edges fixed and one simply supported, subjected to a uniform loading over the entire plate. The second case corresponds to a rectangular plate, with the long edges fixed and the short edges simply supported, subjected to a uniform loading.

$$\sigma_{max} = -\beta * \frac{qb^2}{t^2}$$ (44)

Equation 44 can be used for both cases, by selecting the proper value for the geometry-dependent coefficient β. As with equation 42, q is the distributed load and t is the plate thickness. b is the length of the short side of the plate.

The stresses in the arch roof of the greenhouse subjected to pressure loading were calculated using the well-known relations for a cylindrical pressure vessel. For the nominal case, thermal loading was taken into account as well. Assuming all displacement due to thermal expansion is blocked, the thermal stresses can then be calculated using equation 45

$$\sigma = E * \varepsilon = E * \alpha * \Delta T$$ (45)

E is the Young's modulus of the material, ε is the strain, α is the temperature expansion coefficient and ΔT is the temperature difference.

For the final case, involving a greenhouse without internal pressure, the main design criteria is preventing collapse (buckling) of the structure under applied self-weight and regolith loading.
Here it was assumed that the arch roof carries all loads and the critical buckling load was determined using equation 46 [173].

$$p_{cr} = \beta * (0.855) * \frac{E * t^2}{RL(1 - v^2)^{0.75}} \sqrt{\frac{t}{R}}$$ (46)

P_{cr} is the critical buckling load, β is a coefficient dependent on the ratio between thickness and arch radius, E is the Young's modulus, t is the arch thickness, R is the arch radius, L is the arch length and v is the Poisson's ratio.

6.6.2. Design

The most important (design-driving) load cases were determined by examining the life cycle of the lunar GHM. The load cases which were considered for the structural analysis of the greenhouse structure are listed in Table 37 below.

Table 37: Load types and design properties

Structure configuration	Load type(s)	Investigated property
Stowed	Launch accelerations and shocks	Buckling, Eigenfrequencies
Deployed	Static / Burst Pressure	Max. stress
Deployed	Static / Normal Pressure, Self-weight, Regolith loading, Thermal	Nominal stress
Deployed	Static / Self-weight, Regolith Loading	Buckling

The materials used in the load-bearing structural layers are Al 2024-T4 and Kevlar, similar to the MMOD shielding layer. For these initial calculations, it was assumed that Kevlar behaves as an isotropic material. Relevant properties for these materials are listed in Table 38.

Table 38: Material properties of Al 2024-T4 and Kevlar [153,167]

Property	Al 2024-T4	Kevlar
Density [kg/m^3]	2780	1440
Yield Stress [MPa]	324	1240
Ultimate Stress [MPa]	469	3000
Young's Modulus [GPa]	73.1	76
Poisson's ratio [-]	0.33	0.36
Coefficient of thermal expansion [m/m*K]	$23.2*10^{-6}$	$-4*10^{-6}$

The response of the structure to the different loading cases was calculated using the equations described in the previous section. The design loads and limits used in conjunction with these equations are shown below (see Table 39).

Table 39: Design parameters and coefficients

Property	Value
Launch acceleration, Longitudinal [g]	7
Launch acceleration, Lateral [g]	2.5
Required Eigenfrequency, Longitudinal [Hz]	>31
Required Eigenfrequency, Lateral [Hz]	>10
Nominal pressure [Pa]	101000
Burst pressure [Pa]	404000
Temperature difference [K]	10

After several iterations a design was found which is capable of withstanding the various load scenarios. The thicknesses and weights corresponding to the various structural elements of this design are listed in Table 40.

Table 40: Thickness and weight of the various load-bearing sections

Structure Section	Thickness [mm]	Weight [kg]
Top, rigid	20	5398
Top, flexible	20	2633
Front / Back	80	3145
Bottom, rigid	125	21476
Bottom, flexible	80	6705
Total Structure		39357

The large thicknesses for the end caps and the floor are due to the fact that plate models were used. In follow up design a more realistic honeycomb structure with stiffeners and beams will allow for significant weight reduction.

6.7.   Summary

In this chapter the preliminary design of the lunar GHM structure was detailed. Based on an analysis of the required crop grow area and dimensions of the expected grow system it was found that the greenhouse would have to be unfeasibly large in order to meet the edible biomass production targets. Instead, it was decided to limit the length of the structure to 20 m. Based on estimated and assumed dimensions of the systems, an internal configuration of the GHM was created and the radius of the structure was set at 3 m, leading to an internal volume of 283 m^2.

Along with the internal configuration of the equipment and systems, the interface between the flexible and rigid sections of the structure was selected and interfaces from the GHM to the rest of the lunar base were discussed.

Following this initial sizing of the structure, the various functional layers of the structure were designed. To ensure that the gas loss from the structure is within acceptable limits, the gas retention layer was designed to consist of HDPE, additionally, for fail-safe operation, the gas retention layer is implemented with double-redundancy and a Kevlar felt bleeder cloth is placed between two gas retention layers. The rigid section of the structure is assumed to have negligible permeability and to be puncture-proof.

To protect against (micro-)meteoroids, lunar ejecta and debris, various shielding configurations and materials were investigated for the GHM structure design. Based on the particle fluence, it was determined that there is a 95% chance that no particles bigger than 1,16 g will impact the structure during the mission lifetime and as such the structure was designed to withstand an impact from such a particle. A flexible multi-shock shield made from Kevlar was designed for the flexible section of the structure, while a Whipple shield was found to be most suitable for the rigid sections of the GHM.

The radiation shielding of the structure was designed based representative particle fluences for nominal and solar flare conditions. Using stopping power equations the decrease in particle energy, hence also the radiation dose, can be determined as a result of the shielding thickness, which made it possible to calculate the minimum required shield thickness. Regolith was selected as shielding material, since it is available in-situ on the Moon and therefore the launch mass and cost of the structure can be smaller. A shielding thickness of almost 2,5 m was found to be needed for adequate protection of the interior of the greenhouse.

A first analysis of the thermal environment of the lunar GHM was performed using a one-dimensional two-layer wall model of a simplified rectangular-shaped structure. The outer wall was

taken to be the regolith radiation shielding, while the inner layer was the load-bearing material layer. Hot and cold cases were defined and the temperatures at the exterior surface, inner to outer wall boundary and the interior surface calculated. Using a baseline temperature and assuming that no displacement is possible, the stresses caused by the (blocked) thermal expansion were estimated.

Simplified models of the stowed and deployed greenhouse structure were used to do the initial calculations of the structural response to a number of load cases. Critical buckling loads and eigenfrequencies of the stowed structure were determined to ensure the structure is capable of withstanding the launch conditions. Three load cases were considered for the deployed configuration of the lunar greenhouse, specifically a burst pressure case, where the structure is exposed to 4 times the nominal pressure, a nominal case, where the structure is exposed to nominal pressure, self-loading, regolith loading and thermal loading, and an unpressurized case, where the structure is exposed to self-loading and regolith loading. These cases were used to determine the maximum and nominal stresses and displacements of the structure.

Modeling of the load-bearing structure elements as arches and plates results in a design which is significantly heavier and thicker than necessary. Follow up studies will be able to save mass by reducing thicknesses by introducing more efficient load-bearing elements such as stiffeners.

An overview of the materials, thicknesses and corresponding weights for the different layers are listed in Table 41.

Table 41: Preliminary Design Values for the lunar GHM functional layers

Structural Layer		Material	Thickness	Total Weight [kg]
Flexible	Gas Retention layer (3x)	HDPE	0.15 mm	40
	Bleeder cloth layer (2x)	Kevlar	0.1 mm	27
	MMOD layer	Kevlar	~25 cm	243
	Load-bearing layer, top	Kevlar	20 mm	2633
	Load-bearing layer, bottom	Kevlar	80 mm	6705
	Total – Flexible Sections			**9648**
Rigid	MMOD layer	Al 2024-T4	26.5 cm	4119
	Load-bearing layer, top	Al 2024-T4	20 mm	5398
	Load-bearing layer, front / back	Al 2024-T4	80 mm	3145
	Load-bearing layer, bottom	Al 2024-T4	125 mm	21476
	Total – Rigid Sections			**34138**
Total Structure Weight				
Radiation Layer		Regolith	2.29 m	$3.97*10^{6}$

7. Design Verification

The design calculations discussed in the previous chapter are simplified equations which are useful for initial design purposes. It is necessary, however, to determine whether the results of these preliminary calculations are sufficiently accurate and will lead to an acceptable design.

For this purpose, some design verification was performed and these efforts will be presented in this chapter. Specifically, the radiation shielding calculations and the thermal-structural calculations will be checked using specialized software to model the actual behaviour of the greenhouse structure design. From a comparison between the initial results and the modelled results, conclusions can be drawn regarding the validity of the design and the accuracy of the simplified equations.

7.1.   Finite Element Modelling

The structural and thermal response of the structure was modelled using Finite Element Modelling (FEM) techniques. Models were built using Patran 2011 and then, after defining the load cases and element properties, analysed with MSC Nastran 2012.

The geometry of the stowed and deployed structure models is as described in section 6.6, with the surfaces representing the greenhouse walls modelled as 2D shell elements. The material properties and wall thicknesses mentioned in section 6.6.2 were used to allow for a direct comparison between the FEM results and the analytical calculations.

Mesh seeds were defined to ensure a symmetric mesh and to obtain a finer mesh near the structure edges and material transition regions. The actual mesh consisted of Quad4 elements and was applied using the Hybrid meshing tool with standard settings. Figure 71 shows the meshed models for the stowed (left) and deployed (right) greenhouse structure.
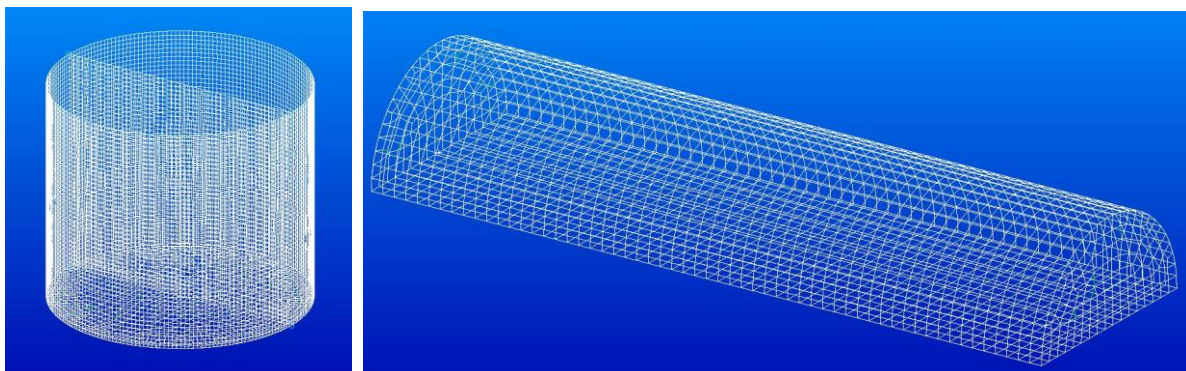
Figure 71: Meshed models for the stowed (left) and deployed (right) configurations of the lunar GHM structure

To determine the eigenfrequencies of the stowed structure, the mass of the structure was modelled using a lumped mass approach. One of the primary lateral eigenmodes of the stowed structure is shown in Figure 72. The corresponding frequency is ~16 Hz, which complies with the demand for an eigenfrequency higher than 10 Hz. Similarly, the eigenfrequency for the other lateral eigenmode complies with the requirements.

The eigenfrequency in the longitudinal direction did not meet the >31 Hz requirement, with eigenmodes in the arches of the rigid sections occurring at lower frequencies

Taking into account the envisioned structure to launcher adapter which would add additional stiffness precisely at these regions, this should not be a problem.
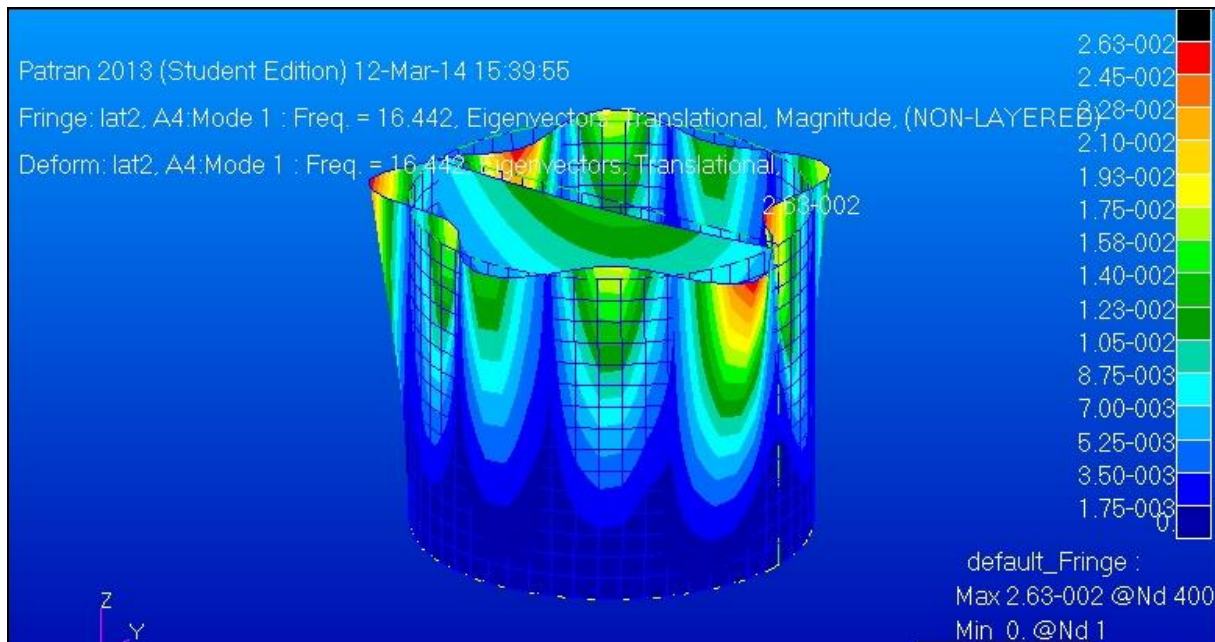
Figure 72: Primary eigenmode of the stowed lunar GHM.

For the buckling analysis, axial and lateral loads were created to simulate the expected launch accelerations of, respectively, 7 g and 2.5g.

Error! Reference source not found. shows the displacement of the structure when subjected to axial load.
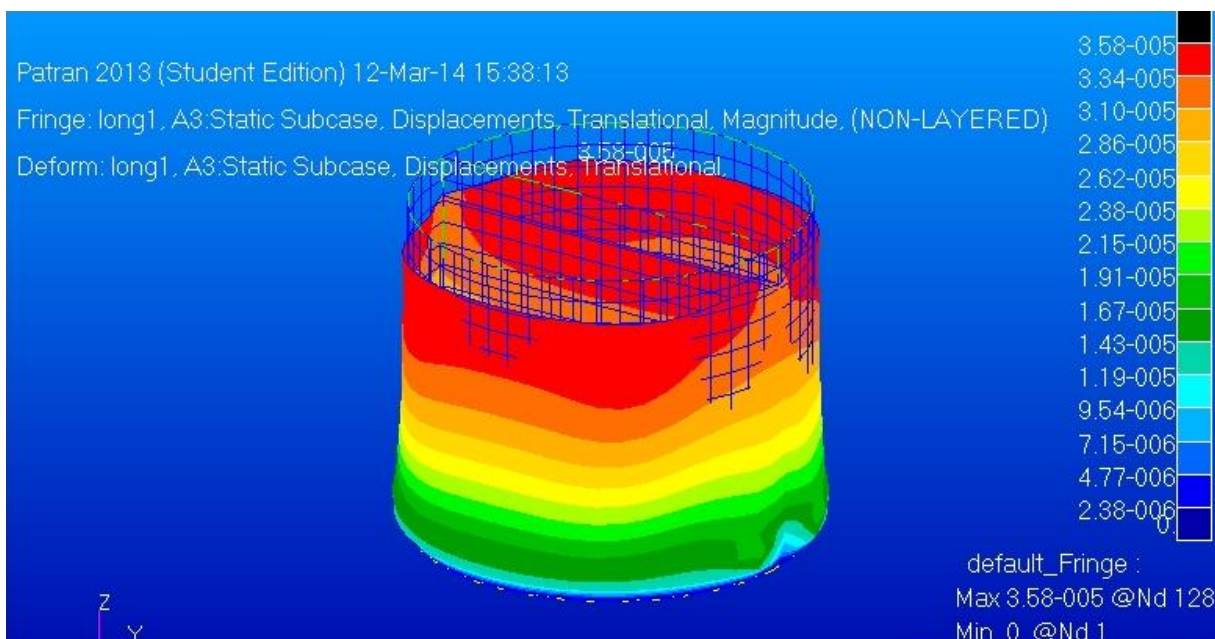
Figure 73: Displacement of stowed configuration subjected to axial acceleration of 7g.

The applied load is significantly lower than the critical buckling load, which means the structure will be capable of withstanding the launch accelerations as expected.

As mentioned in section 6.6, three different loading conditions were analysed for the deployed structure configuration, specifically:

- •Burst pressure (nominal pressure with a safety factor of 4)
- •Nominal conditions (nominal pressure, self-weight, regolith loading and thermal conditions)
- •Non-pressurized (regolith loading and self-weight)

To model the stresses and displacements caused by the nominal thermal conditions, the reference temperature with zero (thermal) stress is taken to be 293 K. Then, a temperature of 303 K was applied to the entire structure. The stresses caused by the temperature difference can be seen in Figure 74.
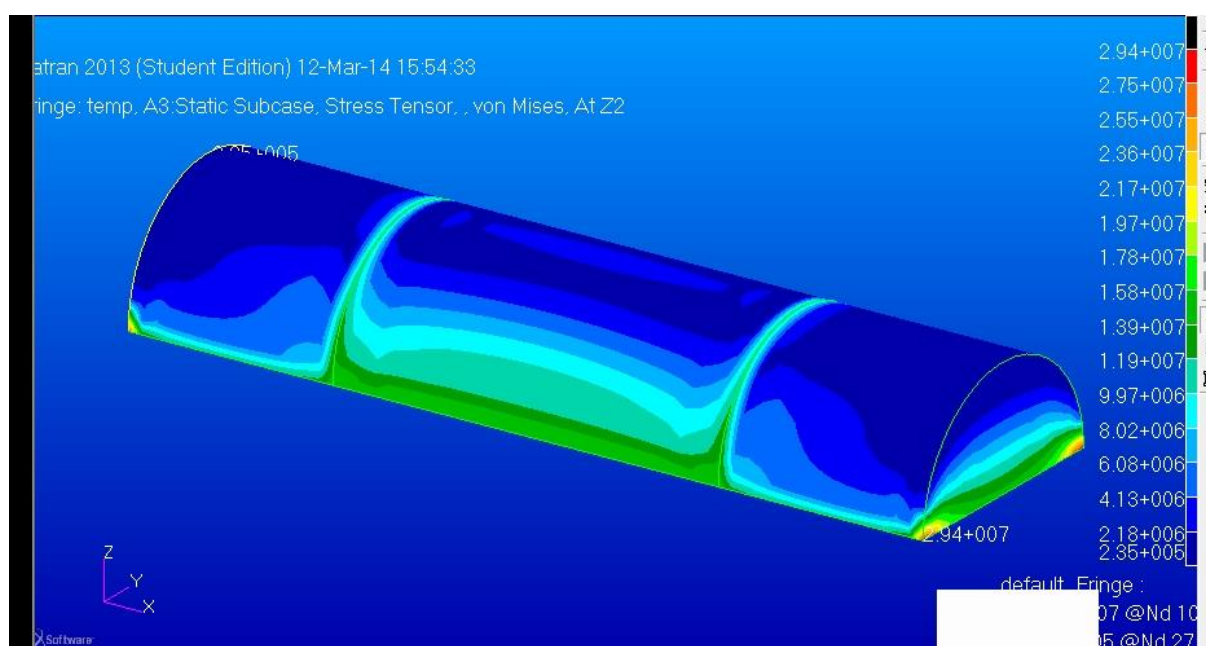
Figure 74: Temperature distribution of the deployed structure

The main structural responses of interest for the deployed structure are the stress and the displacement. The stress and displacement response of the structure to the three load cases can be seen in Figure 75, left and right respectively. From top to bottom, Figure 75 shows the response of the deployed structure for the burst pressure case. Figure 76 shows the stress in the (bottom of the) structure in the nominal case. As expected the stress distribution is quite similar to the burst pressure case. Figure 77 shows the displacement for the structure in the unpressurized case, indicating a flattening of the structure on the top and bulging at the sides.

The burst pressure case was analyzed as non-linear static, while the other two cases were analyzed as linear static.
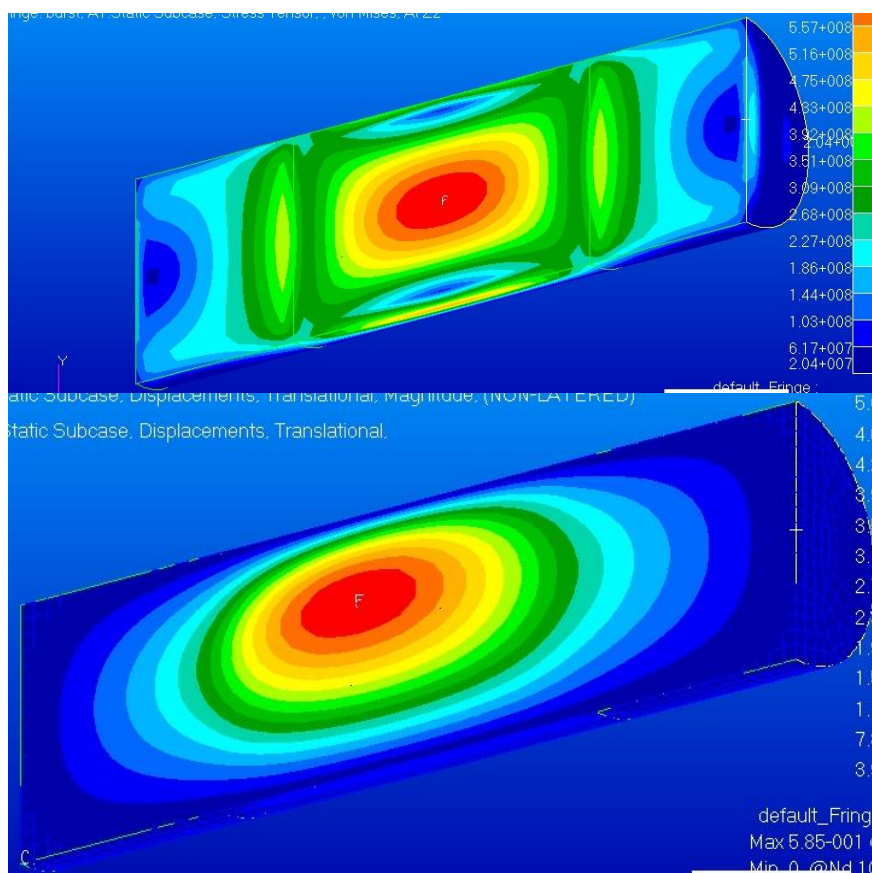
Figure 75: Stress (Top) and Displacement (Bottom) of the deployed structure. Burst pressure case.
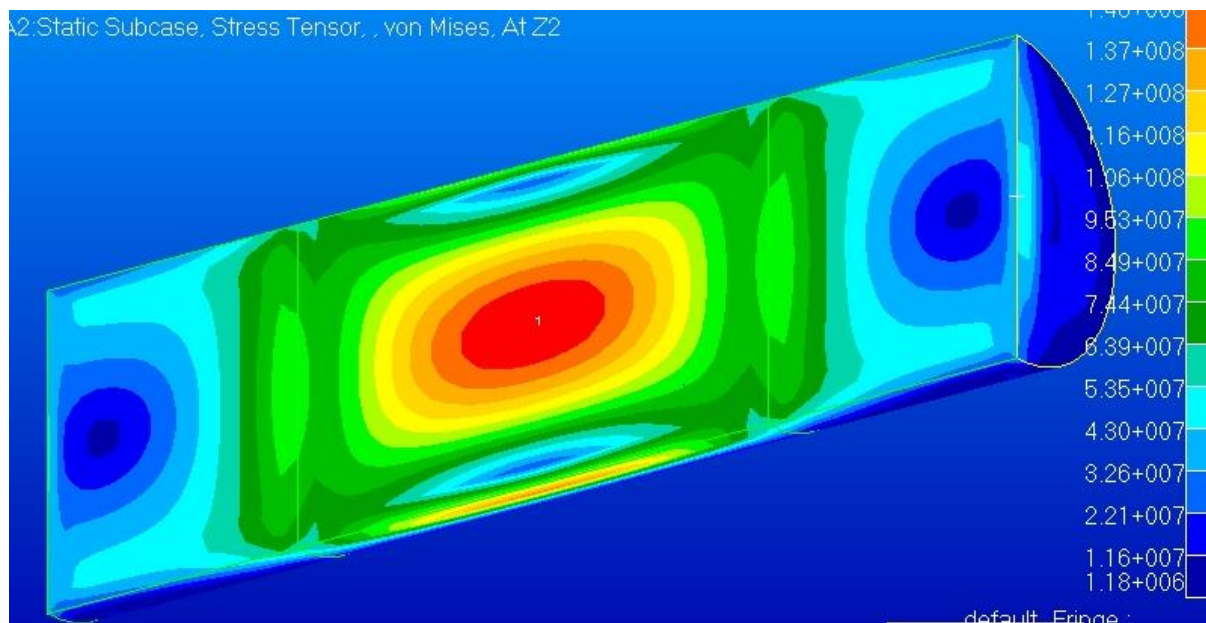
Figure 76: Stress of the deployed structure. Nominal case.
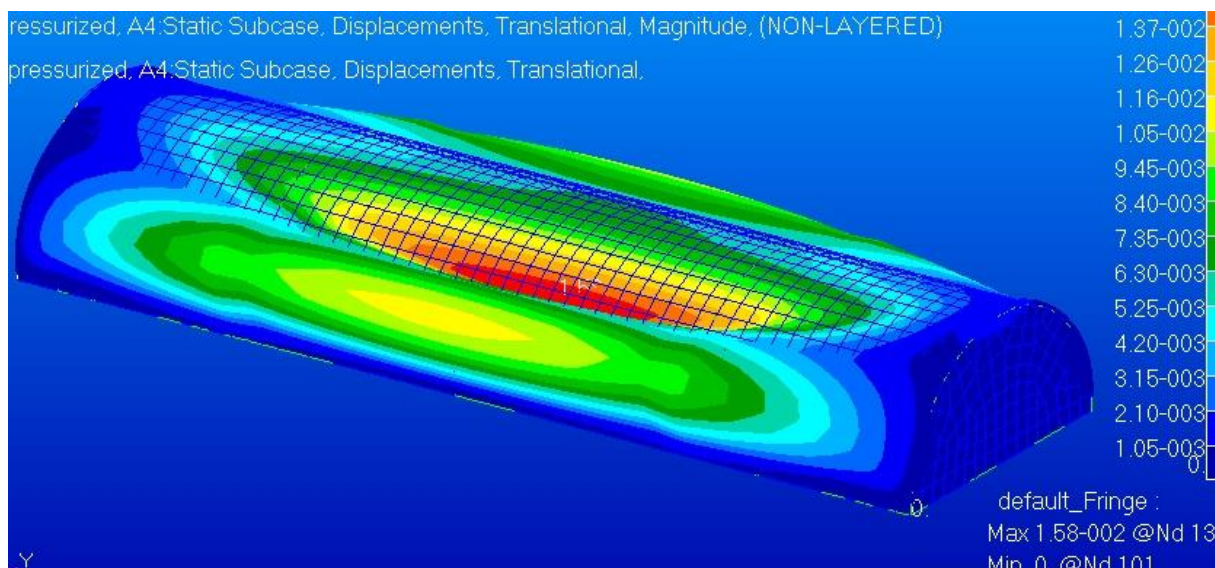
Figure 77: Stress of the deployed structure. Unpressurized case.

Finally, to account for the fact that the Kevlar used in the flexible section of the greenhouse is unlikely to be isotropic, but rather part of a 3D-orthotropic rigidizable composite, the displacement and stresses of the deployed structure are determined using the material properties listed in Table 42 [174]. The Kevlar material was modelled as a triple ply (45/0/-45 degrees) laminate.

The same wall thickness was applied and again non-linear static analysis was used for the burst pressure case. As can be seen in Figure 78 the stress distribution has changed substantially, resulting in an increased stress in the rigid sections of the structure floor.

Table 42: Kevlar composite material properties [174]

Parameter	Value	Parameter	Value
E_{11}, E_{22}	18.5 GPa	G_{12}	0.77 GPa
E_{33}	6.0 GPa	G_{23}, G_{31}	2.715 GPa
ν_{12}	0.25	Density	1230 kg/m^3
ν_{31}, ν_{23}	0.33		
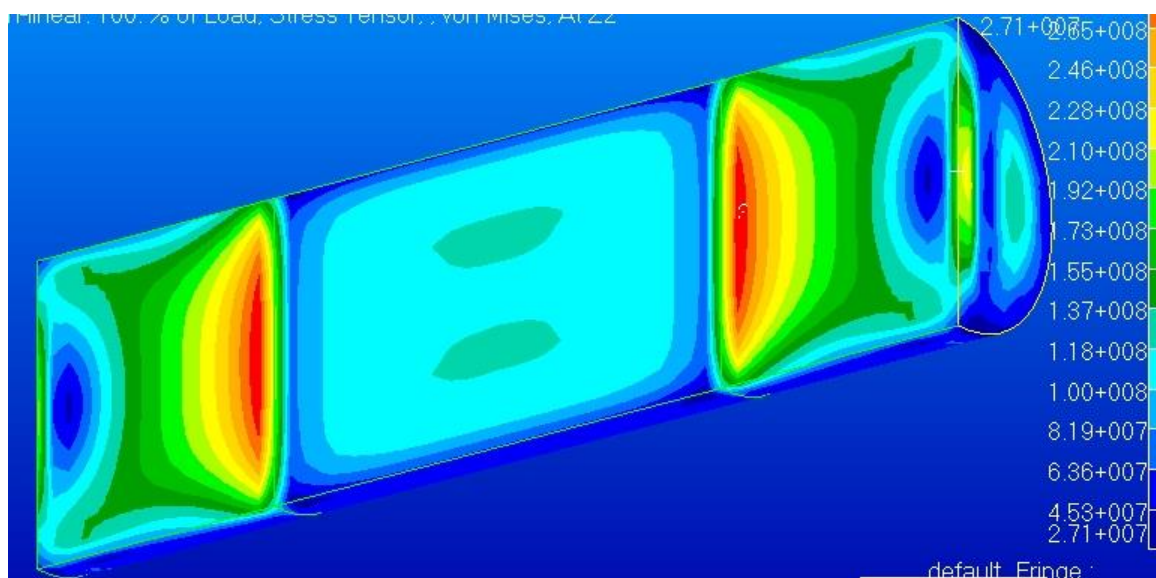
Figure 78: Stress of the deployed structure with 3d-orthotropic Kevlar composite. Burst pressure case

8. Conclusions

The main research question for this thesis was:

What is the optimal design for a (fully-equipped, deployable) Greenhouse module on the Moon?

To facilitate answering this main question, several secondary research questions were formulated.

- What are the requirements for a Lunar Greenhouse Module? (Specifically with regards to the structure)

52 requirements were defined based on a literature review and front-end system engineering tasks, such as a functional analysis and requirements discovery.

- What possible structural designs/configurations would meet the requirements placed on a Lunar Greenhouse Module and which design would be most optimal?

Several design options were presented and evaluated, resulting in a trade-off with the Analytical Hierarchy Process. The selected design is a semi-cylindrical structure with rigid end-caps and a flexible mid-section.

A preliminary design of the various functional layers of the structure was carried out, followed by aa (limited) design verification of the thermal and load-bearing properties of the structure.

It was found that the initial requirement on the amount of plant cultivation area within the greenhouse could not feasibly be met and as such the maximum length of the structure was limited.

The total length of the structure was set to 20 m, the radius of the greenhouse was 3 m and the total weight was ~44000 kg. Al 2024-T4 and Kevlar were the main materials used for load-bearing and micro-meteoroid protection, with layers of HDPE providing (additional) gas retention performance to the flexible section of the structure.

It was envisioned that regolith-filled bags will be placed against the outside of the structure to provide radiation shielding (and also micro-meteoroid shielding). A total regolith thickness of roughly 2,5 m was required to reduce the expected radiation dose per year to less than 250 mSv. This dose is half of the yearly dose limit set by ESA to account for fluctuations in the severity and frequency of solar energetic particle events.

An internal configuration was presented for the greenhouse and an available plant cultivation area of 80 m² was calculated. A possible rigid-to-flexible material interface was presented and a potential design for a structure-to-airlock interface was described.

The conservative nature of the preliminary design was shown through finite element analysis with MSC Nastran.

9. Future Work

The work carried out for this thesis and detailed in this report represents only the very early phase of the development of a lunar greenhouse module. Based on the preliminary results and performed calculations and simulations, it is possible to determine the work items which will need to be addressed in order to further mature the design.

The (non-extensive) list of work items briefly mentioned in this section are divided into groups, based on the corresponding (sub-)systems, such as the GHM systems and the lunar base infrastructure.

Greenhouse subsystems

The design of the greenhouse module structure is partly dependent on the design of the systems within the greenhouse, such as for example the crop cultivation system.

The crop cultivation system (and cultivation scheme) will impact the total amount of plants which can be grown within the GHM at any given time. This, in turn, influences such system aspects as the required nutrient solution flow rate, air flow rate, as well as the power and cooling system requirements. Therefore, an evaluation of (and trade-off between) different cultivation systems (e.g. Grow Units/Grow Pallets/Grow Lids system, wire-culture system) should be performed, and the impact on the structure should be determined.

Similarly, the design of the other systems and the influence on the structure should be investigated.

Lunar base

The lunar GHM will need to interface with a number of other buildings within the lunar base. The exact number of interfaces and their design will depend on the design of these lunar base structures and as such more information will be needed to further mature the greenhouse structure design.

Greenhouse structure

- Trade-off comparison

The concept trade-off discussed in Chapter 5 is of a highly subjective nature, meaning that it might differ from one evaluator to the next. It might be beneficial to gather input from experts in the fields of greenhouses and structure design to obtain a more objective overview of the relative suitability of different concepts.

- Functional Layer Analysis

Based on the literature study of existing concepts which was performed in Chapter 2 it was found that some additional material layers (e.g. flame-retardant and/or puncture-resistant) may need to be placed at the inside of the greenhouse

Gas retention layer

Based on the available literature data and relevant equations, it was determined that a very small thickness of the gas retention layer was sufficient to limit the gas loss rate to acceptably low rates, even when neglecting the impact of the other structural layers and the applied regolith. As such, the gas retention layers might not be necessary and could then be removed from the structure. A scale test could be used to show the validity of such a design decision.

MMOD shielding

- Probability of impact and critical failure

The micrometeoroid and debris shield was designed to ensure a 99% probability of no critical failure over the (roughly 2 year) mission lifetime. However, the regolith shielding which will be applied to the structure to provide protection against radiation will also prevent meteoroid impacts from penetrating the structure. Thus, it should be evaluated whether the MMOD shield layers of the lunar GHM may be reduced in size, or perhaps even removed entirely, without adversely impacting the capabilities of the structure.

- MMOD shield design equations

Ballistic Limit Equations from NASA were used to evaluate different shielding types and to determine the required thicknesses of the shield layers as well as the spacing between layers. These BLEs are based on empirical data and can only be used for a limited set of materials and conditions. Especially for the flexible section of the structure, the number of materials which have been tested is quite limited, so some ballistic tests may be required to determine the actual performance of specific materials.

Radiation shielding

- Engineering design equations

The equations described in section 6.4.1 should be checked for their validity, specifically the relationship between secondary neutron flux and incident primary proton flux. Simple equations for the flux of other secondary particles should be found from literature, or developed, in order to allow for a more accurate first design. If sufficient accuracy cannot be achieved using relatively simple equations, a Monte Carlo simulation may be a better option.

- GEANT4 modeling

GEANT4 radiation modelling was planned to verify the radiation shield design carried out in Chapter 6. This work is ongoing.

Thermal protection design

The thermal environment of the structure should be modelled with increased accuracy by moving from one-dimensional analysis to a full three-dimensional model and taking into account all of the functional layers in the structure walls. The relative orientation of the Sun with respect to the lunar GHM should be considered, as well as the influence of the additional buildings of the lunar base.

Load-bearing structure design

- Material selection and comparison

To allow for stowing and deploying of the structure, while retaining desired properties in the deployed state, a rigidizable material for the flexible section of the structure is likely the best option. Significant work will be needed to select and/or develop a material which can be stored for a long period of time, which is rigidizable through some easily controllable method (e.g. thermal), which has suitable structural characteristics and which does not degrade overly much when exposed to the conditions on the lunar surface.

- Load-bearing members

The structural analysis described in this report has focused on a structure where all the loads are born by the outer walls. A more efficient design can be achieved by adding in load-bearing members (e.g. inflatable arches) in specific locations within the greenhouse.

The optimal location, size and material for such load-bearing members should be investigated, for example as described in [175].

Bibliography

[1]. 'Plants for Human Life Support in Space: A Review of Some NASA Research', 2006, Wheeler, R.M., '2nd Conference on AgroSpace'

[2]. 'Spaceflight Life Support and Biospherics', 1994, Eckart, P.

[3]. 'Moon: Prospective Energy and Material Resources', 2012, Badescu et al., ISBN: 978-3-642-27968-3

[4]. 'Inflatable Deployable Space Structures: Technology Summary', 1998, Freeland et al., IAF-98-1.5.01

[5]. 'United States Patent Office – 3,276,726: Inflation System for Balloon Type Satellites', filed 1965, NASA, last viewed 20-9-2012,

url: http://www.google.com/patents?hl=nl&lr=&vid=USPAT3276726&id=UNJxAAAAEBAJ&oi=fnd&dq=inflation+through+sublimation&printsec=abstract#v=onepage&q=inflation%20through%20sublimation&f=false

[6]. 'New Ultra-Lightweight Stiff Panels for Space Apertures', 2006, Black, J.T., 'University of Kentucky Doctoral Dissertation'

[7]. 'Inflatable Space Structures', 1988, Sasakawa International Center for Space Architecture (SICSA). 'SICSA Outreach: Special Design Project Issue'

[8]. 'Space Station Model', last viewed on 20-9-2012,

url: http://www.nasa.gov/multimedia/imagegallery/image_feature_438.html

[9]. 'Overview of Inflatable Airlock & Related Technologies: Technical Briefing for the Future In-Space Operations Colloquium', 2007, Cadogan, D., last viewed on 20-9-2012,

url:http://spirit.as.utexas.edu/~fiso/telecon/Cadogan_4-25-07/Cadogan%20ILC%20Dover%204-25-07.pdf

[10]. 'Gossamer Spacecraft: Membrane and Inflatable Structures Technology for Space Applications', 2001, Jenkins et al., ISBN: 1-56347-403-4

[11]. 'Spaceborne Antennas for Planetary Exploration', 2006, Imbriale et al., last viewed on 20-9-2012, url: http://descanso.jpl.nasa.gov/Monograph/series8/Descanso8_08.pdf

[12]. 'Soviet Space Flight: The Human Element', Garshnek, V., 1988, 'American Society for Gravitational and Space Biology (ASGSB) bulletin'

[13]. 'The Rochester Sentinel – Friday, Oct. 4, 1963, page 4', last viewed on 20-9-2012,

url: http://news.google.com/newspapers?id=kiRjAAAAIBAJ&sjid=0XMNAAAAIBAJ&pg=4200%2C3569322

[14]. 'System Definition Study of Deployable, Non-Metallic Space Structures', 1984, Goodyear Aerospace, NASA-CR-171090

[15]. 'Large Inflatable Deployable Antenna Flight Experiment Results', 1997, Freeland et al., IAF-97-1.3.01

[16]. 'Inflatable Solar Array Technology', 1999, Cadogan et al., AIAA-99-1075

[17]. 'Planetary and Lunar Missions Under Consideration', last viewed on 24-9-2012,

url: http://nssdc.gsfc.nasa.gov/planetary/prop_missions.html

[18]. 'TransHab: NASA's Large-Scale Inflatable Spacecraft', 2000, de la Fuente et al., 'Proceedings of AIAA Structures, Structural Dynamics and Materials Conference', AIAA 2000-1822

[19]. 'Inflatable Habitats Technology Development', last viewed on 20-9-2012,

url:

http://www.nasaimages.org/luna/servlet/detail/NASAUpdateNUP~7~7~62976~172983:Inflatable-Habitats-Technology-Deve

[20]. 'Nat Geo Textbook Illustrations', Kroll, L., last viewed on 19-11-2012,
url: http://leannekroll.wordpress.com/2010/02/27/nat-geo-textbook-illustrations/

[21]. 'TransHab', last viewed on 19-11-2012, url: http://en.wikipedia.org/wiki/TransHab

[22]. 'Bigelow Aerospace', last viewed on 20-9-2012,
url: http://en.wikipedia.org/wiki/Bigelow_Aerospace

[23]. 'ISAS Deployed Solar Sail Film in Space', last viewed on 21-9-2012,
url: http://www.isas.ac.jp/e/snews/2004/0809.shtml

[24]. 'Development of Deployment System for Small Size Solar Sail Mission', 2008, Mori et al.,
'Transactions of Space Technology Japan'

[25]. 'First Solar Power Sail Demonstration by IKAROS', 2009, Mori et al., last viewed 20-9-2012, url:
http://archive.ists.or.jp/upload_pdf/2009-o-4-07v.pdf

[26]. 'JAXA Today – August 2010 No. 02', last viewed on 20-9-2012,
url: http://www.jaxa.jp/pr/jaxas/pdf/jaxatoday002_p.pdf

[27]. 'IKAROS Solar-Sail Craft Successfully Steers with Strategically Placed LCDs, Using No
Propellant', 2010, last viewed on 20-9-2012,
url:http://www.popsci.com/technology/article/2010-07/ikaros-successfully-changes-attitude-solar-
pressure-alone-using-no-propellant

[28]. 'NASA's First Solar Sail NanoSail-D Deploys in Low-Earth Orbit', last viewed on 21-9-2012, url:
http://www.nasa.gov/mission_pages/smallsats/11-010.html

[29]. 'Gossamer', last viewed on 21-9-2012,
url: http://www.dlr.de/irs/de/desktopdefault.aspx/tabid-6931/11365_read-26354

[30]. 'Large Deployable Technologies for Space', last viewed on 20-9-2012,
url:
http://cordis.europa.eu/search/index.cfm?fuseaction=proj.document&PJ_LANG=EN&PJ_RCN=1252
9234&pid=8

[31]. 'Deploytech', last viewed 20-9-2012, url: http://www.deploytech.eu/index.html

[32]. 'Images from Inside Bigelow Aerospace's Genesis I Released', 2006, last viewed on 12-3-2014,
url: http://www.spaceref.com/news/viewsr.html?pid=21490

[33]. 'Genesis I', last viewed on 12-3-2014, url: http://www.bigelowaerospace.com/genesis-1.php

[34]. 'Inflatable Habitation for the Lunar Base', 1992, Roberts, M., Proceedings of the 2nd Conference
on Lunar Bases and Space Activities

[35]. 'Greenhouse Design for the Mars Environment: Development of a Prototype, Deployable
Dome', 2004, Bucklin et al., 'ISHS Acta Horticulturae 659'

[36]. 'Torus or Dome: Which Makes the Better Martian Home', 1999, Fisher, G.C., last viewed 12-10-
2012, url: http://classes7.com/Torus-Or-Dome-Which-Makes-The-Better-Martian-Home-download-
w27491.pdf

[37]. 'Human friendly architectural design for a small Martian base', 2011, Kozicki, J. and Kozicka, J.,
'Advances in Space Research 48', DOI: 10.1016/j.asr.2011.08.032

[38]. 'The South Pole Greenhouse and Development/Construction of a Lunar Habitat Demonstrator',
2007, Giacomelli, G. and Sadler, P.

[39]. 'Structural Design, Analysis, and Testing of an Expandable Lunar Habitat', 2009, Hinkle et al.,
AIAA 2009-2166, Proceedings of the AIAA Structures, Structural Dynamics, and Materials
Conference

[40]. 'Phase A Design of an Innovative Greenhouse Chamber for Utilisation in a Planetary Research
Base', 2011, Glasgow, L., Master Thesis work for the Cranfield University School of Engineering

[41]. 'Part I: Space Structures and Support Systems', Sasakawa International Center for Space
Architecture (SICSA) Space Architecture Seminar Lecture Series, url: www.sicsa.uh.edu

[42]. 'Concept of a Lunar FARM: Food and Revitalization Module', 2009, Finetto et al., 'Acta
Astronautica 66', DOI: 10.1016/j.actaastro.2009.10.027

[43]. 'Engineering Concepts for Inflatable Mars Surface Greenhouses', 2004, Hublitz et al., 'Advances in Space Research 34', DOI: 10.1016/j.asr.2004.06.002

[44]. 'Inflatable Structures for Mars Base 10', 2012, Sinn, T. and Doule, O., Proceedings of the International Conference on Environmental Systems

[45]. 'Domus I and Dymaxion: Two Concept Designs for Lunar Habitats', 1993, Moore et al., Proceedings of the 9th annual summer conference of the NASA/USRA University Advanced Design Program

[46]. 'Mars Greenhouses: Concepts and Challenges', 2000, Wheeler et al., Proceedings from a 1999 Workshop, NASA TM 2000-208577

[47]. 'Structural Design of a Lunar Habitat', 2006, Ruess et al., 'Journal of Aerospace Engineering'

[48]. 'Lunar Base Design Workshop – IntelliHab', last viewed 12-10-2012,
url: http://67.23.226.3/~austrona/projects/02_lunarbase/presentation_intellihab/index.html

[49]. 'Deployment of Inflatable Space Structures: A Review of Recent Developments', 2000, Salama et al., AIAA-2000-1730

[50]. 'Deployment Control Mechanisms for Inflatable Space Structures', 1999, Cadogan, D.P., Grahne, M.S., '33rd Aerospace Mechanisms Conference'

[51]. 'Rigidizable Materials for use in Gossamer Space Inflatable Structures', 2001, Cadogan, D.P. and Scarborough, S.E., 'Proceedings of AIAA Structures, Structural Dynamics, and Materials Conference', AIAA 2001-1417

[52]. 'Glass transition', last viewed on 19-11-2012,
url: http://en.wikipedia.org/wiki/Glass_transition

[53]. 'Space Inflatable Structures', 2006, Higuchi, K., last viewed on 19-11-2012,
url: http://www.isas.jaxa.jp/e/forefront/2006/higuchi/02.shtml

[54]. 'An Inflatable Rigidizable Truss Structure Based on New Sub-Tg Polyurethane Composites', 2002, Guidanean, K. and Lichodziejewski, D., AIAA 02-1593

[55]. 'Spiral Wrapped Aluminum Laminate Rigidization Technology', 2002, Lichodziejewski et al., AIAA 2002-1701

[56]. 'Light Curing Rigidizable Inflatable Wing', 2004, Allred et al., 'Proceedings of AIAA Structures, Structural Dynamics, and Materials Conference', AIAA 2004-1809

[57]. 'Deployment, Foam Rigidization, and Structural Characterization of Inflatable Thin-film Booms', 2002, Tinker et al., AIAA 2002-1376

[58]. 'Inflatable Material for Space – Synthesis Report', 2003, Aero Sekur

[59]. 'The relationship between the Structural Geometry of a Textile Fabric and its Physical Properties', 1948, Backer, S., 'Textile Research Journal', DOI: 10.1177/004051754801801102

[60]. 'An investigation of Fabric Structure and its relation to certain physical properties', 1950, Hottet, G. H., 'Textile Research Journal', DOI: 10.1177/004051755002001201

[61]. 'Jacquard Carbon Fiber', last viewed on 11-3-2014,
url: http://compositeenvisions.com/raw-fabric-cloth-2/jacquard-carbon-fiber-144/

[62]. 'Carbon and Kevlar cloth', last viewed on 11-3-2014, url: http://www.alibaba.com/product-detail/carbon-and-kevlar-cloth-hybrid-carbon_294169029.html

[63]. 'TN-9: Synthesis, Recommendations & Suggestions for Further Work', 2011, Thales Alenia Space

[64]. 'Aluminium Foam Technology', 2012, Baumeister, J.

[65]. 'Final Report: Assessment of Potential Use of Cellular Materials for Space Applications', 2005, OHB

[66]. 'Self-healing Polymeric Materials: A Review of Recent Developments', 2008, Wu et al., 'Progress in Polymer Science', DOI: 10.1016/j.progpolymsci.2008.02.001

[67]. 'On-orbit Shape Correction of Inflatable Structures', 1994, Salama et al.,

[68]. 'Shape Measurement and Control of Deployable Membrane Structures', 2000, Maji, A.K. and Starnes, M.A., 'Experimental Mechanics', DOI: 10.1007/BF02325040

[69]. 'Intelligent Flexible Materials for Deployable Space Structures (InFlex)', 2006, Cadogan, D.P. et al.

[70]. 'Simulation of Deployment Dynamics of Inflatable Structures', 2000, Salama et al., 'AIAA Journal'

[71]. 'Deployment Simulation Methods for Ultra-Lightweight Inflatable Structures', 2003, Wang, J.T. and Johnson, A.R., NASA-TM-2003-212410

[72]. 'Deployment Simulation of Ultra-Lightweight Inflatable Structures', 2002, Wang, J.T. and Johnson, A.R., AIAA-2002-1261

[73]. 'An incompressible ALE method for fluid-solid interaction', 2004, Dunn, T.A., 'Proceedings from the Nuclear Explosive Code Development Conference (NECDC) 2004'

[74]. 'Modeling and Analysis of the Deployment of a Rolled Inflatable Beam using MSC-Dytran', Lienard, S. and Lefevre Y., AIAA-2005-1968

[75]. 'Deployment Modeling of an Inflatable Solar Sail Spacecraft', 2006, Graybeal et al., 'Proceedings of the AIAA Guidance, Navigation and Controls Conference 2006'

[76]. 'Experimental and Numerical Analysis of a DECSMAR Structure's Deployment and Deployed Performance', 2007, Pollard et al., 'Proceedings of the AIAA Structures, Structural Dynamics, and Materials Conference 2007'

[77]. 'The Moon: Resources, Future Development, and Settlement (2nd Edition)', 2008, Schrunk et al., ISBN: 978-0-387-36055-3

[78]. 'The Constitution and Structure of the Lunar Interior', 2006, Wieczorek et al., 'Reviews in Mineralogy & Geochemistry'

[79]. 'Seismic Detection of the Lunar Core', 2011, Weber et al., 'Science',
DOI: 10.1126/science.1199375

[80]. 'FT-IR/PAS Studies of Lunar Regolith Samples', 2008, Pasieczna-Patkowska et al., 'Acta Physica Polonica A'

[81]. 'Optical Effects of Space Weathering: The Role of the Finest Fraction', 1993, Pieters et al., 'Journal of Geophysical Research'

[82]. 'Lunar Lava Tube Radiation Safety Analysis', 2002, De Angelis et al., 'Journal of Radiation Research'

[83]. 'Lunar Sourcebook: A User's Guide to the Moon', 1991, Heiken et al.,
ISBN: 0-521-33444-6

[84]. 'Lunar Base Agriculture: Soils for Plant Growth', 1989, Ming et al., ISBN: 0-89118-100-8

[85]. 'Lunar Regolith Simulant Materials: Recommendations for Standardization, Production and Usage', 2005, Sibille et al., NASA/TP-2005-XXXXXX

[86]. 'Lunar Settlements',2010, Benaroya et al., ISBN: 978-1-4200-8332-3

[87]. 'Radiation Shielding Properties of Lunar Regolith and Regolith Simulant', 2008, Miller et al., Proceedings of the NASA Lunar Science Institute Lunar Science Conference

[88]. 'Handbook of Lunar Soils', 1983, Morris et al., NASA JSC-19069

[89]. 'Apollo 11: Preliminary Science Report', 1969, NASA SP-214

[90]. 'A 1.5 km-resolution gravity field model of the Moon', 2012, Hirt, C. and Featherstone, W.E., 'Earth and Planetary Science Letters'

[91]. 'Mascons: Lunar Mass Concentrations', 1968, Muller, P.M. and Sjogren, W.L., 'Science'

[92]. 'Magnetic Field of the Moon', last viewed on 19-9-2012,
url: http://en.wikipedia.org/wiki/Magnetic_field_of_the_Moon

[93]. 'Mapping of crustal magnetic anomalies on the lunar near side by the Lunar Prospector electron reflectometer', 2001, Halekas et al., 'Journal of Geophysical Research'

[94]. 'Global mapping of lunar crustal magnetic fields by Lunar Prospector', 2008, Mitchell et al., 'Icarus'

[95]. 'First observation of a mini-magnetosphere above a lunar magnetic anomaly using energetic neutral atoms', 2010, Wieser et al., 'Geophysical Research Letters',

DOI: 10.1029/2009GL041721

[96]. 'The Lunar Atmosphere: History, Status, Current Problems, and Context', 1999, Stern, S.A., 'Reviews of Geophysics'

[97]. 'Lunar Leonids 2000', last viewed on 18-9-2012,
url: http://science.nasa.gov/science-news/science-at-nasa/2000/ast26oct_1/

[98]. 'On the role of dust in the lunar ionosphere', 2011, Stubbs et al., 'Planetary and Space Science', DOI: 10.1016/j.pss.2011.05.011

[99]. 'Lunar Surface Charging: A Global Perspective Using Lunar Prospector Data', 2005, Stubbs et al., ESA SP-643

[100]. 'Lunar Prospector observations of the electrostatic potential of the lunar surface and its response to incident currents', 2008, Halekas et al., 'Journal of Geophysical Research'

[101]. 'Impact of Dust on Lunar Exploration', 2005, Stubbs et al., ESA SP-643

[102]. 'Illumination conditions of the south pole of the Moon derived using Kaguya topography', 2010, Bussey et al., 'Icarus', DOI:10.1016/j.icarus.2010.03.028

[103]. 'Illumination conditions at the lunar polar regions by KAGUYA (SELENE) laser altimeter', 2008, Noda et al., 'Geophysical Research Letters', DOI: 10.1029/2008GL035692

[104]. 'Estimation of solar illumination on the Moon: A theoretical model', 2008, Li et al., 'Planetary and Space Science', DOI: 10.1016/j.pss.2008.02.008

[105]. 'South Pole Illumination Map', last viewed on 19-9-2012,
url: http://lroc.sese.asu.edu/news/index.php?/archives/321-South-Pole-Illumination-Map.html

[106]. 'New NASA temperature maps provide a whole new way of seeing the Moon', last viewed on 19-9-2012,
url: http://newsroom.ucla.edu/portal/ucla/new-nasa-temperature-maps-provide-102070.aspx

[107]. 'Lunar Reconnaissance Orbiter Mission Status', last viewed on 19-9-2012,
url: http://www.iki.rssi.ru/conf/2011-lg/presentations/2_DAY/20110126_Rice(GSFC).pdf

[108]. 'Transient Thermal Model and Analysis of the Lunar Surface and Regolith for Cryogenic Fluid Storage', 2008, Christie et al., NASA/TM-2008-215300

[109]. 'Basics about Radiation', last viewed 20-9-2012,
url: http://www.hicare.jp/en/09/hi03.html

[110]. 'Rad Pro Calculator Frequently Asked Questions', last viewed on 20-9-2012,
url: http://www.radprocalculator.com/FAQ.aspx

[111]. 'Radiation Risk Acceptability and Limitations', Cucinotta, F.A., last viewed on 20-9-2012, url: http://three.usra.edu/articles/AstronautRadLimitsFC.pdf

[112]. 'Radiation exposure in the moon environment', 2012, Reitz et al., 'Planetary and Space Science', DOI: 10.1016/j.pss.2012.07.014

[113]. 'IBEX-Lo observations of energetic neutral hydrogen atoms originating from the lunar surface', 2011, Rodriguez M. et al., 'Planetary and Space Science',
DOI: 10.1016/j.pss.2011.09.009

[114]. 'The ionizing radiation environment on the moon', 2007, Adams et al., 'Advances in Space Research', DOI: 10.1016/j.asr.2007.05.032

[115]. 'The Day the Solar Wind Disappeared', last viewed on 18-9-2012,
url: http://science.nasa.gov/science-news/science-at-nasa/1999/ast13dec99_1/

[116]. 'Isotopic Composition Measured In-Situ in Different Solar Wind Regimes by CELIAS/MTOF on board SOHO', 2001, Kallenbach, R., 'Solar and Galactic Composition: A Joint SOHO/ACE Workshop', DOI: 10.1063/1.1433988

[117]. 'Solar Energetic Particles', 2000, Ryan et al., 'Space Science Reviews'

[118]. 'A characterization of the moon radiation environment for radiation analysis', 2006, Tripathi et al., 'Advances in Space Research', DOI: 10.1016/j.asr.2006.03.016

[119]. 'Solar Energetic Particle Variations', 2003, Reames, D.V., COSPAR-D2.3-E3.3-0032-02

[120]. 'Unified atomic mass unit', last viewed on 20-9-2012,

url: http://physics.nist.gov/cgi-bin/cuu/Value?tukg|search_for=atomic+mass+unit

[121]. 'Basic Mechanisms of Radiation Effects in the Natural Space Environment', 1994, Schwank, J.R.

[122]. 'Geant4', last viewed on 20-9-2012, url: http://geant4.cern.ch/

[123]. 'Revolutionary Concepts of Radiation Shielding for Human Exploration of Space', 2005, Adams Jr. et al., NASA-TM-2005-213688

[124]. 'Space and Planetary Environment Criteria Guidelines for Use in Space Vehicle Development, 1977 Revision', 1977, West Jr. et al., NASA-TM-78119

[125]. 'Meteoroid Environment Model – 1969 [Near Earth to Lunar Surface]', 1969, NASA-SP-8013

[126]. 'Micrometeoroid impacts on the lunar surface', 1997, Vanzani et al., 'Lunar and Planetary Science XXVIII – Proceedings of Lunar and Planetary Science Conference 1997'

[127]. 'In situ dust monitoring on the Moon: an experimental approach', Colangeli et al., last viewed on 20-9-2012,

url:

http://www.google.com/url?sa=t&rct=j&q=in%20situ%20dust%20monitoring%20on%20the%20moon%20an%20experimental%20approach&source=web&cd=3&cad=rja&ved=0CDQQFjAC&url=http%3A%2F%2Fsci.esa.int%2Fscience-e%2Fwww%2Fobject%2Fdoc.cfm%3Ffobjectid%3D42049&ei=29RaUJfKN8bY4QSK8IHYDg&usg=AFQjCNH5Mc24PSziaYpuh20vDQ92Xvbl6g

[128]. 'Greenhouse Module for Space Systems: Statement of Work', 2012, ESA, TEC-MMG/2011/205

[129]. 'Advanced Greenhouse Modules for use within Planetary Habitats', 2011, Schubert et al., Proceedings of the AIAA International Conference on Environmental Systems

[130]. 'NASA Systems Engineering Handbook', 1995, NASA, last viewed on 9-10-2012, url: http://snebulos.mit.edu/projects/reference/NASA-Generic/NASA-STD-8739-8.pdf

[131]. 'Concurrent Engineering Study Report – Vertical Farm', 2012, Schubert et al., DLR-RY-SR-EVACO-2012

[132]. 'Comparison of hydroponic and aeroponic cultivation systems for the production of potato minitubers', 2001, Ritter et al., last viewed on 9-10-2012, url: http://www.springerlink.com/content/q21136170183051l/fulltext.pdf

[133]. 'Spinoff 2006: Progressive Plant Growing has Business Blooming', 2007, NASA, last viewed on 9-10-2012, url: http://ntrs.nasa.gov/archive/nasa/casi.ntrs.nasa.gov/20070019327_2007020222.pdf

[134]. 'Advanced Life Support Baseline Values and Assumptions Document', 2002, NASA, JSC-47804

[135]. 'Candidate Crop Evaluation for Advanced Life Support', 2001, Wheeler et al., last viewed on 9-10-2012, url: http://www.dsls.usra.edu/meetings/bio2001/pdf/033.pdf

[136]. 'System Analysis & Evaluation of Greenhouse Modules within Moon/Mars Habitats', 2012, Zabel, P., Master Thesis work for the Technical University of Bremen

[137]. 'System Analysis and Evaluation of Greenhouse Modules within Moon/Mars Habitats', 2012, Nagendra, N.P., Master Thesis work for the International Space University

[138]. 'ALiSSE criteria for MELiSSA food production technologies', 2011, ESA, TEC-MMG/2011/206

[139]. 'ALISSE: Advanced Life Support System Evaluator, A Tool for ESA & Space Industries', 2009, Brunet, J., Gerbi, O., last viewed on 15-10-2012, url: http://www.congrex.nl/09c13/06_04_Brunet.pdf

[140]. 'Environmental Control & Life Support Systems (CELSS) for MOONBASE 2015', 2000, Koelle, H.H. url: http://server02.fb12.tu-berlin.de/ILR/koelle/ILR-Mitteilungen/Archive/ILR342.pdf

[141]. 'Leak testing of high pressure oxygen and nitrogen tank systems for the Skylab Airlock', 1974, Dutton, R. A. et al., 'NASA N74-10254', url: http://ntrs.nasa.gov/archive/nasa/casi.ntrs.nasa.gov/19740002142_1974002142.pdf

[142]. 'Overview of ILC Dover Programs and Technologies related to Deployable Space Habitats & Structures', 2007, Cadogan, D. and Willey, C., last viewed on 3-5-2013,

url: http://spirit.as.utexas.edu/~fiso/telecon/Cadogan_4-25-07/ILC%20Dover%20Habitation%20Overview%20Short%202-07.pdf

[143]. 'United States Patent Office – 6,881,689 B2: Assembly for Attaching Fabric to Metal and Method of Fabrication therefor', filed 2003, ILC Dover, last viewed on 3-5-2013,
url: http://www.docstoc.com/docs/53493688/Assembly-For-Attaching-Fabric-To-Metal-And-Method-Of-Fabrication-Therefor---Patent-6881689#viewer-area

[144]. 'United States Patent Office – 6,231,010: Advanced structural and inflatable hybrid spacecraft module', filed 1999, NASA, last viewed on 3-5-2013,
url: http://www.patentgenius.com/patent/6231010.html#show-next-page

[145]. 'International Docking System Standard (IDSS) Interface Definition Document (IDD), rev. A', 2011

[146]. 'Permeability Properties of Plastics and Elastomers', 2012, McKeen, L.W., ISBN: 978-1-4377-3469-0

[147]. 'Molecular Mass of Air', last viewed on 28-1-2013,
url: http://www.engineeringtoolbox.com/molecular-mass-air-d_679.html

[148]. 'Predicting the permeability and tensile behaviour of high density polyethylene/tie/polyamide 6 three-layer films', 2004, Huang, C.H. et al., 'Polymer International Vol. 53', DOI: 10.1002/pi1634

[149]. 'Meteoroids & Space Debris', NASA, PD-EC-1102

[150]. 'Micrometeoroid and Orbital Debris (MMOD) Shield Ballistic Limit Analysis Program', 2010, NASA, TM-2009-214789
http://ston.jsc.nasa.gov/collections/TRS/_techrep/TM-2009-214789.pdf ??

[151]. 'Titanium Ti-5Al-2.5 Sn ELI', last viewed on 3-5-2013,
url: http://asm.matweb.com/search/SpecificMaterial.asp?bassnum=MTA521

[152]. 'Aluminium 7075-O ', last viewed on 3-5-2013,
url: http://asm.matweb.com/search/SpecificMaterial.asp?bassnum=MA7075O

[153]. 'Aluminium 2024-T4', last viewed on 3-5-2013,
url: http://asm.matweb.com/search/SpecificMaterial.asp?bassnum=MA2024T4

[154]. '3M Nextel Textiles', 1996, 3M, last viewed on 3-5-2013,
url: http://www.3m.com/market/industrial/ceramics/pdfs/outerspace_apps_brochure.pdf

[155]. 'Atoms, Radiation and Radiation Protection', 2007, Turner, J.E.,
ISBN: 978-3-527-40606-7

[156]. 'Analytic estimates of secondary neutron dose in proton therapy', 2010, Anferov, V., 'Physics in Medicine and Biology', DOI: 10.1088/0031-9155/55/24/008

[157]. 'Semiclassical Estimation of Neutron Stopping Power', 1971, Vora et al., 'Physical Review B', last viewed on 3-5-2013, url: http://prb.aps.org/pdf/PRB/v3/i9/p2929_1

[158]. 'Energy and momentum in Lorentz transformations', Fowler, M., last viewed on 3-5-2013, url: http://galileo.phys.virginia.edu/classes/252/energy_p_reln.html

[159]. 'Mass and Energy', last viewed on 3-5-2013',
url: http://www.launc.tased.edu.au/online/sciences/physics/massener.html

[160]. 'Alpha Particle', last viewed on 3-5-2013,
url: http://www.euronuclear.org/info/encyclopedia/alphaparticle.htm

[161]. 'Neutron interaction with matter', Rinard, P., last viewed on 3-5-2013,
url: http://www.fas.org/sgp/othergov/doe/lanl/lib-www/la-pubs/00326407.pdf

[162]. 'XCOM: Photon Cross Sections Database, Web Version 1.2.', 1999, Berger, M.J. and Hubbell, J.H., National Institute of Standards and Technology, Gaithersburg, MD 20899, USA, Originally published as NBSIR 87-3597 (1987): "XCOM: Photon Cross Sections on a Personal Computer", last viewed on 3-5-2013, url: http://www.nist.gov/pml/data/xcom/index.cfm

[163]. 'Variation in Lunar Neutron Dose Estimates', 2011, Slaba et al., 'Radiation Research', DOI: 10.1667/RR2616.1

[164]. 'Thermal considerations of lunar based systems', Harris, D.K., last viewed on 3-5-2013, url: http://www.eng.auburn.edu/~dbeale/ESMDCourse/Chapter7.htm

[165]. 'Radiative View Factors', last viewed on 3-5-2013, url: http://webserver.dmt.upm.es/~isidoro/tc3/Radiation%20View%20factors.pdf

[166]. 'Performance of Protective Clothing', 1986, Barker et al., ISBN: 0-8031-0461-8, last viewed on 3-5-2013, url: http://books.google.de/books?id=JkaAypWOioAC&pg=PA382&lpg=PA382&dq=emissivity+kevlar&source=bl&ots=Ib48EbeAq9&sig=r-7FKsDgasXpPAlFewmOzrZfEhQ&hl=nl&sa=X&ei=h39RUaaBKe_24QTA_oCwBQ&redir_esc=y#v=onepage&q=emissivity%20kevlar&f=false

[167]. 'DuPont Kevlar 49 Aramid Fiber', last viewed on 3-5-2013, url: http://www.matweb.com/search/datasheet.aspx?matguid=77b5205f0dcc43bb8cbe6fee7d36cbb5&ckck=1

[168]. 'Numerical modelling of lava-regolith heat transfer on the Moon and implications for the preservation of implanted volatiles', 2013, Rumpf et al., 'Journal of Geophysical Research: Planets', DOI: 10.1029/2012JE004131

[169]. 'Thermal Optical Properties of Lunar Dust Simulants', 2012, Gaier et al., 'Journal of Thermophysics and Heat Transfer', DOI: 10.2514/1.T3838

[170]. 'Buckling Analysis', last viewed on 3-5-2013, url: http://www.clear.rice.edu/mech403/HelpFiles/FEA_Buckling_analysis.pdf

[171]. 'Roark's Formulas for Stress and Strain: Seventh Edition', 2001, Young, W. C., Budynas, R. G., ISBN: 0-07-072542-X

[172]. 'ASME Boiler & Pressure Vessel Code Analysis of the 1497 MHz High-Current Cryomodule Helium Vessel', 2007, Wilson, K., JLAB-TN-06-044, last viewed on 12-3-2014, url: http://tnweb.jlab.org/tn/2006/06-044.pdf

[173]. 'Thin Plates and Shells: Theory, Analysis and Applications', 2001, Ventsel, E. and Krauthammer, T., ISBN: 0-8247-0575-0

[174]. 'AM17 Protective functional evaluation of helmet against ballistic impact', 2008, Gerald, Q.Z., last viewed on 3-5-2013, url: http://dynamicslab.mpe.nus.edu.sg/dynamics/project0708/Protective%20Functional%20Evaluation%20of%20helmets%20against%20ballistic%20impact.pdf

[175]. 'Design of internal support structures for an inflatable lunar habitat', 1990, Cameron et al., 'NASA-CR-189996'

[176]. 'Exploring the challenges of habitation design for extended human presence beyond low-earth orbit: Are new requirements and processes needed?', 2008, Robinson, D.K.R. et al.

[177]. 'The Surface Endoskeletal Inflatable Module [SEIM]', Adams, M.C. and Petrov, G.

[178]. 'NASA Habitat Demonstration Unit Project – Deep Space Habitat Overview', 2011, Kennedy, K. et al.

[179]. 'Self-Deployable Lunar Habitat, Part-1: Overall Architectural Design and Deployment, 2012, Polit-Casillas, R.

[180]. 'Lunar Settlement Structures', Ambani et al.

[181]. 'Expandable Habitat Structures for Long Duration Lunar Missions', 2008, Spampinato, P.

[182]. 'Engineering, Design and Construction of Lunar Bases', 2002, Benaroya, H. et al.

[183]. 'Supporting Life on the Moon', 2005, Perino, M.A.

[184]. 'A Review of Technical Requirements for Lunar Structures – Present Status', 2005, Jablonski, A. M., Ogden, K. A., 'International Lunar Conference 2005'

[185]. 'Lunar Base Habitat Designs: Characterizing the Environment, and Selecting Habitat Designs for Future Trade-offs', 1993, Ganapathi, G. B., et al., NASA-CR-195687

[186]. 'MOBITAT2: A Mobile Habitat Based on the TRIGON Construction System', 2006, Howe, A. S., Gibson, I., AIAA 2006-7337

[187]. 'The FLECS expandable module concept for future space missions and an overall description on the material validation', 2006, Mileti, S., et al., 'Acta Astronautica 59' pp. 220-229

[188]. 'G-HOME: Green Habitation Orbital Module for Exploration', 2012, Gatti, L., Lamantea, M., 'Agrospace 2012'

[189]. 'Structural Definition and Mass Estimation of Lunar Surface Habitats for the Lunar Architecture Team Phase 2 (LAT-2) Study', 2008, Dorsey, J. T., et al., 'Earth & Space 2008',
DOI: 10.1061/40988(323)104

[190]. 'Structural health management technologies for inflatable/ deployable structures: Integrating sensing and self-healing', 2010, Brandon, E. J., et al., 'Acta Astronautica 68' pp. 883-903,
DOI: 10.1016/j.actaastro.2010.08.016

[191]. 'HB2: Destination Moon', 2013, Haüplik-Meusburger, S., San-Hwan, L.,
ISBN: 978-3-200-02861-6

[192]. 'Material Property Data', last viewed on 3-5-2013, url: http://matweb.com

[193]. 'Engineering Concepts for Inflatable Mars Surface Greenhouses', Hublitz, I., Technical University of München

[194]. 'The Analytic Hierarchy Process – what it is and how it is used', 1987, Saaty, R.W.,
DOI: 10.1016/0270-0255(87)90473-8

Appendix A. Habitat and Greenhouse concepts
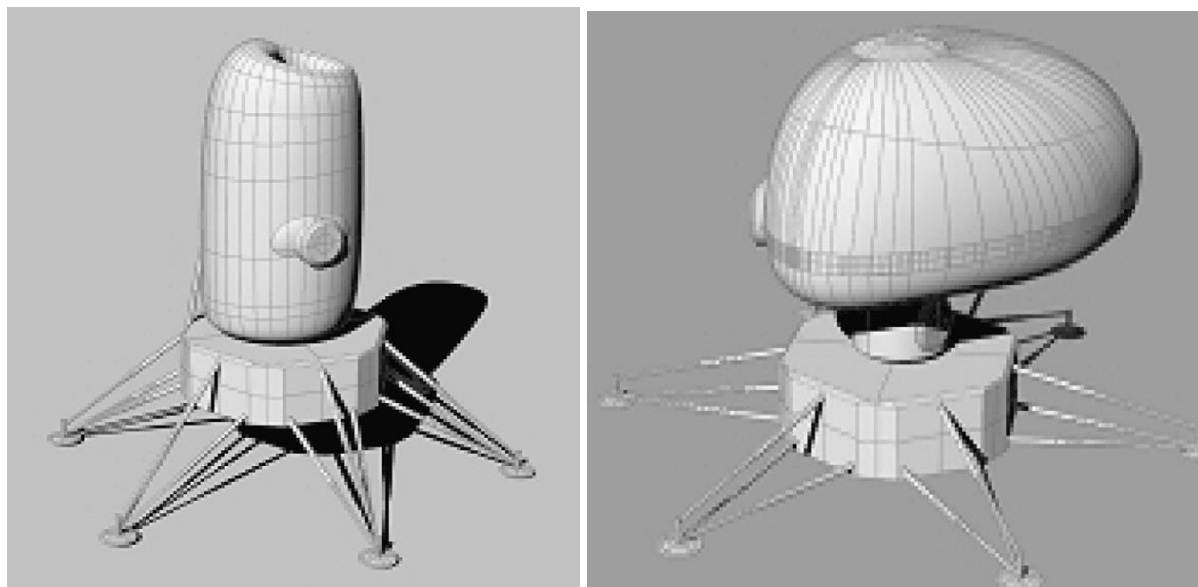
Figure 79: Deployable habitats using inflatable technology [Source: 176]
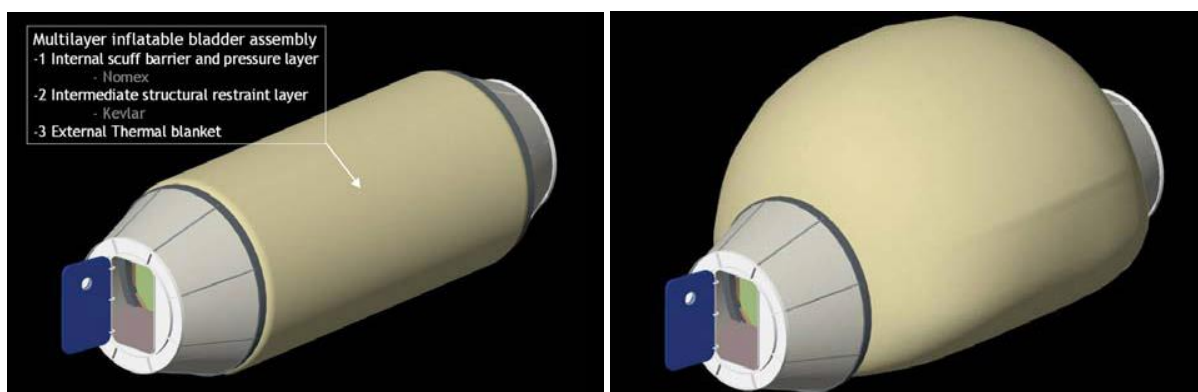
Figure 80: The Surface Endoskeletal Inflatable Module (SEIM) [Source: 177]

Figure 81: NASA Habitat Demonstration Unit concepts (Left) Oklahoma State University concept. (Right) University of Wisconsin-Madison [Source: 178]
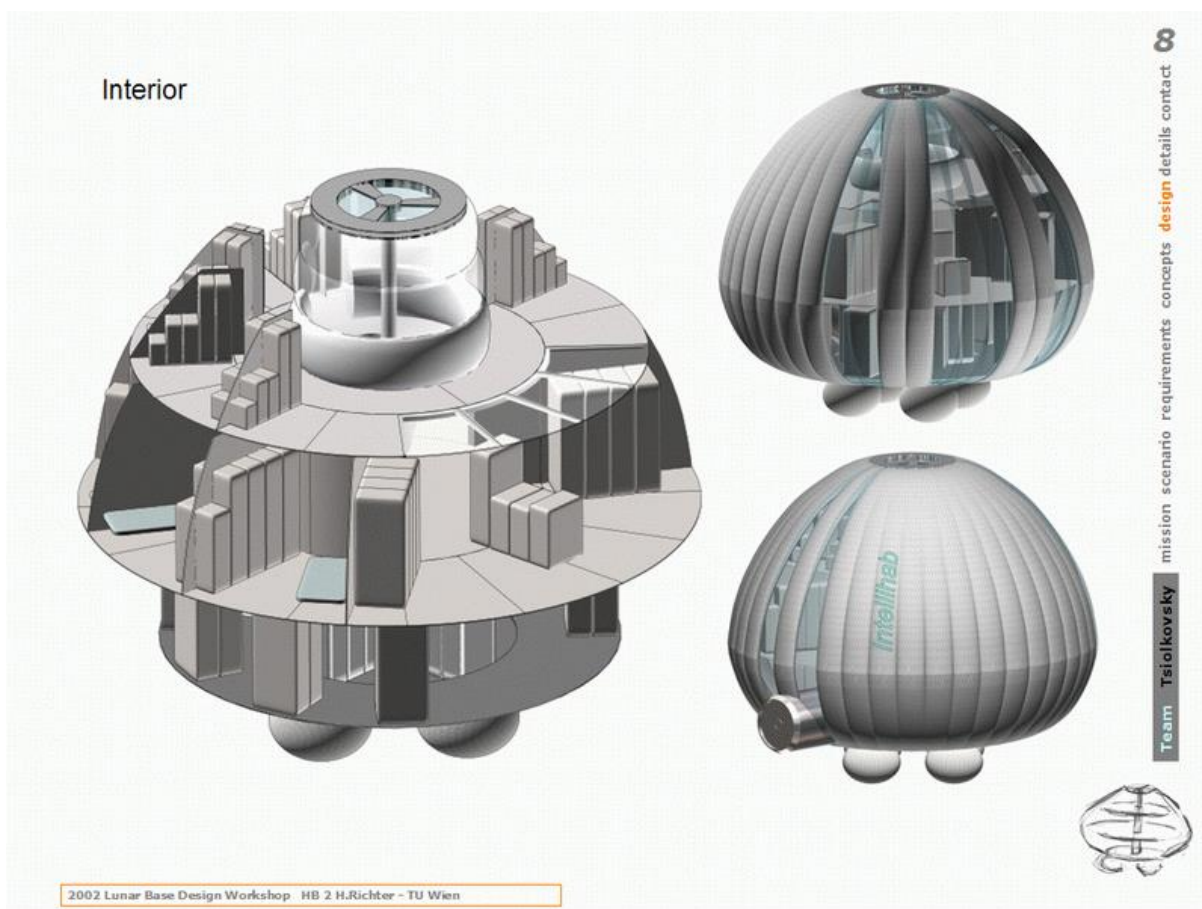
Figure 82: the IntelliHab concept [Source: 48]

Figure 83: SICSA concepts (Left) Interior pop-out structure (Right) MarsLab concept [Source: 41]
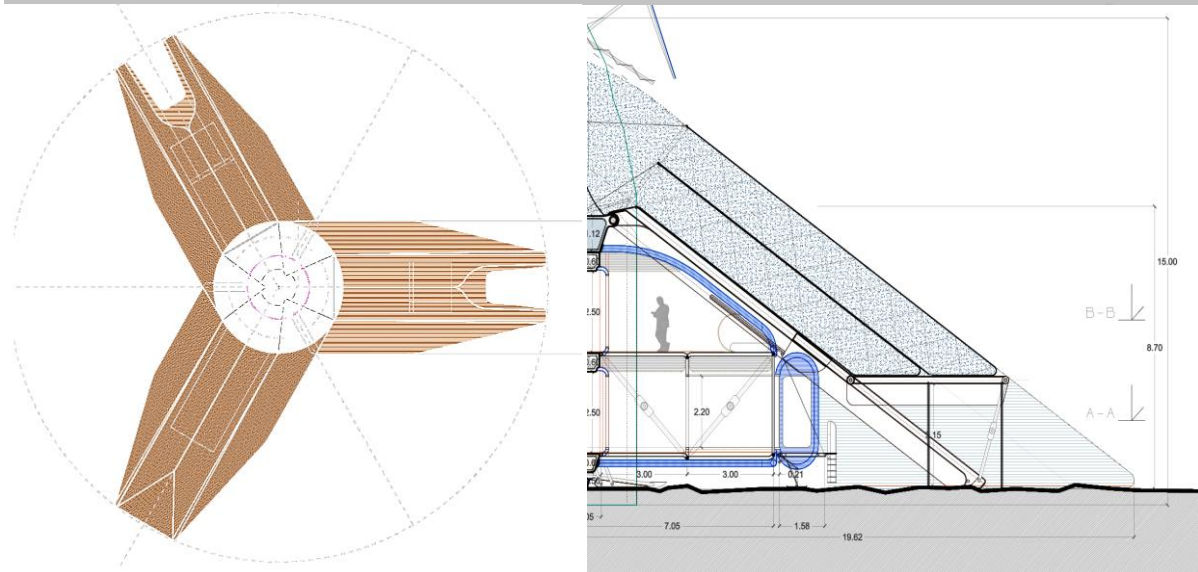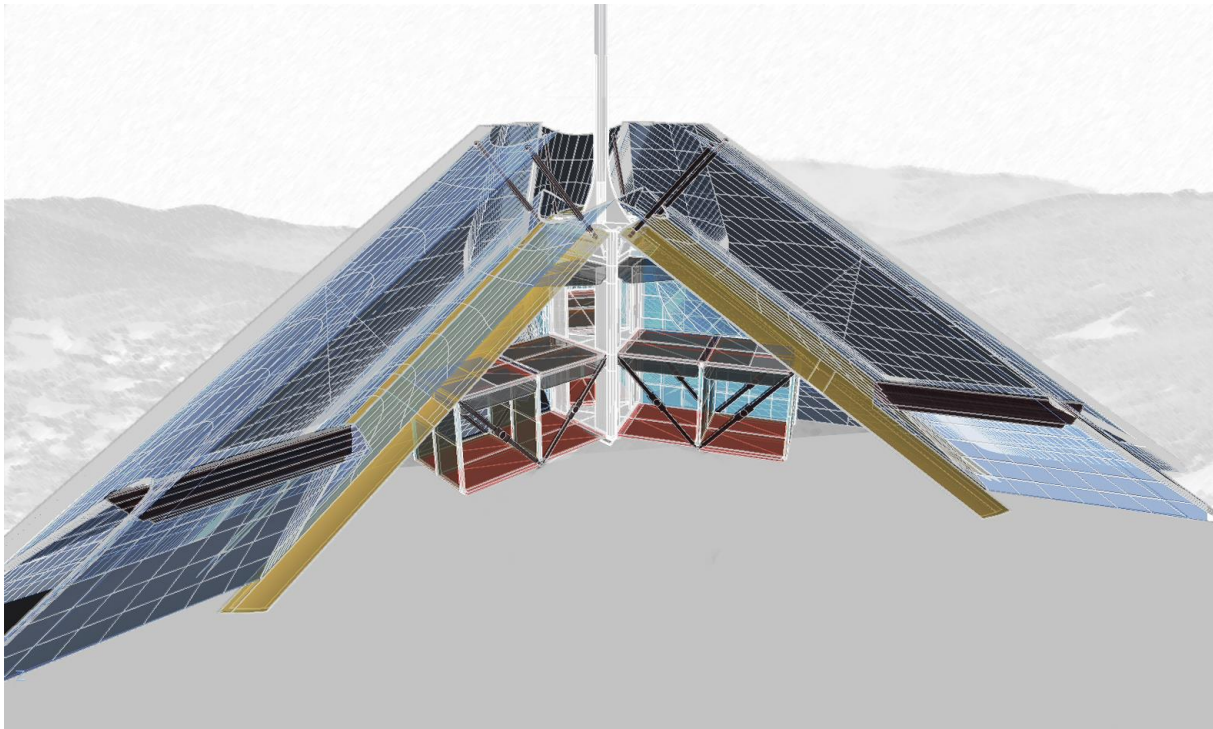
Figure 84: Self-deployable lunar habitat. (Top) Volumetric section (Bottom left) 2D Top view (Bottom right) Partial cross.section [Source: 179]
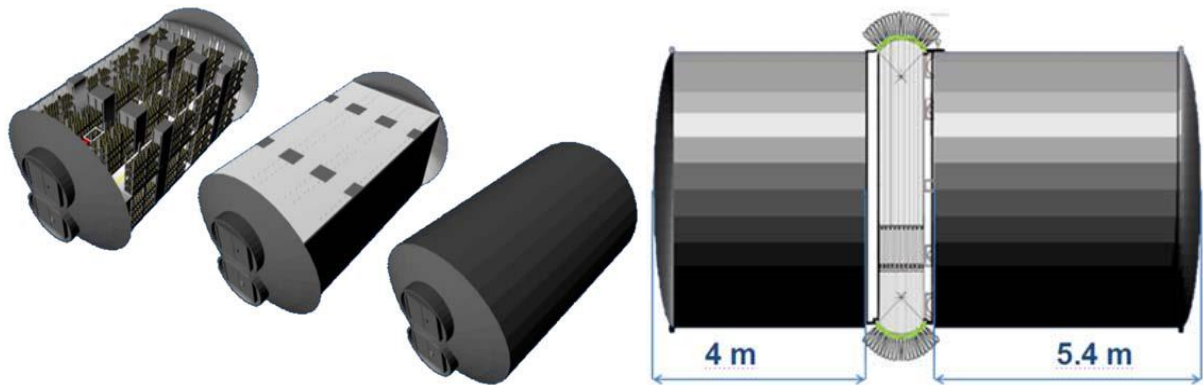
Figure 85: Lunar Farm concept (Left) Rigid solution (Right) Hybrid structure [Source: 42]
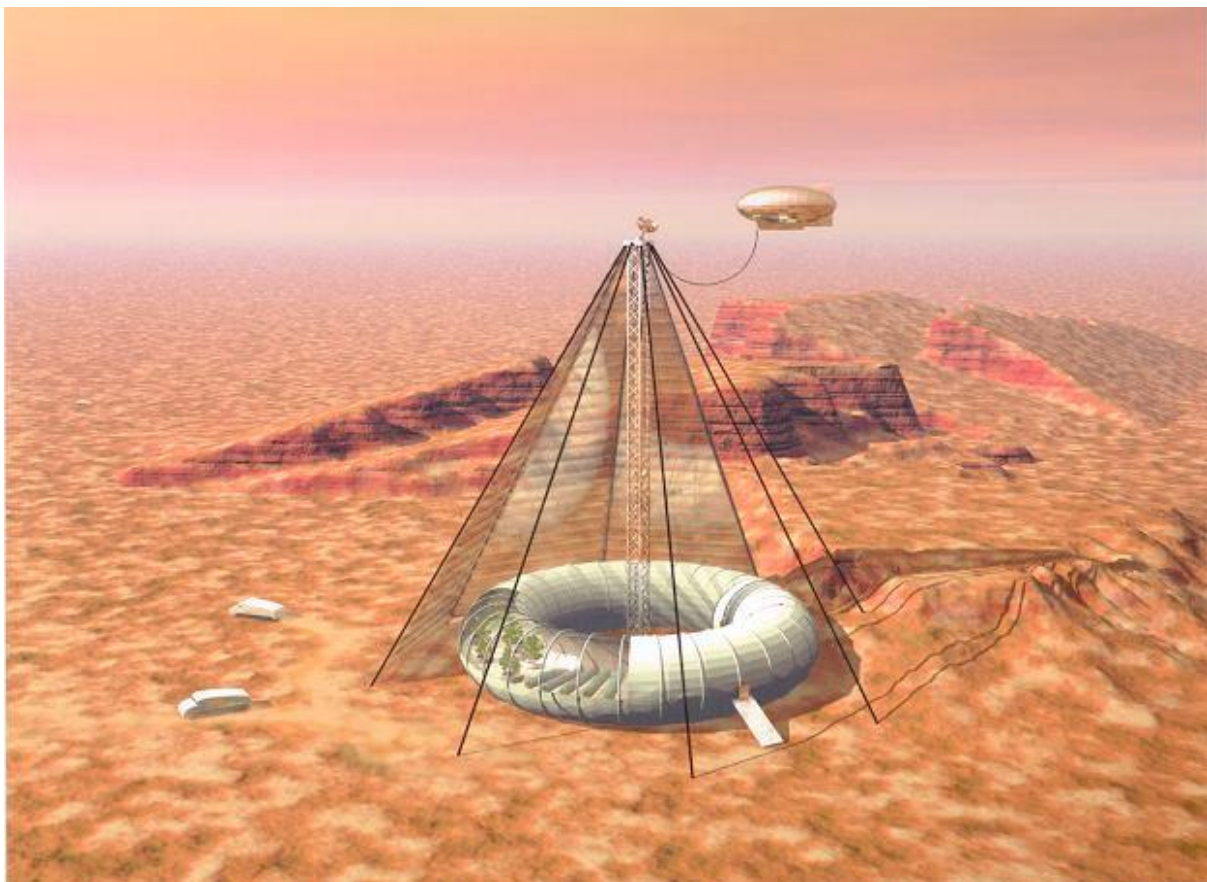
Figure 86: The Independence Torus [Source: 36]

Figure 87: Inflatable structure [Source: 180]

Figure 88: Livermore Habitat Module [Source: 41]

Figure 89: Antarctic Habitat Demonstrator [Source: 181]
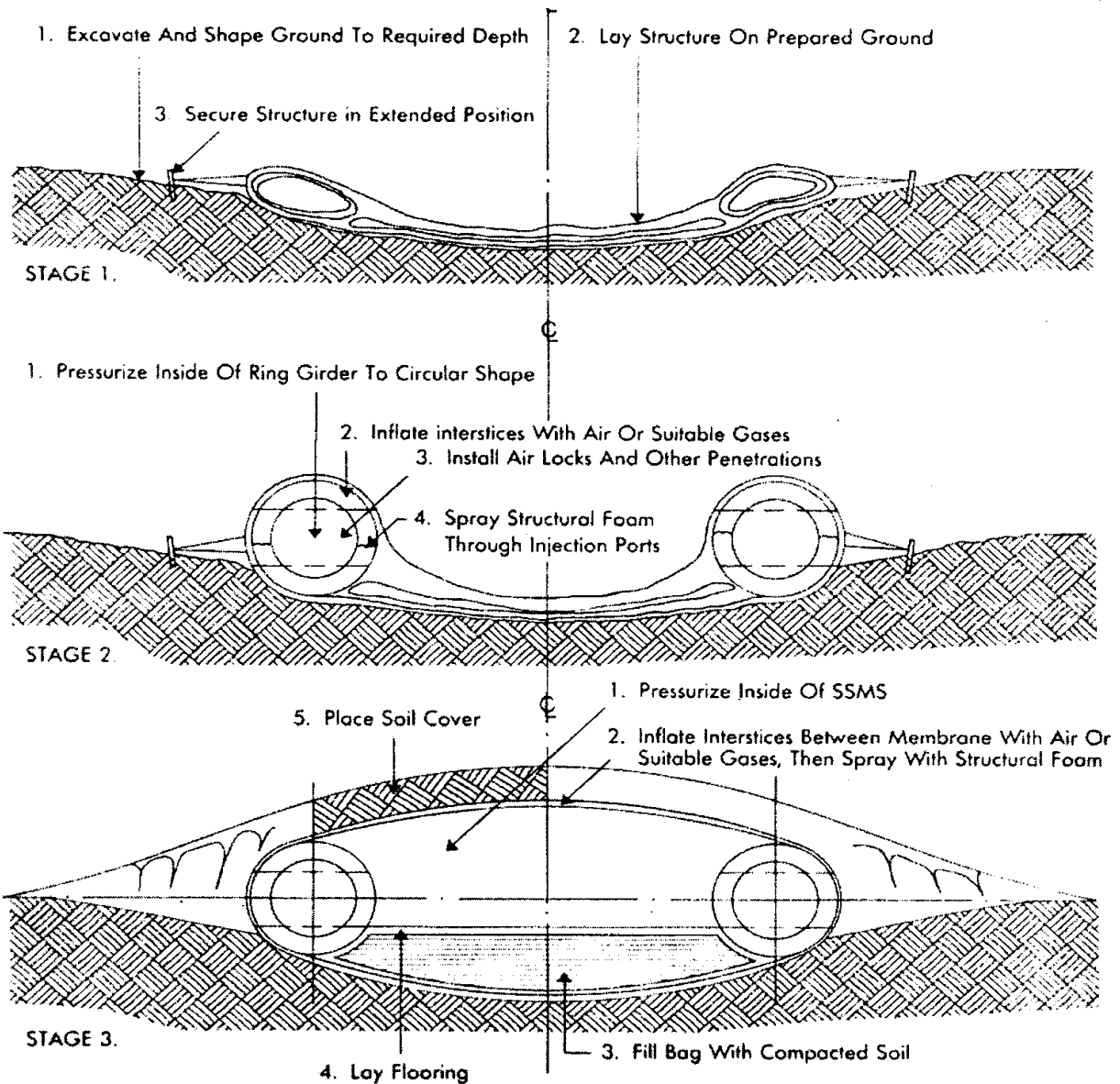
Figure 90: Inflatable membrane structure – construction sequence [Source: 182]
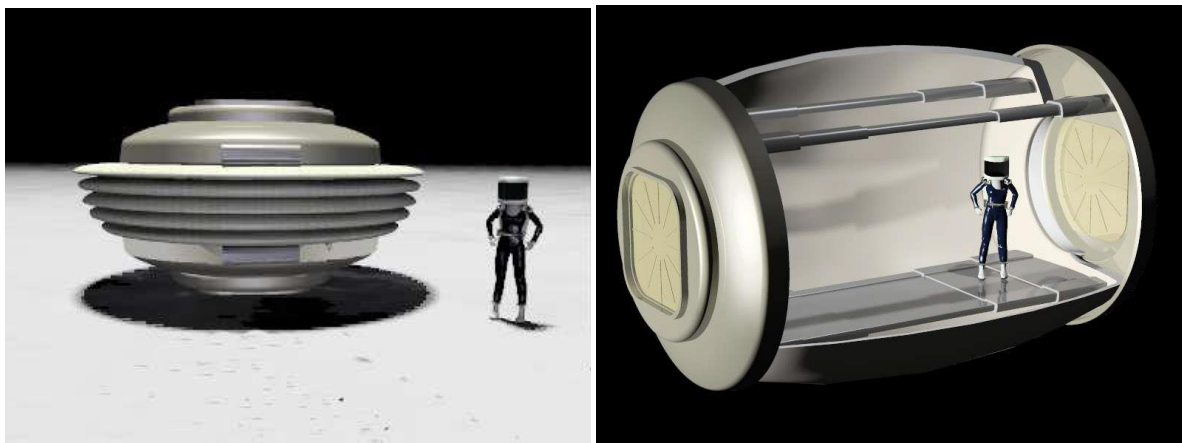
Figure 91: Primary telescopic structure (Left) Stowed configuration (Right) Deployed configuration
[Source: 183]
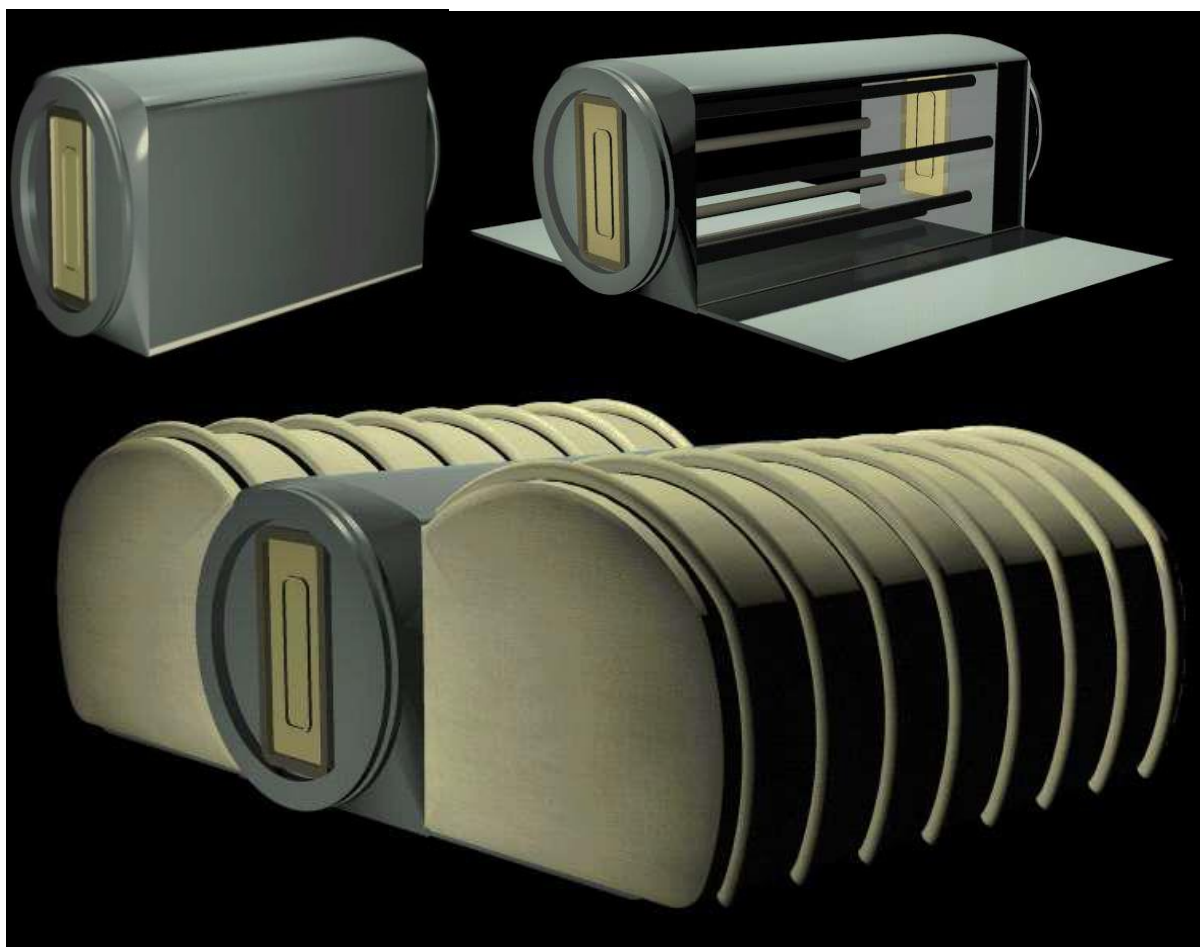
Figure 92: Surface habitat concept: Semi-rigid module [Source: 183]
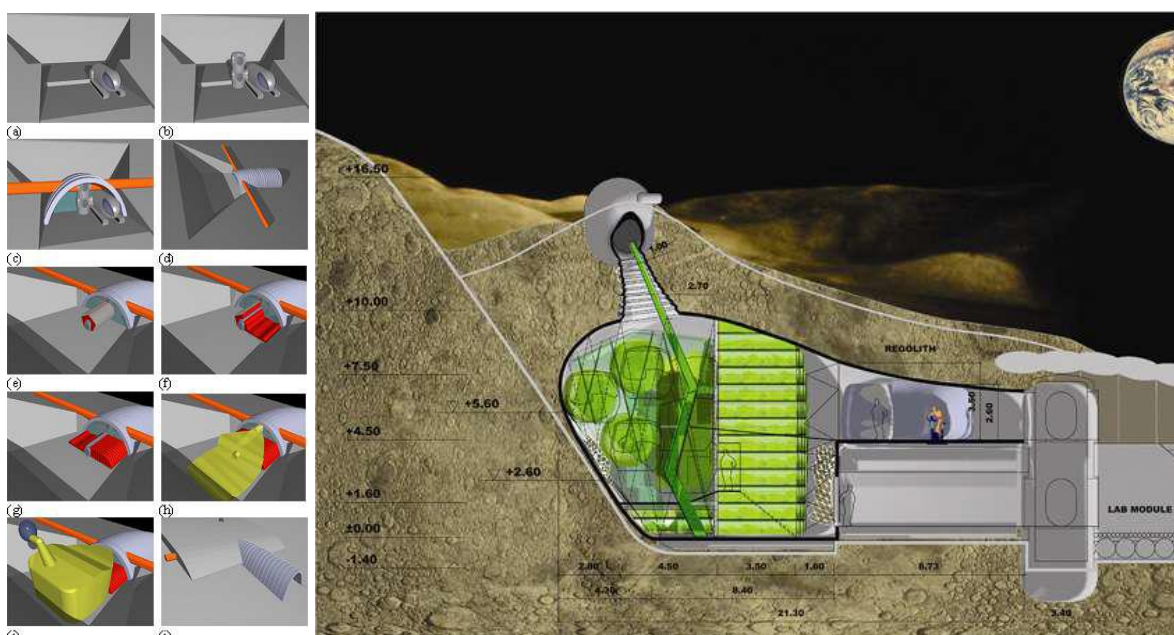
Figure 93: KEPLER lunar base design [Source: 183]
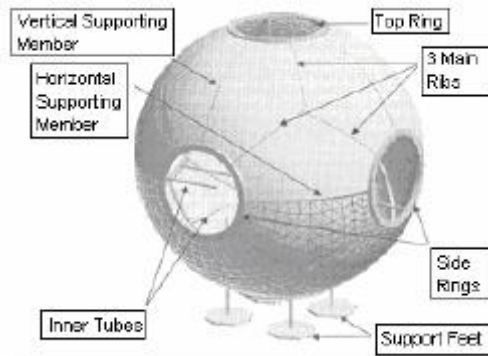
Figure 94: Example of an Inflatable Habitat [184]
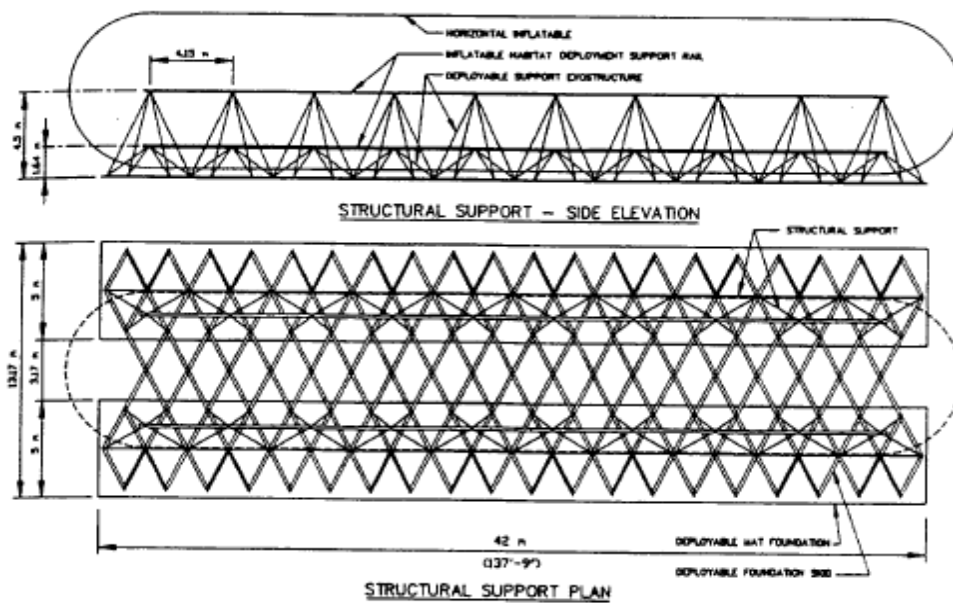
Figure 95: Cylindrical habitat [185]
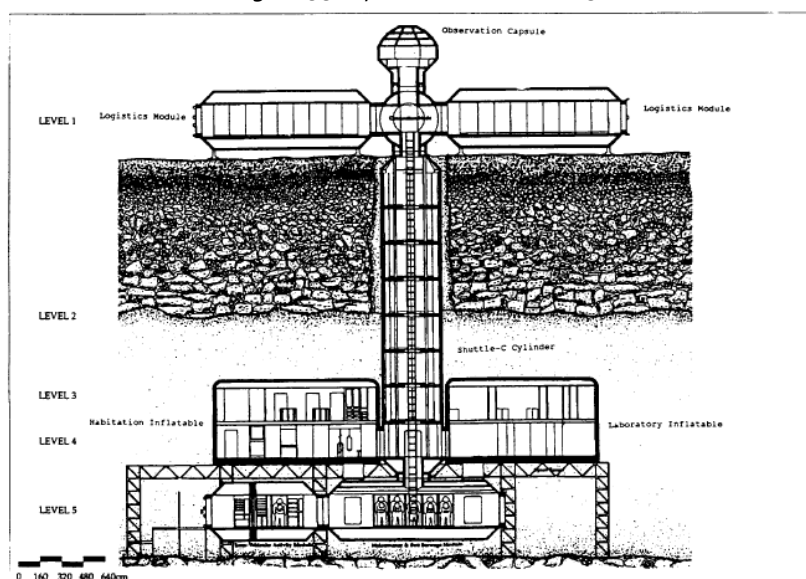
Figure 96: Genesis II Advanced Lunar Outpost [185]
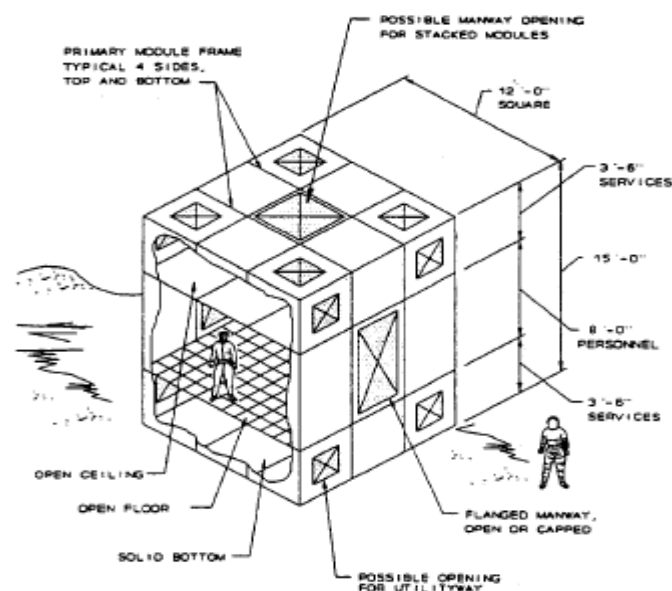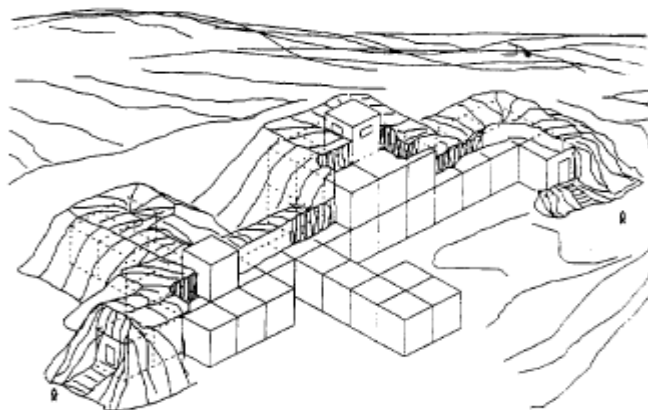
Figure 97: Cubical modular habitat [185]
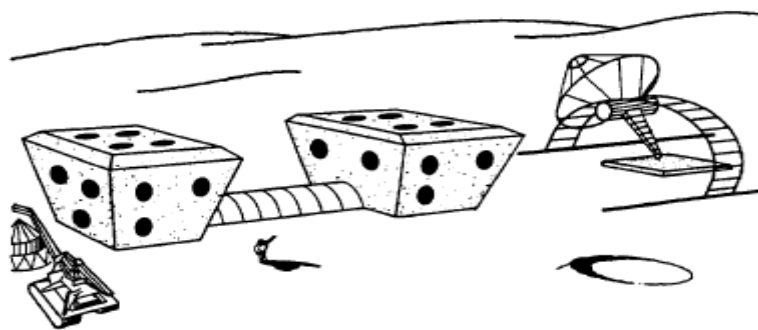
Figure 98: Fused regolith habitat [185]

Figure 99: Mobitat2 habitat in parked position [186]

Figure 100: Top view of the MMOD panels of the FLECS expandable module [187]
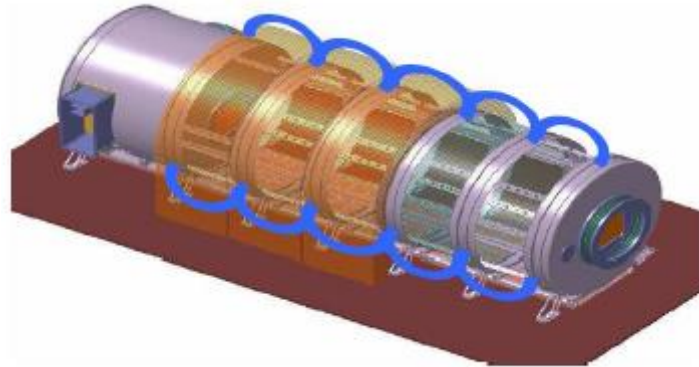
Figure 101: Green Habitation Orbital Module for Exploration [188]
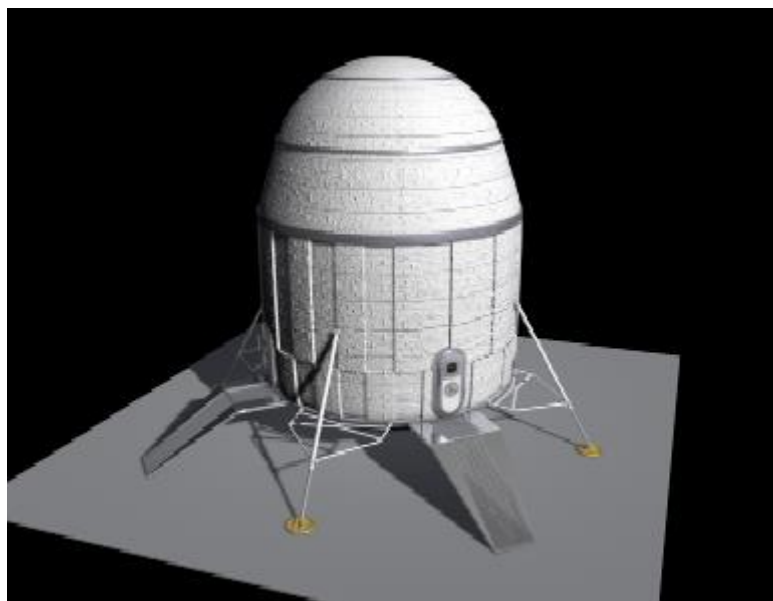
Figure 102: Monolithic concept B geometry [189]
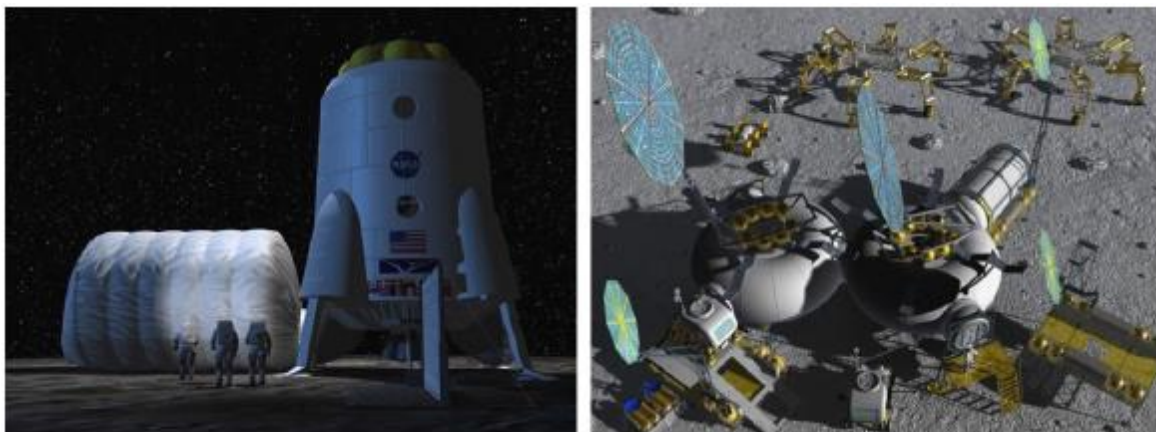
Figure 103: Conceptual views of cylindrical and toroidal inflatable habitats [190]

Figure 104: CyclopsHUB – modular inflatable habitat [191]
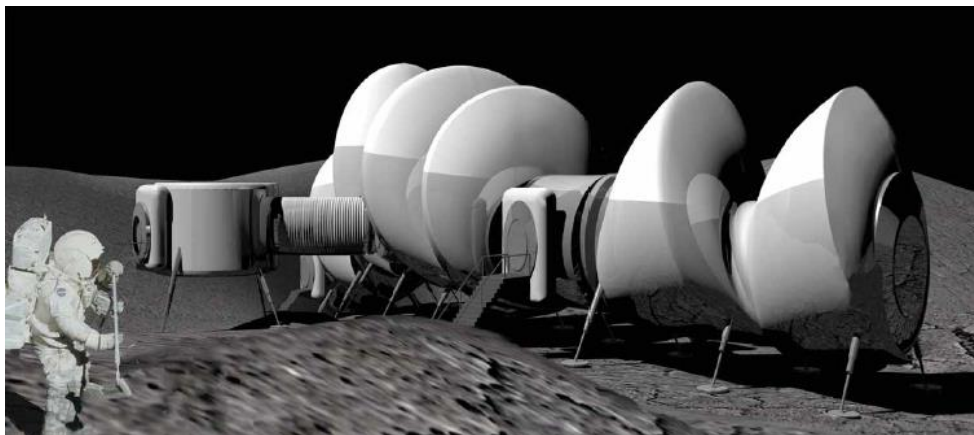
Figure 105: T:W:I:S:T – modular inflatable habitat [191]

Appendix B. Materials for Inflatable Space Structures

During the literature review a number of materials were found which can be used for deployable space structures. A (non-exhaustive) overview of these materials is given in this Appendix.

Note: For a number of materials no data could be found on some of the characteristics. Additionally, for the non-metals, the material properties varied widely between different manufacturers and in this case the median value was used. Furthermore, for several properties, such as impact strength, there are multiple tests which can be used to determine the material performance, leading to possible difference in result. Where possible, the type of test has been indicated for such parameters.

Table 43: Material properties for materials applicable for hybrid and inflatable space structures.
Density, Tensile strength. Tensile modulus and Yield strength
[63,151,152,153,154,166,167,192,193]

Material Name	Density [g/cm^3]	Tensile strength [Mpa]	Tensile modulus [Gpa]	Yield Strength [Mpa]
Kevlar 49	1,44	3600	124	
Twaron 2200	1,44	2950	99	
Dyneema	0,975	3500	115	
Vectran HS	1,41	2900	72	
Poly Benzol Oxylene (PBO)	1,56	5800	180	189,6
Technora	1,39	3400	73	
Spectra 2000	0,97	3250	116	
Ethylene Vinyl alcohol (EVOH)	1,17	57,3	2,16 (??)	66,8 (?? Tensile)
PolyVinyliDene Chloride (PVDC)	1,69			
PolyAmide-Nylon	1,13			70
Polyurethane adhesives	1,21	9,82	0,0638	0,522
Capran Oxyshield OEB (0.6 mil)	1,16			68,9 - 82,7 (TD)
SCLAIRFILM SL-1	0,918		0,17	
PA 6	1,12 - 1,14	48 - 85	2,3 - 2,5	35 - 40
Kapton H				69
Kapton V				69
Kapton E				103,4
Aorimide (Triton)				60,7 (TD) 66,2 (MD)
LaRC CP1 Polyimide (*datasheet)	1,54	87	2	
Kapton 100HN	1,42	231	2,55	69 (MD)
Mylar	1,39	20 [kg/mm2 MD] 24 [TD]	490 [kg/mm2 MD] 510 [TD]	10 [kg/mm2]

Material Name	Density [g/cm^3]	Tensile strength [Mpa]	Tensile modulus [Gpa]	Yield Strength [Mpa]
Tedlar	1,37 - 1,72			
Nextel 312 AF10	2,7	1700	150	
Polyurethane foams (unreinforced)	0,381	13,3	0,111	1,95
Combitherm VPC 140				
Combitherm XX 170				
Urethane coated Nylon				
Urethane coated Polyester scrim				
Amm Flex TM				
Combitherm-Kevlar laminate one sided				
Combitherm-Kevlar laminate two sided				
Kevlar 149	1,47	3450	179	
Spectra 1000	0,97	3000	172	
E37X1 Base resin		64,5	2,69	53,9
Handi-foam two component	0,028	0,317		
Handi-foam one component	0,0192			
Great stuff foam	0,0272	0,154		
Dacron Type 68	1,38		14	
Kevlar 29	1,44	3620	70,3	
Zylon HM	1,56		27	
Nextel 312	2,7	1700 (ult)	150	
Celanese Type 710 polyester	1,38			
Nylon Type 331	1,14			
Toyobo PBO-AS	1,54			
Nomex	1,38	600		
Goretex Teflon	2,1			
Ti-5Al-2.5Sn ELI	4,48	719,936	110,208	
Al 7075-O	2,81	94,978	71,936	
Al 2048	2,75	414,975	70,125	
Al 2024-O	2,78	75,06	72,28	
Al 2219-O	2,84	69,864	72,136	
Viton coating	1,84			
HDPE (Impact Grade)	0,951	13,7	0,702	21,5
Polypropylene (Fiber Grade)	0,525	179	1,59	34,9

Table 44: Material properties for materials applicable for hybrid and inflatable space structures. Impact strength, Breaking strength, Breaking tenacity, Tenacity and Tear Strength [63,151,152,153,154,166,167,192,193]

Material Name	Impact strength	Breaking strength	Breaking tenacity [Mpa]	Tenacity [N/tex]	Tear strength
Kevlar 49			3000	2,08	
Twaron 2200					
Dyneema				3,53	
Vectran HS				2,03	
Poly Benzol Oxylene (PBO)				3,62	
Technora				2,47	
Spectra 2000					
Ethylene Vinyl alcohol (EVOH)					690
PolyVinyliDene Chloride (PVDC)					
PolyAmide-Nylon					
Polyurethane adhesives					32,9 [kN/m]
Capran Oxyshield OEB (0.6 mil)					925-1400, 1000-1400 graves tear
SCLAIRFILM SL-1		34 [MPA MD]			
PA 6	0,44 - 3 [J/cm]				
Kapton H					
Kapton V					
Kapton E					
Aorimide (Triton)					
LaRC CP1 Polyimide (*datasheet)					
Kapton 100HN	0,780 [J]	221 [Mpa]			7,2 [N Graves]
Mylar					
Tedlar					
Nextel 312 AF10		20 - 39 [kg/cm]			
Polyurethane foams (unreinforced)	1,43 [J/cm^2]				84,6 (2,13 kN/m)
Combitherm VPC 140					155 [N]
Combitherm XX 170					40,2 [N]
Urethane coated Nylon					101 [N]

Material Name	Impact strength	Breaking strength	Breaking tenacity [Mpa]	Tenacity [N/tex]	Tear strength
Urethane coated Polyester scrim					393 [N]
Amm Flex TM					55,4 [N]
Combitherm-Kevlar laminate one sided					540 (N)
Combitherm-Kevlar laminate two sided					567 (N)
Kevlar 149					
Spectra 1000				3,09	
E37X1 Base resin					
Handi-foam two component					
Handi-foam one component					
Great stuff foam					
Dacron Type 68				0,741	
Kevlar 29		338 [N ??]	2920	2,03	
Zylon HM				3,71	
Nextel 312					
Celanese Type 710 polyester				0,733	
Nylon Type 331				0,741	
Toyobo PBO-AS				3,71	
Nomex				0,397	
Goretex Teflon				0,15	
Ti-5Al-2.5Sn ELI	44 (Charpy Impact) [J]				
Al 7075-O					
Al 2048	10,3 (Charpy Impact) [J]				
Al 2024-O					
Al 2219-O					
Viton coating					
HDPE (Impact Grade)	1,6 [J/cm] 75,7 [kJ/m2] (Izod Notched)				
Polypropylene (Fiber Grade)	0,3 [J/cm] 3,67 [kJ/m2] (Izod notched)			0,255	

Table 45: Material properties for materials applicable for hybrid and inflatable space structures.
Elongation, Poisson's ratio, Thermal conductivity, Coefficient of thermal expansion
[63,151,152,153,154,166,167,192,193]

Material Name	Elongation at break [%]	Poisson's ratio	Thermal conductivity [W/m*K]	Coefficient of thermal expansion [µm/m*°C]
Kevlar 49	2,9	0,36	0,04	
Twaron 2200	2,9			
Dyneema	3,2			
Vectran HS	3,3		0,37	
Poly Benzol Oxylene (PBO)	3,5			-7,6 (MD) , 7,6 (TD)
Technora	4,6			
Spectra 2000	2,9			
Ethylene Vinyl alcohol (EVOH)	233		0,341	90,4 / 120
PolyVinyliDene Chloride (PVDC)				
PolyAmide-Nylon	55-80			
Polyurethane adhesives	293		0,57	161
Capran Oxyshield OEB (0.6 mil)	55-80 (Machine D) 180-425 (Tensile D)			
SCLAIRFILM SL-1	600			
PA 6	100 - 320		0,245 - 0,27	83 - 120
Kapton H				20
Kapton V				24
Kapton E				12
Aorimide (Triton)				42
LaRC CP1 Polyimide (*datasheet)	16			51
Kapton 100HN	75	0,34	0,12	20 / 32
Mylar	91 (TD) 116 (MD)	0,38 (before yield) 0,58	3,7*10°-4 [cal*cm/cm2*sec*°C]	17
Tedlar				
Nextel 312 AF10				3
Polyurethane foams (unreinforced)	187		0,085	180
Combitherm VPC 140				
Combitherm XX 170				
Urethane coated Nylon				
Urethane coated Polyester				

Material Name	Elongation at break [%]	Poisson's ratio	Thermal conductivity [W/m*K]	Coefficient of thermal expansion [µm/m*°C]
scrim				
Amm Flex TM				
Combitherm-Kevlar laminate one sided				
Combitherm-Kevlar laminate two sided				
Kevlar 149				
Spectra 1000	2,7			
E37X1 Base resin				
Handi-foam two component				
Handi-foam one component				
Great stuff foam				
Dacron Type 68	17			
Kevlar 29	3,6		0,04	
Zylon HM	2,5			
Nextel 312				3
Celanese Type 710 polyester	16,3			
Nylon Type 331	18			
Toyobo PBO-AS	3,5			
Nomex	25		0,035	
Goretex Teflon	35			
Ti-5Al-2.5Sn ELI			7,8	9,4
Al 7075-O			173	23,6
Al 2048			159	23,5
Al 2024-O			193	23,2
Al 2219-O			170	23,3
Viton coating			0,202	
HDPE (Impact Grade)	415			
Polypropylene (Fiber Grade)	268			

Table 46: Material properties for materials applicable for hybrid and inflatable space structures.
Specific heat, Melting point, Glass temperature, Brittleness temperature, Temperature limits
[63,151,152,153,154,166,167,192,193]

Material Name	Specific heat [J/g*°C]	Melting point or decomposition [°C]	Glass temperature [°C]	Brittleness temperature	Temperature limitations
Kevlar 49	1,42	400			Max service temp 149 - 177 °C
Twaron 2200		550			
Dyneema		150			Max service temp 150 °C
Vectran HS	1,26	330		-160	
Poly Benzol Oxylene (PBO)		650			
Technora		550			
Spectra 2000		<170			
Ethylene Vinyl alcohol (EVOH)	2,4	176	60,8		
PolyVinyliDene Chloride (PVDC)					
PolyAmide-Nylon					Max service temp 180 °C
Polyurethane adhesives			-34,4		Min. -54,5 Max. 111
Capran Oxyshield OEB (0.6 mil)					
SCLAIRFILM SL-1					
PA 6	1,592 - 1,7	223	50-75		-70 to 105
Kapton H					
Kapton V					
Kapton E					
Aorimide (Triton)					
LaRC CP1 Polyimide (*datasheet)			263		
Kapton 100HN	1,09		360-410		-269 to 400
Mylar	0,28 [cal/g*°C]	254			Max service temp 150
Tedlar					
Nextel 312 AF10					
Polyurethane foams (unreinforced)				-36,5	-39,1 to 95,9
Combitherm VPC 140					
Combitherm XX 170					
Urethane coated Nylon					

Material Name	Specific heat [J/g*°C]	Melting point or decomposition [°C]	Glass temperature [°C]	Brittleness temperature	Temperature limitations
Urethane coated Polyester scrim					
Amm Flex TM					
Combitherm-Kevlar laminate one sided					
Combitherm-Kevlar laminate two sided					
Kevlar 149		500			Max service temp 425 °C
Spectra 1000		147		-25	
E37X1 Base resin					
Handi-foam two component					
Handi-foam one component					
Great stuff foam					
Dacron Type 68		256			
Kevlar 29	1,42	427-482 °C		-196	Max service temp 149 - 177 °C
Zylon HM		427			
Nextel 312	1,05	1800			
Celanese Type 710 polyester				-55	
Nylon Type 331				-55	
Toyobo PBO-AS					
Nomex	1,47			-157	
Goretex Teflon				-268	
Ti-5Al-2.5Sn ELI					
Al 7075-O					
Al 2048					
Al 2024-O					
Al 2219-O					
Viton coating	1,65				
HDPE (Impact Grade)				-55,4	
Polypropylene (Fiber Grade)		162			

Table 47: Material properties for materials applicable for hybrid and inflatable space structures.
Adhesion strength, Permeability, Corrosion resistance, Abrasion resistance
[63,151,152,153,154,166,167,192,193]

Material Name	Coating adhesion /Adhesion bond strength	Permeability [cc*mm/m^2*day* atm]	Corrosion resistance	Abrasion resistance
Kevlar 49				
Twaron 2200				
Dyneema				
Vectran HS	Excellent			Good
Poly Benzol Oxylene (PBO)				Poor
Technora				
Spectra 2000				
Ethylene Vinyl alcohol (EVOH)		1,13 (H2O) 0,019 (O2)		1,65 [mg/1000 Cycles Taber abrasion]
PolyVinyliDene Chloride (PVDC)		0,0219 (O2)		
PolyAmide-Nylon				
Polyurethane adhesives	2,59 [Mpa]			
Capran Oxyshield OEB (0.6 mil)		140 [g/m^2*day water], 0,23-0,93 [cc/m^2*day O2]		
SCLAIRFILM SL-1		0,47 [Moisture vapor] 236 [O2]		
PA 6				
Kapton H				
Kapton V				
Kapton E				
Aorimide (Triton)				
LaRC CP1 Polyimide (*datasheet)				
Kapton 100HN		3,5 (H20) 9,9 (O2)		
Mylar				
Tedlar				
Nextel 312 AF10		46 - 229 [l/min*dm2]		
Polyurethane foams (unreinforced)				
Combitherm VPC 140		1,09 [cc/m^2*day*atm O2]		
Combitherm XX 170		1,40 [cc/m^2*day*atm O2]		

Material Name	Coating adhesion /Adhesion bond strength	Permeability [cc*mm/m^2*day*atm]	Corrosion resistance	Abrasion resistance
Urethane coated Nylon		257 [cc/m^2*day*atm O2]		
Urethane coated Polyester scrim		399 [cc/m^2*day*atm O2]		
Amm Flex TM		4,97 [cc/m^2*day*atm O2]		
Combitherm-Kevlar laminate one sided		1,55 [cc/m^2*day*atm O2]		
Combitherm-Kevlar laminate two sided		0,311 [cc/m^2*day*atm O2]		
Kevlar 149				
Spectra 1000	Poor			Excellent
E37X1 Base resin				
Handi-foam two component				
Handi-foam one component				
Great stuff foam				
Dacron Type 68				
Kevlar 29	Fair			Poor
Zylon HM				
Nextel 312				
Celanese Type 710 polyester	Excellent			Fair
Nylon Type 331	Excellent			Good
Toyobo PBO-AS				Good
Nomex	Fair			Fair
Goretex Teflon	Poor			Fair
Ti-5Al-2.5Sn ELI			High	
Al 7075-O			medium (C ??)	
Al 2048			low	
Al 2024-O			low (D ??)	
Al 2219-O			low	
Viton coating				
HDPE (Impact Grade)				
Polypropylene (Fiber Grade)				

Table 48: Material properties for materials applicable for hybrid and inflatable space structures.
Shrinkage, Toxicity, Outgassing, Metallizability, Bondability, UV resistance
[63,151,152,153,154,166,167,192,193]

Material Name	Shrinkage [%]	Toxicity	Outgassing [%]	Metalliz-ability	Bond-ability	UV resistance
Kevlar 49	0,1					
Twaron 2200						
Dyneema						
Vectran HS	Minimal (0,1 ??)					Fair
Poly Benzol Oxylene (PBO)				Yes	Yes	
Technora						
Spectra 2000						
Ethylene Vinyl alcohol (EVOH)	-6,99					
PolyVinyliDene Chloride (PVDC)						
PolyAmide-Nylon	1					
Polyurethane adhesives	0,8		0,544			
Capran Oxyshield OEB (0.6 mil)	11 (MD), 2,5 (TD)					
SCLAIRFILM SL-1						
PA 6	0,3 - 2					
Kapton H	0,17		0,02 (CVCM) 0,77 (TML)	Yes	Yes	
Kapton V	0,03		0,02 (CVCM) 0,77 (TML)	Yes	Yes	
Kapton E	0,03			Yes	Yes	
Aorimide (Triton)			<2	Yes	Yes	
LaRC CP1 Polyimide (*datasheet)				Yes	Yes	
Kapton 100HN						
Mylar						
Tedlar						
Nextel 312 AF10						
Polyurethane foams (unreinforced)	0,627					
Combitherm VPC 140		OK				
Combitherm XX 170		OK				
Urethane coated Nylon		OK				
Urethane coated Polyester scrim						

Material Name	Shrinkage [%]	Toxicity	Outgassing [%]	Metalliz-ability	Bond-ability	UV resistance
Amm Flex TM						
Combitherm-Kevlar laminate one sided						
Combitherm-Kevlar laminate two sided						
Kevlar 149						
Spectra 1000						Good
E37X1 Base resin						
Handi-foam two component						
Handi-foam one component						
Great stuff foam						
Dacron Type 68						
Kevlar 29	0,1					Poor
Zylon HM						
Nextel 312						
Celanese Type 710 polyester	1,6					Good
Nylon Type 331	8					Fair
Toyobo PBO-AS						Fair
Nomex	0,5					Good
Goretex Teflon	minimal (0,1 ??)					Excellent
Ti-5Al-2.5Sn ELI						
Al 7075-O						
Al 2048						
Al 2024-O						
Al 2219-O						
Viton coating						
HDPE (Impact Grade)						
Polypropylene (Fiber Grade)	1,75					

Table 49: Material properties for materials applicable for hybrid and inflatable space structures.
Creep, Oxidization resistance, Cure time, Flammability, Puncture resistance
[63,151,152,153,154,166,167,192,193]

Material Name	Creep [%]	Oxidization resistance	Expansion / Cure time	Flammability [LOI]	Puncture resistance
Kevlar 49					
Twaron 2200					
Dyneema					
Vectran HS	Excellent	Excellent		28	
Poly Benzol Oxylene (PBO)	0,0055 (@1500 psi 76 days)			>56	
Technora					
Spectra 2000					
Ethylene Vinyl alcohol (EVOH)					
PolyVinyliDene Chloride (PVDC)					
PolyAmide-Nylon					
Polyurethane adhesives			3680 [minutes]		
Capran Oxyshield OEB (0.6 mil)					
SCLAIRFILM SL-1					
PA 6					
Kapton H					
Kapton V					
Kapton E	0,0065 (@300 psi 76 days)				
Aorimide (Triton)					
LaRC CP1 Polyimide (*datasheet)					
Kapton 100HN				37 (V-0 on UL94 test)	
Mylar	0,9 (@500 psi, 4000+ hrs)				
Tedlar					
Nextel 312 AF10					
Polyurethane foams (unreinforced)				(HB-5VA on UL94 test)	
Combitherm VPC 140					9,59 (??)
Combitherm XX 170					6,91 (??)
Urethane coated Nylon					
Urethane coated Polyester					

Material Name	Creep [%]	Oxidization resistance	Expansion / Cure time	Flammability [LOI]	Puncture resistance
scrim					
Amm Flex TM					
Combitherm-Kevlar laminate one sided					
Combitherm-Kevlar laminate two sided					
Kevlar 149					
Spectra 1000	Poor	Excellent		18-19	
E37X1 Base resin					
Handi-foam two component			0,5 - 1 [minute]		
Handi-foam one component			12-24 [hours]		
Great stuff foam					
Dacron Type 68					
Kevlar 29	Good	Excellent			
Zylon HM					
Nextel 312					
Celanese Type 710 polyester	Good	Good			
Nylon Type 331	Poor	Fair			
Toyobo PBO-AS	Excellent	Excellent			
Nomex	Good	Excellent			
Goretex Teflon	Poor	Excellent			
Ti-5Al-2.5Sn ELI					
Al 7075-O					
Al 2048					
Al 2024-O					
Al 2219-O					
Viton coating					
HDPE (Impact Grade)					
Polypropylene (Fiber Grade)					

Table 50: Material properties for materials applicable for hybrid and inflatable space structures. Solvent resistance, H$_2$O absorption, Coefficient of hygroscopic expansion, Hydrolytic stability, Resistance to flex cracking [63,151,152,153,154,166,167,192,193]

Material Name	Solvent resistance	H2O absorption [%]	Coefficient of hygroscopic expansion [PPM/%RH]	Hydrolytic stability	Resistance to flex cracking
Kevlar 49		3,5			
Twaron 2200					
Dyneema		0			
Vectran HS				Excellent	Good
Poly Benzol Oxylene (PBO)	Excellent	0,8	0,8		Poor
Technora					
Spectra 2000					
Ethylene Vinyl alcohol (EVOH)		7			
PolyVinyliDene Chloride (PVDC)					
PolyAmide-Nylon		9			
Polyurethane adhesives		0,215			
Capran Oxyshield OEB (0.6 mil)					
SCLAIRFILM SL-1					
PA 6		2,0 - 4,0			
Kapton H	Excellent	1,8-2,8	22		
Kapton V	Excellent	1,8-3	17		
Kapton E	Excellent	2,4	9		
Aorimide (Triton)	Excellent	2 to 8			
LaRC CP1 Polyimide (*datasheet)	sol. In MEK, MIBK, CHC13	0,4			
Kapton 100HN		2,8			
Mylar				6	Water content must be <0,1%
Tedlar					
Nextel 312 AF10					
Polyurethane foams (unreinforced)		8,34			
Combitherm VPC 140					
Combitherm XX 170					
Urethane coated Nylon					
Urethane coated Polyester scrim					

Material Name	Solvent resistance	H2O absorption [%]	Coefficient of hygroscopic expansion [PPM/%RH]	Hydrolytic stability	Resistance to flex cracking
Amm Flex TM					
Combitherm-Kevlar laminate one sided					
Combitherm-Kevlar laminate two sided					
Kevlar 149					
Spectra 1000				Excellent	Excellent
E37X1 Base resin					
Handi-foam two component					
Handi-foam one component					
Great stuff foam					
Dacron Type 68					
Kevlar 29		7		Excellent	Poor
Zylon HM					
Nextel 312					
Celanese Type 710 polyester				Good	Excellent
Nylon Type 331				Poor	Excellent
Toyobo PBO-AS				Excellent	
Nomex				Excellent	Good
Goretex Teflon				Excellent	Excellent
Ti-5Al-2.5Sn ELI					
Al 7075-O					
Al 2048					
Al 2024-O					
Al 2219-O					
Viton coating					
HDPE (Impact Grade)					
Polypropylene (Fiber Grade)		0,01			

Appendix C. System Analysis

C.1   Requirements List

Table 51 lists the top level requirements for the overall GHM and in Table 52 the specific requirements related to the GHM structure are presented. A code is assigned to each requirement to ensure that lower level requirements can be traced to a higher level requirement. This ensures that low level requirements flow logically from the initial top level requirements and can be verified later on.

Table 51: Top level requirements for the lunar GHM

Code	Requirement	Rationale
GHM.1	GHM shall successfully be delivered to the surface of the Moon	*To ensure the mission*
GHM.2	GHM shall successfully be utilized to cultivate fresh food	*Main function of the lunar greenhouse*
GHM.3	GHM shall be designed for a mission lifetime of at least twenty-four lunar days (about two years)	*Requirement from the Statement of Work* [128]
GHM.4	GHM shall be designed to provide a safe environment for humans	*Astronauts may be around the Grow Unit for harvesting or maintenance and should be safe while doing so*
GHM.5	GHM shall be designed such that it has minimal mass	*Cost and launch considerations*
GHM.6	GHM shall be designed such that it has minimal launch volume	*Cost and launch considerations*
GHM.7	GHM shall be designed such that it has minimal power consumption	*Cost reduction*
GHM.8	GHM shall be designed such that it has minimal resource consumption	*Cost reduction, development of closed loop life support systems*
GHM.9	GHM shall be designed such that it has minimal mission cost	*Cost reduction*

Table 52: Requirements for the structure of the lunar GHM

Code	Requirement
GHM.1	**GHM shall successfully be delivered to the surface of the Moon**
Struc.1	GHM shall fit within the launcher
Struc.2	GHM shall withstand launch loads
Struc.3	GHM shall withstand loading and environmental conditions experienced during transfer to Moon
Struc.4	GHM shall withstand loads occurring during descent and landing
GHM.2	**GHM shall successfully be utilized to cultivate fresh food**
Struc.5	GHM shall successfully deploy on the Moon
Struc.5.1	*GHM shall automatically inflate on the Moon*
Struc.5.2	*GHM structure shall rigidize after inflation*
Struc.5.3	*GHM shall allow deployment of equipment after rigidization*
Struc.5.4	*GHM shall have a single-point-of-failure free deployment system*
Struc.6	GHM shall withstand loading conditions during operations
Struc.6.1	*GHM structure shall withstand an internal pressure of 1010 mbar*
Struc.6.2	*GHM structure shall support the combined weight of the structure and the equipment*

Code	Requirement
Struc.6.3	*GHM structure shall be designed with a TBD safety factor*
Struc.7	GHM shall connect with lunar base structures
Struc.7.1	*GHM structure shall contain a minimum of two airlocks*
Struc.7.2	*GHM structure shall have interfaces for power supply*
Struc.7.3	*GHM structure shall have interfaces for air flow*
Struc.7.4	*GHM structure shall have interfaces for water and nutrient delivery*
Struc.7.5	*GHM structure failure shall not affect other lunar base structures*
Struc.8	GHM shall maintain internal radiation levels within proscribed limits for plants
Struc.8.1	*GHM shall ensure the nominal absorbed dose of radiation absorbed by plants is below TBD*
Struc.8.2	*GHM shall ensure the peak absorbed dose of radiation absorbed by plants is below TBD*
Struc.9	GHM shall maintain the gas leakage rate below approximately 8.5 g/day
Struc.9.1	*GHM structure shall have an effective permeability of TBD*
Struc.9.2	*GHM structure shall reduce gas leakage at openings and interfaces to TBD*
Struc.9.3	*GHM structure shall prevent hull breach by (micro-)meteorites*
Struc.10	GHM shall have sufficient volume to fit all required subsystems and equipment
GHM.3	**GHM shall be designed for a mission lifetime of at least twenty-four lunar days (about two years)**
Struc.11	GHM structure shall withstand loading conditions during operations for a period of at least twenty-four lunar days
Struc.11.1	*GHM structure shall be designed to withstand loading conditions during operation taking into account radiation-degraded material performance*
Struc.12	GHM structure shall allow maintenance and repair operations
GHM.4	**GHM shall be designed to provide a safe environment for humans**
Struc.13	GHM shall maintain internal radiation levels within proscribed limits for humans
Struc.13.1	*GHM shall ensure the nominal absorbed dose of radiation absorbed by humans is below 250 mSv/year*
Struc.13.2	*GHM shall ensure the peak absorbed dose of radiation absorbed by humans is below 500 mSv/year*
Struc.14	GHM shall maintain the gas leakage rate below approximately 8.5 g/day (See Struc.9)
Struc.15	GHM shall maintain the internal lunar dust concentration below *TBD*
Struc.15.1	*GHM structure shall prevent lunar dust from entering at a rate exceeding TBD*
GHM.5	**GHM shall be designed such that it has minimal mass**
Struc.16	GHM structure shall strive for minimal mass
GHM.6	**GHM shall be designed such that it has minimal launch volume**
Struc.17	GHM structure shall be stowed in the most efficient method
Struc.17.1	*GHM structure shall be stowed such that the internal stress does not exceed TBD*
Struc.17.2	*GHM structure shall be stowed such that deployment is not hindered or prevented*
Struc.17.3	*GHM structure shall be stowed such that the structure occupies a minimal volume*
GHM.7	**GHM shall be designed such that it has minimal power consumption**
Struc.18	GHM structure shall use minimal power
Struc.18.1	*GHM structure shall have a deployment system which uses minimal power*
GHM.9	**GHM shall be designed such that it has minimal mission cost**
Struc.19	GHM structure shall strive for minimal cost

Appendix D. Concept Trade-off

D.1 Analytic Hierarchy Process description

The Analytic Hierarchy Process (AHP) was developed by T.L. Saaty and uses pairwise comparisons to aid in the decision making process.

The first step of the process is to define the criteria which affect the decision making. These criteria are defined in a hierarchy, with criteria being divided into lower level sub-criteria, until the desired level of detail has been achieved. Here it is important to ensure that the criteria on the same hierarchy level are independent to each other.

Once the criteria have been defined, pairwise comparison is performed between the elements of each level of the hierarchy. This is done according to the rating system indicated in Table 53, which is adapted from [194].

Table 53: Rating system for the AHP pairwise comparison

Intensity of importance on an absolute scale	Definition	Explanation
1	Equal importance	Two activities contribute equally to the objective
3	Moderate importance of one over another	Experience and judgment slightly favour one activity over another
5	Essential or strong importance	Experience and judgment strongly favour one activity over another
7	Very strong importance	An activity is strongly favoured and its dominance demonstrated in practice
9	Extreme importance	The evidence favouring one activity over another is of the highest possible order of affirmation
2, 4, 6, 8	Intermediate values between the two adjacent judgments	When compromise is needed

Aside from the ratings listed in the table above, the reasonable assumption of reciprocity is used.
For example, when considering the design of a satellite, mass may be strongly more important than cost, giving it a rating of 5. Due to reciprocity, cost would then have an importance of 1/5 with respect to mass.

The pairwise comparisons between the different criteria on the same hierarchy level are entered into matrices, with a separate matrix for each level of the hierarchy. An example of such a matrix is given below in Table 54.

Table 54: Example of a comparison matrix with 3 elements

	A	B	C
A	1	6	8
B	1/6	1	4
C	1/8	1/4	1

The comparison matrices are then normalized, after which the weights of the different criteria are found by computing the average values of each of the rows of the normalized matrices.

It should be noted that these weights are only with respect to the current hierarchy level and need to be multiplied with the weights of all corresponding higher level criteria before being applied in the final ranking.

Table 55: Normalized comparison matrix with 3 elements and corresponding weights

	A	B	C	Weights
A	24/31	24/29	8/13	0,739055
B	4/31	4/29	4/13	0,191522
C	3/31	1/29	1/13	0,069393

The AHP incorporates a check to ensure that the evaluation is consistent. To do this, the eigenvalue of each element is calculated. This is done by creating a mean matrix, through multiplication of the columns of the initial comparison matrix with the corresponding weights. Then, the sum of each row is calculated to obtain a mean value. This mean value is then divided by the value of the diagonal matrix entry in that row. An example of this process is shown in Table 56.

Table 56: Mean matrix with 3 elements and corresponding mean values and eigenvalues

	A	B	C	Mean values	Eigenvalues
A	0,739055	1,149132	0,555144	2,443331	3,306021
B	0,123176	0,191522	0,277572	0,59227	3,092438
C	0,092382	0,047881	0,069393	0,209656	3,021285

From the eigenvalues of the different elements, the so called maximum eigenvalue is calculated, by taking the sum of the eigenvalues and dividing this by the number of elements, n. For the matrix shown in Table 56, this would yield:

$$\lambda_{max} = \frac{\sum_{i=1}^{n} \lambda_i}{n} = \frac{(3,306021 + 3,092438 + 3,021285)}{3} = 3,139915$$

Using this maximum eigenvalue the consistency index CI is calculated as shown below.

$$CI = \frac{\lambda_{max} - n}{n-1} = \frac{3,139915 - 3}{3 - 1} = 0,069958$$

This consistency index is then finally divided by a random consistency value, R, which is dependent on the size of the matrix, as shown in Table 57.

Table 57: Random consistency, R, as a function of matrix size

Number of elements, n	1	2	3	4	5	6	7	8	9	10
Random consistency, R	0	0	0,52	0,89	1,11	1,25	1,35	1,40	1,45	1,49

Dividing the consistency index, CI, by the random consistency, R, yields the consistency relationship, CR:

$$CR = \frac{CI}{R} = \frac{0,069958}{0,52} \approx 0,13$$

The evaluation can be considered consistent when CR < 0,1. For the example presented here, this is not the case, meaning that there is an inconsistency in the evaluation and the pairwise comparison will need to be reviewed. For example, changing the relative importance of criteria B with respect to criteria C from 4 to 3 would result in a consistent AHP evaluation.

D.2 Pairwise comparisons and intermediate AHP results

This section contains the comparison matrices and the intermediate calculation results for the concept trade-off discussed in chapter 5.

Table 58: Comparison matrix

	Mass	Volume	Reliability	Complexity	Crew Time
Mass	1	0,333333	0,333333	2	5
Volume	3	1	1	5	9
Reliability	3	1	1	4	9
Complexity	0,5	0,2	0,25	1	3
Crew Time	0,2	0,111111	0,11111	0,333333	1

Table 59: Normalized comparison matrix

	Mass	Volume	Reliability	Complexity	Crew Time
Mass	0,129870	0,126050	0,123711	0,162162	0,185185
Volume	0,389610	0,378151	0,371134	0,405405	0,333333
Reliability	0,389610	0,378151	0,371134	0,324324	0,333333
Complexity	0,064935	0,075630	0,092784	0,081081	0,111111
Crew Time	0,025974	0,042017	0,041237	0,027027	0,037037

Table 60: Sums of normalized comparison matrix rows and corresponding weights

	Sums of row entries	Normalized Weights
Mass	0,726979	0,145396
Volume	1,877634	0,375527
Reliability	1,796553	0,359311
Complexity	0,425541	0,085108
Crew Time	0,173292	0,034658

Table 61: Mean matrix

	Mass	Deployed to stowed Volume	Reliability	Complexity	Crew Time
Mass	0,145396	0,125176	0,119770	0,170216	0,173292
Volume	0,436188	0,375527	0,359311	0,425541	0,311926
Reliability	0,436188	0,375527	0,359311	0,340433	0,311926
Complexity	0,072698	0,075105	0,089828	0,085108	0,103975
Crew Time	0,029079	0,041725	0,039923	0,028369	0,034658

Table 62: Mean values and eigenvalues

	Mean values	Eigenvalues
Mass	0,73385	5,047256
Volume	1,908492	5,082171
Reliability	1,823384	5,074671
Complexity	0,426714	5,013787
Crew Time	0,173756	5,013376

Table 63: Consistency check

Maximum eigenvalue	CI	R	CR
5,046252	0,011563	1,11	0,010417